Materials Design for Block Copolymer Lithography

By

Daniel Patrick Sweat

A dissertation submitted in partial fulfillment of

the requirements for the degree of

Doctor of Philosophy

(Chemistry)

at the

UNIVERSITY OF WISCONSIN–MADISON

2014

Date of final oral examination: 8/18/2014

The dissertation is approved by the following members of the Final Oral Committee:

Padma Gopalan, Professor, Materials Science and Engineering
Mahesh K. Mahanthappa, Associate Professor, Chemistry
David M. Lynn, Professor, Chemical and Biological Engineering
Sandro Mecozzi, Associate Professor, Pharmacy
Michael S. Arnold, Associate Professor, Materials Science and Engineering

Abstract

Materials Design for Block Copolymer Lithography

Daniel Patrick Sweat

Under the supervision of Professor Padma Gopalan

at the University of Wisconsin-Madison

Block copolymers (BCPs) have attracted a great deal of scientific and technological interest due to their ability to spontaneously self-assemble into dense periodic nanostructures with a typical length scale of 5 to 50 nm. The use of self-assembled BCP thin-films as templates to form nanopatterns over large-area is referred to as BCP lithography. Directed self-assembly of BCPs is now viewed as a viable candidate for sub-20 nm lithography by the semiconductor industry. However, there are multiple aspects of assembly and materials design that need to be addressed in order for BCP lithography to be successful. These include substrate modification with polymer brushes or mats, tailoring of the block copolymer chemistry, understanding thin-film assembly and developing epitaxial like methods to control long range alignment.

The rational design, synthesis and self-assembly of block copolymers with large interaction parameters (χ) is described in the first part of this dissertation. Two main blocks were chosen for introducing polarity into the BCP system, namely poly(4-hydroxystyrene) and poly(2-vinylpyridine). Each of these blocks are capable of ligating Lewis acids which can increase the

etch contrast between the blocks allowing for facile pattern transfer to the underlying substrate. These BCPs were synthesized by living anionic polymerization and showed excellent control over molecular weight and dispersity, providing access to sub 5-nm domain sizes.

Polymer brushes consist of a polymer chain with one end tethered to the surface and have wide applicability in tuning surface energy, forming responsive surfaces and increasing biocompatibility. In the second part of the dissertation, we present a universal method to grow dense polymer brushes on a wide range of substrates and combine this chemistry with BCP assembly to fabricate nanopatterned polymer brushes. This is the first demonstration of introducing additional functionality into a BCP directing layer and opens up a wide slew of applications from directed self-assembly to biomaterial engineering.

Acknowledgements

While this dissertation represents the culmination of a five year journey through intellectual improvement and research, it was not an adventure taken in isolation. My advisor, my collaborators, my research group, my friends, my family and my girlfriend were all instrumental in aiding me and guiding me through graduate school. Without my advisor, Padma Gopalan, none of these works would have been possible. I would also like to acknowledge my other committee members including Professor Mahesh Mahanthappa, Professor Sandro Mecozzi, Professor David Lynn and Professor Michael Arnold for helpful discussions and comments.

I give special thanks here to Myungwoong Kim, who has been not only a mentor and confidant but also a good friend for the past five years. I pray that we never lose touch as we both move forward in our lives. Myungwoong played a key role in many of these projects and they would have been nigh impossible without his help. I also thank my other group members especially Samantha Schmitt who has always been willing to lend an ear and tell me about her biomaterials problems.

I am thankful to my friends, most of which still live in Lexington, for their constant entertainment and encouragement. I especially thank my parents and my sister, who through their love and prayers have always been a source of strength for me. Finally, I am grateful to my girlfriend, Chuleekorn Chotsuwan, who despite being 8200 miles away in Thailand most of the time, has always been patient and helpful to me during this process.

Thank you all and I wish you all the best.

Contents

Chapter 1. Introduction: Self-Assembly of Block Copolymers and Polymer Brushes

Since the proposal by Hermann Staudinger in the early 1920s on the existence of macromolecules or polymers, the ensuing rise of synthetically derived polymeric materials has undeniably influenced civilization in the past century. From commodity polymers such as polyethylene which comprise a vast array of consumer goods to specialty polymers used in photolithographic processing, these materials all derive their properties from the multitude of repeat units from which they are made. As with most organic (carbon-based) materials, these properties can be tuned to an almost infinite degree through variation of the repeat unit structure. Polymers also display broadly different properties depending on their architecture from linear homopolymers all the way to star copolymers. This ability to tune properties through monomer structure and synthetic technique allows the incorporation of desired functionality into existing systems while preserving the beneficial properties of that system. In this way, it is possible to create a variety of materials for various applications which can aid in solving issues faced in fields as diverse as nanotechnology and cell biology. Some outstanding challenges in the field of nanotechnology consist of scaling down feature sizes for nanolithography to increase transistor count in accord with Moore's Law,[1] which involves both materials design and processing challenges. With that in mind, more detailed background is provided on several of these subjects in the following sections.

1.1. Self-Assembly of Block Copolymers in Bulk and Thin Film

Self-assembly of block copolymer materials (BCPs) in bulk[2] and the subsequent translation of these ordered domains into thin-films[3, 4] has emerged as a powerful method for creating functional nanostructures and templates for various applications. BCPs consist of two or more chemically distinct polymer chains which are covalently linked to each other. In spite of being chemically distinct, they cannot macrophase separate as in a blend of homopolymers and instead self-assemble into dense periodic nanostructures on a typical length scale from 5-50 nm. The self-assembly of the most commonly used diblock copolymers such as poly(styrene-*b*-methyl methacrylate) [P(S-*b*-MMA)],[5-9] poly(styrene-*b*-ethylene oxide) [P(S-*b*-PEO)],[10-14] poly(styrene-*b*-4-vinylpyridine) [P(S-*b*-4VP)][15-19] and poly(styrene-*b*-dimethylsiloxane) [P(S-*b*-DMS)][20-24] is well studied in bulk and to some extent in thin films. The most important parameters that govern the bulk self-assembly or microphase separation are the degree of polymerization (N) of each block, the relative volume fraction ($f_A = 1 - f_B$) and the Flory-Huggins interaction parameter (χ_{AB}). The final morphology results from a compromise between the enthalpic and entropic factors of the two blocks (**Figure 1.1.**).

As the size of the domains scale with $N^{2/3}$, N must be lowered to access smaller domain sizes as desired in nanolithography. However, $\chi_{AB}N$ must be greater than or equal to 10.5 in order to self-assemble which sets a lower limit on N for any given BCP system. Typically χ_{AB} shows both an enthalpic and entropic contribution. The enthalpic contribution is more easily estimated through differences in polarity and can be used for the design of BCPs with a high χ_{AB} and will be discussed in the following sections.

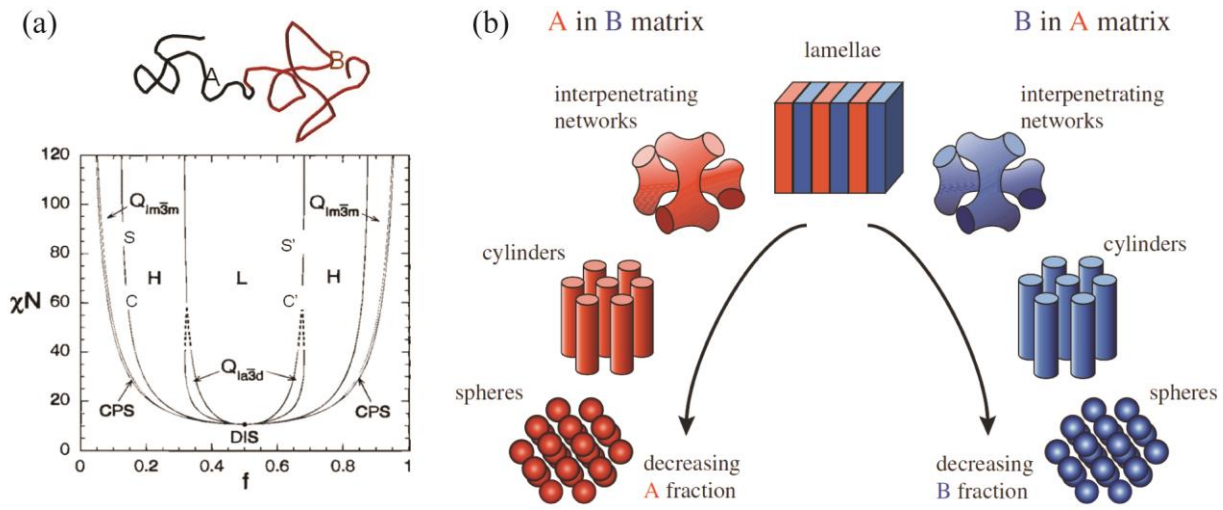

Figure 1.1. (a) Phase diagram of A-*b*-B diblock copolymer showing the transition from disordered (DIS) to ordered nanostructures. Phases are labeled: closed packed spheres (CPS), cylinders (C), hexagonally packed cylinders (H), lamellar (L), Q_{Im3m} (BCC spheres) and Q_{Ia3d} (Bicontinuous cubic).[2] (b) Schematic representation of microstructures formed at varying f_A.[25]

1.1.1. Synthesis of Block Copolymers

BCPs can be synthesized in a variety of different ways including living anionic polymerization, living cationic polymerization, group transfer polymerization, ring-opening metathesis polymerization and controlled radical polymerization (CRP).[26] The most easily applied techniques are the various CRP methods that have been developed such as nitroxide-mediated polymerization (NMP),[27] atom-transfer radical polymerization (ATRP) and its derivatives,[28] and reversible addition-fragmentation chain-transfer (RAFT) polymerization.[29] These CRP methodologies broadly rely on increasing the polymerizing radical lifetime through either a reversibly trapped intermediate or a stabilized radical. Due to the radical-based mechanism, CRP displays a vastly increased monomer scope in comparison to other polymerization mechanisms.[30] Despite the success of CRP in the past 15 years, the resulting BCPs typically display broader dispersity ($Đ = M_w/M_n$) than those derived from living anionic polymerization.[31] Anionic

polymerization also benefits from quantitative conversions enabling facile control over molecular weight and rapid kinetics which simplifies the synthesis of BCPs.[32] As an illustrative example, the synthesis of P(S-*b*-MMA) by three different methods (RAFT, ATRP and anionic) is given in **Figure 1.2**.

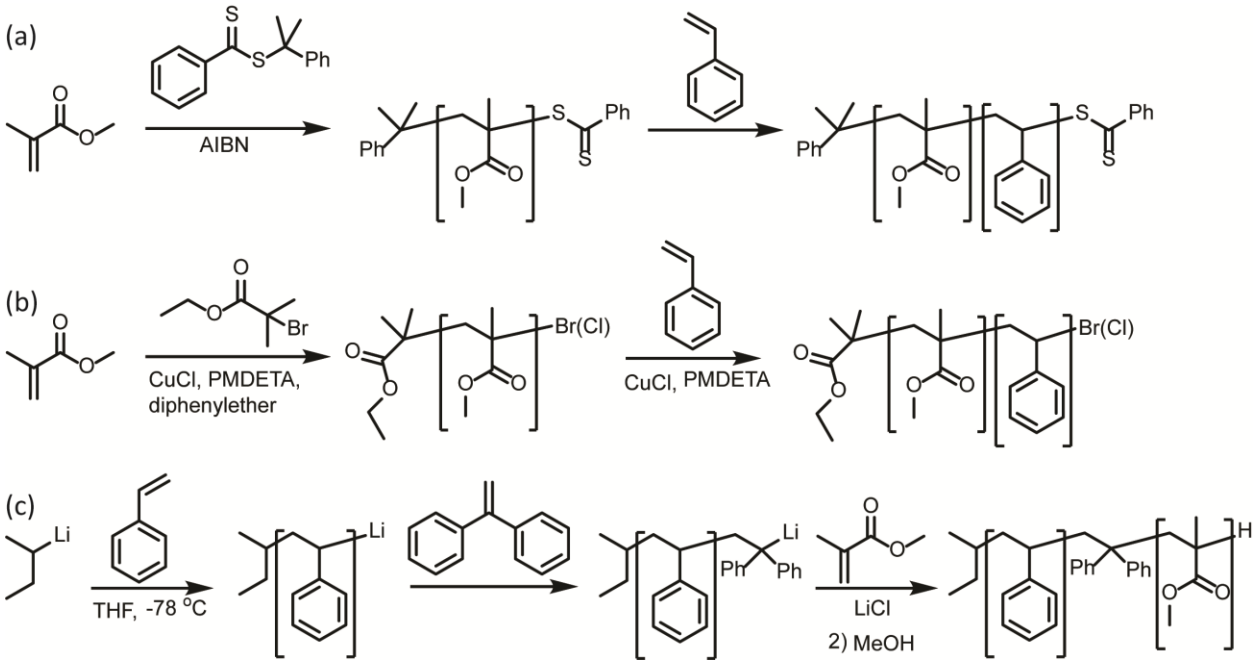

Figure 1.2. Synthetic schemes for the formation of P(S-*b*-MMA) by (a) RAFT, (b) ATRP and (c) living anionic polymerization. Note the reversed order of block formation for the radical methods from anionic polymerization.[6, 33, 34]

While there is currently interest in the community on the use of BCPs with broader dispersity for self-assembly,[35-39] having a BCP with narrow dispersity still has its advantages in using well-established theories in the field to fully understand the thermodynamic factors driving self-assembly. The main drawbacks to anionic polymerization are the stringent conditions necessary during the synthesis (water and oxygen must be rigorously excluded) and the relatively limited monomer scope (e.g. styrenes, dienes, vinylpyridines and methacrylates) due to the need

for carbanion stabilization.[26] Due to the previously mentioned benefits of anionic polymerization, expanding the monomer scope is also a worthwhile endeavor.

Traditional living anionic polymerization was introduced by Szwarc in 1956 using styrene in tetrahydrofuran (THF), initiated by the complex of sodium and naphthalene.[40] Living anionic polymerization has no formal termination step in the mechanism meaning that absent inadvertent or deliberate termination, the chain end anion persists and will react with monomer. In order for the polymerization to proceed in a controlled manner, the rate of initiation should be faster than the rate of propagation so that all chains are started at the same time. The solvent and initiator used affect the relative rates greatly with hydrocarbon solvents generally showing slower rates of initiation and propagation relative to polar solvents such as THF.[41] Polar monomers have generally been an issue for anionic polymerization due to their propensity for side reactions which cause termination of the chain end. While using THF at -78 ^{o}C slows down the rate of most side reactions, it was the introduction of additives and capping agents which allowed the controlled polymerization of polar monomers such as vinylpyridines and methacrylates.[42-44] Lithium chloride has proven invaluable in preventing back-biting reactions during the polymerization of methacrylates and also aids in preventing side reactions during vinylpyridine polymerization. 1,1-diphenylethylene is a sterically hindered alkene which cannot homopolymerize, thus it can be used in excess to quantitatively cap a reactive chain end, generating a bulky anion which prefers conjugate addition rather than direct addition to polar monomers. These techniques have broadened the scope of anionic polymerization considerably beyond the first demonstrations with styrene and dienes.

1.1.2. High χ Block Copolymers

Typically, the product $\chi_{AB}N$ determines if the segregation tendency is weak, intermediate or strong. The strong segregation limit (SSL) is defined as $\chi_{AB}N$ tending to ∞,[45] the intermediate segregation region (ISR) as $10 < \chi_{AB}N < 50$[46] and weak-segregation limit (WSL) as $\chi_{AB}N$ ~10. Well established mean field theories posit that BCPs will not self-assemble below $\chi_{AB}N = 10.5$.[2, 47] If we consider the simplest of these BCPs, namely P(S-*b*-MMA), the magnitude of interaction χ_{AB} between the blocks is low (0.038 at 373 K),[48] hence self-assembly of symmetric compositions with molecular weights less than 28 kg/mol has not been demonstrated by thermal annealing. Oddly, χ_{AB} for P(S-*b*-MMA) shows only a slight dependence on temperature (χ_{AB} = 0.0294 +3.2/T).[48] This behavior is anomalous in many respects due to the large positive entropic contributions to the free energy of mixing. If the second block is changed from PMMA to PEO, PI, P4VP or PDMS, χ_{AB} steadily increases. The increasing unfavorable interaction between the blocks can reduce the self-assembled domain sizes to approximately 5 nm.[10]

For a rough approximation of polarity, solubility parameters can be useful as they have been tabulated for a broad range of homopolymers (**Table 1.1**). In the traditional Flory-Huggins solution theory, there is a direct correlation between χ and the solubility parameter,[49] however this equation only accounts for the enthalpic contributions. For macromolecules, the entropic factors also come into play which can have unanticipated effects on the segregation strength between blocks.[50] Nevertheless, solubility parameters can be used as a rough guide to estimate χ_{AB}. For example, the solubility parameters for polystyrene, poly(dimethylsiloxane) (PDMS) and poly(2-vinylpyridine) (P2VP) are 18.5, 14.9 and 20.6 $(J/cm^3)^{1/2}$, respectively. Compared to P(S-*b*-MMA), both P(S-*b*-DMS) and P(S-*b*-2VP) exhibit much larger χ_{AB}, 0.26 and 0.18, respectively.[23, 51] Further exemplifying this methodology, P(2VP-*b*-DMS) demonstrates an even larger χ_{AB},

estimated at 0.4.[52] Thus, barring unusual enthalpic interactions such as hydrogen bonding, the magnitude of χ_{AB} tracks well with the difference in solubility parameters.

Table 1.1 List of solubility parameters[53, 54] for selected polymers from the literature.

Polymer	**δ (J/cm^3)$^{1/2}$**
poly(*tetra*-fluoroethylene)	12.7
poly(dimethylsiloxane)	14.9
poly(butadiene)	16.2
poly(isoprene)	16.6
poly(styrene)	18.5
poly(ethylene oxide)	20.2
poly(2-vinylpyridine)	20.6
poly(4-hydroxystyrene)	24.55

An important factor to consider during BCP self-assembly is the χ_{AB} between the two blocks which determines both the minimum N necessary for formation of an ordered phase and also the interfacial width according to $\xi \sim 2a/(6\chi)^{1/2}$ which is crucial for achieving a low line-edge roughness.[47, 55] χ_{AB} often takes the expression $\chi(T) = A/T + B$ where A encompasses the enthalpic contribution to the free energy of mixing and B the entropic contribution. As χ_{AB} is inversely related to temperature and a BCP requires a $\chi_{AB}N$ greater than 10.5 to self-assemble, elevated temperatures can cause a BCP to go through the order-to-disorder transition (ODT) which can affect control over the long range order of the domains.[56] A high χ_{AB} offers several advantages in terms of achieving small domain sizes, sharpening the interfacial width of the domains and increasing the distance from the ODT of the BCP.

In order to achieve a high χ_{AB}, some design guidelines can be used to not only achieve small dimensions in bulk and thin-film self-assembly but also engineer in other pre-selected properties. Primarily, the polymer needs to have a high effective interaction parameter in order to reach domain sizes in the sub 5-nm regime. Ideally, the BCP synthesis should be facile, high yielding with controlled molecular weights and dispersity and preferably from commercially available monomers. Scale-up is facilitated if processing of the material can be accomplished using straightforward techniques such as thermal annealing on a hot plate.[57] As small domain sizes generally necessitate thinner films to provide uniform surfaces, a high bulk T_g is useful for maintaining domain integrity. In addition, the degradation temperature should be sufficiently high above the T_g that there is headroom for thermal processing. In order to successfully transfer the pattern from the BCP to the substrate, either intrinsic etch contrast is required or the proper functional groups present in the BCP to increase the etch contrast through seeding techniques. BCPs which have limited intrinsic etch contrast (e.g. P(S-*b*-2VP)) can be seeded with metal ions to yield metallic nanostructures upon plasma treatment either through a solution deposition or a vapor-phase deposition.[58, 59]

1.1.3. Thin-film Self-Assembly

The process of self-assembling a BCP thin film on a substrate and transferring the pattern to the underlying substrate by a subtractive or additive method is known as BCP lithography (**Figure 1.3**).[55, 60, 61] As BCPs self-assemble into dense periodic nanostructures on a length scale between 5 and 50 nm, they are prime candidates to serve as ordered templates for bottom-up patterning as well as growth of nanomaterials. BCP lithography offers both cost and processing advantages over current photolithography. First, BCPs self-assemble into sub 20-nm domain sizes through a thermodynamically driven process, forming densely packed nanostructures which is an

area where photolithography struggles to realize dense line/space or hole patterns.[62, 63] While the semiconductor industry has developed techniques to overcome this limitation (e.g. multiple patterning), introducing extra steps into the patterning process increases cost and lowers the ultimate yield. The second benefit of BCP lithography is that it is a bottom-up self-assembly process without the requirement of expensive photolithography equipment and is inherently scalable due to the nature of the process. Self-assembly can be performed simply by spin-coating the BCP on a Si wafer and heating the substrate on a hot plate, for example. A third benefit of using BCPs for nanolithography is that the interface between the domains is sharp, thus reducing line-edge roughness which increases in importance as the overall feature size decreases, though there is an eventual physical limit to the feature size defined by the interface length.[64] Importantly, BCP lithography is also compatible with currently used semiconductor processing techniques such as spin-coating and baking.[65]

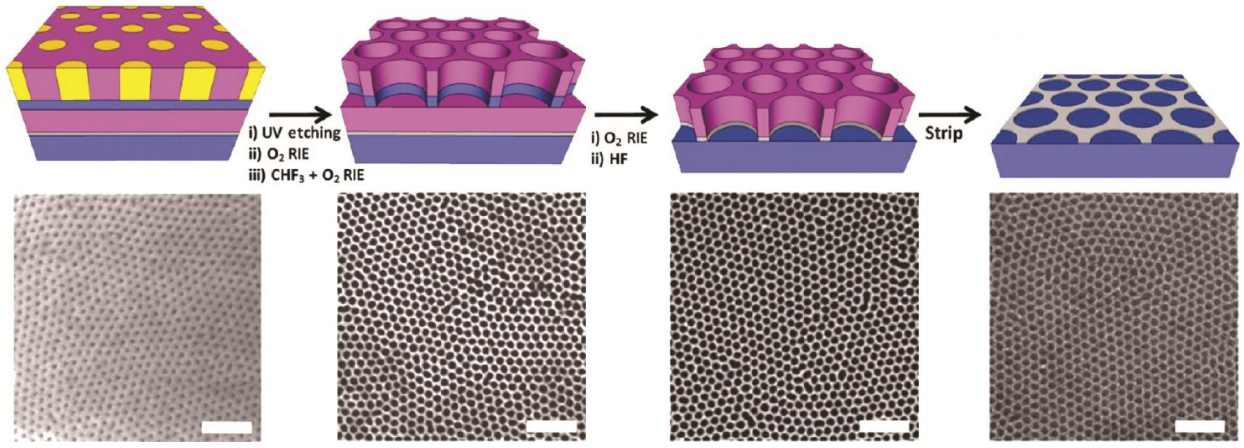

Figure 1.3. Typical process flow for the transfer of the BCP pattern to the underlying substrate through a subtractive process[66] for P(S-*b*-MMA) (scale bars are 200 nm).

1.2. Polymer Brushes

Polymer brushes are coatings which consist of polymer chains tethered to the surface by one chain end.[67] Due to the steric crowding of the polymer chains in close proximity, they adopt a stretched conformation which changes their fundamental properties compared to bulk polymers. Polymer brushes are highly effective at tuning the surface energy of surfaces to which they are attached. The lack of chain entanglement means that the brushes display rapid response to changes in their environment including solvent,[68-71] pH, ion concentration,[72-77] and temperature.[78-83] In addition, polymer brushes have found wide applications in nonbiofouling[84-87] and cell adhesive surfaces.[88-90]

There are two general methods to create polymer brushes, grafting to and grafting from (**Figure 1.4**). Grafting to involves preferential interaction of the polymer or part of the polymer with the surface which is known as physisorption (**Figure 1.4a**).[67] Alternatively, a defined end-group can react with the surface to form a bond which is known as chemisorption (**Figure 1.4b**). Grafting to offers some advantages in that the polymers being grafted can be thoroughly characterized for their molecular weight and composition before attachment and it is experimentally straightforward. However, the technique suffers from slow grafting kinetics, limited chain density and limitations on overall film thickness. As chains graft to the surface, their steric bulk prevents other chains from diffusing to the surface, limiting the ultimate chain density on the surface. The grafting from technique overcomes some of those disadvantages by growing the polymer brushes directly from initiators immobilized on the surface. Grafting from can be accomplished by a variety of different polymerization techniques including anionic,[91, 92] cationic,[93, 94] ring-opening,[95, 96] ring-opening metathesis polymerization[97, 98] and conventional free radical polymerization.[99, 100] However, controlled radical polymerizations have largely become the

workhorse in polymer grafting due to their broad monomer scope, easily tuned polymerization conditions and excellent control over the polymerization. Grafting from allows for control over the rate of brush growth and the thickness of the film.

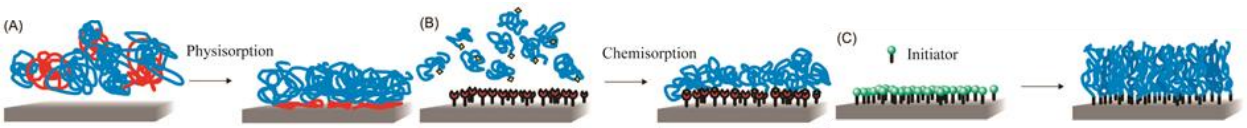

.**Figure 1.4.** Methods of forming polymer brushes by grafting to and grafting from. (a) and (b) demonstrate the two different grafting to methods, while (c) shows the general scheme for grafting from.[67]

Another parameter which is of importance in brush characterization is the chain density or number of polymer chains in a given area. As the distance between grafting points becomes short relative to the polymer radius of gyration (R_g), steric crowding forces the chains to become extended which is what provides some of the unique properties of a brush.[101] Accordingly, the density of initiating sites immobilized on the substrate is important to characterize in order to achieve a brush of high chain density. "High" chain density is also a relative term as each unique polymer will have a different maximum possible chain density. Therefore, a repeat unit with a longer side-chain (e.g. poly(ethylene glycol) monomethyl ether methacrylate) will have a lower maximum chain density than methyl methacrylate and will enter the dense brush regime at lower chain densities.

Surface-initiated atom transfer radical polymerization (SI-ATRP) is a widely used technique for the growth of polymer brushes from substrates due to the wide scope of functionality in the monomer, ease of initiator immobilization on a variety of substrates and experimental conditions that can be tuned.[102] Control in SI-ATRP derives from several factors including the

ratio of Cu^{I} to Cu^{II}, the ligand, the initiating group, the halide and the solvent.[103] The initiator is typically immobilized on the surface using a self-assembled monolayer (SAM) such as alkanethiols for gold surfaces[104] or silyl chlorides[105] for silicon surfaces. SAMs have some drawbacks in their lack of substrate independence necessitating the use of a new system for every new substrate material and typically have limited stability.[67]

1.2.1. Application of Polymer Brushes to Block Copolymer Lithography

A general application of polymer brushes is to create a homogenous energetically non-preferential substrate to control the domain orientation of block copolymers in thin film. Control over the domain orientation is one of the most important criterions for using BCPs in thin film as templates.[106] P(S-*b*-MMA) is the most widely used BCP for lithographic purposes due to the similar surface energy of the domains and the selective removal of the PMMA block by UV-etching. The domain orientation of P(S-*b*-MMA) can be controlled in a variety of ways including electric field,[107] blends of homopolymers or block copolymers,[108] solvent annealing,[109] electro-spray,[110] and chemical modification of the substrate.[5, 111-117] Chemical modification, typically through immobilization of random copolymers of styrene and MMA, has emerged as the primary method for control of the domain orientation for P(S-*b*-MMA) typically in combination with thermal annealing.[113] Following the seminal work by Mansky et al to control the domain orientation of P(S-*b*-MMA) by modifying the substrate to be non-preferential to either block through the grafting of hydroxyl-terminated random copolymers of styrene and methyl methacrylate (**Figure 1.5a**),[5] a number of important advances have emerged. Low molecular weight brushes formed from P(S-*b*-MMA) BCPs were found to be effective at directing the domain orientation for an overlying P(S-*b*-MMA) BCP thin film and they exhibited a different non-preferential window with respect to the fraction of styrene (**Figure 1.5b**).[116] Rather than end-

functionalized polymers, In et al utilized side-chain based hydroxyls for grafting random copolymers[118] and the chemistry was further advanced by the inclusion of photo-patternable acrylate side chains[112] and thermally cross-linkable epoxide side chains.[113] Bates et al demonstrated that the non-preferential layer was not required to contain the same monomers as the block copolymer assembled on it.[119] Interestingly, brushes have also been effective for other block copolymer systems including poly(styrene-*block*-dimethylsiloxane)[20] and poly(styrene-*block*-d,l-lactide) (**Figure 1.5c,d**).[120]

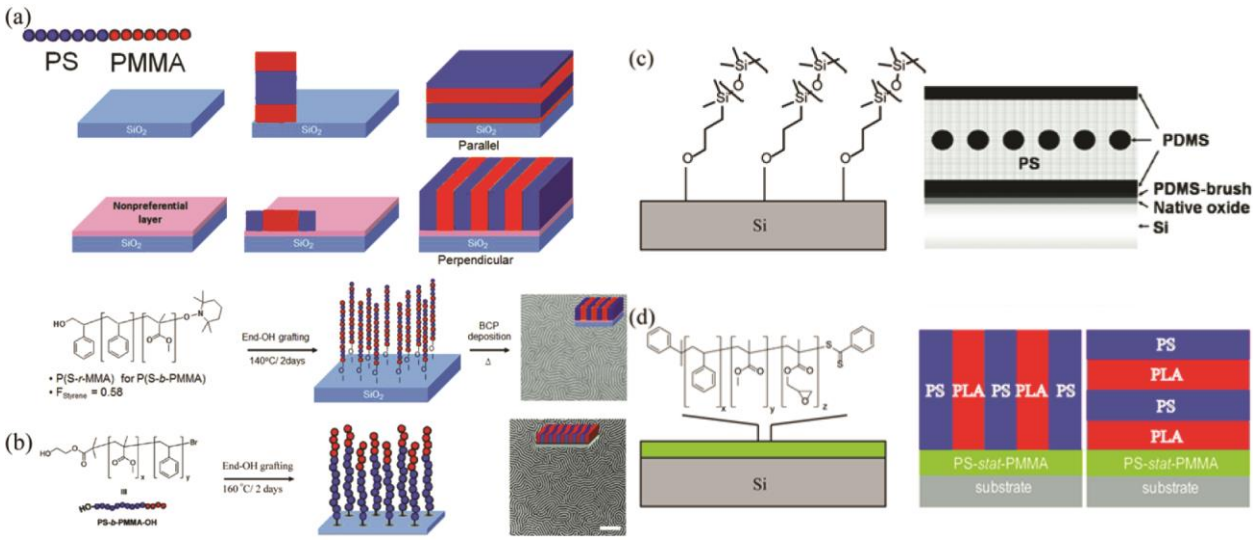

Figure 1.5. Use of polymer brushes or cross-linked films to control BCP domain orientation. (a) P(S-*b*-MMA) domain orientation using a hydroxyl-terminated random copolymer of P(S-*r*-MMA).[5] (b) P(S-*b*-MMA) domain orientation using a hydroxyl-terminated BCP of P(S-*b*-MMA).[116] (c) P(S-*b*-dimethylsiloxane) parallel cylinder orientation through a hydroxyl-terminated poly(dimethylsiloxane) brush.[20] (d) P(S-*b*-d,l-lactide) domain orientation through a cross-linkable random copolymer of P(S-*r*-MMA-*r*-glycidyl methacrylate) with schematic demonstrating perpendicular and parallel orientations of lamellae.[120]

As discussed previously in section 1.1.2, high χ BCPs offer small feature sizes and sharp interfacial boundaries which are necessary in high resolution nanolithography. However, the large difference in polarity between the blocks often extends to a large difference in surface energy as well. Silicon containing blocks such as PDMS and poly(4-trimethylsilylstyrene) have low surface energies and consequently segregate to the free surface readily.[20, 121, 122] Therefore, even if a non-preferential mat is created for these systems on the substrate, the free surface will still be preferential to one block, leading to a parallel orientation or dewetting of the film. One method being investigated to overcome this involves the use of a top-coat which can grant a non-preferential top surface but the design parameters are not clear yet on how to tune the polarity.[123] Increasing attention has been given to non-equilibrium methods (e.g. solvent annealing) rather than thermal annealing due to this inability to readily control the energy of both the substrate and the free surface.[4, 10, 109, 124-126] As the domains continue to decrease in size, another challenge arises in addition to simply ordering the BCP thin film, which is to actually transfer the pattern to the substrate. This is an aspect of BCP lithography which is of active interest to the community and is being explored in different ways: silicon-containing blocks, incorporation of metal ions or metal oxide precursors and cleavable junction points or easily etched blocks.

1.2.2 Patterned Brushes

Brushes can also be patterned on micron and nano-length scales to further applications in analytical sensors, nonbiofouling surfaces and controlled cell adhesion.[127] Brushes can be grown homogeneously on the surface and then patterned via a top-down method such as e-beam lithography[105] or the initiator itself can be patterned before or after deposition (**Figure 1.6**), often involving multiple steps using advanced lithography tools.[128] In an alternative method, von Werne

et al used a photocurable mixture of monomers and inimer to generate nano-sized features on the substrate and then amplified the feature size through SI-ATRP with MMA.[129]

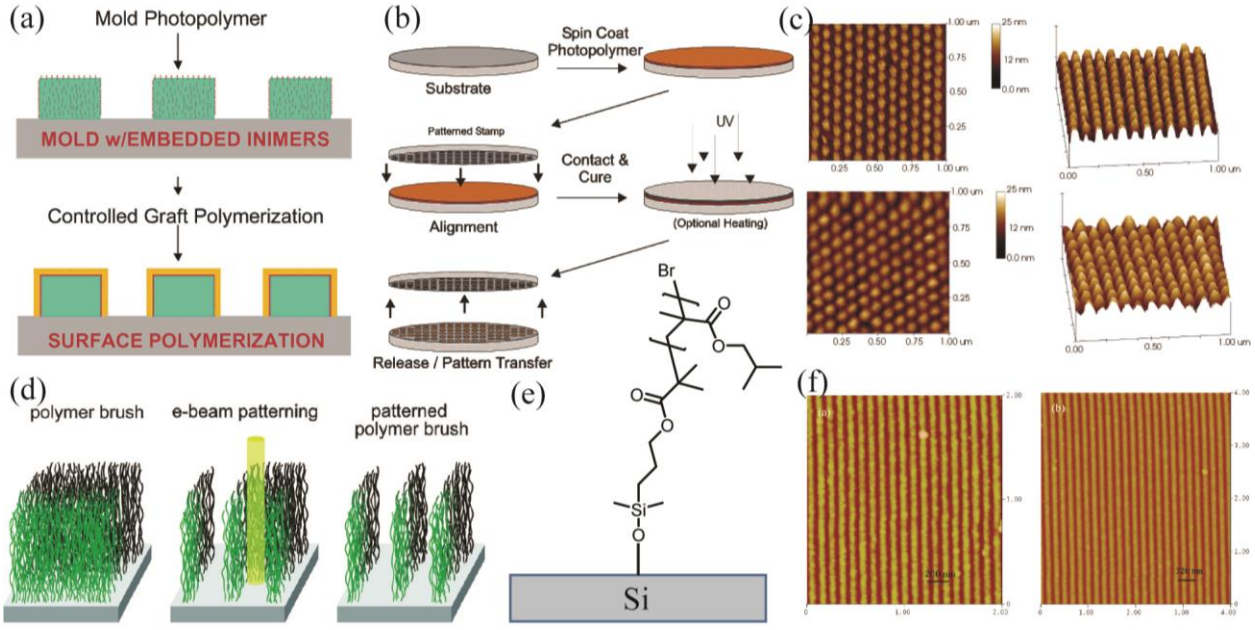

Figure 1.6. (a) Schematic for amplifying feature size through surface-initiated polymerization.[129] (b) Process of forming a nanopattern on the surface by using a photocurable mixture with embedded inimers and imprint lithography (c, top) Shows AFM characterization of the pattern after photocuring, (c,bottom) shows the pattern amplification after SI-ATRP of MMA to increase the feature-size from 60 nm to 75 nm. (c) Schematic depicting the process of patterning a homogeneous polymer brush layer by electron beam lithography.[105] (e) Chemical structure of poly(isobutyl methacrylate) brushes grown from a silyl chloride based initiator. (f) Resulting line and space patterns in poly(isobutyl methacryalate) brushes characterized by AFM at (left) 50 nm lines/100 nm pitch and (right) 80 nm lines/160 nm pitch.

An important application for patterned polymer brushes lies in the field of directed self-assembly (DSA) and specifically the technique known as chemo-epitaxy. This process generates a pattern on the surface with defined geometry and polarity to preferentially interact with one block of a BCP which, under the right conditions, can generate long-range order and reduce defects in the assembled thin film.[64, 130] A typical procedure involves grafting a polymeric brush on the surface (or cross-linking a thin film), applying an electron beam resist such as PMMA and writing a pattern on the resist using E-beam lithography (**Figure 1.7a**). After development, the pattern is exposed to oxygen plasma in order to generate a polar surface in that area and the remaining resist is stripped to reveal the underlying brush. The exposed region can then be backfilled with a non-preferential brush layer to assemble the BCP in a perpendicular fashion. In order to avoid the necessity of using advanced lithography to pattern every substrate, Ji et al developed a technique called molecular transfer printing (MTP) where hydroxyl-functionalized homopolymers are blended into the BCP and through thermal annealing, graft to the surface and transfer the pattern from the assembled BCP (**Figure 1.7c**).

One of the primary challenges remaining in the field of polymer brushes to address is the lack of substrate independence.[127] Being able to use the same chemistry on multiple substrate types would simplify the growth of polymer brushes over large areas on atypical substrates, opening up a slew of new applications. Additionally, polymer brushes which have been patterned on the nano-scale and over large areas at high density would show promise for biomedical applications with the precise locating of cell-adhesive markers and cytophobic background.

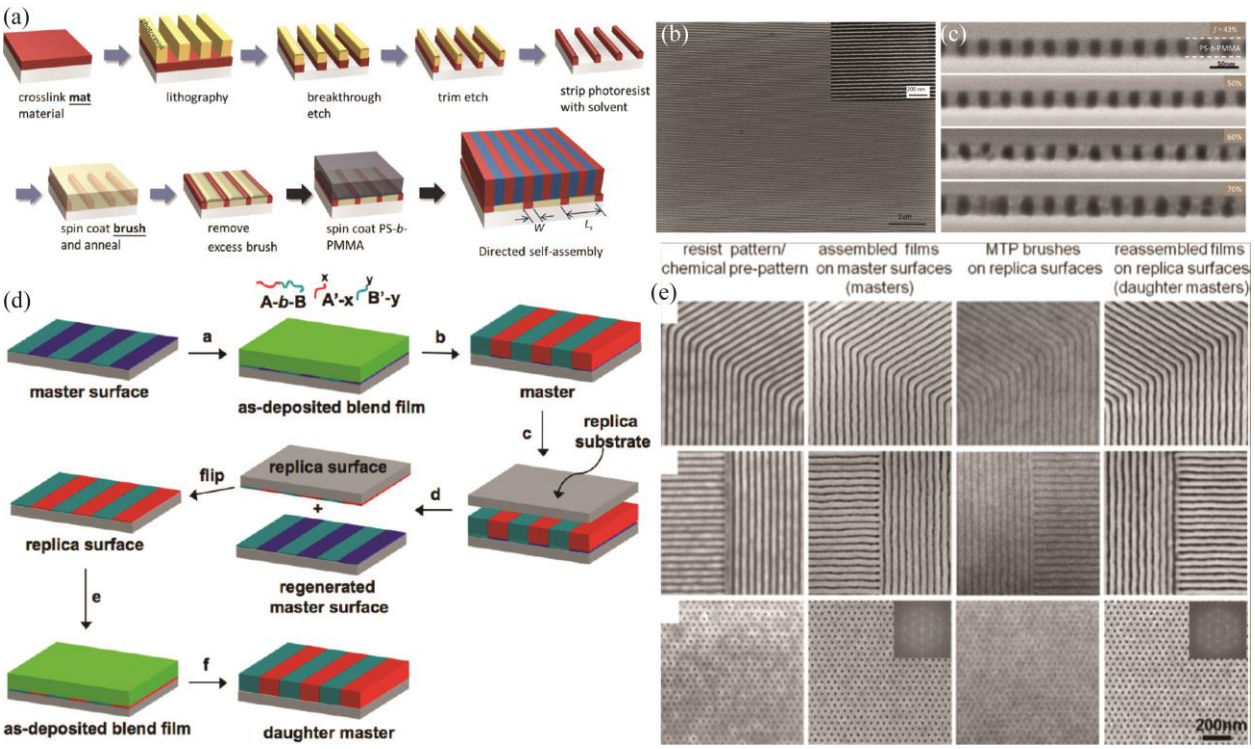

Figure 1.7. (a) Schematic for the creation of a guiding pattern for P(S-*b*-MMA) with density multiplication.[131] (b) SEM image of a lamellar P(S-*b*-MMA) assembled on the pattern showing long range order and registration to the pattern. (c) Cross-sectional SEM images of structures formed after assembly on varying fractions of styrene in the brush. (d) Process flow for MTP where functionalized homopolymers are included in the assembled BCP and designed to react with the substrate, thus transferring the chemical pattern in a 1:1 manner.[132] (e) SEM images demonstrate transfer of the original chemical pattern and DSA of P(S-*b*-MMA) with ability to generate arbitrary shapes.

1.3. Scope of the Dissertation

This dissertation addresses outstanding challenges in the design of appropriate block copolymers to achieve sub 10 nm features in bulk and thin-film, the growth of polymer brushes on atypical substrates and developing methods for their nanopatterning.

In the first half of this dissertation, the synthesis and self-assembly of BCPs predicted to have a high χ parameter between the two blocks is examined through anionic polymerization. The design challenges for high χ BCPs are relatively straightforward in concept; however meeting the criteria necessary for pattern transfer is a more significant challenge. Poly(4-hydroxystyrene) (PHS) is a highly polar polymer with the capability to ligate Lewis acids, significantly increasing its etch resistance but requires a protecting group in order to be polymerized.

In Chapter 2, the synthesis of a monomer, 4-(2-tetrahydropyranyloxy)styrene [OTHPSt], is described which shows excellent control by living anionic polymerization, and allows for deprotection to (PHS) under mild conditions. The versatility of this monomer for living anionic polymerization is aptly demonstrated by the synthesis of four different BCPs, namely P(OTHPSt-*b*-S), P(OTHPSt-*b*-*tert*-butylstyrene), P(OTHPSt-*b*-dimethylsiloxane) and P(OTHPSt-*b*-MAPOSS). After thorough characterization by various techniques, the chemoselective removal of the tetrahydropyranyl group even in the presence of the acid-sensitive siloxane and silsesquioxane blocks was achieved. The mild conditions for deprotection allowed for the first reported synthesis of P(HS-*b*-DMS) and P(HS-*b*-MAPOSS), BCPs which are likely to show high χ parameters and excellent intrinsic etch contrast due to the presence of the silicon-rich block.

Though the OTHPst monomer has been known in the photoresist community since the early 1990's, even basic thermal and chemical characterization of the homopolymers are not documented. The P(OTHPSt) system is further explored in Chapter 3 by the synthesis of a series of P(OTHPSt) homopolymers via living anionic polymerization to quantitatively examine the control over dispersity and molecular weight. For higher molecular weight P(OTHPSt), the T_g plateaus at a value around 125 ^oC and even for a degree of polymerization around 15, the T_g was still remarkably high, allowing facile isolation of the polymer as a powder. To investigate the

reason for this surprising rigidity, the NMR spectrum was analyzed and found that the THP ring has a pronounced effect on the axial vs equatorial preference with the sterically demanding alkoxy phenyl group only being in the axial position. Even for the simplest of the P(HS) BCPs there are no accurate estimates of interaction parameters in the literature. We have quantitatively evaluated the self-assembly of a series of P(HS-*b*-S) BCPs to estimate the effective interaction parameter between the two blocks. Using temperature dependent small angle X-ray scattering (SAXS), a disordered diblock was characterized at elevated temperatures and then modeled to determine χ_{eff} between the blocks. The χ_{eff} demonstrated a remarkably small dependence on temperature and a large entropic contribution. Our studies show that the interaction parameter of this BCP is vastly overestimated in the literature.

While PHS demonstrates remarkable polarity, the high T_g of the PHS block complicates assembly of the BCP. In Chapter 4, the synthesis and detailed characterization of poly(*tert*-butylstyrene-*b*-2-vinylpyridine) [P(tBuSt-*b*-2VP)] is described. This BCP, made from commercially available monomers by living anionic polymerization, shows properties amenable to thermal annealing with a decomposition temperature around 280 ^{o}C and T_g's between 100 and 145 ^{o}C. Symmetric copolymers showed the ability to generate sub 5-nm domains. A series of asymmetric BCPs were also synthesized ranging from PtBuSt spheres to P2VP cylinders. The bulk self-assembly of these BCPs was examined by SAXS and TEM with the smallest cylindrical domains corresponding to a diameter of 5.9 nm. Examining the thin film assembly of the P2VP cylinder forming BCPs yielded parallel arrays of cylinders that were seeded with Pt metal ions and etched to yield arrays of Pt nanowires that were less than 6 nm in diameter. This we believe is an especially promising route to sub 10 nm features.

In Chapters 5, we examine the enabling chemistry for block copolymer lithography, namely the chemistry of surface modifying brushes/mats or copolymers. A single component random copolymer was developed which has an embedded initiator to grow polymer brushes and can be crosslinked into an ultra-thin coating on a range of substrates. This provides a clear advantage over currently used SAMs of initiators which have significant drawbacks in substrate dependence and relatively poor long-term stability. X-ray photoelectron spectroscopy (XPS) was used to characterize the cross-linked surface and determine the absolute concentration of Br (coming from the initiator) in the film. Theoretically, every Br can serve as an initiator for a polymer chain so in order to characterize the initiating efficiency, we quantitatively studied the growth of poly(methyl methacrylate) brushes by surface initiated atom transfer radical polymerization (SI-ATRP). A consistent high chain density was found over the whole time period indicating the control over the polymerization kinetics. We further demonstrated the substrate independence of this system by coating four different surfaces including Si, SiO_2, Au and aluminum oxide. The efficacy of the coating and brush growth on modifying the surface energy was judged by the static water contact angle. This study laid the groundwork for the following system designed with BCP lithography in mind.

The versatility of this chemistry is further exemplified in Chapter 6, where the composition of this initiator embedded coating can be changed on demand to adjust the energetics on the substrate to allow vertical orientation of BCP domains in an overlying film. The dual-functional layer where the cross-linked film serves both as a non-preferential surface for the self-assembly of a P(S-*b*-MMA) BCP and contains embedded initiators for the growth of brushes from the surface. An array of hexagonal PMMA cylinders was generated on the surface and a subtractive process was used to access the initiators on the surface. Through the nanopores, growth of polymer brushes

by SI-ATRP achieved a 15 nm spot size and a dot density (patterned brush domain) of 5×10^{10} cm^{-2}. This is the highest density of patterned brushes by any method reported so far. This is a large area approach, which overcomes many of the limitations of other approaches based on patterning a SAM of initiators by serial top-down lithographic techniques. The chemistry developed through this work on dual functionality lays the groundwork for potentially incorporating a whole range of electronic, biological or optical functionalities in non-preferential layers.

1.3. References

1. Moore, G. E., Cramming More Components onto Integrated Circuits. *Electronics* 1965, pp 114-117.

2. Bates, F. S.; Fredrickson, G. H., Block Copolymer Thermodynamics: Theory and Experiment. *Annu. Rev. Phys. Chem.* **1990,** *41*, 525-557.

3. Park, M.; Harrison, C.; Chaikin, P. M.; Register, R. A.; Adamson, D. H., Block Copolymer Lithography: Periodic Arrays of ~10^{11} Holes in 1 Square Centimeter. *Science* **1997,** *276* (5317), 1401-1404.

4. Tang, C.; Lennon, E. M.; Fredrickson, G. H.; Kramer, E. J.; Hawker, C. J., Evolution of Block Copolymer Lithography to Highly Ordered Square Arrays. *Science* **2008,** *322* (5900), 429-432.

5. Mansky, P.; Liu, Y.; Huang, E.; Russell, T. P.; Hawker, C., Controlling Polymer-Surface Interactions with Random Copolymer Brushes. *Science* **1997,** *275* (5305), 1458-1460.

6. Ham, S.; Shin, C.; Kim, E.; Ryu, D. Y.; Jeong, U.; Russell, T. P.; Hawker, C. J., Microdomain Orientation of PS-b-PMMA by Controlled Interfacial Interactions. *Macromolecules* **2008,** *41* (17), 6431-6437.

7. Russell, T. P.; Coulon, G.; Deline, V. R.; Miller, D. C., Characteristics of the Surface-Induced Orientation for Symmetric Diblock PS/PMMA Copolymers. *Macromolecules* **1989,** *22* (12), 4600-4606.

8. Ryu, D. Y.; Ham, S.; Kim, E.; Jeong, U.; Hawker, C. J.; Russell, T. P., Cylindrical Microdomain Orientation of PS-b-PMMA on the Balanced Interfacial Interactions: Composition Effect of Block Copolymers. *Macromolecules* **2009,** *42* (13), 4902-4906.

9. Stoykovich, M. P.; Kang, H.; Daoulas, K. C.; Liu, G.; Liu, C.-C.; de Pablo, J. J.; Müller, M.; Nealey, P. F., Directed Self-Assembly of Block Copolymers for Nanolithography: Fabrication of Isolated Features and Essential Integrated Circuit Geometries. *ACS Nano* **2007,** *1* (3), 168-175.

10. Park, S.; Lee, D. H.; Xu, J.; Kim, B.; Hong, S. W.; Jeong, U.; Xu, T.; Russell, T. P., Macroscopic 10-Terabit–per–Square-Inch Arrays from Block Copolymers with Lateral Order. *Science* **2009,** *323* (5917), 1030-1033.

11. Mao, H.; Hillmyer, M. A., Nanoporous Polystyrene by Chemical Etching of Poly(ethylene oxide) from Ordered Block Copolymers. *Macromolecules* **2005,** *38* (9), 4038-4039.

12. Mao, H.; Hillmyer, M. A., Macroscopic Samples of Polystyrene with Ordered Three-Dimensional Nanochannels. *Soft Matter* **2006,** *2* (1), 57-59.

13. Neto, C.; James, M.; Telford, A. M., On the Composition of the Top Layer of Microphase Separated Thin PS-PEO Films. *Macromolecules* **2009,** *42* (13), 4801-4808.

14. Tran-Ba, K.-H.; Finley, J. J.; Higgins, D. A.; Ito, T., Single-Molecule Tracking Studies of Millimeter-Scale Cylindrical Domain Alignment in Polystyrene–Poly(ethylene oxide) Diblock Copolymer Films Induced by Solvent Vapor Penetration. *J. Phys. Chem. Lett.* **2012,** *3* (15), 1968-1973.

15. Park, S.; Kim, B.; Wang, J. Y.; Russell, T. P., Fabrication of Highly Ordered Silicon Oxide Dots and Stripes from Block Copolymer Thin Films. *Adv. Mater.* **2008,** *20*, 681-685.

16. Park, S.; Wang, J.-Y.; Kim, B.; Xu, J.; Russell, T. P., A Simple Route to Highly Oriented and Ordered Nanoporous Block Copolymer Templates. *ACS Nano* **2008,** *2* (4), 766-772.

17. Peinemann, K.-V.; Abetz, V.; Simon, P. F. W., Asymmetric Superstructure Formed in a Block Copolymer via Phase Separation. *Nat. Mater.* **2007,** *6* (12), 992-996.

18. Sohn, B.-H.; Yoo, S.-I.; Seo, B.-W.; Yun, S.-H.; Park, S.-M., Nanopatterns by Free-Standing Monolayer Films of Diblock Copolymer Micelles with in Situ Core−Corona Inversion. *J. Am. Chem. Soc.* **2001,** *123* (50), 12734-12735.

19. Liang, C.; Hong, K.; Guiochon, G. A.; Mays, J. W.; Dai, S., Synthesis of a Large-Scale Highly Ordered Porous Carbon Film by Self-Assembly of Block Copolymers. *Angew. Chem. Int. Ed.* **2004,** *43* (43), 5785-5789.

20. Jung, Y. S.; Ross, C. A., Orientation-Controlled Self-Assembled Nanolithography Using a Polystyrene−Polydimethylsiloxane Block Copolymer. *Nano Lett.* **2007,** *7*, 2046-2050.

21. Jung, Y. S.; Ross, C. A., Solvent-Vapor-Induced Tunability of Self-Assembled Block Copolymer Patterns. *Adv. Mater.* **2009,** *21* (24), 2540-2545.

22. Lo, T.-Y.; Chao, C.-C.; Ho, R.-M.; Georgopanos, P.; Avgeropoulos, A.; Thomas, E. L., Phase Transitions of Polystyrene-b-poly(dimethylsiloxane) in Solvents of Varying Selectivity. *Macromolecules* **2013,** *46* (18), 7513-7524.

23. Jung, Y. S.; Jung, W.; Tuller, H. L.; Ross, C. A., Nanowire Conductive Polymer Gas Sensor Patterned Using Self-Assembled Block Copolymer Lithography. *Nano Lett.* **2008,** *8* (11), 3776-3780.

24. Ndoni, S.; Vigild, M. E.; Berg, R. H., Nanoporous Materials with Spherical and Gyroid Cavities Created by Quantitative Etching of Polydimethylsiloxane in Polystyrene−Polydimethylsiloxane Block Copolymers. *J. Am. Chem. Soc.* **2003,** *125* (44), 13366-13367.

25. Grason, G. M., The packing of Soft Materials: Molecular Asymmetry, Geometric Frustration and Optimal Lattices in Block Copolymer Melts. *Phys. Rep.* **2006,** *433* (1), 1-64.

26. Hadjichristidis, N.; Pispas, S.; Floudas, G. A., *Block Copolymers: Synthetic Strategies, Physical Properties, and Applications*. John Wiley & Sons, Inc.: New Jersey, 2003.

27. Quinn, J. D.; Register, R. A., Microphase Separation in Block-Random Copolymers of Styrene, 4-Acetoxystyrene, and 4-Hydroxystyrene. *J. Polym. Sci. Part B: Polym. Phys.* **2009,** *47*, 2106-2113.

28. Chen, X. Y.; Jankova, K.; Kops, J.; Batsberg, W., Hydrolysis of 4-acetoxystyrene Polymers Prepared by Atom Transfer Radical Polymerization. *J. Polym. Sci. Part A: Polym. Chem.* **1999,** *37* (5), 627-633.

29. Kanagasabapathy, S.; Sudalai, A.; Benicewicz, B. C., Reversible Addition-Fragmentation Chain-Transfer Polymerization for the Synthesis of Poly(4-acetoxystyrene) and Poly(4-acetoxystyrene)-block-polystyrene by Bulk, Solution and Emulsion Techniques. *Macromol. Rapid Commun.* **2001,** *22*, 1076-1080.

30. Matyjaszewski, K.; Tsarevsky, N. V., Macromolecular Engineering by Atom Transfer Radical Polymerization. *J. Am. Chem. Soc.* **2014,** *136* (18), 6513-6533.

31. Baskaran, D.; Müller, A. H. E., Anionic Vinyl Polymerization—50 years After Michael Szwarc. *Prog. Polym. Sci.* **2007,** *32* (2), 173-219.

32. Hirao, A.; Goseki, R.; Ishizone, T., Advances in Living Anionic Polymerization: From Functional Monomers, Polymerization Systems, to Macromolecular Architectures. *Macromolecules* **2014,** *47* (6), 1883-1905.

33. Chong, Y. K.; Le, T. P. T.; Moad, G.; Rizzardo, E.; Thang, S. H., A More Versatile Route to Block Copolymers and Other Polymers of Complex Architecture by Living Radical Polymerization: The RAFT Process. *Macromolecules* **1999,** *32* (6), 2071-2074.

34. Erdogan, T.; Unveren, E. E.; Inan, T. Y.; Birkan, B., Well-defined Block Copolymer Ionomers and Their Blend Membranes for Proton Exchange Membrane Fuel Cell. *J. Membr. Sci.* **2009,** *344* (1–2), 172-181.

35. Lynd, N. A.; Hillmyer, M. A., Influence of Polydispersity on the Self-Assembly of Diblock Copolymers. *Macromolecules* **2005,** *38* (21), 8803-8810.

36. Lynd, N. A.; Meuler, A. J.; Hillmyer, M. A., Polydispersity and Block Copolymer Self-Assembly. *Prog. Polym. Sci.* **2008,** *33*, 875-893.

37. Widin, J. M.; Schmitt, A. K.; Schmitt, A. L.; Im, K.; Mahanthappa, M. K., Unexpected Consequences of Block Polydispersity on the Self-Assembly of ABA Triblock Copolymers. *J. Am. Chem. Soc.* **2012,** *134* (8), 3834-3844.

38. Widin, J. M.; Kim, M.; Schmitt, A. K.; Han, E.; Gopalan, P.; Mahanthappa, M. K., Bulk and Thin Film Morphological Behavior of Broad Dispersity Poly(styrene-b-methyl methacrylate) Diblock Copolymers. *Macromolecules* **2013,** *46* (11), 4472-4480.

39. Schmitt, A. K.; Mahanthappa, M. K., Characteristics of Lamellar Mesophases in Strongly Segregated Broad Dispersity ABA Triblock Copolymers. *Macromolecules* **2014,** *47* (13), 4346-4356.

40. Szwarc, M., 'Living' Polymers. *Nature* **1956,** *178*, 1168-1169.

41. Geacintov, C.; Smid, J.; Szwarc, M., Kinetics of Anionic Polymerization of Styrene in Tetrahydrofuran. *J. Am. Chem. Soc.* **1962,** *84*, 2508-2514.

42. Varshney, S. K.; Hautekeer, J. P.; Fayt, R.; Jérôme, R.; Teyssié, P., Anionic polymerization of (meth)acrylic Monomers. 4. Effect of Lithium Salts as Ligands on the "Living" Polymerization of Methyl Methacrylate Using Monofunctional Initiators. *Macromolecules* **1990,** *23*, 2618-2622.

43. Varshney, S. K.; Zhong, X. F.; Eisenberg, A., Anionic Homopolymerization and Block Copolymerization of 4-vinylpyridine and its Investigation by High-Temperature Size-Exclusion Chromatography in N-methyl-2-pyrrolidinone. *Macromolecules* **1993,** *26*, 701-706.

44. Tsitsilianis, C.; Voulgaris, D., Poly(2-vinylpyridine)-based Star-Shaped Polymers. Synthesis of Teteroarm Star (A_nB_n) and Star-Block $(AB)_n$ Copolymers. *Macromol. Chem. Phys.* **1997,** *198* (4), 997-1007.

45. Semenov, A. N., Theory of Block-Copolymer Interfaces in the Strong Segregation Limit. *Macromolecules* **1993,** *26*, 6617-6621.

46. Matsen, M. W.; Bates, F. S., Unifying Weak- and Strong-Segregation Block Copolymer Theories. *Macromolecules* **1996,** *29* (4), 1091-1098.

47. Tseng, Y.-C.; Darling, S. B., Block Copolymers Nanostructures for Technology. *Polymers* **2010,** *2*, 470-489.

48. Russell, T. P.; Hjelm, R. P.; Seeger, P. A., Temperature Dependence of the Interaction Parameter of Polystyrene and Poly(Methyl Methacrylate). *Macromolecules* **1990,** *23*, 890-893.

49. Rubinstein, M.; Colby, R. H., *Polymer physics*. Oxford University Press: New York, 2003.

50. Bates, F. S.; Hillmyer, M. A.; Lodge, T. P.; Bates, C. M.; Delaney, K. T.; Fredrickson, G. H., Multiblock Polymers: Panacea or Pandora's Box? *Science* **2012,** *336* (6080), 434-440.

51. Dai, K. H.; Kramer, E. J., Determining the temperature-dependent Flory interaction parameter for strongly immiscible polymers from block copolymer segregation measurements. *Polymer* **1994,** *35*, 157-161.

52. Jeong, J. W.; Park, W. I.; Kim, M.-J.; Ross, C. A.; Jung, Y. S., Highly Tunable Self-Assembled Nanostructures from a Poly(2-vinylpyridine-b-dimethylsiloxane) Block Copolymer. *Nano Lett.* **2011,** *11*, 4095-4101.

53. Zeng, W.; Du, Y.; Xue, Y.; Frisch, H. L., *Physical Properties of Polymers Handbook*. 2nd ed.; Springer Science: 2007.

54. Brandrup, J.; Immergut, E. H.; Grulke, E. A., *Polymer Handbook*. 4th ed.; Wiley-Interscience: New York, 1999.

55. Black, C. T.; Ruiz, R.; Breyta, G.; Cheng, J. Y.; Colburn, M. E.; Guarini, K. W.; Kim, H.-C.; Zhang, Y., Polymer Self Assembly in Semiconductor Microelectronics. *IBM J. Res. Dev.* **2007,** *51*, 605-633.

56. Mishra, V.; Fredrickson, G. H.; Kramer, E. J., Effect of Film Thickness and Domain Spacing on Defect Densities in Directed Self-Assembly of Cylindrical Morphology Block Copolymers. *ACS Nano* **2012,** *6* (3), 2629-2641.

57. Rincon-Delgadillo, P.; Craig, G.; Gronheid, R.; Nealey, P. F., Scale-up of a Chemo-Epitaxy Flow for Feature Multiplication Using Directed Self- Assembly of Block-Copolymers. *J. Photopolym. Sci. Technol.* **2013,** *26*, 831-839.

58. Chai, J.; Buriak, J. M., Using Cylindrical Domains of Block Copolymers To Self-Assemble and Align Metallic Nanowires. *ACS Nano* **2008,** *2*, 489-501.

59. Wang, Y.; Qin, Y.; Berger, A.; Yau, E.; He, C.; Zhang, L.; Gösele, U.; Knez, M.; Steinhart, M., Nanoscopic Morphologies in Block Copolymer Nanorods as Templates for Atomic-Layer Deposition of Semiconductors. *Adv. Mater.* **2009,** *21*, 2763-2766.

60. Kim, H.-C.; Park, S.-M.; Hinsberg, W. D., Block Copolymer Based Nanostructures: Materials, Processes, and Applications to Electronics. *Chem. Rev.* **2010,** *110* (1), 146-177.

61. Baruth, A.; Rodwogin, M. D.; Shankar, A.; Erickson, M. J.; Hillmyer, M. A.; Leighton, C., Non-lift-off Block Copolymer Lithography of 25 nm Magnetic Nanodot Arrays. *ACS Appl. Mater. Interfaces* **2011,** *3* (9), 3472-3481.

62. Seino, Y.; Yonemitsu, H.; Sato, H.; Kanno, M.; Kato, H.; Kobayashi, K.; Kawanishi, A.; Azuma, T.; Muramatsu, M.; Nagahara, S., Contact Hole Shrink Process Using Directed Self-Assembly. *Proc. of SPIE* **2012,** *8323*, 83230Y.

63. Yi, H.; X.-Y.;, B.; Zhang, J.; Bencher, C.; Chang, L.-W.; Chen, X.; Tiberio, R.; Conway, J.; Dai, H.; Chen, Y., Flexible Control of Block Copolymer Directed Self-Assembly using Small, Topographical Templates: Potential Lithography Solution for Integrated Circuit Contact Hole Patterning. *Adv. Mater.* **2012,** *24*, 3107-3114.

64. Ruiz, R.; Kang, H.; Detcheverry, F. A.; Dobisz, E.; Kercher, D. S.; Albrecht, T. R.; de Pablo, J. J.; Nealey, P. F., Density Multiplication and Improved Lithography by Directed Block Copolymer Assembly. *Science* **2008,** *321*, 936-939.

65. Khaira, G. S.; Qin, J.; Garner, G. P.; Xiong, S.; Wan, L.; Ruiz, R.; Jaeger, H. M.; Nealey, P. F.; de Pablo, J. J., Evolutionary Optimization of Directed Self-Assembly of Triblock Copolymers on Chemically Patterned Substrates. *ACS Macro Lett.* **2014**, 747-752.

66. Kim, M.; Safron, N. S.; Han, E.; Arnold, M. S.; Gopalan, P., Electronic Transport and Raman Scattering in Size-Controlled Nanoperforated Graphene. *ACS Nano* **2012,** *6* (11), 9846-9854.

67. Barbey, R.; Lavanant, L.; Paripovic, D.; Schüwer, N.; Sugnaux, C.; Tugulu, S.; Klok, H.-A., Polymer Brushes via Surface-Initiated Controlled Radical Polymerization: Synthesis, Characterization, Properties, and Applications. *Chem. Rev.* **2009,** *109* (11), 5437-5527.

68. Chen, J.-K.; Hsieh, C.-Y.; Huang, C.-F.; Li, P. M.; Kuo, S.-W.; Chang, F.-C., Using Solvent Immersion to Fabricate Variably Patterned Poly(methyl methacrylate) Brushes on Silicon Surfaces. *Macromolecules* **2008,** *41* (22), 8729-8736.

69. Wolkenhauer, M.; Bumbu, G.-G.; Cheng, Y.; Roth, S. V.; Gutmann, J. S., Investigation of Micromechanical Cantilever Sensors with Microfocus Grazing Incidence Small-Angle X-Ray Scattering. *Appl. Phys. Lett.* **2006,** *89* (5), 054101.

70. Bumbu, G.-G.; Wolkenhauer, M.; Kircher, G.; Gutmann, J. S.; Berger, R., Micromechanical Cantilever Technique: A Tool for Investigating the Swelling of Polymer Brushes. *Langmuir* **2007,** *23* (4), 2203-2207.

71. Granville, A. M.; Boyes, S. G.; Akgun, B.; Foster, M. D.; Brittain, W. J., Synthesis and Characterization of Stimuli-Responsive Semifluorinated Polymer Brushes Prepared by Atom Transfer Radical Polymerization. *Macromolecules* **2004,** *37* (8), 2790-2796.

72. Wu, T.; Gong, P.; Szleifer, I.; Vlček, P.; Šubr, V.; Genzer, J., Behavior of Surface-Anchored Poly(acrylic acid) Brushes with Grafting Density Gradients on Solid Substrates: 1. Experiment. *Macromolecules* **2007,** *40* (24), 8756-8764.

73. Ayres, N.; Boyes, S. G.; Brittain, W. J., Stimuli-Responsive Polyelectrolyte Polymer Brushes Prepared via Atom-Transfer Radical Polymerization. *Langmuir* **2006,** *23* (1), 182-189.

74. Treat, N. D.; Ayres, N.; Boyes, S. G.; Brittain, W. J., A Facile Route to Poly(acrylic acid) Brushes Using Atom Transfer Radical Polymerization. *Macromolecules* **2005,** *39* (1), 26-29.

75. Moya, S. E.; Azzaroni, O.; Kelby, T.; Donath, E.; Huck, W. T. S., Explanation for the Apparent Absence of Collapse of Polyelectrolyte Brushes in the Presence of Bulky Ions. *J. Phys. Chem. B* **2007,** *111* (25), 7034-7040.

76. Sanjuan, S.; Perrin, P.; Pantoustier, N.; Tran, Y., Synthesis and Swelling Behavior of pH-Responsive Polybase Brushes. *Langmuir* **2007,** *23* (10), 5769-5778.

77. Moya, S.; Azzaroni, O.; Farhan, T.; Osborne, V. L.; Huck, W. T. S., Locking and Unlocking of Polyelectrolyte Brushes: Toward the Fabrication of Chemically Controlled Nanoactuators. *Angew. Chem. Int. Ed.* **2005,** *44* (29), 4578-4581.

78. Matsuda, T.; Ohya, S., Photoiniferter-Based Thermoresponsive Graft Architecture with Albumin Covalently Fixed at Growing Graft Chain End. *Langmuir* **2005,** *21* (21), 9660-9665.

79. Xu, F. J.; Zhong, S. P.; Yung, L. Y. L.; Tong, Y. W.; Kang, E.-T.; Neoh, K. G., Thermoresponsive Comb-Shaped Copolymer-Si(1 0 0) Hybrids for Accelerated Temperature-Dependent Cell Detachment. *Biomaterials* **2006,** *27* (8), 1236-1245.

80. Mizutani, A.; Kikuchi, A.; Yamato, M.; Kanazawa, H.; Okano, T., Preparation of Thermoresponsive Polymer Brush Surfaces and Their Interaction with Cells. *Biomaterials* **2008,** *29* (13), 2073-2081.

81. Schild, H. G., Poly(N-isopropylacrylamide): Experiment, Theory and Application. *Prog. Polym. Sci.* **1992,** *17* (2), 163-249.

82. Sun, T.; Wang, G.; Feng, L.; Liu, B.; Ma, Y.; Jiang, L.; Zhu, D., Reversible Switching between Superhydrophilicity and Superhydrophobicity. *Angew. Chem. Int. Ed.* **2004,** *43* (3), 357-360.

83. Schulz, D. N.; Peiffer, D. G.; Agarwal, P. K.; Larabee, J.; Kaladas, J. J.; Soni, L.; Handwerker, B.; Garner, R. T., Phase Behaviour and Solution Properties of Sulphobetaine Polymers. *Polymer* **1986,** *27* (11), 1734-1742.

84. Talarico, T.; Swank, A.; Privalle, C., Autoxidation of Pyridoxalated Hemoglobin Polyoxyethylene Conjugate. *Biochem. Biophys. Res. Commun.* **1998,** *250* (2), 354-358.

85. de las Heras Alarcon, C.; Farhan, T.; Osborne, V. L.; Huck, W. T. S.; Alexander, C., Bioadhesion at Micro-Patterned Stimuli-Responsive Polymer Brushes. *J. Mater. Chem.* **2005,** *15* (21), 2089-2094.

86. Xu, F. J.; Zhong, S. P.; Yung, L. Y. L.; Kang, E. T.; Neoh, K. G., Surface-Active and Stimuli-Responsive Polymer−Si(100) Hybrids from Surface-Initiated Atom Transfer Radical Polymerization for Control of Cell Adhesion. *Biomacromolecules* **2004,** *5* (6), 2392-2403.

87. Herold, D. A.; Keil, K.; Bruns, D. E., Oxidation of Polyethylene Glycols by Alcohol Dehydrogenase. *Biochem. Pharm.* **1989,** *38* (1), 73-76.

88. Mei, Y.; Wu, T.; Xu, C.; Langenbach, K. J.; Elliott, J. T.; Vogt, B. D.; Beers, K. L.; Amis, E. J.; Washburn, N. R., Tuning Cell Adhesion on Gradient Poly(2-hydroxyethyl methacrylate)-Grafted Surfaces. *Langmuir* **2005,** *21* (26), 12309-12314.

89. Bhat, R. R.; Chaney, B. N.; Rowley, J.; Liebmann-Vinson, A.; Genzer, J., Tailoring Cell Adhesion Using Surface-Grafted Polymer Gradient Assemblies. *Adv. Mater.* **2005,** *17* (23), 2802-2807.

90. Singh, N.; Cui, X.; Boland, T.; Husson, S. M., The Role of Independently Variable Grafting Density and Layer Thickness of Polymer Nanolayers on Peptide Adsorption and Cell Adhesion. *Biomaterials* **2007,** *28* (5), 763-771.

91. Jordan, R.; Ulman, A.; Kang, J. F.; Rafailovich, M. H.; Sokolov, J., Surface-Initiated Anionic Polymerization of Styrene by Means of Self-Assembled Monolayers. *J. Am. Chem. Soc.* **1999,** *121* (5), 1016-1022.

92. Advincula, R.; Zhou, Q.; Park, M.; Wang, S.; Mays, J.; Sakellariou, G.; Pispas, S.; Hadjichristidis, N., Polymer Brushes by Living Anionic Surface Initiated Polymerization on Flat Silicon (SiO_x) and Gold Surfaces: Homopolymers and Block Copolymers. *Langmuir* **2002,** *18* (22), 8672-8684.

93. Jordan, R.; Ulman, A., Surface Initiated Living Cationic Polymerization of 2-Oxazolines. *J. Am. Chem. Soc.* **1998,** *120* (2), 243-247.

94. Zhao, B.; Brittain, W. J., Synthesis of Tethered Polystyrene-block-Poly(methyl methacrylate) Monolayer on a Silicate Substrate by Sequential Carbocationic Polymerization and Atom Transfer Radical Polymerization. *J. Am. Chem. Soc.* **1999,** *121* (14), 3557-3558.

95. Choi, I. S.; Langer, R., Surface-Initiated Polymerization of l-Lactide: Coating of Solid Substrates with a Biodegradable Polymer. *Macromolecules* **2001,** *34* (16), 5361-5363.

96. Wang, Y.; Chang, Y.-C., Grafting of Homo- and Block Co-polypeptides on Solid Substrates by an Improved Surface-Initiated Vapor Deposition Polymerization. *Langmuir* **2002,** *18* (25), 9859-9866.

97. Harada, Y.; Girolami, G. S.; Nuzzo, R. G., Catalytic Amplification of Patterning via Surface-Confined Ring-Opening Metathesis Polymerization on Mixed Primer Layers Formed by Contact Printing. *Langmuir* **2003,** *19* (12), 5104-5114.

98. Kong, B.; Lee, J. K.; Choi, I. S., Surface-Initiated, Ring-Opening Metathesis Polymerization: Formation of Diblock Copolymer Brushes and Solvent-Dependent Morphological Changes. *Langmuir* **2007,** *23* (12), 6761-6765.

99. Biesalski, M.; Rühe, J., Preparation and Characterization of a Polyelectrolyte Monolayer Covalently Attached to a Planar Solid Surface. *Macromolecules* **1999,** *32* (7), 2309-2316.

100. Huang, W.; Skanth; Baker, G. L.; Bruening, M. L., Surface-Initiated Thermal Radical Polymerization on Gold. *Langmuir* **2001,** *17* (5), 1731-1736.

101. Halperin, A.; Tirrell, M.; Lodge, T. P., Tethered Chains in Polymer Microstructures. In *Macromolecules: Synthesis, Order and Advanced Properties*, Springer Berlin Heidelberg: 1992; Vol. 100/1, pp 31-71.

102. Edmondson, S.; Osborne, V. L.; Huck, W. T. S., Polymer Brushes *via* Surface-Initiated Polyermizations. *Chem. Soc. Rev.* **2004,** *33*, 14-22.

103. Matyjaszewski, K.; Xia, J. H., Atom Transfer Radical Polymerization. *Chem. Rev.* **2001,** *101*, 2921-2990.

104. Kaholek, M.; Lee, W.-K.; Ahn, S.-J.; Ma, H.; Caster, K. C.; LaMattina, B.; Zauscher, S., Stimulus-Responsive Poly(N-isopropylacrylamide) Brushes and Nanopatterns Prepared by Surface-Initiated Polymerization. *Chem. Mater.* **2004,** *16* (19), 3688-3696.

105. Rastogi, A.; Paik, M. Y.; Tanaka, M.; Ober, C. K., Direct Patterning of Intrinsically Electron Beam Sensitive Polymer Brushes. *ACS Nano* **2010,** *4* (2), 771-780.

106. Stoykovich, M. P.; Nealey, P. F., Block Copolymers and Conventional Lithography. *Mater. Today* **2006,** *9* (9), 20-29.

107. Morkved, T. L.; Lu, M.; Urbas, A. M.; Ehrichs, E. E.; Jaeger, H. M.; Mansky, P.; Russell, T. P., Local Control of Microdomain Orientation in Diblock Copolymer Thin Films with Electric Fields. *Science 273* (5277), 931-933.

108. Kitano, H.; Akasaka, S.; Inoue, T.; Chen, F.; Takenaka, M.; Hasegawa, H.; Yoshida, H.; Nagano, H., Control of the Microdomain Orientation in Block Copolymer Thin Films with Homopolymers for Lithographic Application. *Langmuir* **2007,** *23* (11), 6404-6410.

109. Xuan, Y.; Peng, J.; Cui, L.; Wang, H.; Li, B.; Han, Y., Morphology Development of Ultrathin Symmetric Diblock Copolymer Film via Solvent Vapor Treatment. *Macromolecules* **2004,** *37* (19), 7301-7307.

110. Hu, H.; Rangou, S.; Kim, M.; Gopalan, P.; Filiz, V.; Avgeropoulos, A.; Osuji, C. O., Continuous Equilibrated Growth of Ordered Block Copolymer Thin Films by Electrospray Deposition. *ACS Nano* **2013,** *7* (4), 2960-2970.

111. Ryu, D. Y.; Shin, K.; Drockenmuller, E.; Hawker, C. J.; Russell, T. P., A Generalized Approach to the Modification of Solid Surfaces. *Science* **2005,** *308*, 236-239.

112. Han, E.; In, I.; Park, S.-M.; La, Y.-H.; Wang, Y.; Nealey, P. F.; Gopalan, P., Photopatternable Imaging Layers for Controlling Block Copolymer Microdomain Orientation. *Adv. Mater.* **2007,** *19*, 4448-4452.

113. Han, E.; Stuen, K. O.; La, Y.-H.; Nealey, P. F.; Gopalan, P., Effect of Composition of Substrate-Modifying Random Copolymers on the Orientation of Symmetric and Asymmetric Diblock Copolymer Domains. *Macromolecules* **2008,** *41*, 9090-9097.

114. Han, E.; Stuen, K. O.; Leolukman, M.; Li, C.-C.; Nealey, P. F.; Gopalan, P., Perpendicular Orientation of Domains in Cylinder-Forming Block Copolymer Thick Films by Controlled Interfacial Interactions. *Macromolecules* **2009,** *42*, 4896-4901.

115. Han, E.; Gopalan, P., Cross-Linked Random Copolymer Mats As Ultrathin Nonpreferential Layers for Block Copolymer Self-Assembly. *Langmuir* **2010,** *26*, 1311-1315.

116. Han, E.; Leolukman, M.; Kim, M.; Gopalan, P., Resist Free Patterning of Nonpreferential Buffer Layers for Block Copolymer Lithography. *ACS Nano* **2010,** *4*, 6527-6534.

117. Bates, C. M.; Strahan, J. R.; Santos, L. J.; Mueller, B. K.; Bamgbade, B. O.; Lee, J. A.; Katzenstein, J. M.; Ellison, C. J.; Willson, C. G., Polymeric Cross-Linked Surface Treatments for Controlling Block Copolymer Orientation in Thin Films. *Langmuir* **2011,** *27*, 2000-2006.

118. In, I.; La, Y.-H.; Park, S.-M.; Nealey, P. F.; Gopalan, P., Side-Chain-Grafted Random Copolymer Brushes as Neutral Surfaces for Controlling the Orientation of Block Copolymer Microdomains in Thin Films. *Langmuir* **2006,** *22* (18), 7855-7860.

119. Bates, C. M.; Strahan, J. R.; Santos, L. J.; Mueller, B. K.; Bamgbade, B. O.; Lee, J. A.; Katzenstein, J. M.; Ellison, C. J.; Willson, C. G., Polymeric Cross-Linked Surface Treatments for Controlling Block Copolymer Orientation in Thin Films. *Langmuir* **2011,** *27* (5), 2000-2006.

120. Keen, I.; Yu, A.; Cheng, H.-H.; Jack, K. S.; Nicholson, T. M.; Whittaker, A. K.; Blakey, I., Control of the Orientation of Symmetric Poly(styrene)-block-poly(d,l-lactide) Block Copolymers Using Statistical Copolymers of Dissimilar Composition. *Langmuir* **2012,** *28* (45), 15876-15888.

121. Cushen, J. D.; Bates, C. M.; Rausch, E. L.; Dean, L. M.; Zhou, S. X.; Willson, C. G.; Ellison, C. J., Thin Film Self-Assembly of Poly(trimethylsilylstyrene-b-d,l-lactide) with Sub-10 nm Domains. *Macromolecules* **2012,** *45*, 8722-8728.

122. Pitet, L. M.; Wuister, S. F.; Peeters, E.; Kramer, E. J.; Hawker, C. J.; Meijer, E. W., Well-Organized Dense Arrays of Nanodomains in Thin Films of Poly(dimethylsiloxane)-b-poly(lactide) Diblock Copolymers. *Macromolecules* **2013,** *46*, 8289-8295.

123. Bates, C. M.; Seshimo, T.; Maher, M. J.; Durand, W. J.; Cushen, J. D.; Dean, L. M.; Blachut, G.; Ellison, C. J.; Willson, C. G., Polarity-Switching Top Coats Enable Orientation of Sub–10-nm Block Copolymer Domains. *Science* **2012,** *338* (6108), 775-779.

124. Kim, S. H.; Misner, M. J.; Xu, T.; Kimura, M.; Russell, T. P., Highly Oriented and Ordered Arrays from Block Copolymers via Solvent Evaporation. *Adv. Mater.* **2004,** *16* (3), 226-231.

125. Li, M.; Douki, K.; Goto, K.; Li, X.; Coenjarts, C.; Smilgies, D. M.; Ober, C. K., Spatially Controlled Fabrication of Nanoporous Block Copolymers. *Chem. Mater.* **2004,** *16* (20), 3800-3808.

126. Bosworth, J. K.; Black, C. T.; Ober, C. K., Selective Area Control of Self-Assembled Pattern Architecture Using a Lithographically Patternable Block Copolymer. *ACS Nano* **2009,** *3* (7), 1761-1766.

127. Chen, T.; Amin, I.; Jordan, R., Patterned Polymer Brushes. *Chem. Soc. Rev.* **2012,** *41*, 3280-3296.

128. Steenackers, M.; Lud, S. Q.; Niedermeier, M.; Bruno, P.; Gruen, D. M.; Feulner, P.; Stutzmann, M.; Garrido, J. A.; Jordan, R., Structured Polymer Grafts on Diamond. *J. Am. Chem. Soc.* **2007,** *129* (50), 15655-15661.

129. von Werne, T. A.; Germack, D. S.; Hagberg, E. C.; Sheares, V. V.; Hawker, C. J.; Carter, K. R., A Versatile Method for Tuning the Chemistry and Size of Nanoscopic Features by Living Free Radical Polymerization. *J. Am. Chem. Soc.* **2003,** *125*, 3831-3838.

130. Segalman, R. A., Directing Self-Assembly Toward Perfection. *Science* **2008,** *321* (5891), 919-920.

131. Liu, C.-C.; Ramírez-Hernández, A.; Han, E.; Craig, G. S. W.; Tada, Y.; Yoshida, H.; Kang, H.; Ji, S.; Gopalan, P.; de Pablo, J. J.; Nealey, P. F., Chemical Patterns for Directed Self-Assembly

of Lamellae-Forming Block Copolymers with Density Multiplication of Features. *Macromolecules* **2013,** *46* (4), 1415-1424.

132. Ji, S.; Liu, C.-C.; Liu, G.; Nealey, P. F., Molecular Transfer Printing Using Block Copolymers. *ACS Nano* **2009,** *4* (2), 599-609.

Chapter 2. Synthesis of Poly(4-hydroxystyrene)-based Block Copolymers Containing Acid-Sensitive Blocks by Living Anionic Polymerization

The contents of this chapter have been published in *J. Polym. Sci. Part A: Polym. Chem.* **2014**, *52*, 1458-1468. Authors are: Sweat, Daniel. P.; Yu, Xiang; Kim, Myungwoong; Gopalan, Padma.

Author contributions: Daniel did the synthesis and characterization of the OTHP monomer, developed anionic polymerization, synthesis of the PS diblocks, developed deprotection conditions and characterized all diblocks. Xiang Yu synthesized the MAPOSS, PDMS and PtBS diblocks and developed deprotection conditions for the PDMS and MAPOSS diblocks. Myungwoong participated in the design of experiments and data interpretation. All authors contributed towards writing the manuscript.

2.1. Abstract

Living anionic polymerization of an acetal protected 4-hydroxystyrene monomer, (4-(2-tetrahydropyranyloxy)styrene) (OTHPSt), and the chain extension of the poly(OTHPSt) anion with a variety of monomers including styrene, 4-*tert*-butylstyrene, methacryloyl polyhedral oligomeric silsesquioxane (MAPOSS) and hexamethylcyclotrisiloxane is demonstrated. The P(OTHPSt) homopolymer has a glass transition temperature well above room temperature which facilitates handling and purification of the protected poly(4-hydroxystyrene) (PHS). The resulting diblock copolymers have narrow dispersities <1.05. Chemoselective mild deprotection conditions for the P(OTHPSt) block were identified to prevent simultaneous degradation of the MAPOSS or

dimethylsiloxane (DMS) block, thus allowing for the first reported synthesis of P(HS-*b*-DMS) and P(HS-*b*-MAPOSS).

2.2. Introduction

Block copolymers (BCPs) have attracted considerable scientific interest due to their ability to spontaneously self-assemble into a variety of dense, periodic nanostructures with a typical length scale of 5-50 nm.[1-5] In the last two decades, advances in controlled radical polymerization have provided for an ever-widening degree of functionalities to be incorporated into BCPs;[6] however, living anionic polymerization does provide a high degree of control over polymer structure, near quantitative conversions and rapid kinetics.[7] Although anionic polymerization is a powerful technique, one of its major limitations is the strongly basic environment resulting from the carbanions present in solution, which necessitates the use of only certain classes of monomers and protecting groups.[8] For carbanionic propagating species, the monomer scope is generally limited to dienes, styrenes, vinylpyridines and (meth)acrylates as these groups are able to stabilize the carbanion through resonance delocalization.[9] Various substituents can be placed on the monomer (e.g. 4-*tert*-butylstyrene) to change the polymer properties as long as they remain compatible with the basic environment.

Of the numerous substituted polystyrenes commonly encountered, poly(4-hydroxystyrene) (PHS) is a highly polar (Hildebrand solubility parameter 24.55 $(J/cm^3)^{1/2}$) derivative of polystyrene (PS) which has been used more commonly as a chemically amplified resist.[10, 11] In addition to conferring solubility in basic aqueous solutions, the phenol group is amenable to a wide array of transformations, thus opening up a facile pathway for post-functionalization. Due to the acidic phenol proton, 4-hydroxystyrene itself is not stable to most polymerization conditions, therefore a variety of protected derivatives such as 4-acetoxystyrene (AcOS), and 4-*tert*-butoxystyrene

(tBuOS) have been developed. AcOS is the preferred monomer for controlled radical polymerization and has been used with all three major techniques (nitroxide-mediated polymerization, atom transfer radical polymerization and reversible addition fragmentation chain transfer polymerization).[12-14] The acetoxy group is however not stable to anionic polymerization, hence tBuOS and 4-*tert*-butyldimethylsiloxystyrene are commonly employed protected monomers for synthesis of PHS containing polymers by anionic polymerization.[15-18] These protecting groups while stable during the anionic polymerization, also require relatively drastic post synthesis deprotection conditions, such as refluxing with 5% HCl in 1,4-dioxane or reaction with tetrabutylammonium fluoride which limits the options for added functionalities in the second block of the BCP.

In small molecule chemistry, acetals are well-known protecting groups for alcohols due to the facile protection chemistry as well as removal under mild conditions.[19] Of the acetal protected styrenic monomers, recently Natalello et al.[20] reported the anionic polymerization of 4-(1-ethoxy ethoxy)styrene using THF at -90 ^{o}C. This first report on the use of an acetal protected hydroxystyrene to create functional BCPs through an anionic route resulted in fairly well-controlled BCPs, although the dispersity at lower molecular weights was relatively broad (1.09 at 3.1 kDa). They successfully demonstrated chain extension using 2-vinylpyridine (2VP) to generate P(HS-*b*-2VP) BCPs after rapid deprotection at room temperature with HCl. The BCPs were subsequently used to grow poly(ethylene oxide) from the hydroxystyrene block for use as pH-sensitive surfactants. This method offers a new anionic route through acetal protected monomers for functional BCPs and subsequent functionalization of PHS. The resulting 4-(1-ethoxy ethoxy)styrene polymer has a glass transition temperature (T_g) below room temperature, making isolation of the product after polymerization cumbersome.

Another acetal protecting group is the 2-tetrahydropyranyl (THP) ether, which is stable to a wide variety of bases and nucleophiles and is removed easily under a variety of conditions. THP-protected 4-hydroxystyrene, [4-(2-tetrahydropyranyloxy)styrene] (OTHPSt), has been used as a chemically amplified resist since the early 90s where the polymer P(OTHPSt) was synthesized by free radical polymerization.[21] P(OTHPSt) exhibits a T_g of 110 ^oC and good thermal stability up to 280 ^oC.[21] Remarkably, to date, there are no published studies in the literature on the details of anionic polymerization of this monomer to synthesize BCPs. We believe that OTHPSt monomer is an ideal protected 4-hydroxystyrene derivative for anionic polymerization due to the relatively high T_g of the polymer combined with the mild deprotection conditions afforded by the acetal protecting groups.

In this article, we describe a THP-protected derivative of 4-hydroxystyrene (OTHPSt), that is, stable to living anionic polymerization in THF at -78 ^oC and demonstrate chain extension to form a variety of different BCPs. The deprotection conditions for P(OTHPSt) can be tuned such that even acid-sensitive Si-O-Si linkages in dimethylsiloxane (DMS) and methacryloyl polyhedral oligomeric silsesquioxane (MAPOSS) were stable, thus allowing for the first reported synthesis of P(HS-*b*-DMS) and P(HS-*b*-MAPOSS). We examine the reactivity of the P(OTHPSt) anion to show efficient crossover to a variety of monomers. All of the BCPs exhibited excellent control by anionic polymerization with dispersities of 1.02-1.05 as measured by gel permeation chromatography (GPC). Due to the well-controlled anionic polymerization and ease of polymer purification and deprotection, OTHPSt is an excellent monomer for the preparation of PHS containing monodispersed polymers, thus allowing the synthesis of BCPs previously not possible by sequential living anionic polymerization.

2.3. Experimental Section

Materials. All reagents were purchased from Aldrich Chemical Co. and used as received unless otherwise stated. Polymerizations were performed under argon atmosphere or by using home-built high-vacuum break seal glassware.[22] Tetrahydrofuran (THF) was dried over sodium/benzophenone ketyl and freshly distilled before use. Benzene was stirred over H_2SO_4 for 1 week then separated, washed with aq. NaOH, dried over Na_2SO_4 and distilled from CaH_2. 1 mL of styrene and a small amount of *n*-butyllithium were added and stirred overnight to generate poly(styryl)lithium which was used as an indicator in the benzene solution, yielding a red color while dry. 4-(2-tetrahydropyranyloxy)styrene (OTHPSt) was prepared according to a modified literature procedure.[21] Styrene (St) and 4-*tert*-butylstyrene (tBuSt) were distilled first from CaH_2 under vacuum and then di-*n*-butylmagnesium and stored at -20 ^oC. 1,1-diphenylethylene (DPE) was distilled from *n*-butyllithium under vacuum and stored in ampoules after diluting with THF. 3-(3,5,7,9,11,13,15-Heptaisobutylpentacyclo-[9.5.1.3,915,1517,13]octasiloxan-1-yl)propyl methacrylate (MAPOSS) was purchased from Hybrid Plastics and recrystallized from methanol (MeOH) and dried in a vacuum oven at 60 ^oC for 24 h then dissolved in THF at 1.0 M concentration and stored in ampoules at -20 ^oC. Hexamethylcyclotrisiloxane (D_3) was stirred over CaH_2 at 50 ^oC overnight then distilled under vacuum. D_3 was then added to a solution of poly(styryl)lithium in benzene and stirred for 2 hours. The D_3 solution in benzene was distilled into ampoules under vacuum and stored at -20 ^oC. Lithium chloride (LiCl) was heated at 110 ^oC for 48 hours, dissolved into THF at 0.5 M concentration then degassed and sealed under vacuum. MeOH was degassed under vacuum. s*ec*-Butyllithium (*s*-BuLi, 1.4 M in cyclohexane) was diluted with hexanes to approximately 0.2 M and stored in ampoules under vacuum at -20 ^oC. The solution was calibrated by polymerization of a known volume of styrene in benzene overnight and determination of the

molecular weight by gel permeation chromatography (GPC). Pyridine was stirred over CaH_2 overnight before distillation into ampoules with chlorotrimethylsilane resulting in a pyridine/ chlorotrimethysilane solution (2/1 v/v).

4-(2-tetrahydropyranyloxy)benzaldehyde. To a suspension of 4-hydroxybenzaldehyde (61.1 g, 0.5 mol) in 750 mL dichloromethane was added 3,4-2*H*-dihydropyran (58.9 g, 0.7 mol) and pyridinium *p*-toluenesulfonate (0.67 g, 2.7 mmol). The reaction was stirred under nitrogen at room temperature and monitored by thin layer chromatography ($CHCl_3$ eluent) until complete conversion, approximately 1 h. The reaction was quenched with a saturated solution of sodium carbonate and allowed to stir for 10 min. The layers were separated and the organic layer washed with aq. sodium carbonate twice and water once. The organic layer was dried over sodium sulfate and solvent removed by rotary evaporation. The resulting crude oil was used without further purification. Typical yield, 98 g, 95%. ^{1}H NMR (400 MHz, $CDCl_3$) δ 9.89 (s, 1H), 7.87 – 7.78 (m, 2H), 7.20 – 7.12 (m, 2H), 5.54 (t, J = 3.1 Hz, 1H), 3.85 (ddd, J = 11.3, 9.9, 3.1 Hz, 1H), 3.63 (dtd, J = 11.4, 4.0, 1.4 Hz, 1H), 2.10 – 1.92 (m, 1H), 1.89 (ddd, J = 7.6, 4.9, 3.2 Hz, 2H), 1.81 – 1.53 (m, 3H).

4-(2-tetrahydropyranyloxy)styrene (OTHPSt). 4-(2-tetrahydropyranyloxy)benzaldehyde (93 g, 0.45 mol) was dissolved in 1200 mL of THF and methyltriphenylphosphonium bromide (250 g, 0.7 mol) was added with vigorous stirring under nitrogen. The flask was cooled via an external ice bath and a solution of potassium *tert*-butoxide (100 g, 0.89 mol) in 300 mL THF was added dropwise over 30 minutes. After the addition was complete, the reaction was stirred overnight at room temperature. The reaction was then filtered over celite to remove various salts and the filtrate was concentrated to approximately 500 mL. This suspension was then poured into 1500 mL hexanes with vigorous stirring and the suspension

filtered over celite. Concentration, precipitation and filtration steps were repeated once more. Solvent was removed by rotary evaporation and the orange residue was distilled under high vacuum (b.p. ~110-120 ^{o}C (oil bath temperature), approx. 1 torr) to yield a colorless oil (60 g, 65% yield). For anionic polymerization, OTHPSt was distilled further from CaH_2 and then NaH under high vacuum and sealed into ampoules after diluting with THF to approximately 50% v/v. ^{1}H NMR (300 MHz, $CDCl_3$) δ 7.37 – 7.31 (m, 2H), 7.04 – 6.96 (m, 2H), 6.65 (dd, J = 17.6, 10.8 Hz, 1H), 5.60 (dd, J = 17.6, 1.0 Hz, 1H), 5.41 (t, J = 3.3 Hz, 1H), 5.12 (dd, J = 10.9, 1.0 Hz, 1H), 3.89 (ddd, J = 11.3, 9.3, 3.2 Hz, 1H), 3.59 (dtd, J = 11.4, 4.1, 1.6 Hz, 1H), 2.22 – 1.46 (m, 6H). ^{13}C NMR (75 MHz, $CDCl_3$) δ 157.07, 136.53, 131.50, 127.51, 116.70, 112.04, 96.54, 62.22, 30.57, 25.45, 19.00.

Anionic Polymerization of OTHPSt and Chain Extension with St (Example Procedure for St-1). A flame-dried round bottom flask with PTFE stopcock was cooled under argon. 40 mL of THF was transferred to the flask by syringe and cooled to -78 ^{o}C. *s*-BuLi was added until a yellow color persisted in solution and was used to wash the sides of the flask. The THF solution was warmed to room temperature until the color disappeared. After cooling the solution to -78 ^{o}C again, 0.11 mL *s*-BuLi (1.4 M) was added to the flask. 4 mL of 50% v/v OTHPSt (~10 mmol) was then added to the initiator solution and an orange color immediately appeared. The polymerization was stirred for 30 minutes before an aliquot was taken by syringe and quickly quenched in degassed MeOH. 3 mL (32 mmol) St was then added rapidly to the flask with no apparent color change. The polymerization was stirred for an additional 30 minutes before being quenched by degassed MeOH. The polymerization was slowly poured into 400 mL of MeOH to precipitate the P(OTHPSt-*b*-St) BCP. The polymer was recovered by vacuum filtration as a white powder. The resulting powder was dried under vacuum at room temperature (4.9 g, 95% yield).

^{1}H NMR (300 MHz, $CDCl_3$) δ 7.2 – 6.1 (Ar-H), 5.4 - 5.2 (C-H), 4 – 3.8 (C-H), 3.65 – 3.5 (C-H), 2.3 – 1.1 (C-H_2 and backbone).

Anionic Polymerization of OTHPSt and Chain Extension with tBuSt (Example Procedure for tBuSt-1). A reactor was made with ampoules containing 4 mL 50% v/v OTHPSt solution (~10 mmol), 1.8 mL (10 mmol) tBuSt, 0.8 mL *s*-BuLi (0.2 M) and 2 mL MeOH sealed by break-seals. The reactor was pumped down to high vacuum and flame dried. THF was cryo-transferred into the reactor using liquid nitrogen (~50-75 mL). After finishing the THF transfer, the reactor was sealed from the vacuum line using a torch and the THF melted at -78 ^{o}C. Once the THF melted, *s*-BuLi was introduced to the solution before adding the ampoule of OTHPSt. An orange color immediately developed and the reaction was stirred for 30 min. Then, an aliquot was taken from the flask and sealed behind a stopcock for analysis by GPC. tBuSt was then added to the solution which developed a red color immediately, then quickly faded back to orange and was stirred for 30 min. MeOH was used to terminate the polymerization and the THF solution was slowly poured into MeOH to precipitate the P(OTHPSt-*b*-tBuSt) BCP and the resulting white powder was recovered by vacuum filtration. The powder was dried under vacuum at room temperature (3.8 g, 98% yield). ^{1}H NMR (300 MHz, THF-d_8) δ 7.2 – 6.1 (Ar-H), 5.4 - 5.2 (C-H), 3.95 – 3.75 (C-H), 3.6 – 3.4 (C-H), 2.2 – 1.1 (C-H_2, backbone and tBu).

Chain Extension with D_3 (Example Procedure for DMS-2). A reactor was made with ampoules containing 4 mL 50% v/v OTHPSt solution (~10 mmol), 1.4 mL *s*-BuLi (0.2 M), 3.6 mL 40% w/v D_3/benzene solution (~ 6.6 mmol D_3) and 2 mL pyridine/ 1 mL chlorotrimethylsilane. The procedure in the previous section was followed to generate the P(OTHPSt) anion. An aliquot of P(OTHPSt) anion was taken for GPC analysis and the solution of D_3 in benzene was then added to the P(OTHPSt) anion solution and the orange/red color of the OTHPSt anion slowly

disappeared. The flask was warmed to 25 °C and stirred for 2 h to reach approximately 50% conversion.[23] The polymerization was terminated by adding the solution of chlorotrimethylsilane and pyridine 1/2 v/v. The resulting solution was poured slowly into MeOH to precipitate the P(OTHPSt-*b*-DMS) BCP and the resulting white powder was recovered by vacuum filtration and dried at room temperature under vacuum (2.5 g, 75% yield). ^{1}H NMR (500 MHz, THF-d_8) δ 6.95 – 6.2 (Ar-H), 5.4 - 5.2 (C-H), 4 – 3.85 (C-H), 3.65 – 3.5 (C-H), 2.2 – 1.1 (C-H_2 and backbone), 0.08 (s, C-H_3). ^{29}Si NMR (100 MHz, THF-d_8) δ -22.0 (s).

Chain Extension with MAPOSS (Example Procedure for MAPOSS-1). A reactor was made with ampoules containing 4 mL 50% v/v OTHPSt solution (~10 mmol), 2.4 mL *s*-BuLi (0.48 mmol, 0.2 M), DPE (0.45 g, 2.5 mmol), LiCl solution (5 mL, 2.5 mmol), MAPOSS solution (1.7 mL, ~1.7 mmol) and 5 mL MeOH. After achieving high vacuum in the reactor and transfer/melting of THF at -78 °C, the LiCl solution was added to the flask, then *s*-BuLi. OTHPSt was then added to the flask and stirred for 30 min. At this point, DPE was added to the flask which immediately generated a dark red color. The reaction was stirred for 10 min and then an aliquot was removed from the flask and sealed behind a stopcock. The solution of MAPOSS in THF was then added rapidly to the polymerization and the solution immediately became colorless. The solution was further stirred for 1 h and then quenched by the addition of degassed MeOH. The solution was then poured slowly into MeOH to precipitate the P(OTHPSt-*b*-MAPOSS) BCP and the resulting white powder was recovered by vacuum filtration and dried at room temperature under vacuum (3.2 g, 95% yield). ^{1}H NMR (500 MHz, THF-d_8) δ 7.3 – 6.1 (Ar-H), 5.45 - 5.2 (C-H), 4 – 3.75 (C-H), 3.6 – 3.4 (C-H), 2.2 – 1.15 (CH_2 and backbone), 1.1 – 0.9 (C-H_3 + C-H), 0.75 – 0.55 (C-H_2). ^{29}Si NMR (100 MHz, THF-d_8) δ -67.6 (s), -67.9 (s).

Deprotection of P(OTHPSt-*b*-St) or P(OTHPSt-*b*-tBuSt). 1.0 g of BCP was dissolved in 50 mL THF and then an additional 50 mL of EtOH was added. It was not necessary to maintain a clear solution for deprotection purposes. At this point, 0.1 mL of concentrated aq. HCl (12 M) was added and the solution stirred overnight (cloudy solutions turned clear rapidly after addition of acid). After ^{1}H-NMR spectroscopy confirmed complete deprotection, the solution was poured into water and then the powder was collected by filtration which was dried at room temperature under vacuum (yield = quantitative). ^{1}H NMR (**P(HS-*b*-St)**, 400 MHz, THF-d_8) δ 7.95 – 7.65 (O-H), 7.2 – 6.2 (Ar-H), 2.3 – 1.1 (backbone). ^{1}H NMR (**P(HS-*b*-tBuSt)**, 300 MHz, THF-d_8) δ 7.95 – 7.65 (O-H), 7.25 – 6.1 (Ar-H), 2.3 – 1.0 (backbone and tBu)

Deprotection of P(OTHPSt-*b*-DMS) or P(OTHPSt-*b*-MAPOSS). 1.0 g of BCP was dissolved in 50 mL THF and then 50 mL of ethanol was added. More THF was added if the solution became cloudy. 5 mL conc. aq. HCl was diluted to 50 mL with water. Approximately 0.06 mL dilute HCl solution was added to the polymer solution and then stirred until ^{1}H-NMR spectroscopy confirmed complete deprotection. Note that extended reaction time or higher acid concentration led to Si-O-Si degradation for both siloxane and silsesquioxane. After deprotection was complete, the solution was poured into water for precipitation followed by collecting the powder by vacuum filtration and drying at room temperature under vacuum (yield = quantitative). ^{1}H NMR (**P(HS-*b*-DMS)**, 500 MHz, THF-d_8) δ 8.15 – 7.8 (O-H), 6.8 – 6.2 (Ar-H), 2.2 – 1.1 (backbone), 0.08 (s, C-H_3). ^{29}Si NMR (100 MHz, THF-d_8) δ -22.0 (s). ^{1}H NMR (**P(HS-*b*-MAPOSS)**, 500 MHz, THF-d_8) δ 8.0 – 7.65 (O-H), 7.2 – 6.9 (Ar-H, DPE), 6.75 – 6.15 (Ar-H, PHS), 2.2 – 1.2 (backbone), 1.1 – 0.9 (C-H_3 + C-H), 0.75 – 0.55 (C-H_2). ^{29}Si NMR (100 MHz, THF-d_8) δ –67.6 (s), -67.9 (s).

Characterization. ^{1}H NMR, ^{13}C NMR and ^{29}Si spectra were recorded in $CDCl_3$ or THF-d_8 using a Bruker Avance-400, Varian MercuryPlus 300 or Bruker Avance-500 spectrometer with

the residual solvent peak as internal reference ($CDCl_3$ 7.26 ppm, THF-d_8 3.58 ppm). GPC was performed using a Viscotek 2210 system equipped with three Waters columns (HR 4, HR 4E, HR 3) and a 1 mL/min flow rate of THF as eluent at 30 °C. Monodisperse PS standards ranging from 1 kDa to 400 kDa were used for calibration. Thermal gravimetric analysis was performed on a TA Instruments Q500 using a heating rate of 10 ^{o}C per minute under a nitrogen atmosphere. Differential scanning calorimetry was performed on a TA Instruments Q100 using a heating and cooling rate of 10 ^{o}C per minute for three cycles. Glass transition temperatures were determined from the third cycle.

2.4. Results and Discussion

To study the living anionic polymerization of OTHPSt, we first synthesized the monomer in large quantities, with high yield and a high degree of purity. The literature procedure where the first step is THP protection of 4-hydroxybenzaldehyde and the second step is a Wittig methenylation reaction was modified, by using a more efficient acid catalyst (pyridinium *p*-toluenesulfonate), and solvent for the first step. A yield of >95% in under an hour was achieved compared to the 2-3 days as previously reported with HCl saturated ethyl acetate.[21, 24] The Wittig coupling was also modified by taking into account the exothermic nature of the reaction and mixing the THP-protected benzaldehyde with methyltriphenylphosphonium bromide in THF while cooling with an ice bath before slow addition of a solution of potassium *tert*-butoxide in THF. This allowed for a typical yield of 60-70% over the two steps and excellent purity by distillation under high vacuum.

In order to purify the monomer for anionic polymerization, a first distillation from CaH_2 and a second distillation from NaH were carried out to remove residual traces of water. Due to its

high boiling point (~110 ^{o}C), typical dehydrating agents such as di-*n*-butylmagnesium cannot be used as they cause extensive polymerization before monomer can be recovered, possibly due to Lewis acid catalyzed deprotection of the THP group. NaH, however, was found to be quite effective for the removal of water without causing excessive polymerization during the distillation. The viscous monomer was diluted with dry THF before use. To start with, we used the standard anionic polymerization conditions for polar monomers, namely -78 ^{o}C in THF as solvent.[9] In fact, the very first anionic polymerization worked extremely well giving a moderate molecular weight of 6.4 kDa relative to PS standards with a very low dispersity of 1.03. While the efficient homopolymerization of OTHPSt was encouraging, for sequential polymerization to be feasible, chain extension of the living P(OTHPSt) anion with a second monomer should also be efficient. To test this, we chose to use styrene due to its well-controlled anionic polymerization and high propagation rate in THF (**Figure 2.1**).[25] BCPs were synthesized by the sequential addition of styrene to the living OTHPSt anion. After terminating the polymerization with methanol and precipitation, the resulting BCPs were characterized by GPC, ^{1}H-NMR spectroscopy, TGA and DSC. Given the fast propagation rate for styrene in THF at -78 ^{o}C, the narrow distribution of the BCPs demonstrates fast initiation of styrene by the living P(OTHPSt) anion. The chain extension proceeded with a remarkable lack of side reactions to yield P(OTHPSt-*b*-St) BCPs with molecular weights around 34 kDa and low dispersities of 1.04 (**Table 2.1**). From these initial studies, the control over polymerization was exceptional as the targeted degree of polymerization was attained by varying the monomer to initiator ratio while maintaining narrow molecular weight distributions. All polymers precipitated from methanol as white powders, making the handling more straightforward than poly(4-(1-ethoxy ethoxy)styrene) which is a viscous oil.[20]

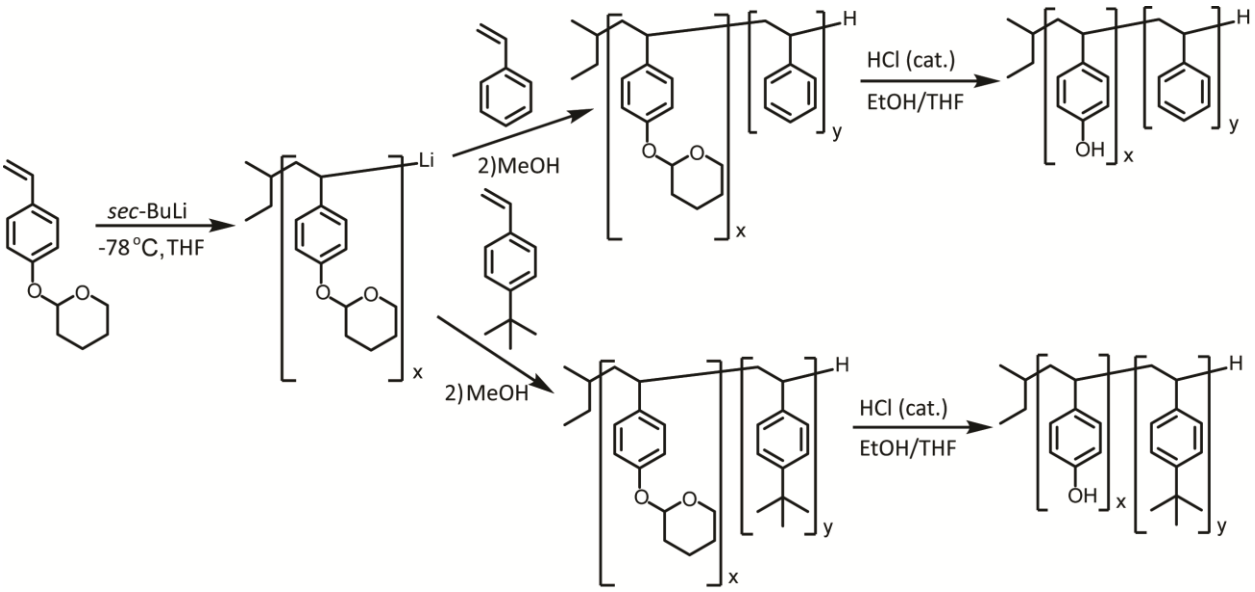

Figure 2.1. Synthetic route for P(HS-*b*-St) and P(HS-*b*-tBuSt) by anionic polymerization.

Table 2.1. Characteristic Data for BCPs Synthesized by Chain Extension of P(OTHPSt) as the First Block.

Sample	2nd block	M_n P(OTHPSt) (kg/mol)[a]	M_n (BCP) (kg/mol)[a]	$Đ$[a]	F_{OTHPSt}[b]	T_g (°C)[c]	T_g (°C)[d]
St-1	St	9.0	33.8	1.04	0.26	90, 108	177, 110
St-2	St	13.3	33.2	1.04	0.40	110	181, 110
tBuSt-1	tBuSt	9.8	20.1	1.02	0.49	134	177, 152
tBuSt-2	tBuSt	8.3	29.8	1.03	0.32	140	175, 150
tBuSt-3	tBuSt	42.1	54.7	1.03	0.78	130	188, 162
MAPOSS-1	MAPOSS	3.3	5.3	1.04	0.87	95	148
MAPOSS-2	MAPOSS	17.2	21.2	1.03	0.91	125	180
DMS-1	DMS	11.7	13.7	1.03	0.72	-	185
DMS-2	DMS	5.5	9.5	1.05	0.51	-	167

[a]Determined by GPC using PS standards. [b]Mol fraction of P(OTHPSt) determined using ^{1}H-NMR. [c]Determined by DSC from the third heating cycle for the protected BCP. [d]Determined by DSC from the third heating cycle for the deprotected BCP.

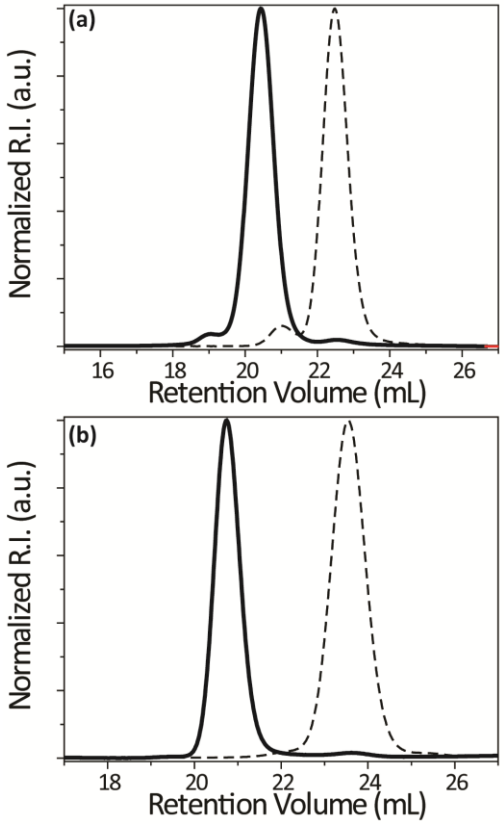

Figure 2.2. GPC chromatograms for P(OTHPSt) homopolymer (dashed) and after chain extension (solid) with (a) St (**St-2**) and (b) tBuSt (**tBuSt-2**).

We also examined a styrene derivative with higher hydrophobicity, namely 4-*tert*-butylstyrene (tBuSt) which also has a higher T_g than PS, making it a potentially interesting block for applications in BCP lithography.[26] The chain extension by tBuSt was equally well-controlled as St, yielding BCPs with targeted molecular weights between 20 and 55 kDa with dispersities between 1.02 and 1.03 (**Table 2.1**). Example GPC chromatograms for the St and tBuSt systems, shown in **Figure 2.2**, depict a clean shift to lower elution volume upon chain extension while

maintaining the narrow distribution of the homopolymer. The small shoulders at the high molecular weight end in the homopolymer traces were an artifact due to dimerization of the highly reactive living anion by oxygen during removal of the aliquot and termination by MeOH.

Thermal characterization by TGA showed a two-step degradation with the first step at ~280 ^{o}C corresponding to the loss of the THP group, followed by complete degradation of the polymer (**Figure 2.S1**). DSC of the protected polymer gave the expected T_g's, ~110 ^{o}C for PS and 130 to 140 ^{o}C for PtBuSt. Interestingly, a transition for the P(OTHPSt) block was not observed except for **St-1** where an endothermic peak was observed at 90 ^{o}C. The P(OTHPSt) homopolymer itself shows an endothermic transition around 110-120 ^{o}C (**Figure 2.S2**).

A wide variety of acids have been used for the deprotection of THP ethers with stronger acids greatly increasing the rate.[19] Typically, 1.0 g of BCP was dissolved in 50 mL of THF followed by the addition of 50 mL of ethanol (EtOH). With the tBuSt BCPs, these conditions resulted in a cloudy solution which rapidly turned clear upon the addition of 0.1 mL of concentrated aq. HCl (12 M). Under these conditions, deprotection was quantitative by ^{1}H-NMR in <15 min at room temperature. **Figure 2.3** shows a comparison of ^{1}H-NMR spectra for a protected and deprotected BCP (**tBuSt-2**). The peaks from the acetal were distinctly defined making integration of the relevant regions straightforward.

The deprotected BCPs demonstrate remarkably different thermal characteristics compared to the protected BCPs as the TGA shows a single step-degradation starting at ~ 340 ^{o}C and the thermal transitions observed from DSC are in good agreement with the typical T_g for PHS (~ 180 ^{o}C). The solubility of the BCPs also changes considerably as the deprotected polymer is no longer soluble in solvents which do not accept hydrogen bonds (e.g., chloroform), another indicator of

successful deprotection. Thus, P(OTHPSt) provides a viable anionic route to rapid and straightforward access to well-defined PHS based BCPs.

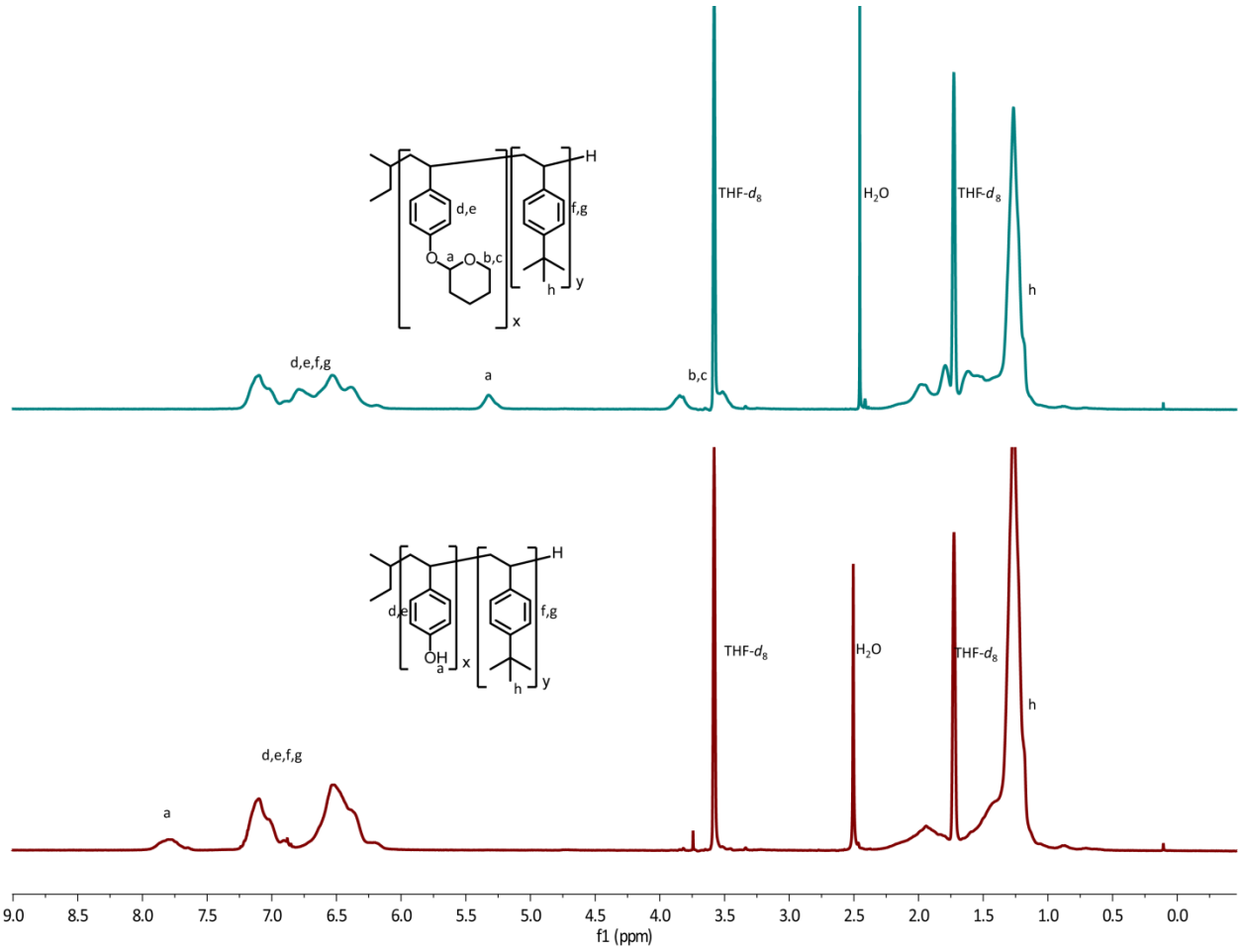

Figure 2.3. ^{1}H-NMR spectra for protected **tBuSt-2** (top) and deprotected **tBuSt-2** (bottom) in THF-d_8.

To demonstrate the versatility of this method, we examined the chain extension of inherently acid-sensitive monomers that have previously not been synthesized with a PHS block. As mentioned earlier, current methods for the deprotection of protected PHS derivatives tend to be quite harsh, thus preventing the incorporation of acid-sensitive blocks into PHS-based BCPs. In fact, some of the most useful and interesting blocks are inherently more sensitive due to the

functionality they carry. PDMS, for example, is an extremely hydrophobic polymer known to have strong segregation strength with most polymers, and oxidizes into SiO_2 upon exposure to O_2 plasma making it useful for hybrid materials, compatibilizers in blends, as well as for fabrication of hard masks for pattern transfer.[27]

To synthesize P(HS-*b*-DMS), we followed a procedure typically used for P(S-*b*-DMS) as the reactivity of the P(OTHPSt) anion is similar to the PS anion. While the growth of PDMS suffers from an equilibration reaction at high conversion, 50% conversion can be achieved in two hours while maintaining good control over the polymerization.[23] Therefore, we first polymerized OTHPSt in THF at -78 ^oC to generate the living anion and added a solution of D_3 in benzene to the polymerization mixture (**Figure 2.4**). The orange color of the anion slowly faded and the reaction was warmed to room temperature while stirring in a water bath. After polymerizing for two hours, the reaction was quenched by the addition of excess chlorotrimethylsilane (TMSCl) and precipitated into methanol. After stirring for 15 minutes, the initially suspended white powder dissolved into the methanol to form a clear solution. Upon evaporation of the methanol, only PHS homopolymer remained. The HCl generated from the reaction of the excess TMSCl with methanol likely drove two different reactions, both deprotecting the P(OTHPSt) to PHS and also degrading the PDMS block of the BCP, yielding a methanol soluble polymer and aptly demonstrating the acid-sensitivity of PDMS. Thus, we synthesized another P(OTHPSt-*b*-DMS) BCP, this time quenching with a 2:1 mixture of pyridine and TMSCl, to absorb the generated HCl during polymer precipitation.

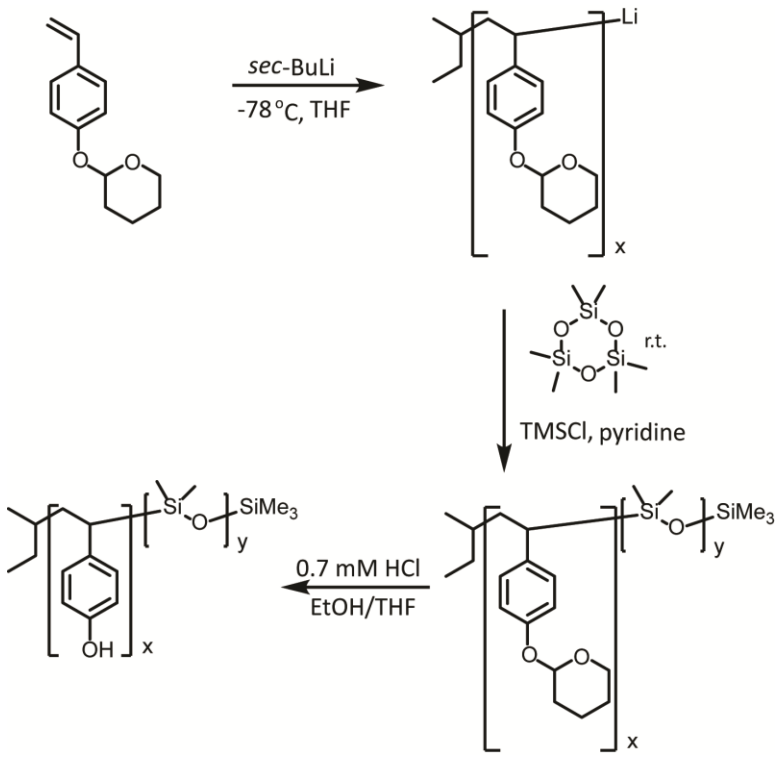

Figure 2.4. Synthetic scheme for P(HS-*b*-DMS).

With these modifications in the procedure, we obtained P(OTHPSt-*b*-DMS) BCPs with varying fractions of P(OTHPSt) and narrow dispersities. **Figure 2.5a** shows a representative GPC chromatograph with well-controlled chain extension from the P(OTHPSt) homopolymer to the P(OTHPSt-*b*-DMS) BCP. For the deprotection of the OTHP block in the P(OTHPSt-*b*-DMS) BCP, we had to reexamine the acidolysis method as our initial studies showed that adding even a small amount (40 µL) of concentrated HCl (12 M) was sufficient to degrade the PDMS block. Varying the acid strength by using trifluoroacetic acid (TFA) and acetic acid (AcOH) also resulted in complete degradation of the PDMS block. Serendipitously, we discovered that the addition of 60 µL diluted HCl (1.2 M) was able to deprotect the P(OTHPSt) block without degrading PDMS. This roughly corresponds to 0.7 mM HCl in the solution, which quantitatively catalyzes the deprotection of the THP groups within 3 hours with good chemoselectivity.

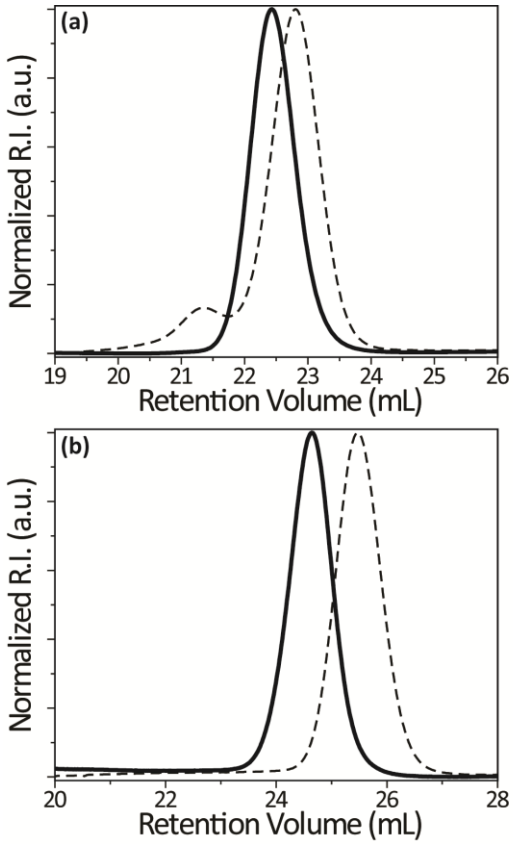

Figure 2.5. GPC chromatograms of P(OTHPSt) homopolymer (dashed) and after chain extension (solid) with (a) DMS (**DMS-1**) and (b) MAPOSS (**MAPOSS-1**).

The presence of the PDMS block was confirmed by both ^{1}H-NMR (large singlet at approximately 0.1 ppm) and ^{29}Si-NMR (singlet at -22 ppm) both before and after removal of the THP groups (**Figure 2.6**, full ^{29}Si spectra are given in **Figure 2.S3**). Integration of the aryl peak to PDMS peak ratio remained the same before and after deprotection (4.0:5.3 vs 4.0:5.4, respectively), also providing clear evidence of an intact PDMS block. Thermal characterization demonstrates the difference between the protected and deprotected BCPs as TGA again shows a two-step degradation for the protected BCP and a single step degradation for the deprotected BCP. Upon deprotection, the PHS T_g was observed readily (**Figure 2.S4**). Thus, we successfully synthesized P(HS-*b*-DMS), a heretofore unknown BCP.

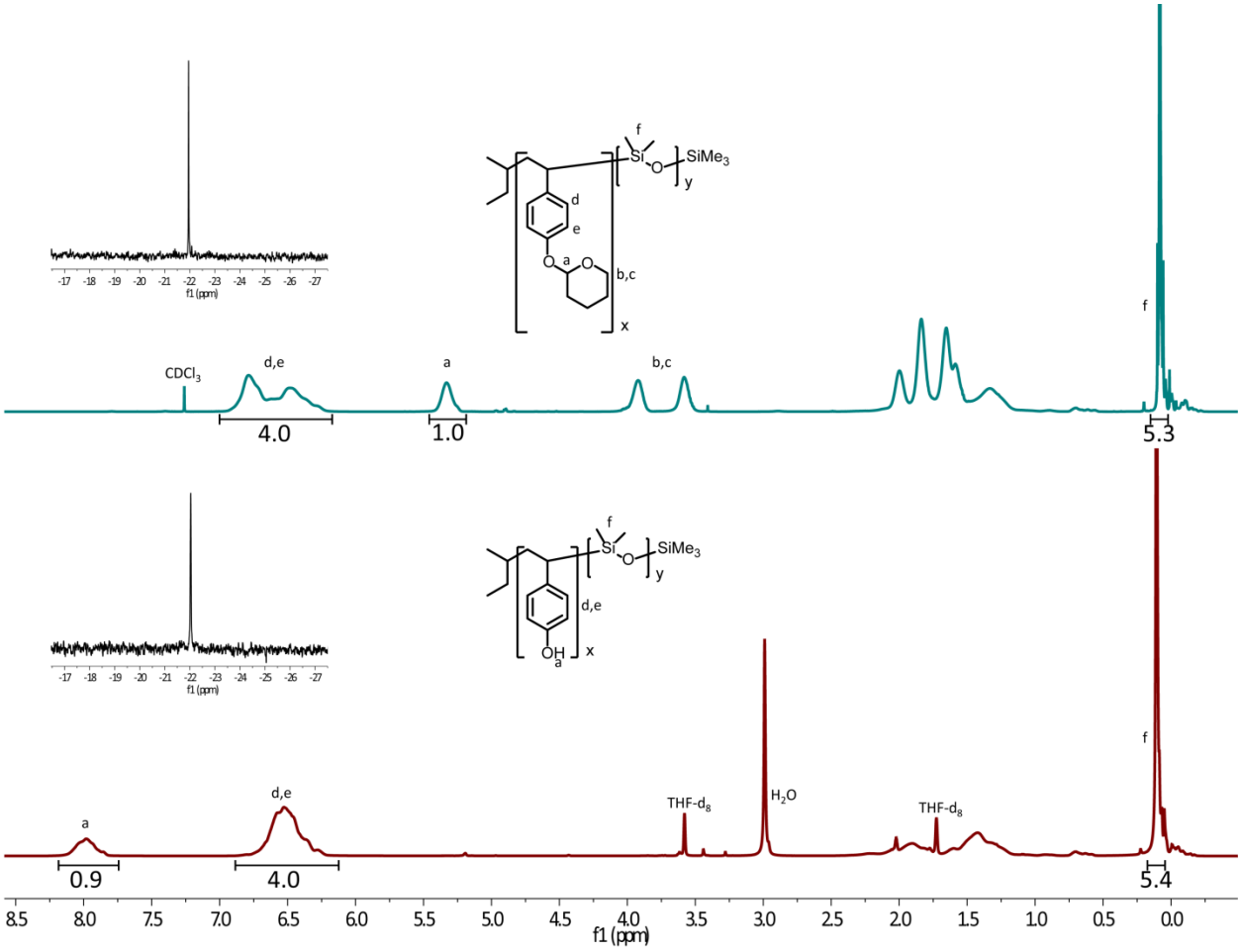

Figure 2.6. ^{1}H-NMR spectra (inset: ^{29}Si-NMR) for protected (top) **DMS-2** and deprotected (bottom) **DMS-2**.

Similar to PDMS, we were interested in other precursors for inorganic-organic hybrid polymers. The anionic polymerization of a silsesquioxane-based block has been previously shown, namely a methacrylate functionalized isobutyl substituted polyhedral oligomeric silsesquioxane (MAPOSS).[28, 29] So far, the same Si-O-Si chemical stability issues as PDMS have prevented the synthesis of a PHS-*b*-PMAPOSS BCP. In order to maintain a controlled polymerization of MAPOSS (and methacrylates in general), it was necessary to add LiCl to the polymerization which aids in preventing back-biting reactions during methacrylate propagation as well as end-capping

the P(OTHPSt) anion with 1,1-diphenylethylene (DPE) which serves to both increase the steric bulk of the anion as well as lower the reactivity through increased delocalization (**Figure 2.7**).[30] By doing so, P(OTHPSt-*b*-MAPOSS) BCPs were successfully synthesized in a well-controlled manner, maintaining a low dispersity even at low molecular weights (**Table 2.1**). **Figure 2.5b** shows a clear shift to lower elution volume upon adding MAPOSS to the polymerization solution as well as the narrow peak shape during crossover and propagation.

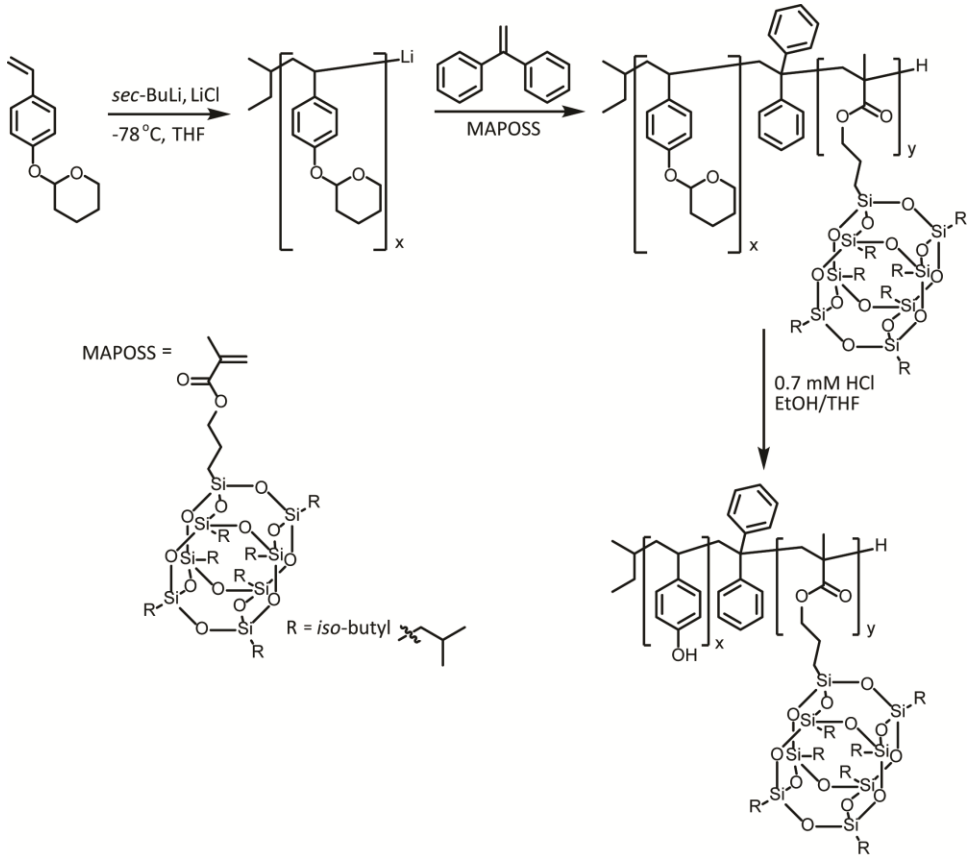

Figure 2.7. Synthetic scheme for P(HS-*b*-MAPOSS).

For deprotection, the optimized conditions for P(HS-*b*-DMS) were used, namely 0.7 mM HCl in EtOH/THF. These conditions were equally effective for P(HS-*b*-MAPOSS) as judged by ^{1}H and ^{29}Si-NMR (**Figure 2.8**, full ^{29}Si spectra given in **Figure 2.S5**). The two peaks from the *iso*-

butyl substituents on MAPOSS are clearly intact at 1.0 and 0.6 ppm in the ^{1}H-NMR spectrum while the ^{29}Si-NMR spectrum shows the expected set of two peaks around -68 ppm both before and after deprotection. Integration of the aryl protons to the two *iso*-butyl proton peaks on MAPOSS remained consistent before and after deprotection (4:6.6 and 2.6 vs 4:6.6 and 2.5, respectively). The protected BCP shows the expected two-step degradation by TGA and a single-step degradation after deprotection (**Figure 2.S6**). By DSC, going from the protected BCP to the deprotected BCP, a clear shift in T_g to higher temperature was observed, consistent with chemoselective removal of the THP groups to yield P(HS-*b*-MAPOSS).

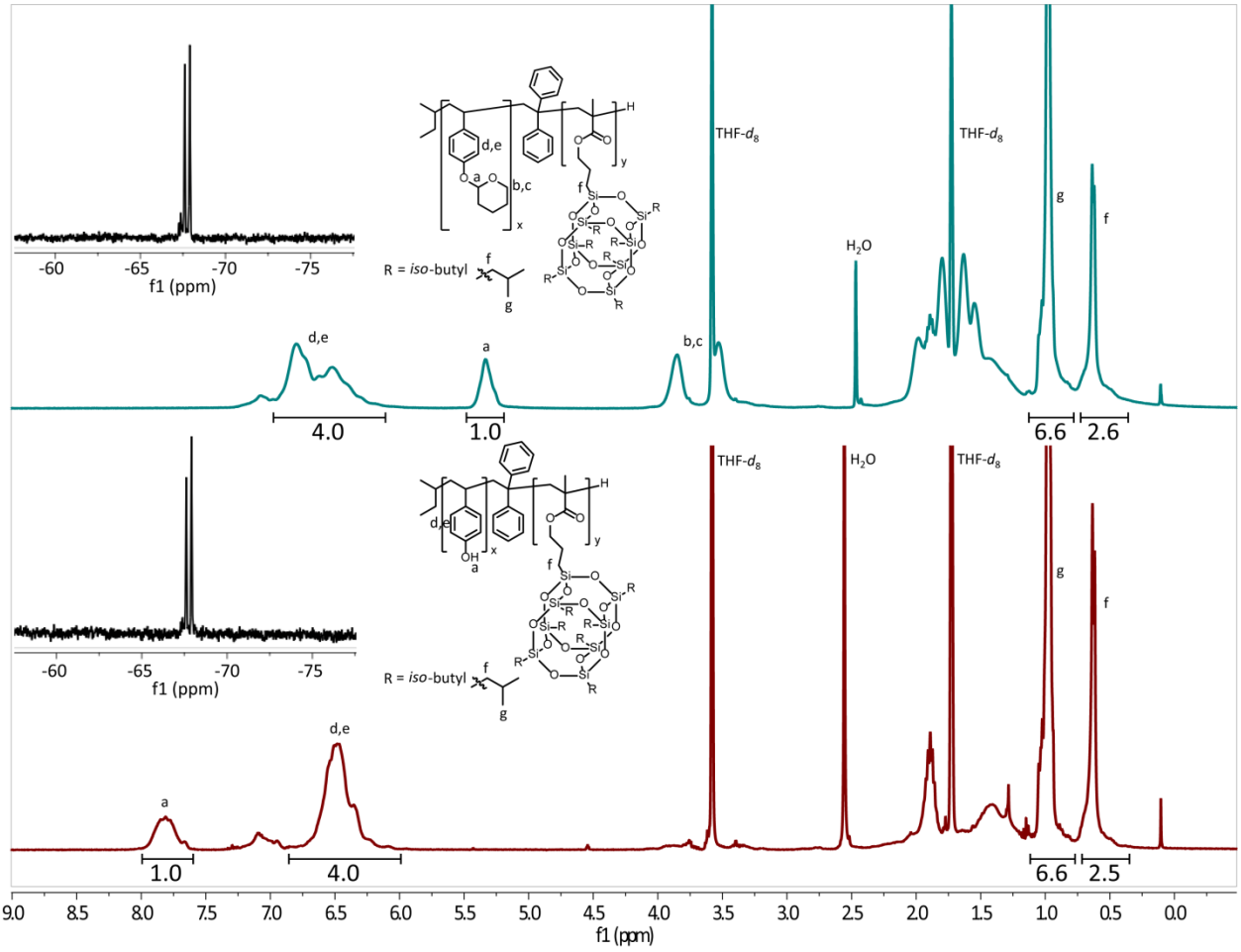

Figure 2.8. ^{1}H-NMR spectra (inset: ^{29}Si-NMR) for protected (top) **MAPOSS-2** and deprotected

(bottom) **MAPOSS-2**.

2.5. Conclusions

In this article, we have demonstrated the well-controlled anionic polymerization of a THP protected 4-hydroxystyrene, OTHPSt. This previously unexplored monomer, OTHPSt, constitutes an ideal protected version of 4-HS for living anionic polymerization. While the THP ether has excellent stability to both basic conditions and nucleophiles, it can be cleaved under mild acidic conditions. This is particularly important as it opens up a broad spectrum of monomer functionalities that can be incorporated in the second block. The glass transition temperature is well above room temperature which facilitates handling and purification of the protected PHS polymer. We examined the chain extension of the P(OTHPSt) anion to generate a variety of BCPs including styrene, *tert*-butylstyrene, dimethylsiloxane and MAPOSS blocks. By tuning the deprotection conditions using catalytic amounts of HCl, THP groups were removed without affecting the acid-sensitive Si-O-Si linkages in siloxane and silsesquioxane blocks. These BCPs with DMS and MAPOSS could not be accessed by any of the previous methods due to their acid sensitivity. Detailed morphological studies for these BCPs are currently ongoing.

2.6. Supporting Information

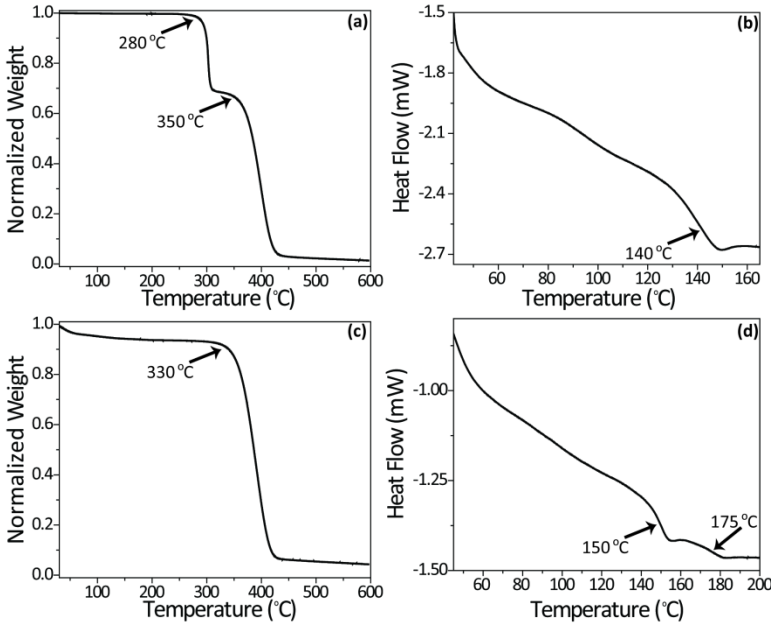

Figure 2.S1. (a) and (c) TGA for **tBuSt-3** before and after deprotection, respectively. (b) and (d) DSC for **tBuSt-2** before and after deprotection, respectively.

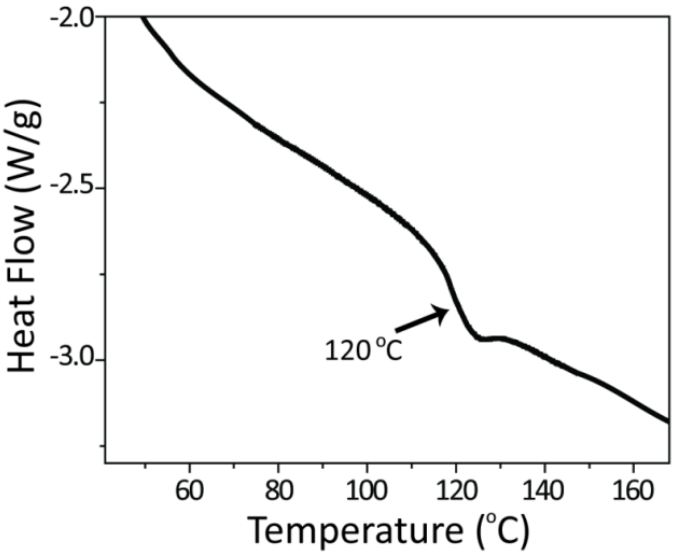

Figure 2.S2. DSC for P(OTHPSt).

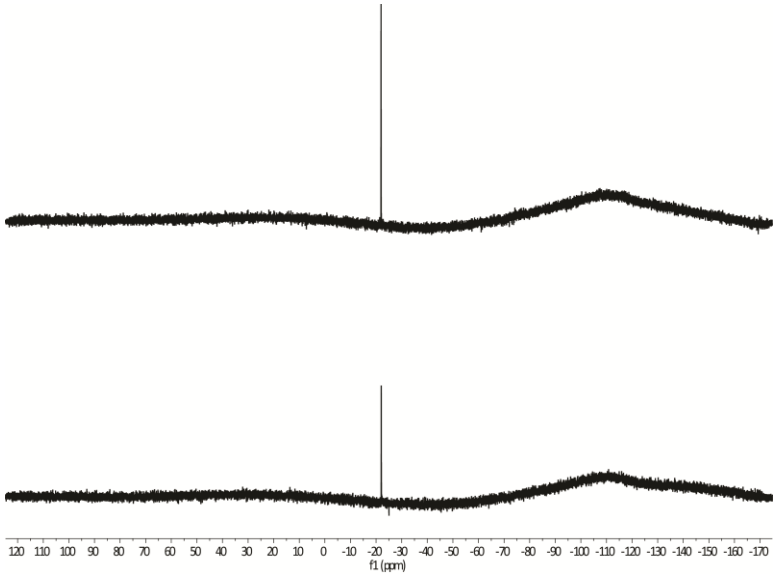

Figure 2.S3. ^{29}Si NMR spectra for **DMS-2** before (top) and after (bottom) deprotection.

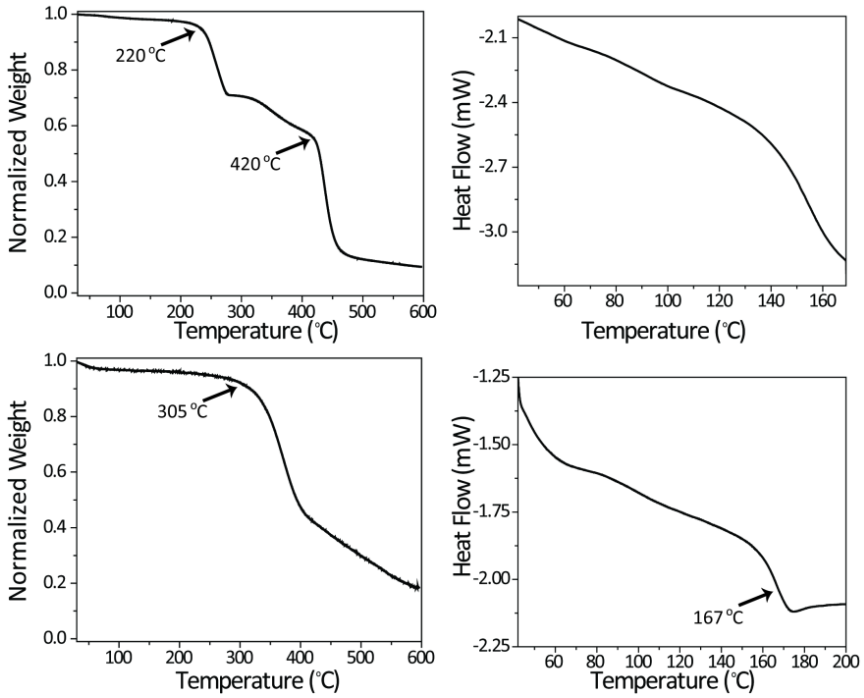

Figure 2.S4. (a) and (c) TGA for **DMS-2** before and after deprotection, respectively. (b) and (d) DSC for **DMS-2** before and after deprotection, respectively.

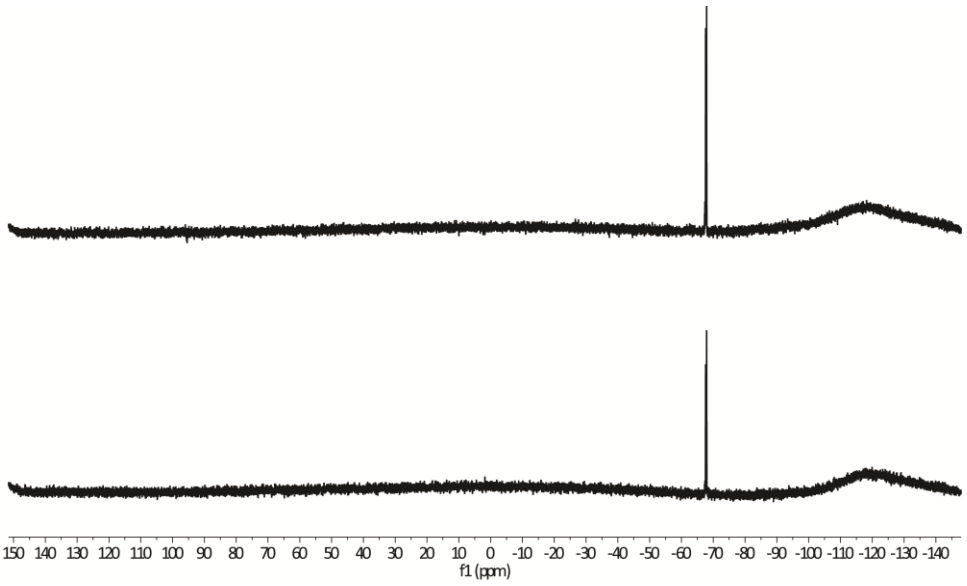

Figure 2.S5. ^{29}Si NMR spectra for **MAPOSS-1** before (top) and after (bottom) deprotection.

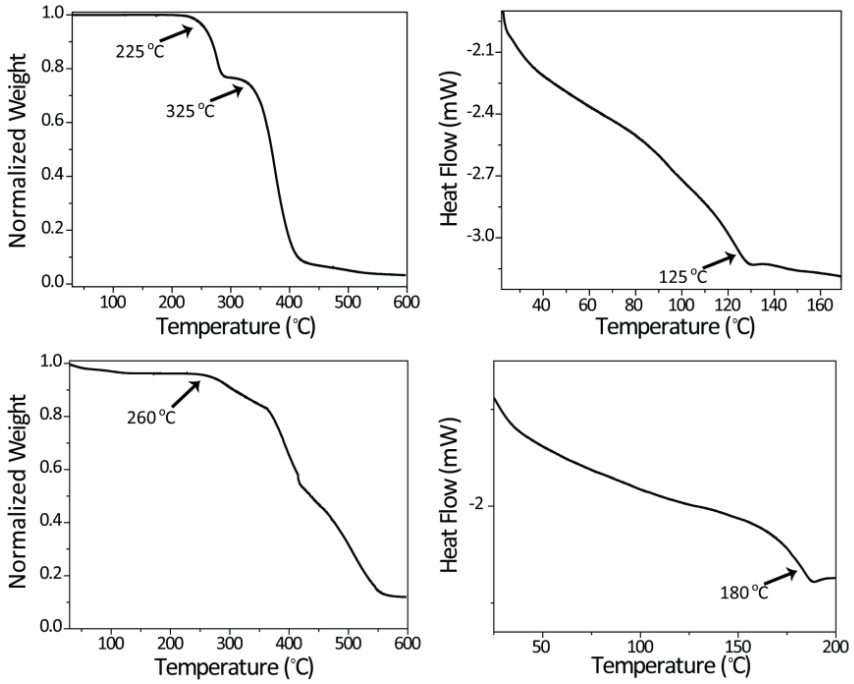

Figure 2.S6. (a) and (c) TGA of **MAPOSS-2** before and after deprotection, respectively. (b) and (d) DSC of **MAPOSS-2** before and after deprotection, respectively.

2.7. References

1. Bates, F. S.; Fredrickson, G. H., Block Copolymer Thermodynamics: Theory and Experiment. *Annu. Rev. Phys. Chem.* **1990,** *41*, 525-557.

2. Park, M.; Harrison, C.; Chaikin, P. M.; Register, R. A.; Adamson, D. H., Block Copolymer Lithography: Periodic Arrays of ~1011 Holes in 1 Square Centimeter. *Science* **1997,** *276* (5317), 1401-1404.

3. Park, S.; Kim, B.; Wang, J. Y.; Russell, T. P., Fabrication of Highly Ordered Silicon Oxide Dots and Stripes from Block Copolymer Thin Films. *Adv. Mater.* **2008,** *20*, 681-685.

4. Park, S.; Lee, D. H.; Xu, J.; Kim, B.; Hong, S. W.; Jeong, U.; Xu, T.; Russell, T. P., Macroscopic 10-Terabit–per–Square-Inch Arrays from Block Copolymers with Lateral Order. *Science* **2009,** *323* (5917), 1030-1033.

5. Tang, C.; Lennon, E. M.; Fredrickson, G. H.; Kramer, E. J.; Hawker, C. J., Evolution of Block Copolymer Lithography to Highly Ordered Square Arrays. *Science* **2008,** *322* (5900), 429-432.

6. Braunecker, W. A.; Matyjaszewski, K., Controlled/living radical polymerization: Features, developments, and perspectives. *Prog. Polym. Sci.* **2007,** *32* (1), 93-146.

7. Baskaran, D.; Müller, A. H. E., Anionic vinyl polymerization—50 years after Michael Szwarc. *Prog. Polym. Sci.* **2007,** *32* (2), 173-219.

8. Hirao, A.; Loykulnant, S.; Ishizone, T., Recent advance in living anionic polymerization of functionalized styrene derivatives. *Prog. Polym. Sci.* **2002,** *27* (8), 1399-1471.

9. Hadjichristidis, N.; Pispas, S.; Floudas, G. A., *Block Copolymers: Synthetic Strategies, Physical Properties, and Applications*. John Wiley & Sons, Inc.: New Jersey, 2003.

10. Brandrup, J.; Immergut, E. H.; Grulke, E. A., *Polymer Handbook*. 4th ed.; Wiley-Interscience: New York, 1999.

11. Fréchet, J. M. J.; Matuszczak, S.; Reck, B.; Stover, H. D. H.; Willson, C. G., Chemically amplified imaging materials based on electrophilic aromatic substitution: poly[4-(acetoxymethyl)styrene-co-4-hydroxystyrene]. *Macromolecules* **1991,** *24*, 1746-1754.

12. Chen, X. Y.; Jankova, K.; Kops, J.; Batsberg, W., Hydrolysis of 4-acetoxystyrene polymers prepared by atom transfer radical polymerization. *J. Polym. Sci. Part A: Polym. Chem.* **1999,** *37* (5), 627-633.

13. Kanagasabapathy, S.; Sudalai, A.; Benicewicz, B. C., Reversible Addition-Fragmentation Chain-Transfer Polymerization for the Synthesis of Poly(4-acetoxystyrene) and Poly(4-acetoxystyrene)-block-polystyrene by Bulk, Solution and Emulsion Techniques. *Macromol. Rapid Commun.* **2001,** *22*, 1076-1080.

14. Quinn, J. D.; Register, R. A., Microphase Separation in Block-Random Copolymers of Styrene, 4-Acetoxystyrene, and 4-Hydroxystyrene. *J. Polym. Sci. Part B: Polym. Phys.* **2009,** *47*, 2106-2113.

15. Dobrosielska, K.; Takano, A.; Matsushita, Y., Creation of Hierarchical Nanophase-Separated Structures via Supramacromolecular Self-Assembly from Two Asymmetric Block Copolymers with Short Interacting Sequences Giving Hydrogen Bonding Interaction. *Macromolecules* **2009,** *43* (2), 1101-1107.

16. Dobrosielska, K.; Wakao, S.; Takano, A.; Matsushita, Y., Nanophase-Separated Structures of AB Block Copolymer/C Homopolymer Blends with Complementary Hydrogen-Bonding Interactions. *Macromolecules* **2008,** *41* (20), 7695-7698.

17. Hirao, A.; Higashihara, T., Synthesis of Branched Polymers by Means of Living Anionic Polymerization. 13. Synthesis of Well-Defined Star-Branched Polymers via an Iterative Approach Using Living Anionic Polymers. *Macromolecules* **2002,** *35* (19), 7238-7245.

18. Kuo, S.-W.; Tung, P.-H.; Chang, F.-C., Syntheses and the Study of Strongly Hydrogen-Bonded Poly(vinylphenol-b-vinylpyridine) Diblock Copolymer through Anionic Polymerization. *Macromolecules* **2006,** *39* (26), 9388-9395.

19. Greene, T. W.; Wuts, P. G. M., *Protective Groups in Organic Synthesis*. 2nd ed.; Wiley-Interscience: New York, 1991.

20. Natatello, A.; Tonhauser, C.; Frey, H., Anionic Polymerization of *para*-(1-Ethoxy ethoxy)styrene: Rapid Access to Poly(*p*-hydroxystyrene) Copolymer Architectures. *ACS Macro Lett.* **2013,** *2*, 409-413.

21. Hesp, S. A. M.; Hayashi, N.; Ueno, T., Tetrahydropyranyl- and Furanyl-Protected Polyhydroxystyrene in Chemical Amplification Systems. *J. Appl. Polym. Sci.* **1991,** *42*, 877-883.

22. Hadjichristidis, N.; Iatrou, H.; Pispas, S.; Pitsikalis, M., Anionic Polymerization: High Vacuum Techniques. *J. Polym. Sci. Part A: Polym. Chem.* **2000,** *38*, 3211-3234.

23. Bellas, V.; Iatrou, H.; Hadjichristidis, N., Controlled Anionic Polymerization of Hexamethylcyclotrisiloxane. Model Linear and Miktoarm Star Co- and Terpolymers of Dimethylsiloxane with Styrene and Isoprene. *Macromolecules* **2000,** *33*, 6993-6997.

24. Miyashita, M.; Yoshikoshi, A.; Grieco, P. A., Pyridinium p-toluenesulfonate. A mild and efficient catalyst for the tetrahydropyranylation of alcohols. *J. Org. Chem.* **1977,** *42*, 3772-3774.

25. Geacintov, C.; Smid, J.; Szwarc, M., Kinetics of Anionic Polymerization of Styrene in Tetrahydrofuran. *J. Am. Chem. Soc.* **1962,** *84*, 2508-2514.

26. Kennemur, J. G.; Hillmyer, M. A.; Bates, F. S., Synthesis, Thermodynamics, and Dynamics of Poly(4-*tert*-butylstyrene-*b*-methyl methacrylate). *Macromolecules* **2012,** *45*, 7228-7236.

27. Jung, Y. S.; Jung, W.; Tuller, H. L.; Ross, C. A., Nanowire Conductive Polymer Gas Sensor Patterned Using Self-Assembled Block Copolymer Lithography. *Nano Lett.* **2008,** *8* (11), 3776-3780.

28. Hirai, T.; Leolukman, M.; Hayakawa, T.; Kakimoto, M.-a.; Gopalan, P., Hierarchical Nanostructures of Organosilicate Nanosheets within Self-Organized Block Copolymer Films. *Macromolecules* **2008,** *41* (13), 4558-4560.

29. Hirai, T.; Leolukman, M.; Jin, S.; Goseki, R.; Ishida, Y.; Kakimoto, M.-A.; Hayakawa, T.; Ree, M.; Gopalan, P., Hierarchical Self-Assembled Structures from POSS-Containing Block Copolymers Synthesized by Living Anionic Polymerization. *Macromolecules* **2009,** *42*, 8835-8843.

30. Varshney, S. K.; Hautekeer, J. P.; Fayt, R.; Jérôme, R.; Teyssié, P., Anionic polymerization of (meth)acrylic monomers. 4. Effect of lithium salts as ligands on the "living" polymerization of methyl methacrylate using monofunctional initiators. *Macromolecules* **1990,** *23*, 2618-2622.

Chapter 3. Phase Behavior of Poly(4-hydroxystyrene-block-styrene) Synthesized by Living Anionic Polymerization of an Acetal Protected Monomer

The contents of this chapter have been accepted in *Macromolecules* (DOI: 10.1021/ma501126t) with coauthors Sweat, Daniel P.; Kim, Myungwoong; Schmitt, Adam K.; Perroni, Dominic V.; Fry, Charles G.; Mahanthappa, Mahesh K.; Gopalan, Padma.

Author contributions: The synthesis and characterization of the BCPs were done by Daniel; NMR analysis was done by Daniel in consultation with Dr. Fry. Calculation of interaction parameter was done in collaboration with Prof. Mahanthappa's group (Dominic and Adam). Experimental design and interpretation of data was done by Daniel and Myungwoong. All authors contributed towards writing the manuscript.

3.1. Abstract

We have synthesized a series of poly(4-(2-tetrahydropyranyloxy)styrene) [P(OTHPSt)] homopolymers by living anionic polymerization of the protected monomer (OTHPSt) in tetrahydrofuran at -78 ^{o}C, with excellent control over molecular weight and dispersity. The high T_g of P(OTHPSt) led to facile purification and isolation of the polymer as a powder. Characterization of the POTHPSt homopolymer by Nuclear Overhauser Effect Spectroscopy confirms the strong preference for the axial position of the relatively sterically demanding alkoxy phenyl group. By sequential monomer addition, a series of low to high molecular weight P(OTHPSt-*b*-S) BCPs with narrow dispersities were synthesized. Quantitative deprotection of the THP groups yielded poly(4-hydroxystyrene-*b*-styrene) [P(HS-*b*-S)] with tunable molecular

weights and compositions. The solid-state and melt-phase self-assembly of these diblocks was investigated using synchrotron small angle X-ray scattering (SAXS) and transmission electron microscopy (TEM). Mean-field theory analysis of the temperature-dependent correlation-hole scattering for a disordered diblock was used to determine the interaction parameter as $\chi_{HS/S}(T) = (4.39 \pm 0.83)/T + (0.109 \pm 0.002)$, which is approximately four times larger than that of poly(styrene-*b*-methyl methacrylate) with the same disproportionately high contribution of entropy to the free energy of mixing.

3.2. Introduction

Block copolymers (BCPs) have attracted a great deal of interest for their ability to spontaneously self-assemble into dense periodic nanostructures with accessible length scales of 5–50 nm.[1-5] In this thermodynamically-driven self-assembly process, the order parameters that govern the resulting size of the domains are the copolymer volume fraction (composition) f_A, and the segregation strength χN, wherein N is the segment density normalized degree of polymerization and χ is the effective interaction parameter that quantifies the thermodynamic repulsion between the homopolymer blocks.[5] Well-established mean-field theories predict that coil-coil diblock copolymer self-assemble only when $\chi N \geq 10.5$,[6] neglecting monomer concentration fluctuation effects.[7] Below this critical value of χN, the BCP is disordered. For a given segmental interaction parameter χ, the degree of polymerization may be adjusted so that $\chi N \geq 10.5$ to force the BCP to self-assemble. The resulting domain sizes for lamellar diblock copolymers scale as $d \propto \chi^{1/6} N^{\alpha}$ wherein $\alpha = 2/3$ for strongly segregated systems[8] and $\alpha = 1/2$ for weakly segregated copolymers.[9] Thus, this scaling relation establishes a lower limit on the accessible domain sizes of ordered block copolymer morphologies.[6, 10-11] This domain spacing limitation is aptly demonstrated by poly(styrene-*b*-methyl methacrylate) [P(S-*b*-MMA)], one of the most widely used BCPs for self-

assembly in thin film and for pattern transfer. The small surface energy difference between the PS and PMMA blocks facilitates P(S-*b*-MMA) thin film self-assembly, while the ability to selectively remove the PMMA block simplifies pattern transfer to the underlying substrate.[12-14] However, the relatively small and temperature insensitive $\chi_{MMA/S} = 2.87/T + 0.0209$ for this system limits the minimum feature size to ~ 24 nm pitch for a lamellar morphology.[15-16]

One approach to accessing smaller feature sizes in nanotemplating and nanolithography using BCPs is to develop copolymers with greater chemical incompatibility between the homopolymer segments, *i.e.* to increase χ between the blocks. A straightforward means of increasing χ is to increase the difference in polarity between the blocks. For example, poly(styrene-*b*-dimethylsiloxane) [P(S-*b*-DMS)] has χ ~ 0.26 at 22 °C, while poly(styrene-*b*-2-vinylpyridine) [P(S-*b*-2VP)] exhibits χ ~ 0.18, both of which are significantly higher than P(S-*b*-MMA).[17-18] Tabulated values of the Hildebrand solubility parameters for various polymers allow a first-order estimate of their relative polarities, and hence their chemical incompatibilities. For example, the solubility parameters for PS, PMMA, PDMS and P2VP are 18.5, 19.0, 15.5 and 20.6 $(J/cm^3)^{1/2}$, respectively, thus demonstrating that differences in solubility parameters track with the magnitude of χ.[19-20] Poly(4-hydroxystyrene) [PHS] is a common polymer that has a high solubility parameter (24.55 $(J/cm^3)^{1/2}$), indicating its relatively high polarity and hydrophilicity.[21] Additionally, PHS exhibits good solubility in a variety of common hydrogen-bond accepting solvents such as tetrahydrofuran (THF) and acetone, rendering it easier to handle than other highly polar polymers such as poly(4-vinyl pyridine). The phenolic OH provides a functional handle amenable to a wide variety of transformations and post-functionalization reactions, while also conferring solubility in basic aqueous solutions and the ability to ligate Lewis acids such as metal oxide precursors. These

chemical attributes have made protected derivatives of PHS useful components in chemically-amplified resists for photolithography.[22]

Surprisingly, χ has not been quantified for a wide variety of simple, well-known polymer systems such as P(HS-*b*-S). From the solubility parameter formalism, one anticipates that χ = 0.68.[23] This large value of χ was invoked to explain the prevalence of ordered microdomains over large temperature ranges even when M_n is small.[24] A recent paper by Jarnagin et al.[25] estimated $\chi_{S/HS}$ at 2.2 based on the scaling law, i.e. the ratio of observed domain size to calculated N for P(HS-*b*-S). The polymers were made by nitroxide-mediated polymerization (NMP) (12.8 and 29.2 kg/mol, $Đ$ = 1.2) and the self-assembly involved a non-equilibrium solvent annealing method using acetone (a preferential solvent for PHS) to promote ordering which is known to swell domain size considerably.[26] Hence the exact extent of incompatibility even between PS and PHS blocks is not known.

We recently demonstrated the facile synthesis of PHS-based BCPs by living anionic polymerization of 4-(2-tetrahydropyranyl)oxystyrene (OTHPSt), a monomer readily synthesized in two steps from 4-hydroxybenzaldehyde, followed by mild acetal deprotection to yield narrow dispersity copolymers ($Đ$ = 1.02-1.05) with predictable molecular weights.[27] Due to its well-controlled polymerization, ease of polymer purification, and mild acid-catalyzed deprotection, OTHPSt is an extremely attractive monomer for the preparation of monodisperse PHS homopolymers and BCPs previously inaccessible by sequential living anionic polymerizations. Our initial report focused primarily on the synthesis and molecular characterization of several previously unknown BCPs including P(HS-*b*-DMS), which exploit our mildly acidic acetal deprotection conditions to unmask the latent PHS block.

Here we present the synthesis and molecular characterization of a series of narrow dispersity PHS and P(HS-*b*-S) BCPs with variable compositions and molecular weights derived from anionic polymerization of OTHPSt monomer, along with studies of their bulk phase behavior. As part of our studies, we also investigate the molecular weight-dependence of the T_g of P(OTHPSt) and show that T_g >> 22 °C even at low M_n, thus facilitating convenient polymer isolation and purification as a powder. Detailed NMR characterization of the monomer and the POTHPSt homopolymer in solution highlights how the anomeric effect directs cyclic acetal ring conformations, which when taken with the T_g data, indicates substantial rigidity of the resulting polymer chains. Quantitative deprotection of the THP protected hydroxyl group with aqueous HCl occurs within minutes at 22 °C, giving rapid access to a range of PHS copolymers. Bulk morphological characterization of these BCPs by small-angle X-ray scattering (SAXS) and transmission electron microscopy (TEM) confirms their ability to microphase separate into lamellar and cylindrical morphologies. By analyzing the temperature-dependent correlation-hole scattering data associated with a disordered P(HS-*b*-S) BCP using mean-field theory, we estimate the value of $\chi_{S/HS}$ to be four times larger than $\chi_{MMA/S}$, with a similarly weak temperature-dependent chemical incompatibility.

3.3. Experimental Section

Reagents. All solvents and reagents were purchased from Sigma-Aldrich Chemical Company (Milwaukee, WI, U.S.A.) and used without further purification unless specified. Tetrahydrofuran (THF) was freshly distilled from Na/benzophenone ketyl. 4-(2-tetrahydropyranyloxy)styrene and block copolymers with styrene were synthesized according to the literature procedure.[27] Anionic polymerizations were terminated using MeOH that was sparged with Ar for 10 min to remove dissolved oxygen.

Anionic polymerization of OTHPSt. An oven-dried flask equipped with a PTFE stopcock was cooled under argon and 40 mL of THF was added. The flask was cooled to -78 °C and *sec*-butyllithium (1.4 M in cyclohexane) (***caution***: *sec*-butyllithium is a highly reactive, pyrophoric reagent; handle with care) was added dropwise until a yellow color persisted. The flask was slowly warmed to room temperature until the solution became colorless and then chilled to -78 °C. A measured amount of *sec*-butyllithium (example: 0.11 mL, 0.154 mmol *sec*-BuLi) was added for the desired molecular weight and the desired volume of OTHPSt/THF solution (example: 4 mL, ~10 mmol) was injected into the flask with stirring, yielding an orange/red color from the living anion. After 30 min, methanol was added to quench the chain end and the THF solution was slowly poured into 400 mL MeOH to precipitate the P(OTHPSt) homopolymer. The polymer was quantitatively recovered by vacuum filtration as a white powder. The resulting powder was dried under vacuum at 22 °C overnight. ^{1}H NMR ($CDCl_3$, 500 MHz) δ 7.00-6.15 (4H), 5.43-5.20 (1H), 4.01-3.79 (1H), 3.67-3.42 (1H), 2.35-1.00 (9H). ^{13}C NMR ($CDCl_3$, 125 MHz) δ 155.01, 139.59-137.92, 128.43, 115.65, 96.3, 61.86, 46.90-41.80, 39.54, 30.48, 25.26, 18.84.

Typical method for deprotection of P(OTHPSt) and P(OTHPSt-*b*-S). 1.0 g P(OTHPSt) was dissolved in 50 mL of THF and 50 mL of ethanol was added. A catalytic amount of concentrated $HCl_{(aq)}$ (typically, 0.1-1.0 mL) was added and the solution stirred until the ^{1}H NMR spectrum in THF-d_8 indicated complete deprotection. (Since the reaction is acid-catalyzed, the amount of acid only affects the rate of the reaction.) The resulting solution was then precipitated into 500 mL of hexanes to yield a white powder that was collected by vacuum filtration. The powder was redissolved in 25 mL THF and precipitated into 300 mL of hexanes, isolated by filtration, and dried under vacuum at 22 °C.

Characterization. ^{1}H NMR and ^{13}C NMR spectra were recorded in $CDCl_3$ or THF-d_8 using a Bruker Avance-500, Bruker Avance-400 or a Varian MercuryPlus 300 spectrometer with TMS as internal reference. Quantitative ^{1}H NMR utilized a 10 s relaxation delay between pulses. 2-D Nuclear Overhauser Effect Spectroscopy (NOESY) was performed on a Bruker Avance-500 spectrometer. Size exclusion chromatograhy (SEC) was performed using a Viscotek 2210 system equipped with three Waters columns (HR 4, HR 4E, HR 3) and a 1 mL/min flow rate of THF as eluent at 30 °C. SEC analysis relied on a calibration curve constructed from nine narrow dispersity PS standards with M_n = 1–400 kg/mol. Tetra-detector SEC was performed using a Viscotek VE2001 equipped with TDA-302 (light scattering detectors at 7° and 90°, and four capillary viscometer in addition to a refractive index detector) with 1 mL/min THF eluent at 40 ^{o}C. Thermogravimetric analysis (TGA) was performed on a TA Instruments Q500 using a heating rate of 10 ^{o}C /min under a nitrogen atmosphere. Differential scanning calorimetry (DSC) was performed on a TA Instruments Q100 using a heating and cooling rate of 10 °C/min for three cycles. Glass transition temperatures were determined from the third heating cycle. SAXS samples were solvent cast by the slow evaporation of THF solutions (5 wt% polymer in THF) and followed by annealing at 160 ^{o}C for 48 h under vacuum. SAXS analysis employed either a Rigaku SMAX-300 instrument with a MM002+ micro-focus X-ray source operating at 40.5 W using Cu Kα radiation or the 12-ID-B beamline at the Advanced Photon Source (APS) at Argonne National Laboratory, using a beam energy of 12 keV (1.033 Å). The sample-to-detector distance in both cases was rigorously calibrated using a silver behenate standard (d_{001} = 5.838 nm). Temperature-dependent SAXS studies used a Linkam DSC stage with a 5 min thermal pre-equilibration delay prior to data collection at a given temperature. Synchrotron SAXS data were analyzed using publicly available Igor Pro procedures.[28] The SAXS samples were further prepared for TEM by

embedding in epoxy (Eponate 12 with DMP-30, Ted Pella) and subsequently sectioned at 22 °C using a diamond knife to produce 70-90 nm thick samples. The sections were placed on 200 mesh Cu grids and exposed to either I_2 vapor overnight or immersed in 0.5 wt% Cs_2CO_3(*aq*) for 15 min to preferentially stain the PHS block. TEM samples were imaged using a Phillips CM120 operating at 80 kV accelerating voltage in bright-field mode.

3.4. Results and Discussion

Synthesis and Thermal Characterization of the P(OTHPSt) homopolymer

The anionic polymerization of OTHPSt was carried out using *sec*-butyllithium as the initiator in THF at -78 °C (**Figure 3.1**).[27] For polymerization of styrene under identical reaction conditions, faster chain propagation is typically observed and results in broader molar mass dispersities ($Đ = M_w/M_n$ = 1.07–1.25).[29] However, OTHPSt polymerization exhibits a high degree of control as evidenced by $Đ \leq 1.04$ for all reactions (**Table 3.1**). POTHPSt homopolymers with M_n = 3–37 kg/mol were synthesized by this method. The "livingness" of these polymerizations was further confirmed by the conformance of the experimentally observed molecular weight to that theoretically calculated by M_n = [OTHPSt]/[*s*BuLi], as well as the observed narrow molecular weight distributions (Figure 1a) even at molecular weights as low as M_n = 3.1 kg/mol (**Figure 3.2b**).

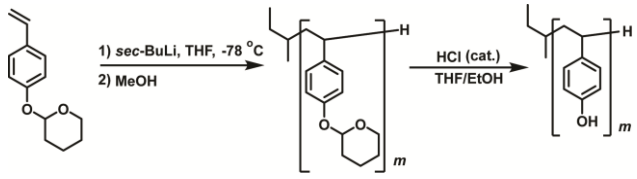

Figure 3.1. Synthesis of Narrow Dispersity PHS by Anionic Polymerization of OTHPSt and Subsequent Acid-Catalyzed Deprotection.

Table 3.1. Molecular Characterization of P(OTHPSt) Homopolymers from Anionic Polymerization.

Sample	M_n *(kg/mol)*[a]	M_n *(kg/mol)*[b]	$Đ$[a]	T_g *(°C)*
1H	3.1	3.1	1.03	103
2H	5.6	7.5	1.04	114
3H	6.4	8.0	1.03	114
4H	10.4	13.6	1.04	122
5H	37.5	-[c]	1.02	126

[a]Determined by GPC using polystyrene standards. [b]Determined by quantitative ^{1}H NMR end group analysis comparing the *sec*-butyl methyl peaks from 0.5-0.8 ppm with the acetal peak at 5.3 ppm. [c]End group could not be accurately integrated due to low ^{1}H NMR peak intensity.

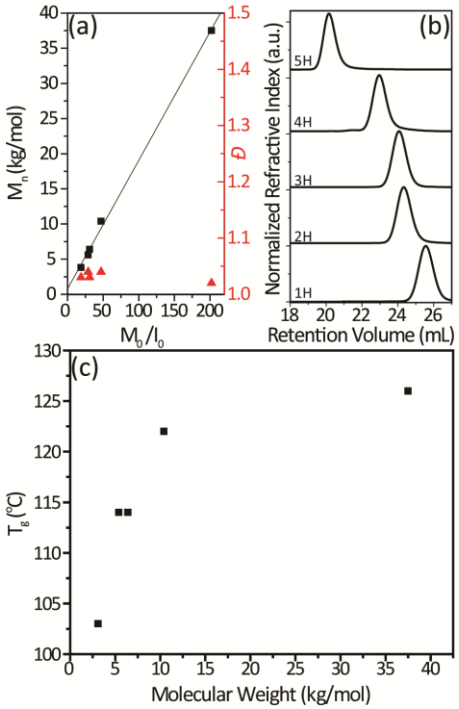

Figure 3.2. (*a*) Experimentally determined M_n *versus* the initial monomer to initiator ratio ($[M_0]/[I_0]$), and the resulting dispersities $Đ$. (*b*) GPC chromatograms for the P(OTHPSt) homopolymers demonstrating narrow dispersities throughout the molecular weight range

examined (data has been shifted vertically for clarity). (*c*) A plot of T_g versus M_n for P(OTHPSt), showing a plateau T_g ~ 126 °C when $M_n \geq 15$ kg/mol.

In order to assess the thermal stability and melt processability of P(OTHPSt), we conducted thermogravimetric analysis (TGA) and differential scanning calorimetry (DSC) on these homopolymers. TGA indicates a two-step thermal decomposition, with the onset of the first decomposition T_{d1} ~ 255 °C and the second decomposition T_{d2} ~ 350 °C (**Figure 3.S1**). Approximately 35% of the total sample weight is lost in the first step, which quantitatively correlates with the loss of the THP ring. Hence, thermal deprotection of the THP group occurs upon annealing the polymer at elevated temperatures. DSC measurements indicate that the T_g's for these homopolymers range from 103-126 °C, showing a plateau value close to ~ 126 °C when $M_n \geq 15$ kg/mol (**Figure 3.1c**, see **Figure 3.S2** for DSC heating curves).

Spectroscopic Characterization of OTHPSt monomer and P(OTHPSt) homopolymer

Given the observed glassy nature of the P(OTHPSt) homopolymers at low molecular weights and the presence of a stereo-center in the THP ring of every monomer unit, we sought to gain deeper molecular insights into the conformational behavior of the OTHPSt monomer and its homopolymers using solution ^{1}H NMR spectroscopy. Detailed assignments of the peaks for either the monomer, or the homopolymers have not been reported so far. ^{1}H NMR spectra for the monomer OTHPSt indicate that the proton located on the carbon stereocenter between the two acetal oxygens (**g** proton in **Figure 3.S3**) is split into a triplet with J = 3.3 Hz, strongly suggesting an equatorial orientation with slow ring inversion on the NMR time scale at room temperature. The strong axial preference of the sterically demanding alkoxy phenyl group aptly demonstrates how the anomeric effect can dictate ring conformations.[30] The protons on the methylene adjacent

to the ring oxygen (**k** protons in **Figure 3.S3**) show a large difference in chemical shift with the downfield resonance exhibiting a ddd coupling pattern (J = 11.3, 9.3, 3.2 Hz) and the upfield resonance exhibiting a dtd pattern (J = 11.3, 4.1, 1.6 Hz). The 11.3 Hz splitting likely arises from the geminal coupling between the two protons, while the Karplus relationship shows that vicinal protons with large dihedral angles or eclipsed conformations have larger coupling constants. Thus, the downfield resonance for **k** corresponds to the axial proton and upfield corresponds to the equatorial proton. To definitively assign the six aliphatic proton resonances (δ 1.5–2.0 ppm) and the aromatic protons, we used two-dimensional Nuclear Overhauser Effect Spectroscopy (NOESY) to garner information on through-space dipole-dipole interactions over distances ≤ 5 Å (Figure S3). As would be expected from the resonance structures of the monomer, the aromatic protons *ortho* to the oxygen (protons **e**) are shifted upfield relative to the *meta* protons (protons **d**).

With the information gained from analysis of the monomer spectrum, we examined the 2D-NOESY spectrum for P(OTHPSt), which exhibited similar features as the monomer (**Figure 3.3**). Protons **g** and **k** are still easily distinguished while **h**, **i**, and **j** remain in their relative locations although the lines are broadened as expected for a polymer. One stark difference from the monomer peak assignments is that the two aromatic resonances have essentially switched position with **e** being downfield of **d**, most likely due to the polymer backbone strongly shielding the protons *ortho* to it. Due to the line broadening arising from the increased conformational variability of the polymeric species in solution, it is difficult to determine if the same preference for the axial position is maintained in the polymer as in the monomer. While these NMR studies provide previously unreported details of structural characterization for the monomer and the homopolymer, the fact that these are solution derived structures limit its direct translation to bulk properties. However from experimental observations by DSC it is clear that the tetrahydropyran (THP) ring

confers rigidity upon the polymer, similar to the rigidity afforded by cyclohexyl substituents on other polymers (e.g. cyclohexyl methacrylate *vs* *n*-hexyl methacrylate).[31] As compared to another acetal protected hydroxystyrene, poly(*p*(1-ethoxy ethoxy)styrene), that bears a flexible and acyclic side-chain, the T_g of P(OTHPSt) is over 100 °C higher.[32]

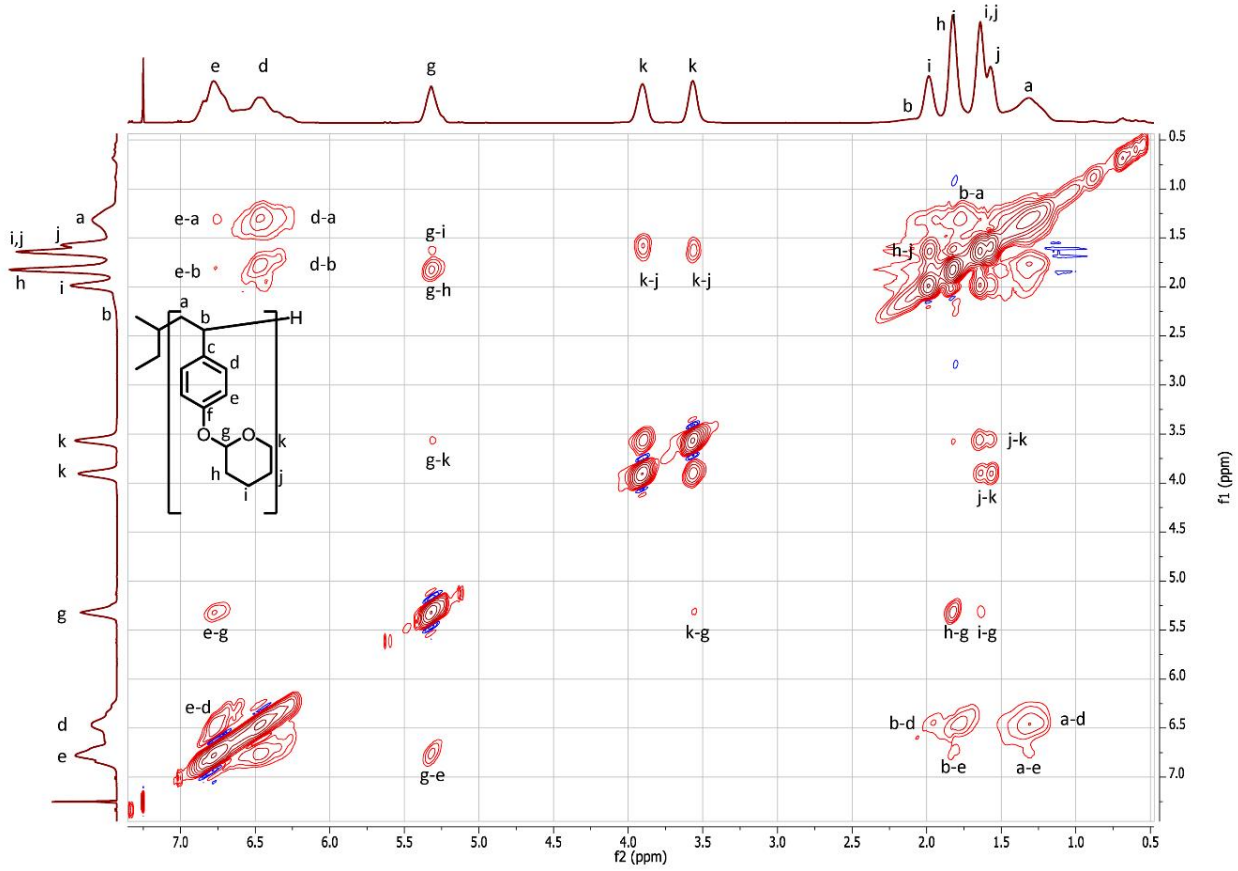

Figure 3.3. 2D-NOESY spectrum for P(OTHPSt) (2H), showing full assignment of the proton peaks. Note that backbone proton b lies under the sharper i and h resonances (2.2 to 1.7 ppm).

Synthesis and Molecular Characterization of P(HS-*b*-S) Block Copolymers

We synthesized a series of BCPs with M_n = 6.2–50.4 kg/mol and PHS volume fractions f_{PHS} ~ 0.3–0.6 by the sequential addition of styrene to the living P(OTHPSt) anion after withdrawing an aliquot of the first segment for molecular weight analysis (**Figure 3.4**).[27] Upon

terminating the polymerization with methanol and subsequent isolation, the resulting BCPs were characterized at a molecular level by a combination of GPC, ^{1}H NMR spectroscopy, TGA and DSC both prior to and after deprotection of the THP moiety (**Table 3.2**).

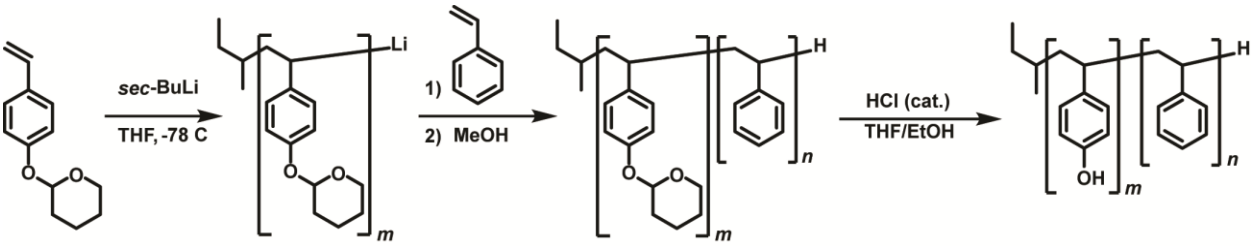

Figure 3.4. Synthesizing P(OTHPSt-*b*-S) and P(HS-*b*-S) BCPs by Sequential Living Anionic Polymerization.

Table 3.2. Molecular and Morphological Characteristics of P(OTHPSt-*b*-S) BCPs.

Sample	$M_{n,OTHPSt}$ ***(kg/mol)***[a]	$M_{n,overall}$ ***(kg/mol)***[a]	$Đ$[a]	f_{PHS}[b]	**N**[c]	T_g (^{o}C)[d]	T_g (^{o}C)[e]	L_0 **(morphology)**[f]
4k-2k	4.3 (6.5)[g]	6.2 (9.0)[g]	1.14	0.58	85[g]	96, 107	157, 107	Disordered
7k-6k	6.8 (12.5)[g]	13.0 (17.9)[g]	1.07	0.55	116	96, 109	165, 117	11.8 nm (LAM)
9k-25k	9.0	33.8	1.04	0.26	365	90, 108	177, 110	23.4 nm (HEX)
13k-21k	13.3	33.2	1.04	0.4	326	110	181, 110	21.7 nm (LAM)
16k-35k	16.0	50.4	1.09	0.33	519	107	180, 107	33.1 nm (LAM)

[a] Determined by SEC using polystyrene standards. [b] PHS volume fraction determined using the homopolymer densities at 25 °C: ρ(PHS) = 1.16 g/cm^3 and ρ(PS) = 1.05 g/cm^3.[24] [c] Total segment density normalized degree of polymerization based on 118 Å^3 reference volume. [d] P(OTHPSt-*b*-S) T_g determined by DSC during the third heating cycle. [e] P(HS-*b*-S) T_g determined by DSC during the third heating cycle. [f] Determined by synchrotron SAXS at 25 °C. [g] Determined by quantitative ^{1}H NMR end group analysis comparing the *sec*-butyl methyl peaks from 0.5-0.8 ppm with the acetal peak at 5.3 ppm.

The thermal characteristics for the protected and deprotected diblocks are tabulated in **Table 3.2**. The THP group in each of these protected BCPs was removed by acidolysis with 0.1 M HCl in THF/ethanol (50:50 *v/v*) at 22 °C. Quantitative deprotection of the THP moieties along the block copolymer chains was verified using ^{1}H NMR (**Figure 3.4**). After deprotection, TGA indicates a single degradation step with an onset near 350 °C (**Figure 3.S4**) that is consistent with the polymer backbone decomposition observed in the above P(OTHPSt) homopolymers. The fully deprotected polymer exhibited the higher T_g's expected for PHS at ~180 ^{o}C (**Figure 3.5**). We note that each of these diblock copolymers exhibits two distinct glass transition temperatures corresponding to those of the PHS and PS blocks, which suggests the possibility that they are microphase separated. However, Lodge and co-workers have previously noted that the presence of two T_g's in the absence of any X-ray scattering data does not necessarily imply the melt microphase separation of a block copolymer.[33]

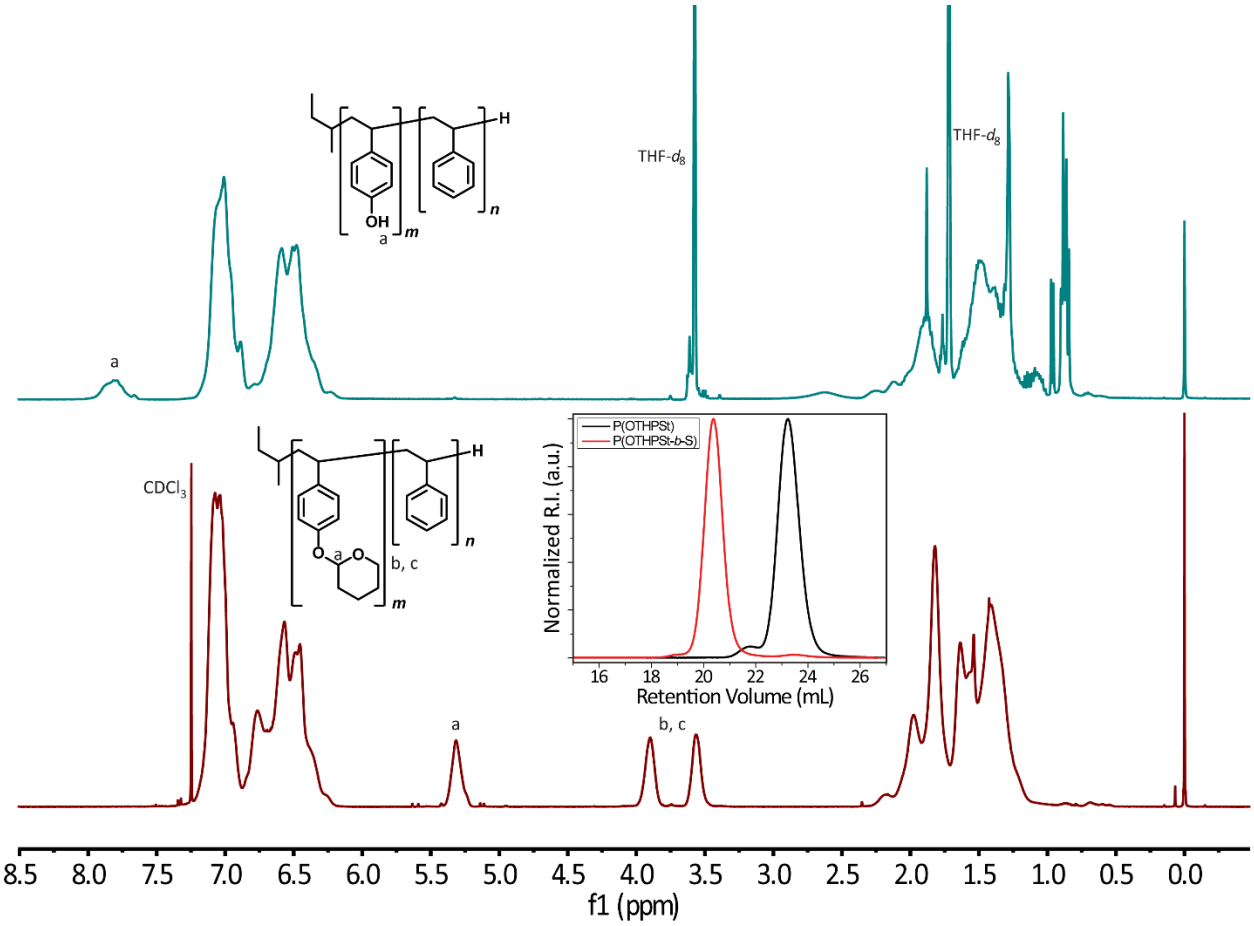

Figure 3.4. ^{1}H NMR spectra of **9k-25k** prior to (bottom, $CDCl_3$) and after (top, THF-d_8) deprotection with 0.1 M HCl in THF/ethanol (50:50 *v/v*). Inset shows GPC profiles of the quenched P(OTHPSt) aliquot prior to styrene addition (*black*) and the resulting P(OTHPSt-*b*-S) diblock **9k-25k** (red) from the sequential chain extension block copolymerization.

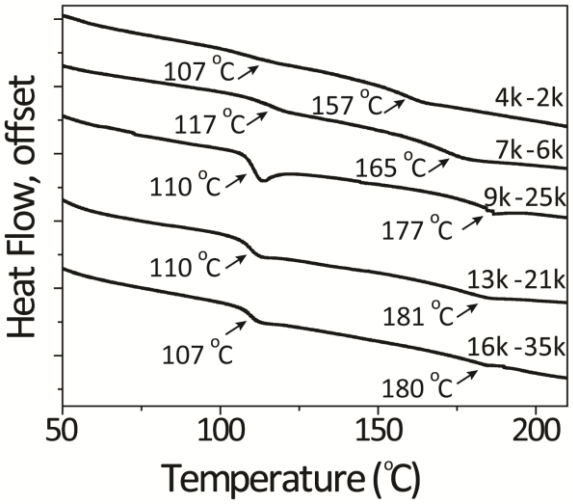

Figure 3.5. DSC heating curves for the deprotected BCPs showing the expected increase in T_g with increasing PHS block M_n, which reaches a plateau value of ~180 °C. Data has been shifted vertically for clarity.

Morphological Characterization of the BCPs

Given the interest in P(HS-*b*-S) diblock copolymers as self-assembling nanotemplates with small domain sizes,[34-38] we studied the morphological behavior of the diblocks listed in **Table 3.2**. We systematically examined the self-assembly of both the protected and deprotected BCPs using small angle X-ray scattering (SAXS). None of the solvent-cast protected BCPs showed any signs of microphase separation by SAXS, hence the samples were annealed under vacuum at 160 °C for various amounts of time to partially thermally deprotect the P(OTHPSt) blocks (*vide infra*). After annealing for only 3 h, **13k-21k** showed characteristic scattering peaks for a lamellar morphology. Increasing the annealing times led to sharper peaks and larger domain spacing (**Figure 3.6**), consistent with an increase in the chemical incompatibility of the segments in the BCPs. Thus, the annealed samples were dissolved in THF-d_8 and characterized by ^{1}H NMR spectroscopy (**Figure 3.S5**). NMR revealed the deprotection of the THP group during thermal annealing. After 24 h at

160 °C, over 90% of THP was removed in a first-order reaction (Figure 5, inset), as discerned from the linearity of the $\ln([OTHP]_t/[OTHP]_0)$ versus time curve. As the samples were easily re-dissolved for NMR analysis, this thermal deprotection is clearly a clean process with no side reactions that yields microphase separated BCP morphologies *in situ* as well as at a temperature below T_g of one of the blocks. This interesting observation furnishes a new means for dynamically dictating the desired morphology by controlling the extent of deprotection, and the loss of dihydropyran has a plasticizing effect on the BCP film which further facilitates long-range ordering of the morphology.

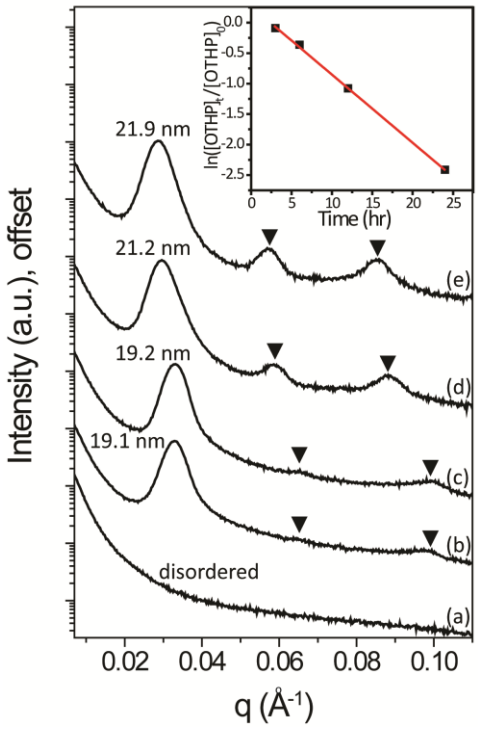

Figure 3.6. SAXS curves for protected **13k-21k** annealed at 160 °C for (a) 1 hr, (b) 3 hrs, (c) 6 hrs, (d) 12 hrs and (e) 24 hrs (data has been shifted vertically for clarity), where the peak markers indicated the calculated peak positions for a lamellar morphology based on the position of the principal scattering peak. Inset shows plot of $\ln([OTHP]_t/[OHTP]_0)$ as a function of annealing time

as measured by ^{1}H NMR spectroscopy of the acetal proton at 5.3 ppm vs the total aryl protons demonstrating the first-order nature of the thermal deprotection reaction.

While the ability to thermally deprotect the THP group during annealing may be beneficial for *in situ* thin film self-assembly, we employed the chemical deprotection method in producing samples for complete morphological characterization of P(HS-*b*-S) phase behavior. All of the chemically deprotected diblocks were annealed at 160 ^{o}C for 48 h under vacuum and shown to microphase separate into phase-segregated morphologies by SAXS, except for **4k-2k** which exhibited only correlation hole-scattering associated with a disordered diblock copolymer (**Figure 3.7**). 160 ^{o}C was chosen as a compromise between annealing kinetics and the propensity for ordered PHS BCPs to self cross-link when heated above their T_g.[39] Hence, the morphologies observed may not reflect the true equilibrium morphology. **7k-6k**, **13k-21k,** and **16k-35k** showed lamellar morphologies while **9k-25k** formed hexagonally-packed cylinders of PHS in a PS matrix. The domain size ranges from L_0 = 33.1 nm for **16k-35k** to 11.8 nm for **7k-6k**. This large range of accessible L_0 values suggests that the magnitude of the χ parameter between PS and PHS is quite large. Interestingly, the processing conditions can have a large effect on the resulting BCP morphology. A sample of chemically deprotected 13k-21k cast from THF solution demonstrates an ordered lamellar morphology with a L_0 ~19 nm (**Figure 3.S6**). Annealing the sample at 160 ^{o}C causes the SAXS profile to become broad, indicative of a microphase segregated morphology lacking long-range order (**Figure 3.7**). Thermal deprotection of the P(OTHPSt-*b*-S) 13k-21k BCP at 160 ^{o}C for 72 h yields a well-ordered lamellar morphology with a L_0 = 21.9 nm and a deprotection extent > 99% by ^{1}H NMR spectroscopy (**Figure 3.S6**). Thus, the relatively low annealing temperature may not enable adoption of the equilibrium structure for the higher molecular weight BCPs such as 13k-21k and 16k-35k.

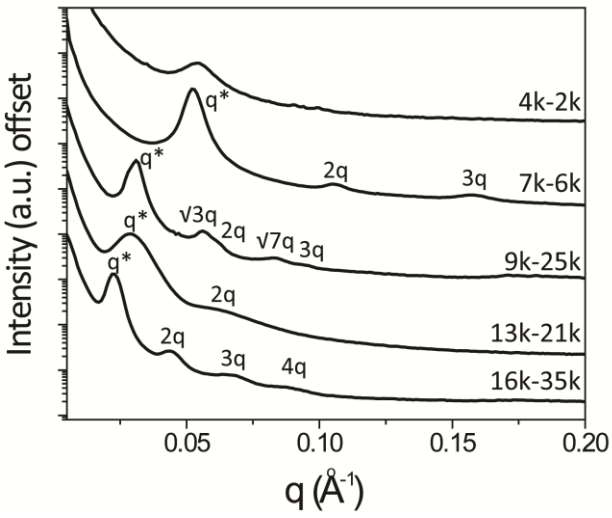

Figure 3.7. Synchrotron SAXS patterns for deprotected BCPs annealed at 160 °C for 48 h under vacuum. Data has been shifted vertically for clarity.

Representative transmission electron microscopy (TEM) images of the two morphologies formed by these polymers were obtained by using two different staining agents (**Figure 3.8**). Attempts to stain these samples with RuO_4 vapor did not yield the preferential staining required for high contrast TEM imaging, as both blocks became overstained in only a 5 min exposure to the metal oxide vapor. **9k-25k** was successfully stained using Cs_2CO_3(aq), which led to incorporation of Cs^+ ions into the PHS domain and **13k-21k** was stained with I_2(*g*) as lamellae are easier to visualize than dot structures. The periodicities measured from the images match well with those ascertained from the synchrotron SAXS data.

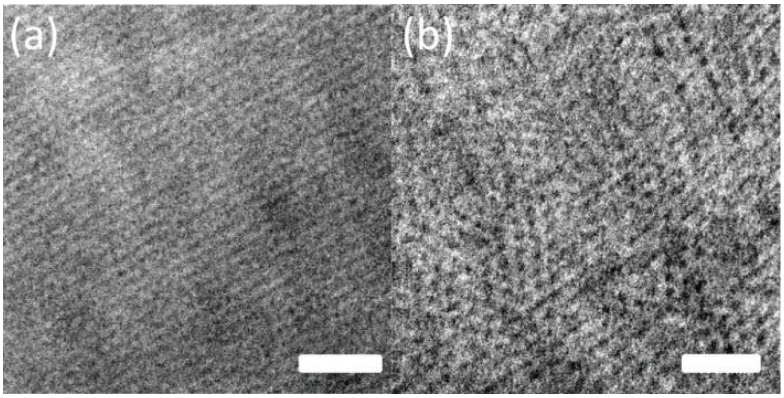

Figure 3.8. TEM micrographs of (a) **13k-21k** and (b) **9k-25k**. PHS is the darker phase. Scale bar is 100 nm. Periodicities are 21.5 nm for (a) and 22.5 nm for (b).

Quantitative Determination of $\chi_{HS/S}$

Domain sizes as small as approximately L_0 ~14 nm have been previously reported in P(HS-*b*-S) at temperatures up to 300 °C,[24] which have been attributed to the large χ = 0.68 measured in polymer blend miscibility studies.[16, 23, 40] However, there are discrepancies in the reported $\chi_{HS/S}$ values in the literature. The aforementioned $\chi_{HS/S}$ in conjunction with mean-field theory implies that a symmetric copolymer would microphase separate at overall copolymer degree of polymerization as low as N = 15, yet this claim contradicts our experimental observation that **4k-2k** with N = 85 is melt disordered. The value of N used was determined from quantitative ^{1}H-NMR end-group analysis. The M_n values obtained from end group analysis are quite accurate as the initiator peaks (0.5-0.8 ppm) for the low molecular weight samples do not have any overlap with other peaks (see NOESY **Figure 3.3** and **Figure 3.S7**). For the lowest molecular weight used for $\chi_{HS/S}$ determination, SEC with light scattering analyses were also conducted to determine the absolute molecular weight (9.0 kg/mol from NMR end group analysis, 9.2 kg/mol from SEC with light scattering), which agrees quite closely to the end group analysis values. Using this sample,

we opted to directly estimate the $\chi(T)$ using mean-field theory analysis of temperature-dependent correlation-hole SAXS data for this polymer.[6] The correlation-hole scattering patterns for **4k-2k** were acquired at T = 170, 190, 210 and 230 ^{o}C (above the T_g's of the BCP). These data were fit using the equations of state governing a disordered BCP (see **section 3.6** for details of the calculation). Plotting the calculated χ values as a function $1/T$ (in degrees K) yields the temperature-dependent expression $\chi_{HS/S}(T) = (4.39 \pm 0.83)/T + (0.109 \pm 0.002)$ (**Figure 3.9a**). Thus, the $\chi_{HS/S}$ is largely independent of temperature due to large entropic contributions to the free energy of mixing. While P(S-*b*-MMA) copolymer phase behavior is governed by a similarly weak temperature-dependent χ parameter, there is no definitive explanation for the observed small enthalpic and large entropic contributions.[41] At a reference temperature of 150 °C, the $\chi_{S/MMA} \sim 0.028$ while $\chi_{HS/S} = 0.119$ is four times larger. We note that although our observed $\chi_{HS/S}$ is much smaller than that previously reported, the value seems reasonable and comparable to other diblock copolymer systems that are known to furnish small microphase separated domain spacings useful in nanotemplating applications. We also note that Maurer *et al*. have previously reported that a single χ parameter may not consistently apply to both polymer blend and block copolymer phase behavior.[42] For visual comparison, we have plotted $\chi(T)$ for three other BCP systems containing a PS block in **Figure 3.9b** as compared to the results presented here for P(HS-*b*-S).[15, 41]

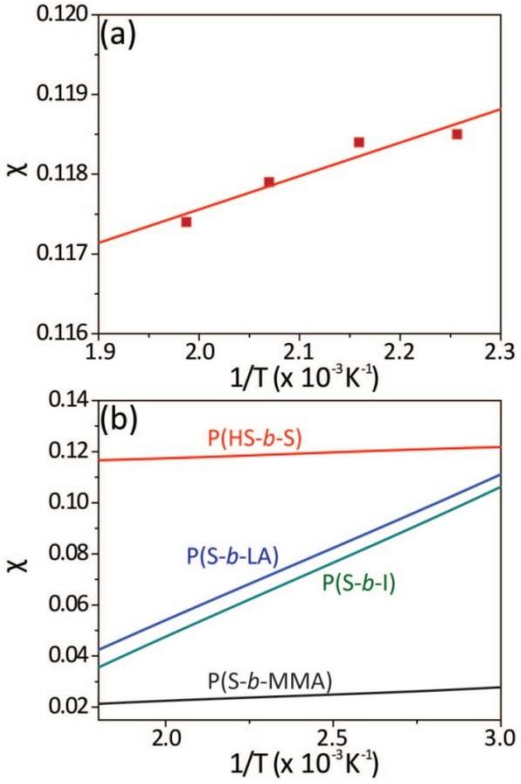

Figure 3.9. (a) $\chi_{HS/S}$ vs $1/T$ plotted using the values obtained from fitting the temperature-dependent correlation-hole SAXS data and the line of best fit. (b) χ vs $1/T$ plotted for three other styrene-containing BCP systems.

3.5. Conclusions

In summary, we have used living anionic polymerization of a tetrahydropyranyl acetal protected 4-hydroxystyrene (OTHPSt) to synthesize a series of P(OTHPSt) homopolymers and P(HS-*b*-S) BCPs with excellent molecular weight and dispersity control over a broad M_n range. The high T_g of P(OTHPSt) allows for its facile preparation, isolation, and purification as a powder. These BCPs may be thermally deprotected by a controlled first-order reaction upon annealing at 160 °C under vacuum, which suggests a means for dynamically tuning the microphase separated morphology in both bulk and thin films by analogy to poly(*tert*-butyl acrylate) block copolymers.[43] For preparative purposes, complete and rapid deprotection may also be affected using dilute

HCl(*aq*). SAXS and TEM studies demonstrated that these P(HS-*b*-S) copolymers self-assemble into well-defined lamellar and hexagonally-packed cylindrical morphologies. Mean-field theory fitting of the temperature-dependent correlation-hole scattering derived a P(HS-*b*-S) disordered diblock enabled the determination of $\chi_{HS/S}(T) = (4.39 \pm 0.83)/T + (0.109 \pm 0.002)$, which is four times larger than $\chi_{MMA/S}$ and exhibits similarly large entropic and small enthalpic contributions to the free energy of mixing. Although it is lower than most of the values previously reported in the literature, the $\chi_{HS/S}(T)$ is consistent with the experimentally observed molecular weight threshold for microphase separation anticipated from mean-field theory. On the basis of this temperature-dependent $\chi_{HS/S}(T)$, we estimate that the smallest accessible domain spacing with the HS/S monomer system is $L_0 = 11.6$ nm. Thus, this well-defined anionic polymerization route provides access to high χ PHS-based BCPs with very small domain sizes.

3.6. Supporting Information

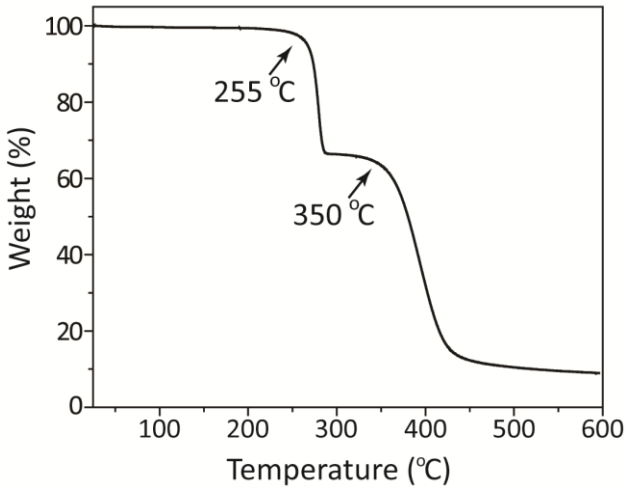

Figure 3.S1. TGA curve for P(OTHPSt) polymer 4H demonstrating two thermal decomposition waves: (1) T_{d1} ~ 255 °C corresponding to the thermal deprotection of the THF moiety, and (2) T_{d2} ~ 350 °C corresponding to the PS backbone degradation.

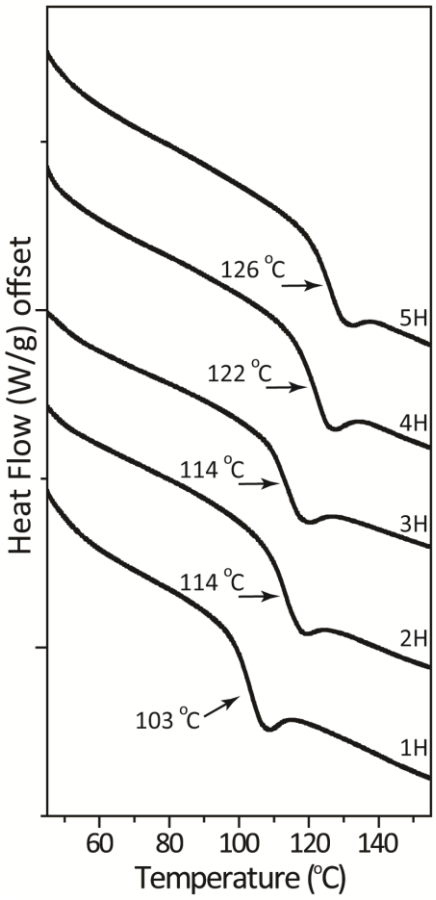

Figure 3.S2. DSC curves for the five P(OTHPSt) homopolymers (taken from the third heating cycle, endo is down), showing that T_g increases to a plateau value of ~ 126 °C as the homopolymer M_n increases.

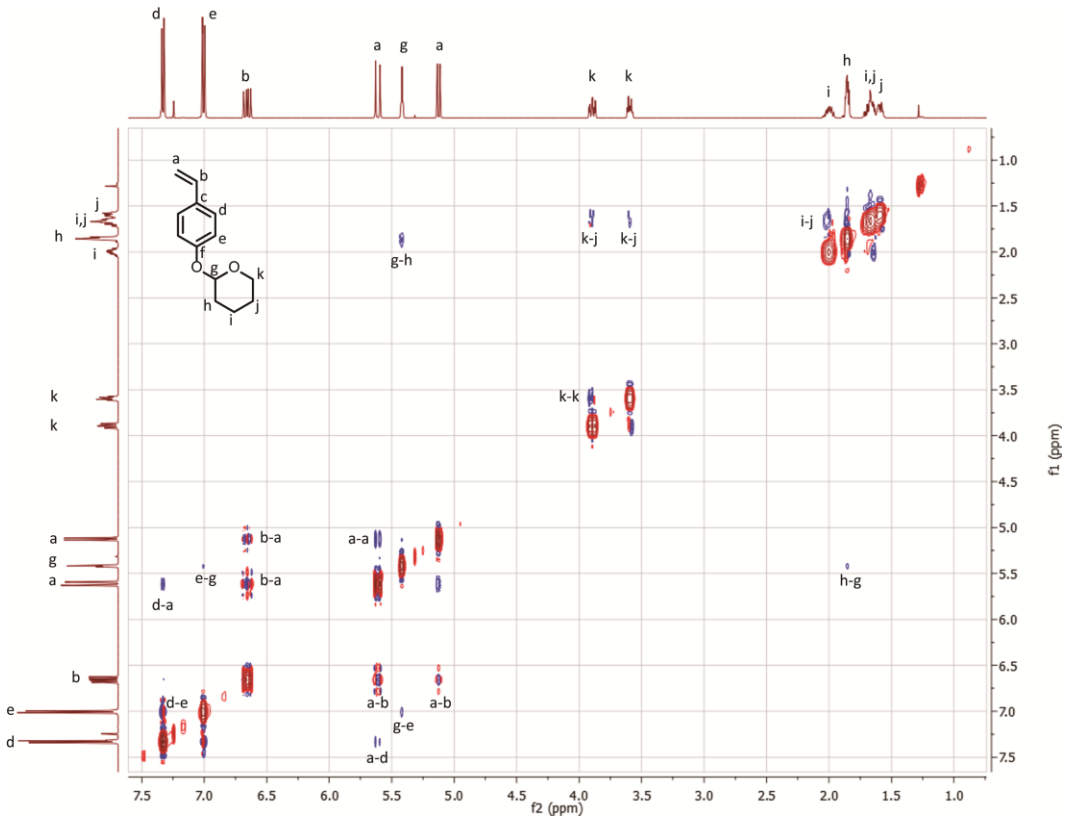

Figure 3.S3. 2D-NOESY plot for OTHPSt showing full proton assignments.

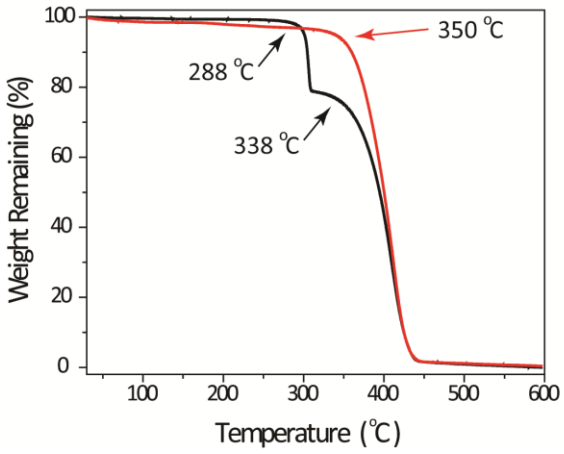

Figure 3.S4. TGA curves for protected P(OTHPSt-*b*-S) (*black*) and deprotected P(HS-*b*-S) (*red*) **13k**-**21k** with degradation onset temperatures listed. These data are consistent with the observed thermal deprotection of the THP moiety at ~ 255 °C.

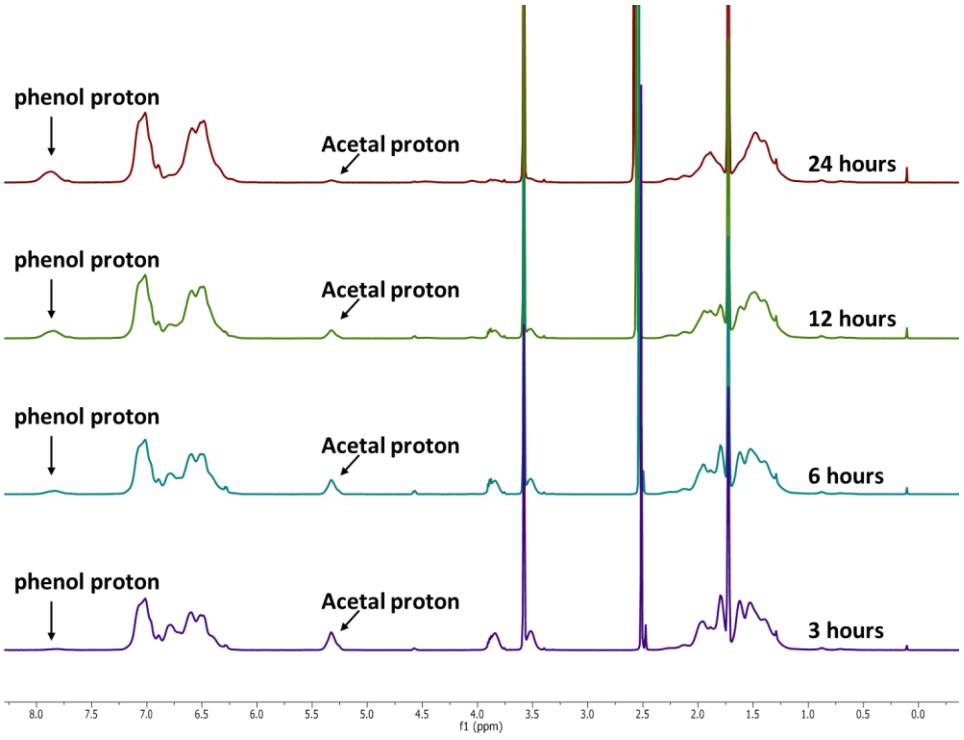

Figure 3.S5. ^{1}H NMR spectra for protected **13k-21k** vacuum annealed at 160 °C from 3 h to 24 h.

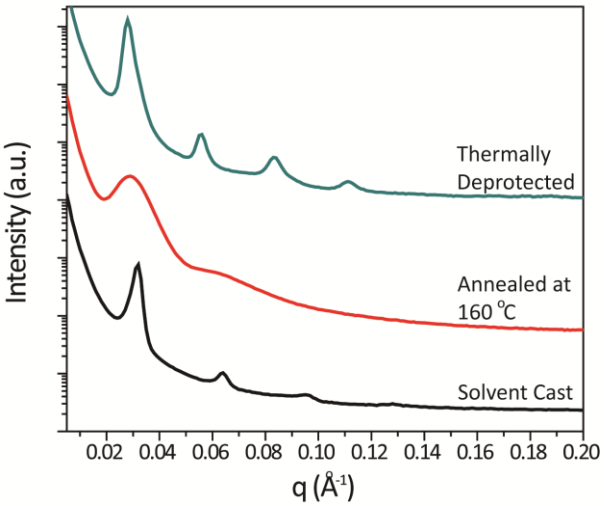

Figure 3.S6. Synchrotron SAXS curves for (black) chemically deprotected 13k-21k cast from THF solution, (red) the solvent cast sample annealed at 160 °C for 48 hours and (teal) protected

13k-21k cast from THF solution and annealed at 160 °C for 72 hours (>99% deprotection by NMR).

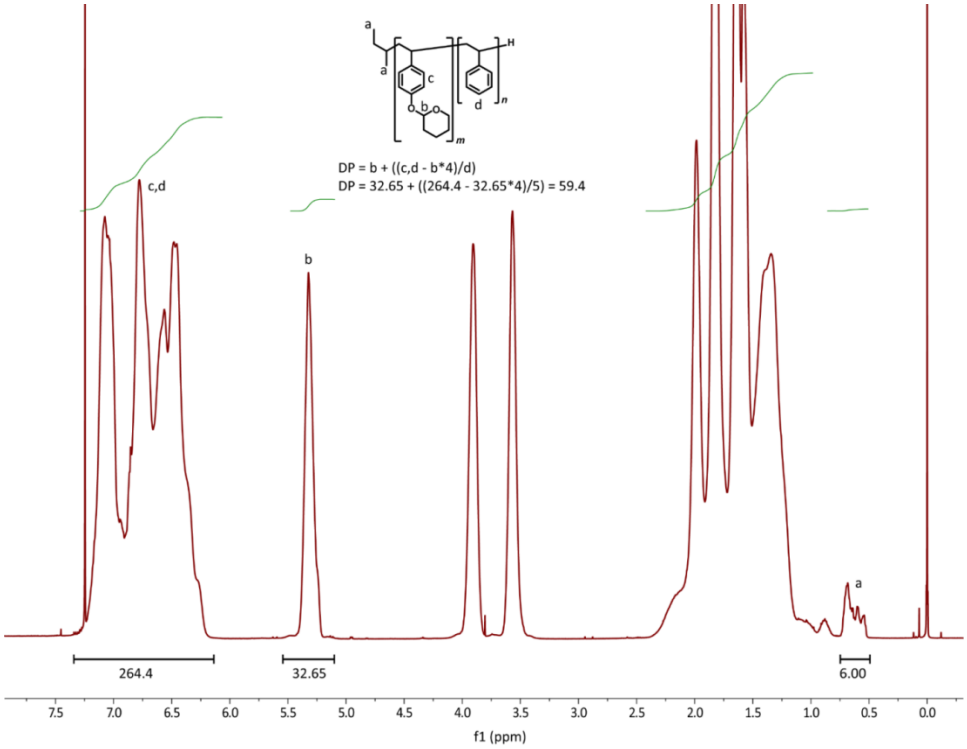

Figure 3.S7. ^{1}H NMR spectrum of **4k-2k** showing the end group analysis. The chemical DP of 59.4 calculated above corresponds to a volume normalized DP of 85.

Determination of $\chi_{HS/S}$ by synchrotron SAXS

The equations governing the disordered state scattering of a block copolymer are shown below.

$$I(q) = \frac{A_0}{\frac{S(q)}{W(q)} - 2\chi}$$

$$S(q) = \langle S_{PS,PS} \rangle + 2\langle S_{PS,PHS} \rangle + \langle S_{PHS,PHS} \rangle$$

$$W(q) = \langle S_{PS,PS} \rangle \cdot \langle S_{PHS,PHS} \rangle - \langle S_{PS,PHS} \rangle^2$$

$$\langle S_{X,X}(q) \rangle = r_c {f_X}^2 {g^{(2)}}_X(q)$$

$$\langle S_{PS,PHS}(q) \rangle = r_c f_{PS} f_{PHS} {g^{(1)}}_{PS}(q) {g^{(1)}}_{PHS}(q)$$

$$r_c = \frac{(v_{PS}N_{PS} + v_{PHS}N_{PHS})}{(v_{PS} \cdot v_{PHS})^2}$$

$$g^{(1)}{}_X(q) = \frac{1}{y_X(q)} \cdot \left\{1 - [y_X(q) \cdot (Đ_X - 1) + 1]^{-(Đ_X - 1)^{-1}}\right\}$$

$$g^{(2)}{}_X(q) = \frac{2}{y_X(q)^2} \cdot \left\{-1 + [y_X(q) \cdot (Đ_X - 1) + 1]^{-(Đ_X - 1)^{-1}}\right\}$$

$$y_X(q) = \frac{N_X {a_X}^2}{6} \cdot q^2$$

where I(q) is the scattered intensity from the diblock copolymer melt, S(q) and W(q) together are the correlation function of the diblock copolymer, A_0 is a fitting variable, r_c is the molar volume normalized degree of polymerization of the diblock copolymer, $g^{(i)}{}_x$(q) is a modified Debye function, and y_x(q) is the dimensionless wave vector. Additionally, f is the volume fraction occupied by a homopolymer segment, v is the molar volume calculated using the bulk densities for each block at 140 °C (ρ(PHS) = 1.079 g/cm^3, ρ(PS) = 0.969 g/cm^3), N is the volume degree of polymerization calculated using a 118 Å^3 reference volume, $Đ$ is the dispersity index, and a is the statistical segment length (normalized by the homopolymer melt density).

Table 3.S1. Fixed parameters used for determination of $\chi_{HS/S}$

Segment	***f***	***N***	***v* (cm^{3}mol^{-1})**	***Đ***
PS	0.44	37.4	107.5	1.10
PHS	0.56	47.4	111.4	1.04

Because the diblock copolymer is very small and is expected to have a large χ parameter, the copolymer chains in the disordered phase remains stretched. In order to accommodate this high degree of chain stretching (non-Gaussian chain conformations), the statistical segment lengths of each homopolymer segment are allowed to vary in the fitting routine. In addition to fitting the statistical segment lengths of each block, the background intensity, scattering intensity and χ parameter were also adjustable. The final fitted values of the statistical segment length are a(PS) = 7.6 Å, and a(PHS) = 9.8 Å.

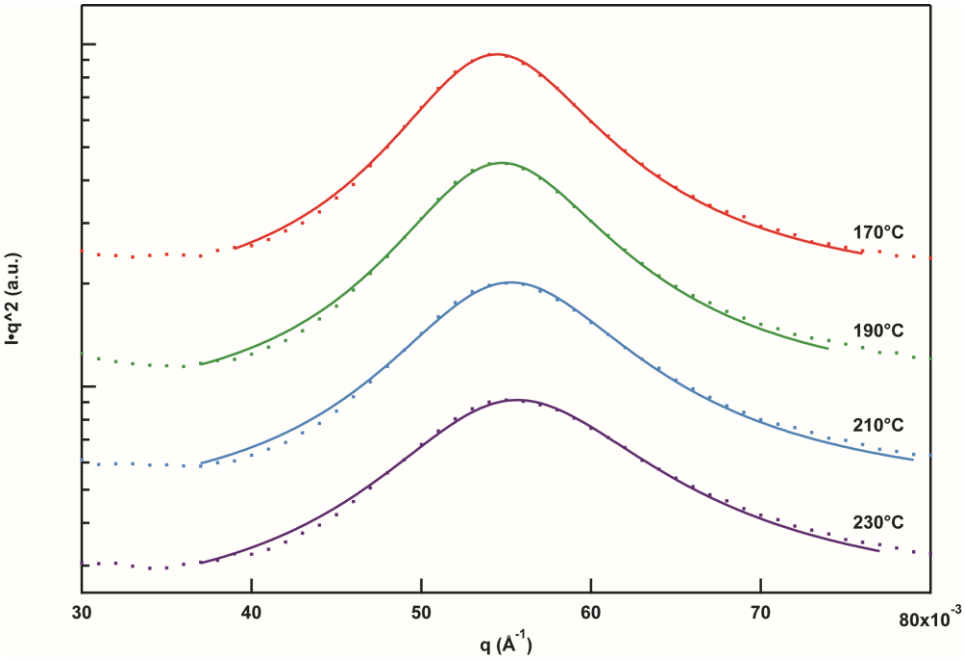

Figure 3.S8. Temperature-dependent synchrotron small-angle x-ray scattering data (dots) with disordered scattering fits (lines).

The temperature-dependent X-ray scattering is shown in **Figure 3.18** along with the theoretical fits to determine χ. As the temperature increases, the correlation-hole scattering intensity decreases and the peak width increases corresponding to a decrease in interaction parameter. The fitting values for the temperature-dependent $\chi(T)$ parameters at the corresponding temperatures are shown in **Table 3.S2**.

Table 3.S2. χ(T) values from mean-field fitting of the correlation-hole scattering for	
Temperature (°C)	**$\chi_{HS/S}$(T)**
170	0.1185
190	0.1184
210	0.1179
230	0.1174

From these values, we find that $\chi_{HS/S}(T) = (4.39 \pm 0.83)/T + (0.109 \pm 0.002)$.

3.7. References

1. Stoykovich, M. P.; Nealey, P. F., Block Copolymers and Conventional Lithography. *Mater. Today* **2006,** *9* (9), 20-29.

2. Hawker, C. J.; Russell, T. P., Block Copolymer Lithography: Merging "Bottom-Up" with "Top-Down" Processes. *MRS Bull.* **2005,** *30*, 952-966.

3. Marencic, A. P.; Register, R. A., Controlling Order in Block Copolymer Thin Films for Nanopatterning Applications. *Annu. Rev. Chem. Biomol. Eng.* **2010,** *1*, 277-297.

4. Hamley, I. W., Ordering in Thin Films of Block Copolymers: Fundamentals to Potential Applications. *Prog. Polym. Sci.* **2009,** *34*, 1161-1210.

5. Bates, F. S.; Fredrickson, G. H., Block Copolymer Thermodynamics: Theory and Experiment. *Annu. Rev. Phys. Chem.* **1990,** *41*, 525-557.

6. Leibler, L., Theory of Microphase Separation in Block Copolymers. *Macromolecules* **1980,** *13*, 1602-1617.

7. Fredrickson, G. H.; Bates, F. S., Dynamics of Block Copolymers: Theory and Experiment. *Annu. Rev. Mater. Sci.* **1996,** *26*, 501-550.

8. Semenov, A. N., Theory of Block Copolymer Interfaces in the Strong Segregation Limit. *Macromolecules* **1993,** *26*, 6617-6621.

9. Matsen, M. W.; Bates, F. S., Unifying Weak- and Strong-Segregation Block Copolymer Theories. *Macromolecules* **1996,** *29* (4), 1091-1098.

10. Hashimoto, T.; Shibayama, M.; Kawai, H., Domain-Boundary Structure of Styrene-Isoprene Block Copolymer Films Cast from Solution. 4. Molecular-Weight Dependence of Lamellar Microdomains. *Macromolecules* **1980,** *13*, 1237-1247.

11. Hasegawa, H.; Tanaka, H.; Yamasaki, K.; Hashimoto, T., Bicontinuous microdomain morphology of block copolymers. 1. Tetrapod-network structure of polystyrene-polyisoprene diblock polymers. *Macromolecules* **1987,** *20*, 1651-1662.

12. Cheng, J. Y.; Sanders, D. P.; Truong, H. D.; Harrer, S.; Friz, A.; Holmes, S.; Colburn, M.; Hinsberg, W. D., Simple and Versatile Methods to Integrate Directed Self-Assembly with Optical Lithography Using a Polarity-Switched Photoresist. *ACS Nano* **2010,** *4*, 4815-4823.

13. Han, E.; Kim, M.; Gopalan, P., Chemical Patterns from Surface Grafted Resists for Directed Assembly of Block Copolymers. *ACS Nano* **2012,** *6*, 1823-1829.

14. Thurn-Albrecht, T.; Steiner, R.; DeRouchey, J.; M. Stafford, C.; Huang, E.; Bal, M.; Tuominen, M.; Hawker, C. J.; Russell, T. P., Nanoscopic Templates from Oriented Block Copolymer Films. *Adv. Mater.* **2000,** *12*, 787-791.

15. Widin, J. M.; Kim, M.; Schmitt, A. K.; Han, E.; Gopalan, P.; Mahanthappa, M. K., Bulk and Thin Film Morphological Behavior of Broad Dispersity Poly(styrene-b-methyl methacrylate) Diblock Copolymers. *Macromolecules* **2013,** *46*, 4472-4480.

16. Russell, T. P.; Hjelm, R. P.; Seeger, P. A., Temperature dependence of the interaction parameter of polystyrene and poly(methyl methacrylate). *Macromolecules* **1990,** *23*, 890-893.

17. Jung, Y. S.; Chang, J. B.; Verploegen, E.; Berggren, K. K.; Ross, C. A., A Path to Ultranarrow Patterns Using Self-Assembled Lithography. *Nano Lett.* **2010,** *10*, 1000-1005.

18. Dai, K. H.; Kramer, E. J., Determining the temperature-dependent Flory interaction parameter for strongly immiscible polymers from block copolymer segregation measurements. *Polymer* **1994,** *35*, 157-161.

19. Barton, A. F., *CRC Handbook of Solubility Parameters and Other Cohesion Parameters.* CRC Press: Boca Raton, FL, 1991.

20. Haynes, W. M., *CRC Handbook of Chemistry and Physics*. 92nd ed.; Taylor & Francis: 2011-2012.

21. Brandrup, J.; Immergut, E. H.; Grulke, E. A., *Polymer Handbook*. Fourth ed.; Wiley-Interscience: New York, 1999; Vol. 7, p 702-711.

22. Ayothi, R.; Yi; Cao, H. B.; Yueh, W.; Putna, S.; Ober, C. K., Arylonium Photoacid Generators Containing Environmentally Compatible Aryloxyperfluoroalkanesulfonate Groups. *Chem. Mater*. **2007,** *19*, 1434-1444.

23. Zhu, K. J.; Chen, S. F.; Ho, T.; Pearce, E. M.; Kwei, T. K., Miscibility of Copolymer Blends. *Macromolecules* **1990,** *23*, 150-154.

24. Han, S. H.; Kim, J. K.; Pryamitsyn, V.; Ganesan, V., Phase Behavior of Binary Blends of Block Copolymers Having Hydrogen Bonding. *Macromolecules* **2011,** *44*, 4970-4976.

25. Jarnagin, N. D.; Cheng, J.; Peters, A.; Yeh, W.-M.; Lawson, R. A.; Tolbert, L. M.; Henderson, C. L., Investigation of High χ Block Copolymers for Directed Self-Assembly: Synthesis and Characterization of PS-b-PHOST. *Proc. of SPIE* **2012,** *8323*, 832310.

26. Cushen, J. D.; Bates, C. M.; Rausch, E. L.; Dean, L. M.; Zhou, S. X.; Willson, C. G.; Ellison, C. J., Thin Film Self-Assembly of Poly(trimethylsilylstyrene-b-d,l-lactide) with Sub-10 nm Domains. *Macromolecules* **2012,** *45*, 8722-8728.

27. Sweat, D. P.; Yu, X.; Kim, M.; Gopalan, P., Synthesis of Poly(4-hydroxystyrene)-Based Block Copolymers Containing Acid-Sensitive Blocks by Living Anionic Polymerization. *J. Polym. Sci. Part A: Polym. Chem.* **2014,** *52*, 1458-1468.

28. Schmitt, A. K.; Mahanthappa, M. K. Computer Code for Materials Scientists: Igor Pro Procedures for Analyzing Dynamic Light Scattering, Rheology, and Synchrotron X-ray Scattering Data. 2013.

29. Bhattacharyya, D. N.; Lee, C. L.; Smid, J.; Szwarc, M., Reactivities and Conductivities of Ions and Ion Pairs in Polymerization Processes. *J. Phys. Chem.* **1965,** *69*, 612-623.

30. Juraisti, E.; Cuevas, G., Recent Studies of the Anomeric Effect. *Tetrahedron* **1992,** *48* (24), 5019-5087.

31. van Krevelen, D. W.; te Nijenhuis, K.; *Properties of Polymers*, 4th ed.; Elsevier: Oxford, 2009.

32. Natatello, A.; Tonhauser, C.; Frey, H., Anionic Polymerization of *para*-(1-Ethoxy ethoxy)styrene: Rapid Access to Poly(*p*-hydroxystyrene) Copolymer Architectures. *ACS Macro Lett.* **2013,** *2*, 409-413.

33. Lodge, T. P.; Wood, E. R.; Haley, J. C., Two calorimetric glass transitions do not necessarily indicate immiscibility: The case of PEO/PMMA. *J. Polym. Sci. Part B: Polym. Phys.* **2006,** *44*, 756-763.

34. Zhao, J. Q.; Pearce, E. M.; Kwei, T. K.; Jeon, H. S.; Kesani, P. K.; Balsara, N. P., Micelles Formed by a Model Hydrogen-Bonding Block Copolymer. *Macromolecules* **1995,** *28*, 1972-1978.

35. Zhao, J. Q.; Pearce, E. M.; Kwei, T. K., Binary and Ternary Blends of Polystyrene-block-Poly(p-hydroxystyrene). *Macromolecules* **1997,** *30*, 7119-7126.

36. Asari, T.; Matsuo, S.; Takano, A.; Matsushita, Y., Three-Phase Hierarchical Structures from AB/CD Diblock Copolymer Blends with Complemental Hydrogen Bonding Interaction. *Macromolecules* **2005,** *38*, 8811-8815.

37. Matsushita, Y., Creation of Hierarchically Ordered Nanophase Structures in Block Polymers Having Various Competing Interactions. *Macromolecules* **2007,** *40*, 771-776.

38. Dobrosielska, K.; Wakao, S.; Takano, A.; Matsushita, Y., Nanophase-Separated Structures of AB Block Copolymer/C Homopolymer Blends with Complementary Hydrogen-Bonding Interactions. *Macromolecules* **2008,** *41*, 7695-7698.

39. Sipos, L.; Som, A.; Faust, R.; Richard, R.; Schwarz, M.; Ranade, S.; Boden, M.; Chan, K., Controlled Delivery of Paclitaxel from Stent Coatings Using Poly(hydroxystyrene-b-isobutylene-b-hydroxystyrene) and Its Acetylated Derivative. *Biomacromolecules* **2005,** *6* (5), 2570-2582.

40. Bates, F. S., Measurement of the correlation hole in homogeneous block copolymer melts. *Macromolecules* **1985,** *18*, 525-528.

41. Kennemur, J. G.; Hillmyer, M. A.; Bates, F. S., Synthesis, Thermodynamics, and Dynamics of Poly(4-tert-butylstyrene-b-methyl methacrylate). *Macromolecules* **2012,** *45*, 7228-7236.

42. Maurer, W. W.; Bates, F. S.; Lodge, T. P.; Almdal, K.; Mortensen, K.; Fredrickson, G. H., Can a single function for χ account for block copolymer and homopolymer blend phase behavior? *J. Chem. Phys.* **1998,** *108* (7), 2989-3000.

43. La, Y.-H.; Edwards, E. W.; Park, S.-M.; Nealey, P. F., Directed Assembly of Cylinder-Forming Block Copolymer Films and Thermochemically Induced Cylinder to Sphere Transition: A Hierarchical Route to Linear Arrays of Nanodots. *Nano Lett.* **2005,** *5* (7), 1379-1384.

Chapter 4. Rational Design of a Block Copolymer with a High Interaction Parameter

This work was done in collaboration with Kim, Myungwoong; Larson, Steven R.; Choi, Jonathan W.; Choo, Youngwoo; Osuji, Chinedum O.; Gopalan, Padma.*(Submitted August 2014)*

Author contributions: Daniel designed, synthesized and characterized the BCPs. Myungwoong contributed to the design and interpretation of experiments. Steve contributed towards the synthesis of low molecular weight samples. Jonathan contributed towards thin-film assembly studies. The temperature dependent SAXS measurements were done in Prof. Osuji's lab at Yale with his student Youngwoo. All authors contributed towards writing the manuscript.

4.1. Abstract

A series of poly(4-*tert*-butylstyrene-*block*-2-vinylpyridine) [P(tBuSt-*b*-2VP)] block copolymers (BCPs) with varying volume fractions, molecular weights and narrow dispersities was synthesized from the commercially available monomers by sequential living anionic polymerization. The copolymers were thoroughly characterized by ^{1}H NMR spectroscopy, size exclusion chromatography, thermal gravimetric analysis and differential scanning calorimetry (DSC). To examine the effect of the *tert*-butyl group on the effective interaction parameter (χ_{eff}) relative to poly(styrene-*block*-2-vinylpyridine) [(P(S-*b*-2VP)], the self-assembly of symmetric copolymers was characterized by small angle X-ray scattering (SAXS) and transmission electron microscopy. Order-to-disorder transitions (ODTs) were identified by both DSC and SAXS on five copolymers, to define the equation $\chi_{eff}(T) = (67.9 \pm 1.3)/T - (0.0502 \pm 0.0029)$, which shows a higher enthalpic contribution to χ_{eff} than P(S-*b*-2VP) and approximately 1.5 times larger χ_{eff}. This

enables a minimum full pitch of 9.6 nm for the symmetric copolymers. Asymmetric copolymers were also examined for bulk self-assembly by SAXS and TEM, exploring both P2VP and PtBuSt cylindrical phases with diameters as small as 6 nm. Feasibility of thin film assembly by thermal annealing was demonstrated for P2VP cylinder forming BCPs to yield parallel cylinders that were seeded with Pt ions and etched to yield Pt nanowires with diameters as small as 5.8 nm.

4.2. Introduction

Block copolymers (BCPs) are capable of self-assembling via a thermodynamically driven process into a variety of nanostructures with typical domain sizes between 5 and 50 nm.[1-4] This process is governed by several factors including the relative volume fraction of one block ($f_A = 1 - f_B$), the degree of polymerization (N) and the Flory-Huggins interaction parameter (χ).[1] The volume fraction and degree of polymerization can be varied extensively for any given copolymer system but χ is a parameter which nominally depends on temperature only for that BCP, though in practice molecular weight and composition dependencies also have been observed.[5-8] A symmetric ($f_A = f_B$) BCP will only self-assemble when χ_{eff} (effective segmental interaction parameter) is greater than or equal to 10.5.[9, 10] This provides the lower limit of N for self-assembly of any given copolymer system. The resulting domain sizes also scale with $N^{2/3}$ for a strongly segregated system ($\chi N >> 10.5$) which means that every BCP has a minimum feature size which can be achieved. There is considerable interest in developing BCPs with sub-10 nm and even sub-5 nm features for future nodes of nanolithography through the use of directed self-assembly.[11-15]

There are some basic design guidelines that can be followed to achieve these small dimensions in bulk and thin-film self-assembly of BCPs along with engineering in other desirable properties. Fundamentally, the polymer should exhibit a large effective interaction parameter in order to achieve small domain sizes. In order to successfully compete with mainstream BCPs such

as poly(styrene-*b*-methyl methacrylate) [P(S-*b*-MMA)], poly(styrene-*b*-2-vinylpyridine) [P(S-*b*-2VP)] and poly(styrene-*b*-dimethylsiloxane) [P(S-*b*-DMS)], the BCP should be straightforward to synthesize in high yield with controllable molecular weights and dispersity and preferably from commercially available monomers. It is also beneficial if processing of the material is accomplished with conventional methods such as thermal annealing with a hot plate in order to facilitate scale-up.[16] The glass transition and degradation temperatures should be suitable for needed processing conditions. Finally, it is necessary to have the right functional moieties to provide etch contrast between the domains in order to facilitate pattern transfer. BCPs which have limited intrinsic etch contrast (e.g. P(S-*b*-2VP) or poly(styrene-*b*-4-vinylpyridine) [P(S-*b*-4VP)]) can be seeded with metal ions to yield metallic nanostructures upon plasma treatment either through a solution deposition or a vapor-phase deposition.[17, 18]

In order to achieve smaller domain sizes, high-χ_{eff} BCP systems have been developed by increasing the difference in polarity between the blocks.[10, 19-21] Poly(dimethylsiloxane) (among other silicon-containing blocks such as poly(4-trimethylsilylstyrene)[19]) has been effective at increasing the segregation strength with other blocks including styrene (8 nm diameter cylinders),[22, 23] 2-vinylpyridine (6 nm diameter cylinders)[24] and *d,l*-lactide (12 nm diameter cylinders).[21] Despite their usefulness in pattern transfer through conversion to silicon oxide, silicon-containing blocks have low surface energies which promote segregation to the free surface.[25] This complicates thin film assembly through the formation of a silicon-rich layer at the free surface.

P(S-*b*-2VP), on the other hand, is a common all-organic BCP that is considered to have a high χ_{eff} parameter.[26, 27] P(S-*b*-4VP) is equally valuable, though the position of nitrogen in the pyridine ring and the resultant higher polarity of P4VP leads to complications in synthesis and

characterization.[28-30] Thus, P(S-*b*-2VP) has been mainly used for a variety of different applications including photonic gels, ordered gold dot arrays through micelle templating and the formation of metal nanowire arrays mainly due to the easily functionalized pyridine unit.[17, 31, 32] Recently, poly(4-*tert*-butylstyrene) [P(tBuSt)] was introduced as a more hydrophobic version of styrene in a variety of BCPs including with ethylene oxide, 4-vinylpyridine and methyl methacrylate.[33-35] In a seminal work, Kennemur et al. synthesized P(tBuSt-*b*-MMA) and thoroughly investigated the effect of PtBuSt on χ_{eff} compared to P(S-*b*-MMA) which demonstrated a 10-fold increase in the enthalpic contribution to χ_{eff}.[33] In our work, we examine a new BCP, namely P(tBuSt-*b*-2VP), to see if the χ_{eff} can be significantly increased compared to P(S-*b*-2VP) and how that translates to bulk and thin film self-assembly. From the previously stated design guidelines, P(tBuSt-*b*-2VP) should be an ideal BCP as it can exhibit a high χ_{eff}, can be synthesized using sequential anionic polymerization with commercially available monomers, processed by thermal annealing and can be seeded with metal ions by a solution treatment[18] or subjected to vapor-phase deposition of metal oxide precursor to seed oxides to increase etch contrast between the domains.[36, 37]

Using sequential living anionic polymerization, we synthesized a series of P(tBuSt-*b*-2VP) BCPs with varying molecular weights and symmetric compositions to determine the χ_{eff} by order-to-disorder transition (ODT) analysis. Using differential scanning calorimetry (DSC) and temperature-dependent small angle X-ray scattering (SAXS), we identified five BCPs with accessible ODTs which allowed determination of χ_{eff} for the system. The replacement of PS with PtBuSt increased the χ_{eff} 1.5 times mainly through a larger enthalpic contribution to χ_{eff} which furnished sub-5 nm domains (full pitch 9.6 nm). We also examine asymmetric BCPs for their self-assembly in bulk and in thin film. BCPs ranging from PtBuSt spheres to P2VP cylinders were synthesized via the same sequential anionic polymerization method and showed cylinder diameters

as small as 5.9 nm. Thin film self-assembly was accomplished via spin-coating from a toluene solution and thermal annealing on the native oxide to form arrays of P2VP cylinders parallel to the substrate. The cylinders were seeded with Pt metal ion complexes and etched to yield arrays of Pt nanowires with 5.8 ± 0.5 nm diameter.

4.3. Experimental Section

Reagents. All reagents were purchased from Sigma-Aldrich Co. (Milwaukee, WI) and used as received unless otherwise specified. Tetrahydrofuran (THF) was freshly distilled from Na/benzophenone ketyl. 4-*tert*-butylstyrene (tBuSt) was sequentially distilled from CaH_2 and di-*n*-butylmagnesium under vacuum and then stored at 0 ^oC under argon. 2-vinylpyridine (2VP) was sequentially distilled from CaH_2 and triethylaluminum under vacuum and then stored at 0 ^oC under argon. Lithium chloride was dried in the oven at 140 ^oC under vacuum for 48 hours then stored in the desiccator. 1,1-diphenylethylene (DPE) was distilled from *n*-BuLi under vacuum and stored at 22 ^oC under argon. Methanol was sparged with argon for 10 minutes to remove dissolved oxygen.

Anionic polymerization of P(tBuSt-*b*-2VP). The following is a general procedure for the synthesis of P(tBuSt-*b*-2VP). An oven-dried flask was loaded with 30 mg LiCl and cooled under argon to room temperature. 40 mL of THF was added to the flask and cooled in a -78 ^oC bath. s*ec*-butyllithium (1.4 M in cyclohexane) was added dropwise until a yellow color persisted. The flask was then removed from the bath and kept at room temperature until colorless. At this point, the flask was chilled to -78 ^oC and a measured amount of *sec*-BuLi was added (typical 0.11 mL, 0.154 mmol) with vigorous stirring. tBuSt (typical 1.0 mL, 5.5 mmol) was then injected rapidly into the center of the flask using a syringe and stirred for 30 minutes. At this point, 0.1 mL DPE was added to the flask and the orange anion turned dark red immediately. A small aliquot was removed from the solution and rapidly quenched in methanol for analysis. 2VP (typical 1.5 mL, 9.2 mmol) was

then injected rapidly into the center of the flask and polymerized for 20 minutes. No color change was noticed after the addition of 2VP. Sparged MeOH was used for terminating the polymerization and the resulting colorless solution was poured into water to precipitate the block copolymer. The BCP was dried under vacuum at 60 ^{o}C for 24 to 48 hrs and yield was typically quantitative. ^{1}H NMR (500 MHz, $CDCl_3$) δ 8.5-8.0 (1H from 2VP), 7.25-6.0 (3H from 2VP, 4H from tBuSt), 2.5-1.0 (3H from 2VP, 12H from tBuSt).

Chemical and physical characterization. ^{1}H NMR and ^{13}C NMR spectra were recorded in $CDCl_3$ using a Bruker Avance-500 spectrometer with TMS as internal reference. Quantitative ^{1}H NMR utilized a 10 s relaxation delay between pulses. Heteronuclear single quantum coherence (HSQC) spectra were acquired using standard parameters. Size exclusion chromatography (SEC) was performed using a Viscotek 2210 system equipped with three Waters columns (HR 4, HR 4E, HR 3) and a 1 mL/min flow rate of THF as eluent at 30 °C. SEC analysis relied on a calibration curve constructed from nine narrow dispersity PS standards with M_n = 1–400 kg/mol. Thermogravimetric analysis (TGA) was performed on a TA Instruments Q500 using a heating rate of 10 ^{o}C /min under a nitrogen atmosphere. Differential scanning calorimetry (DSC) was performed on a TA Instruments Q100 using a heating and cooling rate of 10 °C/min for two cycles. Glass transition temperatures and order to disorder transitions (ODTs) were determined from the second heating cycle. Matrix assisted laser desorption ionization time of flight (MALDI-TOF) mass spectrometry of low molecular weight P(tBuSt-*b*-2VP) BCPs was performed using α-cyano-4-hydroxycinnamic acid as the matrix on a Bruker Ultraflex-III instrument operating at 20 kV.

Bulk self-assembly. SAXS samples were solvent cast by the slow evaporation of THF solutions (5 wt% polymer in THF) and followed by annealing at 190 ^{o}C for 24 h under vacuum. SAXS analysis used a Rigaku SMAX-300 instrument with a MM002+ micro-focus X-ray source

operating at 40.5 W using Cu Kα radiation (λ = 0.15418 nm). The resulting 2D SAXS patterns were rigorously calibrated using a silver behenate standard (d_{001} = 5.838 nm). The patterns were integrated azimuthally to provide intensity versus q plots ($q = 4\pi\sin(\theta)/\lambda$) where 2θ is the scattering angle and λ is the X-ray wavelength. Temperature-dependent SAXS studies used a home-built temperature controlled stage with the sample sandwiched between two thin Kapton windows. A 10 min thermal pre-equilibration delay was employed prior to data collection at a given temperature. The SAXS samples were further prepared for TEM by embedding in epoxy (Eponate 12 with DMP-30, Ted Pella) and subsequently sectioned at 22 °C using a diamond knife to produce 70-90 nm thick samples. The sections were collected onto 200 mesh Cu grids and exposed to I_2 vapor overnight to preferentially stain the P2VP block. TEM samples were imaged using a Phillips CM120 operating at 80 kV accelerating voltage in bright-field mode.

Thin film self-assembly. Si wafers were cleaned using piranha acid (7:3 H_2SO_4:30% H_2O_2, ***caution*****:** strongly oxidizing solution) at 75 ^oC for 30 minutes then washed copiously with DI water before being dried under a stream of air. P2VP cylinder forming BCPs were dissolved in toluene at 1 wt% concentration and then spin-coated on the Si wafers at 4000 rpm and acceleration rate of 4000 rpm/s. The substrates were then annealed at 190 ^oC for 24 hours under vacuum followed by slow cooling to room temperature. The substrates were then submerged in an aqueous solution of 0.9% HCl and 10 mM Na_2PtCl_4 for 18 hours before being rinsed with DI water and blown dry with a stream of air. The films were then imaged using a LEO 1530 scanning electron microscope operating at 1 kV accelerating voltage. Metal ion seeded films were exposed to 20 W oxygen plasma.

4.4. Results and Discussion

Synthesis. Poly(*tert*-butylstyrene-*block*-2-vinylpyridine) P(tBuSt-*b*-2VP) BCPs were synthesized by living anionic polymerization using the sequential addition of monomers (**Figure 4.1**). In fact, tBuSt can be used in an identical manner as styrene for the synthesis of most BCPs but in general remains more well-controlled than styrene under the same conditions.[20] 1,1-diphenylethylene (DPE) was used to end-cap the P(tBuSt) anion before the addition of 2VP to reduce the chance of chain termination during cross-over from the highly nucleophilic styrenyl anion.[28, 38] Lithium chloride was also included as an additive to reduce side reactions from the reactive 2VP group.[39] These techniques were successful for the synthesis of well-controlled BCPs with dispersity ($Đ = M_w/M_n$) less than 1.10. The main difference at this point from P(S-*b*-2VP) is that the BCPs do not precipitate in hexanes due to the greater solubility of PtBuSt in non-polar solvents, thus water was used for precipitation as it is a non-solvent for the two blocks. A series of both symmetric and asymmetric compositions were synthesized as listed in **Table 4.1** and **4.3** respectively.

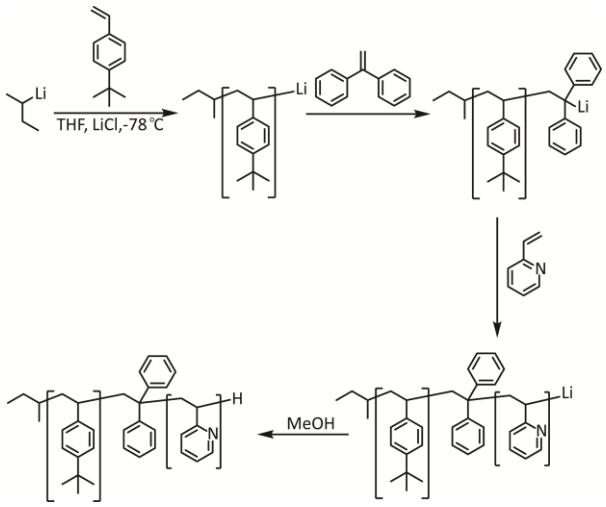

Figure 4.1. Synthetic scheme for the living anionic polymerization of P(tBuSt-*b*-2VP) by sequential addition.

Table 4.1. Chemical and morphological characterization for the symmetric compositions of P(tBuSt-*b*-2VP).

Sample	M_n PtBuSt (kg/mol)[a]	M_n BCP (kg/mol)[a]	$Đ$[a]	T_g (°C)[b]	f_{P2VP}[c]	L_0 (nm)[d]
1.7k-0.9k	1.7	2.6	1.08	71	0.44	-
2.2k-1.4k	2.2	3.6	1.07	76	0.47	-
2.5k-1.9k	2.5	4.4	1.07	77	0.49	-
3.0k-1.5k	3.0	4.5	1.09	94, 81	0.52	9.6
2.8k-2.0k	2.8	4.8	1.07	107, 90	0.46	9.7
3.1k-1.9k	3.1	5.0	1.07	107, 89	0.54	10.1
3.2k-2.8k	3.2	6.0	1.06	103, 86	0.49	11.1
4.2k-3.7k	4.2	7.9	1.08	108, 91	0.59	13.3
4.4k-4.5k	4.4	8.9	1.05	117, 93	0.52	14.4
5.3k-4.7k	5.3	10	1.04	134, 98	0.44	16.8
6.0k-4.9k	6.0	10.9	1.03	134, 99	0.53	17.3
5.3k-6.2k	5.3	11.5	1.04	128, 98	0.56	18.1
8.4k-7.6k	8.4	16	1.05	142, 100	0.48	23.2
7.3k-11.6k	7.3	18.9	1.04	138, 100	0.65	26.9
17.4k-23.2k	17.4	40.6	1.08	147, 102	0.69	50.3

a – Determined by SEC using PS standards. b – Determined by DSC from the second heating cycle. c – Determined by ^{1}H NMR using the bulk densities of PtBuSt and P2VP at 25 °C (ρ(PtBuSt) 0.95 g/cm^3 and ρ(P2VP) 1.15 g/cm^3).[6, 7] d – Determined from the principal SAXS scattering peak ($D = 2\pi/q$).

Spectral and thermal characterization. To characterize the BCPs, we first used size exclusion chromatography (SEC) to determine the molecular weight and the dispersity relative to PS standards and ^{1}H NMR spectroscopy to calculate the volume fraction (**Figure 4.2**). Due to the low bulk density of PtBuSt, a larger mole fraction of P2VP was necessary to achieve a symmetric volume fraction. There are a few distinguishing features in the NMR spectrum, such as: one of the

P2VP protons is far downfield at 8.0 to 8.5 ppm (proton d in **Figure 4.2**) while there is a prominent singlet at 1.2 ppm for the *tert*-butyl protons (proton b in **Figure 4.2**). This provides a straightforward way to determine the molar ratio between the two blocks through both the aryl and aliphatic proton regions.

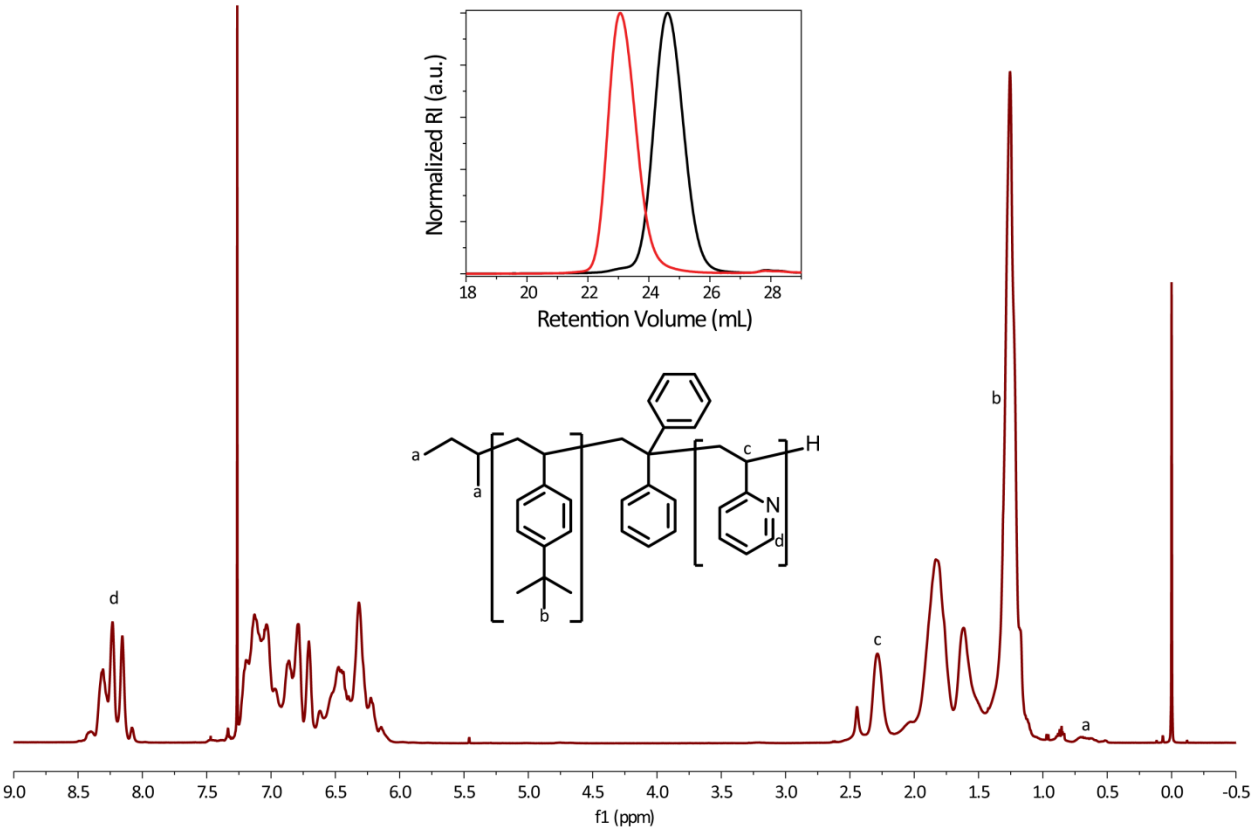

Figure 4.2. ^{1}H NMR spectrum in $CDCl_3$ of **5.3k-6.2k** showing relevant labeled peaks. *Inset*: SEC chromatogram showing the PtBuSt homopolymer (black) and the chain-extended P(tBuSt-*b*-2VP) (red) (**4.4k-4.5k**).

In order to further analyze the NMR spectrum, we used the two-dimensional technique heteronuclear single quantum coherence (HSQC) spectroscopy which correlates proton and carbon signals (**Figure 4.S1**, quaternary carbons do not show any cross peaks, red peaks are CH and CH_3 groups, blue are CH_2). In the HSQC, several prominent peaks are split out allowing better

resolution of the protons that comprise the 1D proton spectrum (**Figure 4.S1**). The two methyls in the *sec*-butyl initiating group are clearly visible at 0.5 to 0.8 ppm and do not overlap with other resonances. The *tert*-butyl group overlaps with the backbone CH_2 peaks which exhibit a broad resonance in the aliphatic region. Interestingly, the CH backbone carbons are quite different between the PtBuSt and P2VP blocks (about 5 ppm different in the ^{13}C spectrum). These resonances overlap with each other and the broad methylene backbone peaks in the proton 1D spectrum while the HSQC allows for direct visualization of the relative intensities. More importantly, the lack of overlapping peaks with the initiator protons (marked as 'a' in **Figure 4.2**) shown in HSQC enables us to rely on quantitative integration from ^1H NMR to directly determine *N* for the lower molecular weight BCPs.

Thermal gravimetric analysis (TGA) was used to quantify the thermal headroom of the polymer for thin film processing. TGA indicated that the degradation onset began at 280 ^oC (**Figure 4.S2**) so we limited our maximum temperature to 265 ^oC. We then used differential scanning calorimetry (DSC) for determination of the glass transition temperatures (T_g) for the various symmetric BCPs (**Figure 4.3**). The three lowest molecular weight BCPs exhibited only a single T_g possibly indicating a disordered morphology. As the molecular weight increases, two T_g's appear and gradually increase in temperature up to their respective maximums for the two blocks (~100 ^oC for P2VP and ~145 ^oC for PtBuSt). Interestingly, a small endothermic peak was observed at temperatures above the T_g's for five of the lower molecular weight BCPs (**Figure 4.S3**). These are indicative of an order-to-disorder transition (ODT),[10] and will be discussed further in the ODT analysis section.

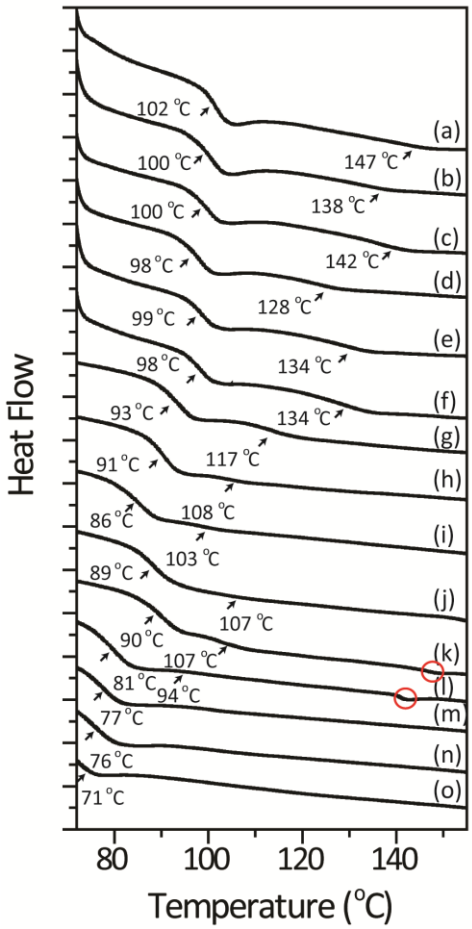

Figure 4.3. DSC heating curves for the symmetric BCPs. T_g values from the midpoint of the transition are listed below each curve. Data was shifted vertically for clarity. (a) 17.4k-23.2k, (b) 7.3k-11.6k, (c) 8.4k-7.6k, (d) 5.3k-6.2k, (e) 6.0k-4.9k, (f) 5.3k-4.7k, (g) 4.4k-4.5k, (h) 4.2k-3.7k, (i) 3.2k-2.8k, (j) 3.1k-1.9k, (k) 2.8k-2.0k, (l) 3.0k-1.5k, (m) 2.5k-1.9k, (n) 2.2k-1.4k, (o) 1.7k-0.9k. Red circles indicate ODTs seen in (l) and (k).

Bulk self-assembly of the symmetric BCPs. In order to examine the molecular weight limits for self-assembly for the P(tBuSt-*b*-2VP) system, we used small angle X-ray scattering (SAXS) and transmission electron microscopy (TEM) to confirm the dimensions and morphology present. After annealing the BCP samples at 190 °C for 24 hours, the samples were examined by

SAXS at room temperature (**Figure 4.4**). The three lowest molecular weight copolymers showed a disordered or "correlation hole"[8] type scattering while the rest correspond to a lamellar morphology. The smallest ordered sample has a L_0 of 9.6 nm, indicating the ability of the copolymer to make sub-5 nm domains. TEM also confirmed the lamellar morphologies for the BCPs examined and the domain sizes correlate well with that measured by SAXS (**Figure 4.5**).

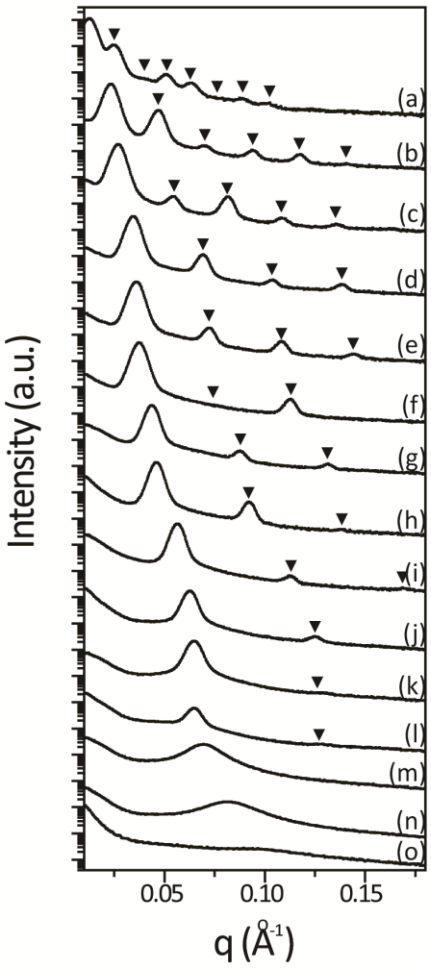

Figure 4.4. Room temperature SAXS patterns for the symmetric copolymers. Triangles indicate calculated lamellar peak positions based upon q*. Data was shifted vertically for clarity. (a) 17.4k-23.2k, (b) 7.3k-11.6k, (c) 8.4k-7.6k, (d) 5.3k-6.2k, (e) 6.0k-4.9k, (f) 5.3k-4.7k, (g) 4.4k-4.5k, (h)

4.2k-3.7k, (i) 3.2k-2.8k, (j) 3.1k-1.9k, (k) 2.8k-2.0k, (l) 3.0k-1.5k, (m) 2.5k-1.9k, (n) 2.2k-1.4k, (o) 1.7k-0.9k.

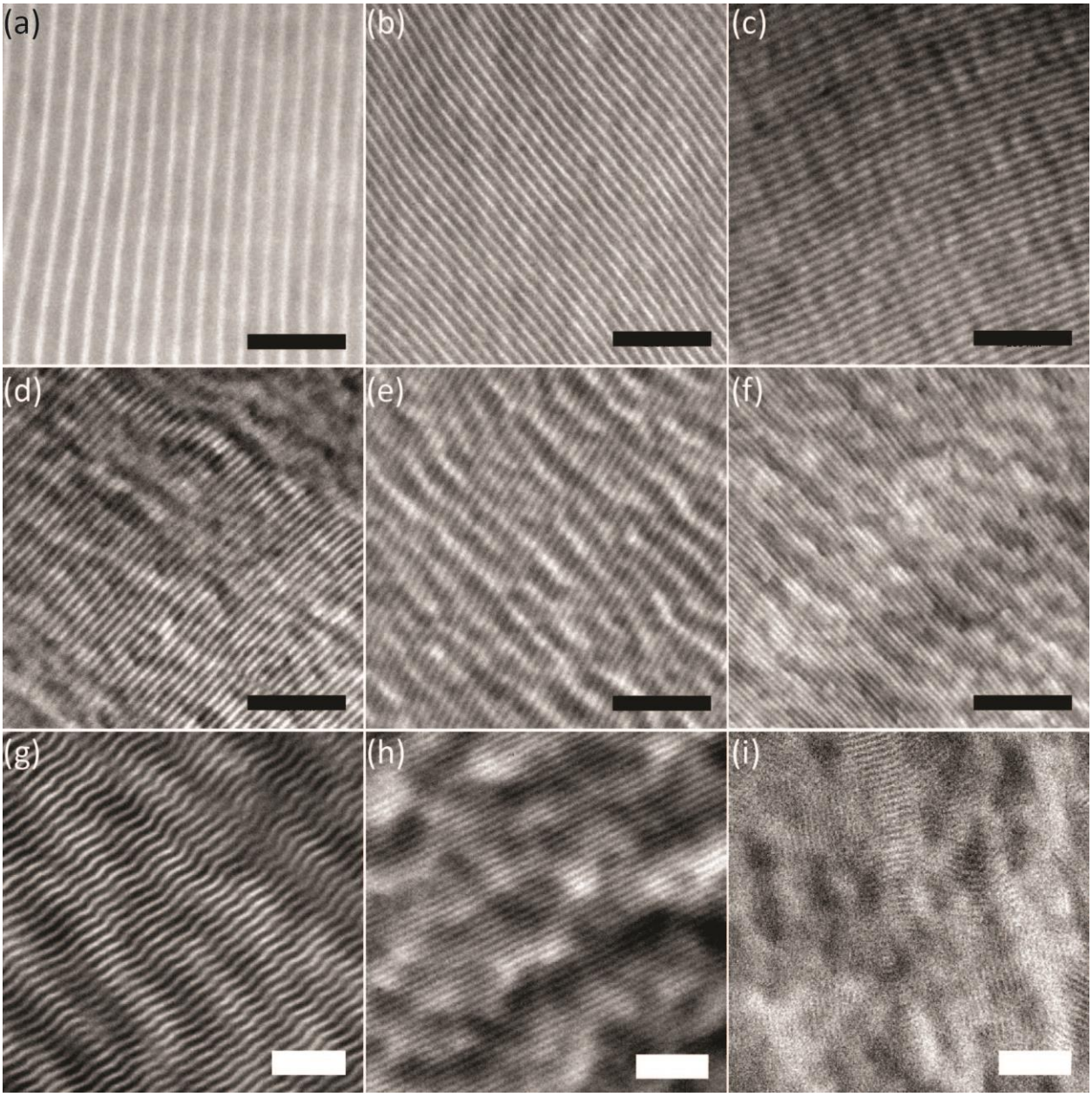

Figure 4.5. TEM images of the symmetric copolymers (black scale bar = 200 nm, white scale bar = 100 nm). (a) 17.4k-23.2k, (b) 7.3k-11.6k, (c) 8.4k-7.6k, (d) 5.3k-6.2k, (e) 6.0k-4.9k, (f) 5.3k-4.7k, (g) 4.4k-4.5k, (h) 3.2k-2.8k, (i) 2.8k-2.0k.

ODT analysis for the symmetric BCPs. Well-established mean field theories posit that when $\chi_{eff}N \geq 10.5$ for a symmetric ($f_A = 0.5$) BCP, it will self-assemble into a lamellar morphology.[10] ODTs can be observed by a variety of different methods including variable temperature SAXS, dynamic mechanical analysis and more recently, DSC.[10, 33, 40] By analyzing the ODTs for a series of BCPs as a function of molecular weight, an equation for $\chi(T) = \alpha/T + \beta$ can be readily established. However, this analysis is vitally dependent on an accurate value for the degree of polymerization (N), which we have referenced to a volume of 118 $Å^3$ to allow direct comparisons with other systems. In order to determine N, we employed quantitative ^1H NMR spectroscopy to analyze the six methyl protons in the initiator fragment to the total polymer peaks (**Table 4.2**). This method is effective for low molecular weight copolymers where the initiator or end-group can be cleanly integrated. End-group analysis is quite accurate for this particular system as the HSQC shows that no other signals reside in the same area of the proton spectrum, thus allowing for reliable integration (*vide supra*). To confirm that the NMR analysis gave an accurate value, we used matrix-assisted laser desorption ionization time-of-flight (MALDI-TOF) mass spectrometry to quantitatively determine the molar mass and distribution for two of the BCPs (3.2k-2.8k and 2.8k-2.0k, spectra are given in **Figure 4.S4**). Analysis of the MALDI-TOF spectra showed almost identical results as the NMR quantification (the difference was less than one normalized repeat unit for each), thus providing additional confidence in the NMR method.

Table 4.2. Experimental values for M_n and ODT for selected symmetric BCPs.

	$\mathbf{M_n}$[a]	$\boldsymbol{Đ}$[b]	**N**[c]	**ODT**[d]	$\boldsymbol{\chi_{eff}}$[e]
3.0k-1.5k	6820	1.09	90.0	132	0.1167
2.8k-2.0k	6736	1.07	91.5	140	0.1148

3.1k-1.9k	6995	1.07	92.5	142	0.1135
3.2k-2.8k	8113	1.06	111.0	195	.09460
4.2k-3.7k	9700	1.08	127.8	240	.08216

a – Determined by quantitative ^{1}H NMR using the six methyl initiator protons at 0.5-0.8 ppm. b – Determined by SEC relative to PS standards (2.8k-2.0k and 3.2k-2.8k also confirmed by MALDI-TOF). c – Based on 118 Å^3 reference volume. d – Determined from DSC heating curves, confirmed by SAXS. e – Calculated via the equation $\chi_{eff} = 10.5/N$.

DSC can be used to determine ODT by examining small reversible endothermic peak in some systems.[10, 41] To further confirm the transition as an ODT, we employed temperature-dependent SAXS to directly observe the ordering of the BCP. By heating the BCP to a disordered state, followed by slow cooling, we were able to clearly identify the ODT for all five BCPs using the plot of I^{-1} vs. T^{-1} to find mid-point temperature of the transition,[33] and the temperatures coincided well with those obtained from DSC (**Figure 4.S4** shows the DSC traces, **Figure 4.6** shows an example of ODT determination by SAXS, other SAXS curves in **Figure 4.S5**).

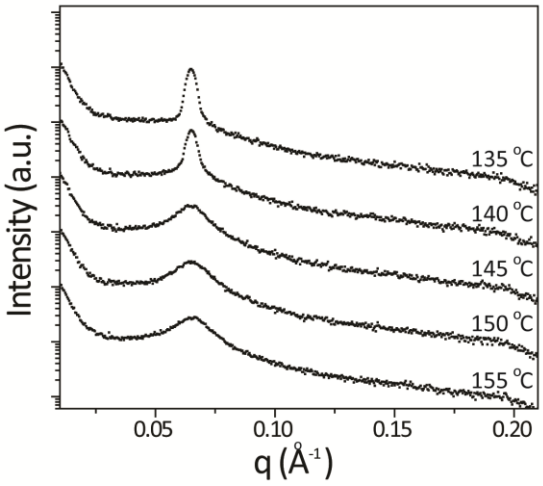

Figure 4.6. SAXS spectra showing the discontinuous rise in intensity of the q* peak upon cooling through the ODT (2.8k-2.0k, ODT at 145 ^{o}C by DSC). Data was shifted vertically for clarity.

Using the calculated values for χ_{eff} at the determined ODTs to plot χ_{eff} vs T^{-1} shows the expected linear relationship (**Figure 4.7a**). Analysis by linear regression gives the expression

$$\chi_{eff} = \frac{67.9 \pm 1.3}{T} - (0.0502 \pm 0.0029)$$

which shows a large enthalpic contribution and a negative entropic contribution. The large enthalpic contribution allows for a considerable range of temperature (132 ^{o}C to 240 ^{o}C) to encounter accessible ODTs for a range of *N* from 90 to 128. In order to compare with the calculated χ_{eff} for P(S-*b*-2VP), we recalculated the expression for P(S-*b*-2VP) using a reference volume of 118 Å^3 from the original $\chi_{eff}(T) = 63/T - 0.033$ (derived from chemical degree of polymerization estimated using SEC and NMR) to $\chi_{eff}(T) = 45.4/T - 0.024$.[10, 26, 33] This indicates that P(tBuSt-*b*-2VP) has a large increase to the enthalpic contribution in comparison to P(S-*b*-2VP) which enables the BCP to self-assemble into sub-5 nm domain sizes. Interestingly, the increase in χ_{eff} is perhaps not as dramatic a change as that seen in P(tBuSt-*b*-MMA) where the enthalpic contribution increased 10-fold relative to P(S-*b*-MMA). This suggests that the nature of the interaction between PS and P2VP is different from PS and PMMA as the interaction parameter for P(S-*b*-MMA) is characterized by a small enthalpic contribution and positive entropic contribution while P(S-*b*-2VP) has the more standard negative entropic contribution and moderate temperature dependence.[8, 33] We postulate that the *tert*-butyl group is successful at screening weak noncovalent interactions between the aryl and ester moieties in PS and PMMA respectively, that are not present in P(S-*b*-2VP).[33] Therefore, the increase in χ_{eff} likely stems from the increased hydrophobicity of

PtBuSt relative to PS. As a visual comparison, we present a plot of χ_{eff} vs T^{-1} for a variety of BCPs (**Figure 4.7b**).

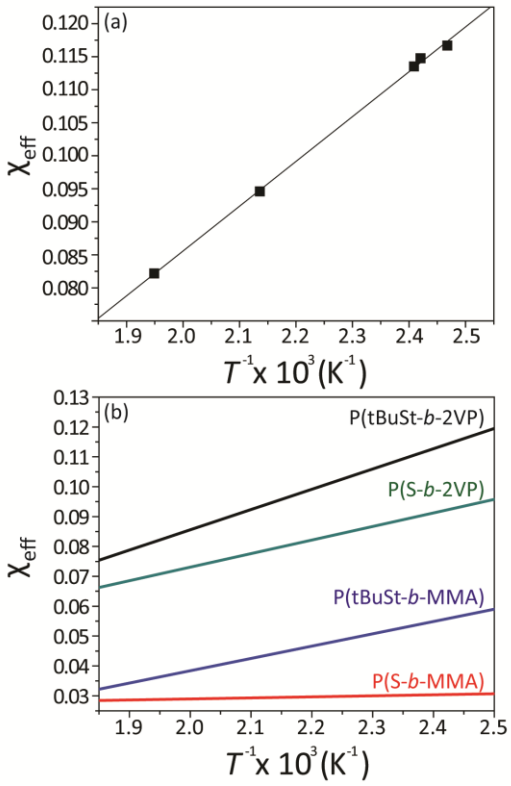

Figure 4.7. (a) Linear dependence of χ_{eff} vs T^{-1} using experimental ODTs and $\chi_{eff}N$ = 10.5. (b) Comparison of χ_{eff} vs T^{-1} for a variety of relevant BCPs showing the increased χ_{eff} for P(tBuSt-*b*-2VP).

Synthesis and self-assembly of asymmetric BCPs in bulk. A series of asymmetric P(tBuSt-*b*-2VP) BCPs was synthesized following the same general scheme as previously given (**Table 4.3**). We targeted a variety of volume fractions going from PtBuSt sphere forming to P2VP cylinder forming BCPs in order to comprehensively study the self-assembly of this BCP.

Table 4.3. Chemical and morphological characterization of the asymmetric compositions of P(tBuSt-*b*-2VP).

Sample	M_n PtBuSt (kg/mol)[a]	M_n BCP (kg/mol)[a]	$Đ$[a]	T_g (°C)[b]	f_{P2VP}[c]	L_0 (morphology)[d]
3.0k-15.8k	3.0	18.8	1.05	100	0.87	16.8 nm (sphere)
2.7k-5.8k	2.7	8.5	1.04	80	0.71	14.1 nm (cyl)
7.7k-4.3k	7.7	11.4	1.04	136, 101	0.31	20.2 nm (cyl)
6.1k-1.6k	6.1	7.7	1.04	128, 98	0.23	14.2 nm (cyl)
11.9k-3.0k	11.9	14.9	1.04	139, 100	0.19	23.0 nm (cyl)

a – Determined by SEC using PS standards. b – Determined by DSC from the second heating cycle. c – Determined by ^{1}H NMR using the bulk densities of PtBuSt and P2VP at 25 °C (ρ(PtBuSt) 0.95 g/cm^3 and ρ(P2VP) 1.15 g/cm^3).[6, 7] d – Determined from the principal SAXS scattering peak (D = 2π/q) then multiplying by 2/√3 for cylindrical phases, D for spheres is given as 2π/q due to the low degree of long range order.

Four of the five BCPs display well-resolved cylindrical morphologies by SAXS while the most asymmetric BCP (3.0k-15.8k, f_{P2VP} 0.87) presented a relatively ill-defined higher order peak (**Figure 4.8c**). Examination by TEM revealed that this BCP was phase segregated but the morphology did not exhibit long range order or regularity. Instead, it was more a collection of disordered spheres (**Figure 4.9a**).[42] The smallest copolymers achieved domain sizes of 14.1 and 14.2 nm which correspond to cylinder diameters of 5.9 nm. The domain sizes measured from TEM correlated well with those calculated from SAXS.

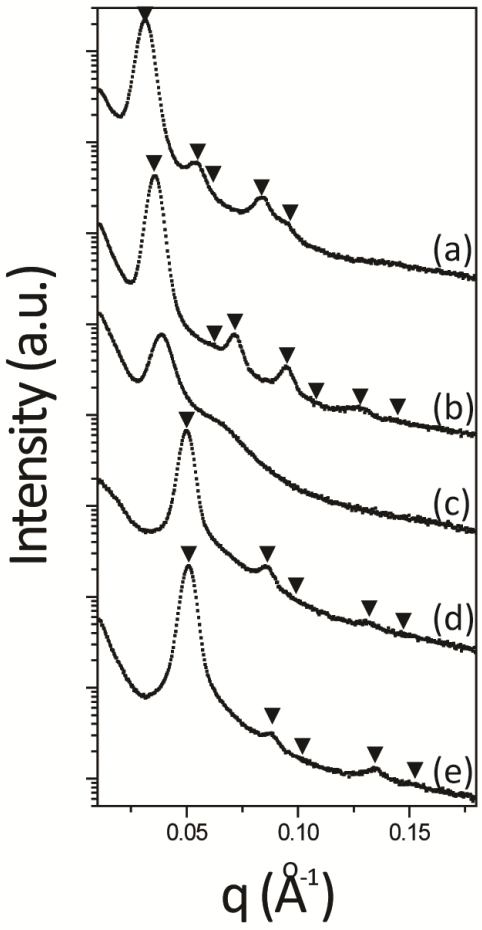

Figure 4.8. SAXS curves for the various asymmetric BCPs. (a) 11.9k-3.0k, (b) 7.7k-4.3k, (c) 3.0k-15.8k, (d) 6.1k-1.6k, (e) 2.7k-5.8k. Black triangles represent calculated peak positions for a hexagonal cylinder morphology (i.e. q*, √3q*, √4q*, √7q* etc.). Data was shifted vertically for clarity.

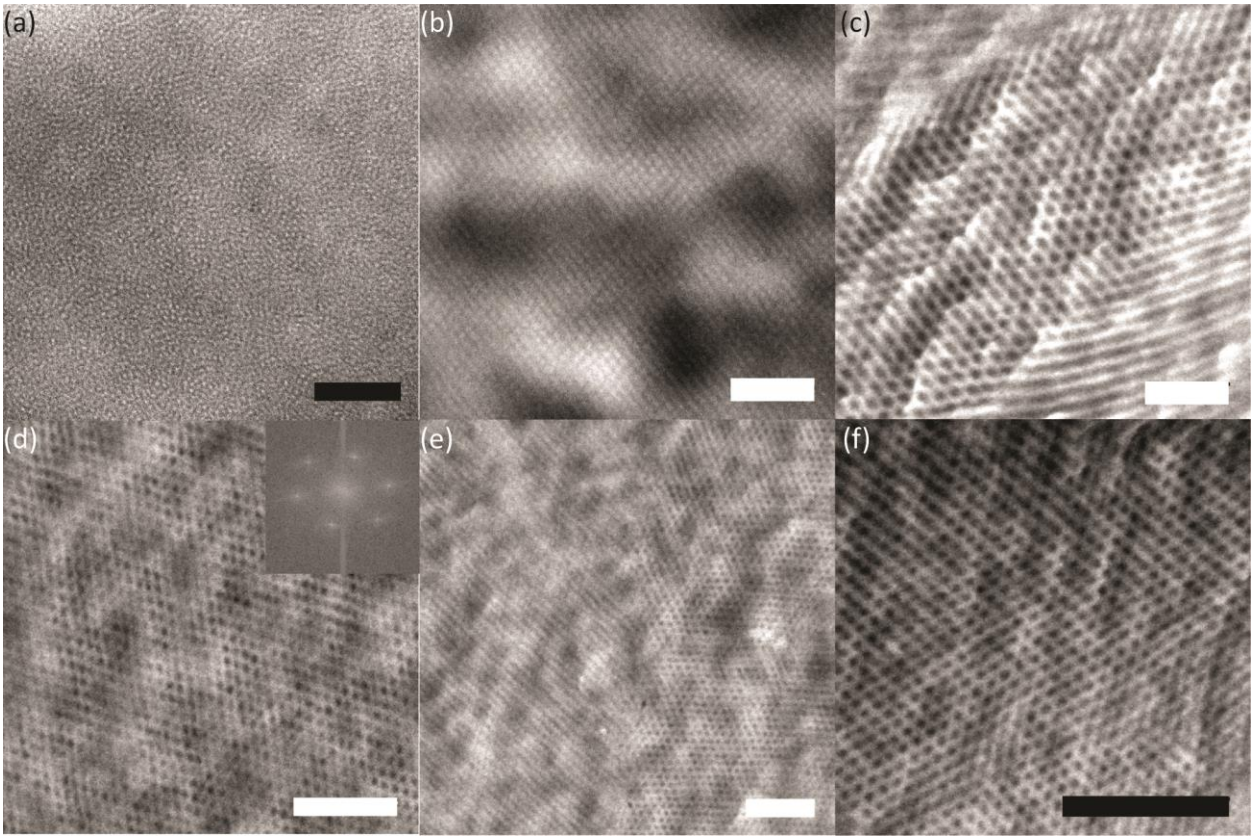

Figure 4.9. TEM micrographs of the asymmetric BCPs showing the morphologies provided by increasing the volume fraction of PtBuSt, P2VP was preferentially stained with I_2 vapor and appears dark. White scale bar = 100 nm, black scale bar = 200 nm. (a) 3.0k-15.8k (disordered PtBuSt spheres), (b) 2.7k-5.8k (PtBuSt cylinders), (c) 7.7k-4.3k (P2VP cylinders), (d) 6.1k-1.6k (P2VP cylinders, inset: FFT showing hexagonal packing), (e) 6.1k-1.6k showing a grain boundary, (f) 11.9k-3.0k (P2VP cylinders).

Self-assembly of asymmetric BCPs in thin film. With the bulk morphology well-characterized, we studied the self-assembly of P2VP cylinder forming BCPs in thin film. We used conditions reported[17] for the assembly of P2VP parallel cylinders in P(S-*b*-2VP), namely spin-coating from a toluene solution onto an oxide surface and then thermal annealing at elevated temperatures. We chose 190 ^{o}C as it is well above the two T_g's for the BCP and annealed for 24

hours to reach thermodynamic equilibrium. In order to improve contrast between the blocks to image by top-down scanning electron microscopy (SEM), we used the metal seeding technique developed for P(S-*b*-2VP) using a solution of sodium chloroplatinate in 0.9% HCl.[17] Well-ordered parallel cylinders were observed over the entire surface after thermal annealing (**Figure 4.10a**). Lower molecular weight BCPs showed a hole and island type morphology. With the small domain size for 6.1k-1.6k yielding cylinders in sub 6-nm dimension (**Figure 4.10b**), the seeded film was etched approximately halfway using oxygen plasma to reveal an array of Pt nanowires which exhibited a diameter equivalent to the parent BCP (5.8 ± 0.5 nm, before and after etching) (**Figure 4.S6**). Therefore, this result strongly suggests that it is feasible to utilize this BCP to define nanostructures in sub-10 nm dimension that can be used as a template for nanolithography.

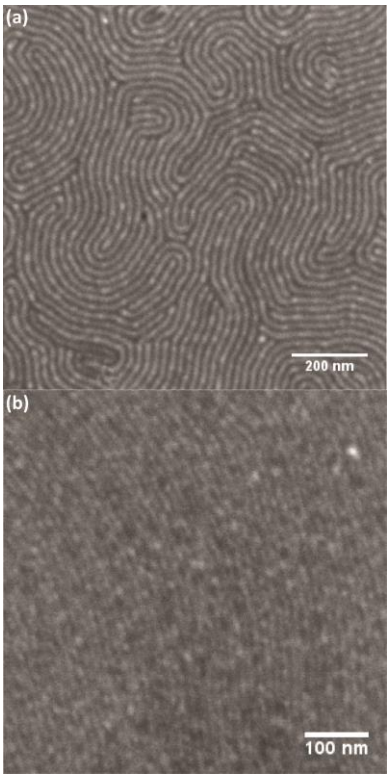

Figure 4.10. Top-down SEM micrographs for thermally annealed thin films of (a) 11.9k-3.0k with a cylinder diameter of 11.1 ± 1.6 nm and (b) 6.1k-1.6k with a cylinder diameter of 5.8 ± 0.5 nm.

4.5. Conclusions

We have demonstrated the synthesis of a series of P(tBuSt-*b*-2VP) BCPs by sequential anionic polymerization which yielded BCPs with controllable molecular weight and low dispersity. P(tBuSt-*b*-2VP) is a glassy copolymer with good thermal stability up to 280 ^{o}C that can be easily synthesized from commercially available monomers. Thorough analysis of the self-assembled morphology by SAXS and TEM demonstrated a minimum full pitch of 9.6 nm for a symmetric BCP. Through mean-field analysis of five BCPs with accessible ODTs, we determined that $\chi_{eff}(T) = (67.9 \pm 1.3)/T - (0.0502 \pm 0.0029)$ which is approximately 1.5 times larger in magnitude in comparison with P(S-*b*-2VP). We also demonstrated the self-assembly of asymmetric BCPs with both PtBuSt and P2VP minority domains with cylinder domains as small as 5.9 nm and a L_0 of 14.1 nm. Preliminary results show the feasibility of thin-film assembly of these new BCPs using thermal processing. Using a solution of anionic Pt complexes in aqueous HCl, the P2VP domains were seeded and partially etched with oxygen plasma to yield Pt nanowire arrays. In summary, the facile synthesis of this BCP from commercially available monomers, high χ_{eff} leading to sub 5-nm domains, and the easily tunable and accessible ODTs make it an appealing candidate for high-resolution block copolymer lithography. The BCP has all the properties which have made P(S-*b*-2VP) a widely used system while increasing the interaction parameter between the blocks substantially.

4.6. Supporting Information

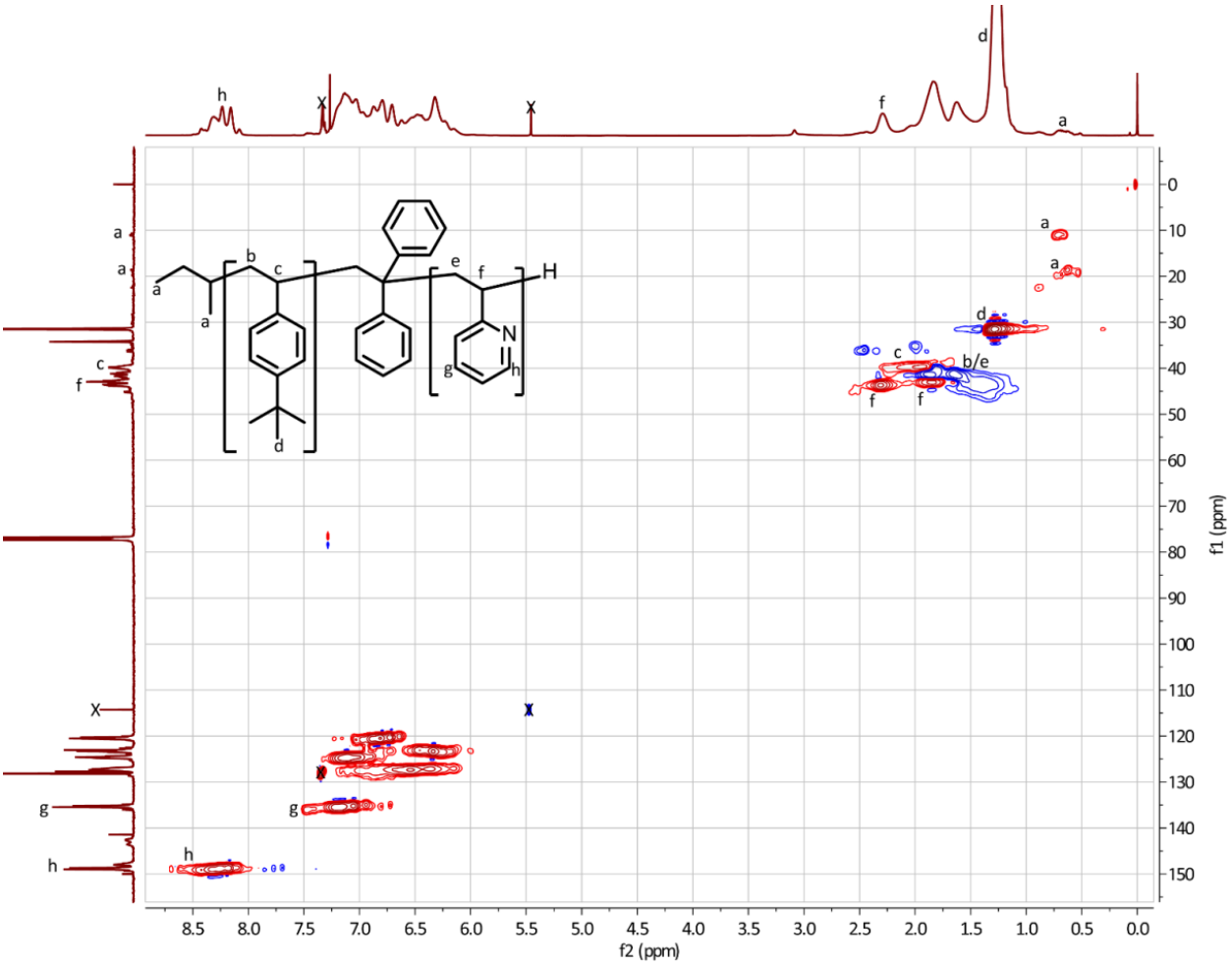

Figure 4.S1. Heteronuclear single-quantum coherence (HSQC) of 2.8k-2.0k, clearly showing the initiator methyl peaks along with the *tert*-butyl groups as separate from the backbone and the aryl protons. X denotes peaks from unreacted DPE.

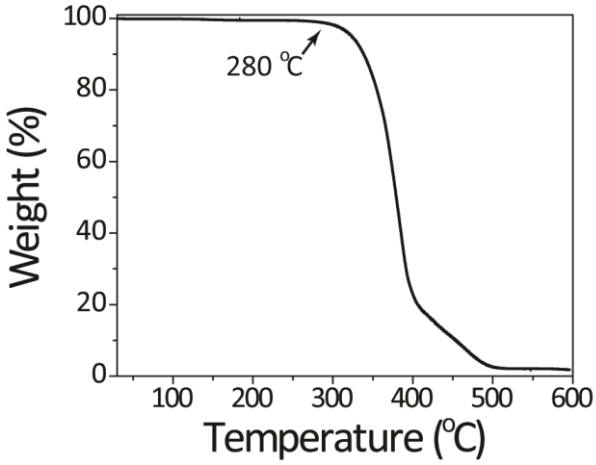

Figure 4.S2. Thermal gravimetric analysis (TGA) curve for 6.1k-1.6k showing an initial degradation at 280 °C.

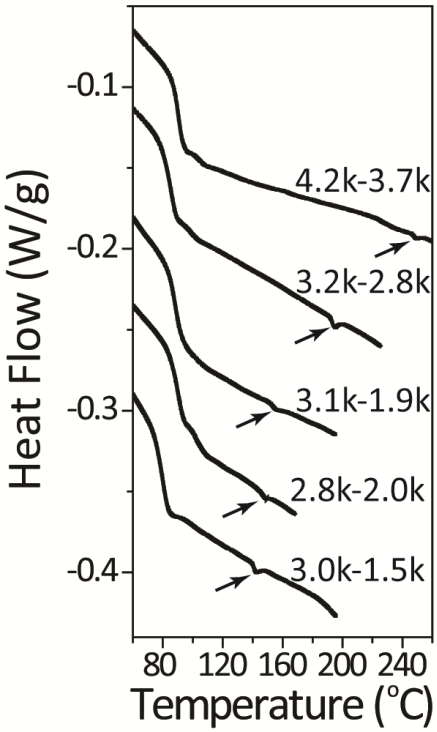

Figure 4.S3. DSC heating scans demonstrating the small endothermic peaks corresponding to ODTs for the five BCPs. Data was shifted vertically for clarity.

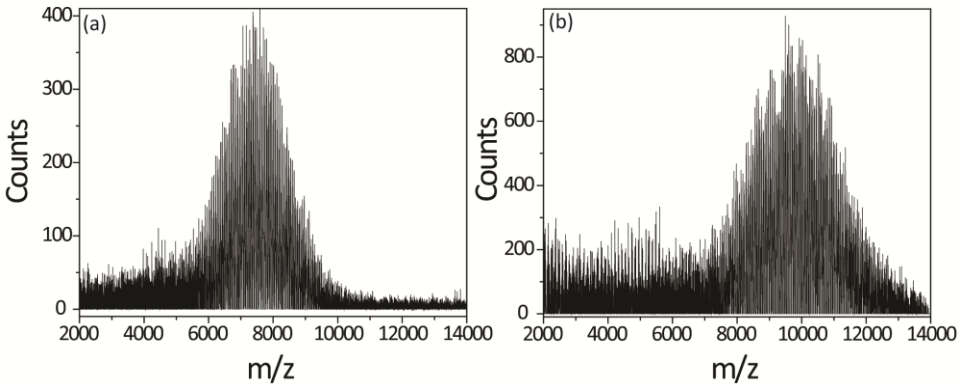

Figure 4.S4. MALDI-TOF spectra for (a) 2.8k-2.0k and (b) 3.2k-2.8k.

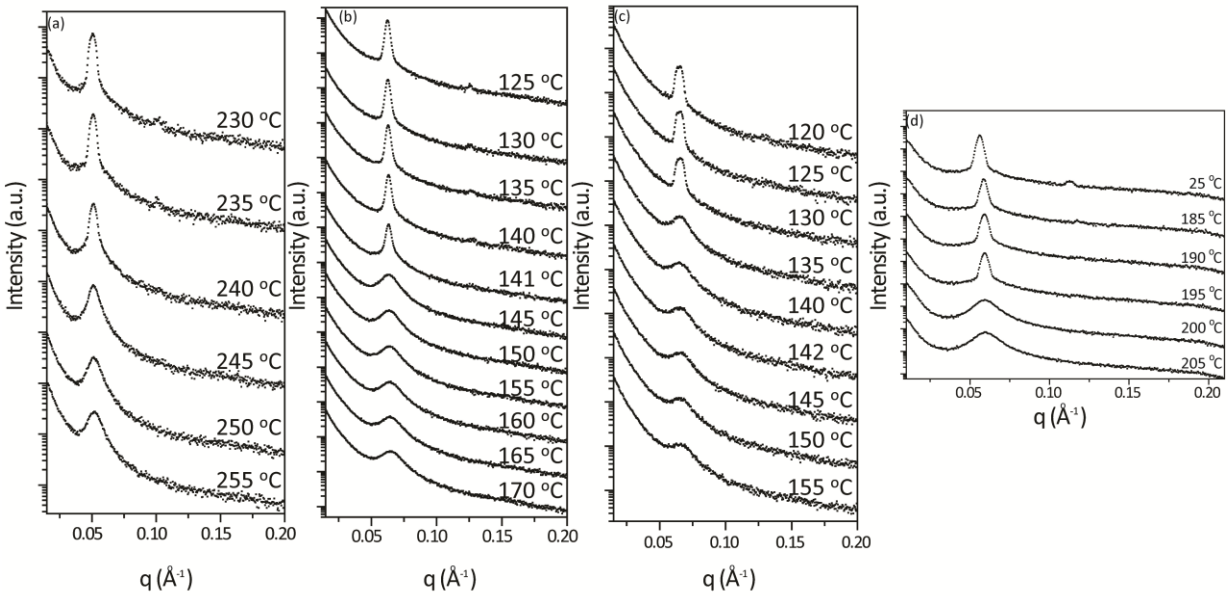

Figure 4.S5. Temperature dependent SAXS data to determine ODTs. (a) 4.2k-3.7k, (b) 3.1k-1.9k, (c) 3.0k-1.5k, (d) 3.2k-2.8k. Data was shifted vertically for clarity.

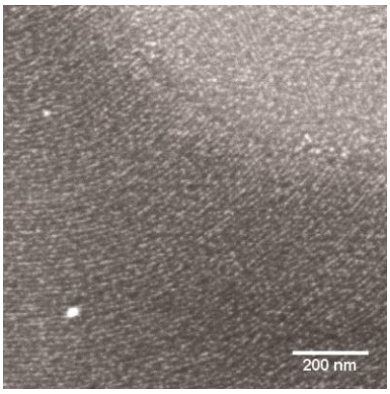

Figure 4.S6. Top-down SEM images of ~6 nm Pt nanowires derived from a thin film of 6.1k-1.6k that was seeded with Pt and etched with oxygen plasma.

4.7. References

1. Bates, F. S.; Fredrickson, G. H., Block Copolymer Thermodynamics: Theory and Experiment. *Annu. Rev. Phys. Chem.* **1990,** *41*, 525-557.

2. Semenov, A. N., Theory of Block-Copolymer Interfaces in the Strong Segregation Limit. *Macromolecules* **1993,** *26*, 6617-6621.

3. Thurn-Albrecht, T.; Steiner, R.; DeRouchey, J.; M. Stafford, C.; Huang, E.; Bal, M.; Tuominen, M.; Hawker, C. J.; Russell, T. P., Nanoscopic Templates from Oriented Block Copolymer Films. *Adv. Mater.* **2000,** *12*, 787-791.

4. Stoykovich, M. P.; Nealey, P. F., Block Copolymers and Conventional Lithography. *Mater. Today* **2006,** *9* (9), 20-29.

5. Nedoma, A. J.; Robertson, M. L.; Wanakule, N. S.; Balsara, N. P., Measurements of the Composition and Molecular Weight Dependence of the Flory-Huggins Interaction Parameter. *Macromolecules* **2008,** *41* (15), 5773-5779.

6. Gehlsen, M. D.; Weimann, P. A.; Bates, F. S.; Harville, S.; Mays, J. W.; Wignall, G. D., Synthesis and characterization of poly(vinylcyclohexane) derivatives. *J. Polym. Sci. Part B: Polym. Phys.* **1995,** *33* (10), 1527-1536.

7. Han, S. H.; Kim, J. K.; Pryamitsyn, V.; Ganesan, V., Phase Behavior of Binary Blends of Block Copolymers Having Hydrogen Bonding. *Macromolecules* **2011,** *44*, 4970-4976.

8. Russell, T. P.; Hjelm, R. P.; Seeger, P. A., Temperature dependence of the interaction parameter of polystyrene and poly(methyl methacrylate). *Macromolecules* **1990,** *23*, 890-893.

9. Leibler, L., Theory of Microphase Separation in Block Copolymers. *Macromolecules* **1980,** *13*, 1602-1617.

10. Kennemur, J. G.; Yao, L.; Bates, F. S.; Hillmyer, M. A., Sub-5 nm Domains in Ordered Poly(cyclohexylethylene)-block-poly(methyl methacrylate) Block Polymers for Lithography. *Macromolecules* **2014,** *47*, 1411-1418.

11. Li, M. Q.; Coenjarts, C. A.; Ober, C. K., Patternable Block Copolymers. *Adv. Polym. Sci.* **2005,** *190*, 183.

12. Hamley, I. W., Ordering in Thin Films of Block Copolymers: Fundamentals to Potential Applications. *Prog. Polym. Sci.* **2009,** *34*, 1161-1210.

13. Albert, J. N. L.; Epps III, T. H., Self-assembly of block copolymer thin films. *Mater. Today* **2010,** *13* (6), 24-33.

14. Bates, F. S.; Hillmyer, M. A.; Lodge, T. P.; Bates, C. M.; Delaney, K. T.; Fredrickson, G. H., Multiblock Polymers: Panacea or Pandora's Box? *Science* **2012,** *336*, 434-440.

15. Luo, M.; Epps III, T. H., Directed Block Copolymer Thin Film Self-Assembly: Emerging Trends in Nanopattern Fabrication. *Macromolecules* **2013,** *46*, 7567-7579.

16. Rincon-Delgadillo, P.; Craig, G.; Gronheid, R.; Nealey, P. F., Scale-up of a Chemo-Epitaxy Flow for Feature Multiplication Using Directed Self- Assembly of Block-Copolymers. *J. Photopolym. Sci. Technol.* **2013,** *26*, 831-839.

17. Chai, J.; Buriak, J. M., Using Cylindrical Domains of Block Copolymers To Self-Assemble and Align Metallic Nanowires. *ACS Nano* **2008,** *2*, 489-501.

18. Wang, Y.; Qin, Y.; Berger, A.; Yau, E.; He, C.; Zhang, L.; Gösele, U.; Knez, M.; Steinhart, M., Nanoscopic Morphologies in Block Copolymer Nanorods as Templates for Atomic-Layer Deposition of Semiconductors. *Adv. Mater.* **2009,** *21*, 2763-2766.

19. Cushen, J. D.; Bates, C. M.; Rausch, E. L.; Dean, L. M.; Zhou, S. X.; Willson, C. G.; Ellison, C. J., Thin Film Self-Assembly of Poly(trimethylsilylstyrene-b-d,l-lactide) with Sub-10 nm Domains. *Macromolecules* **2012,** *45*, 8722-8728.

20. Sweat, D. P.; Yu, X.; Kim, M.; Gopalan, P., Synthesis of Poly(4-hydroxystyrene)-Based Block Copolymers Containing Acid-Sensitive Blocks by Living Anionic Polymerization. *J. Polym. Sci. Part A: Polym. Chem.* **2014,** *52*, 1458-1468.

21. Pitet, L. M.; Wuister, S. F.; Peeters, E.; Kramer, E. J.; Hawker, C. J.; Meijer, E. W., Well-Organized Dense Arrays of Nanodomains in Thin Films of Poly(dimethylsiloxane)-b-poly(lactide) Diblock Copolymers. *Macromolecules* **2013,** *46*, 8289-8295.

22. Park, S.-M.; Liang, X.; Harteneck, B. D.; Pick, T. E.; Hiroshiba, N.; Wu, Y.; Helms, B. A.; Olynick, D. L., Sub-10 nm Nanofabrication via Nanoimprint Directed Self-Assembly of Block Copolymers. *ACS Nano* **2011,** *5*, 8523-8531.

23. Jung, Y. S.; Chang, J. B.; Verploegen, E.; Berggren, K. K.; Ross, C. A., A Path to Ultranarrow Patterns Using Self-Assembled Lithography. *Nano Lett.* **2010,** *10*, 1000-1005.

24. Jeong, J. W.; Park, W. I.; Kim, M.-J.; Ross, C. A.; Jung, Y. S., Highly Tunable Self-Assembled Nanostructures from a Poly(2-vinylpyridine-b-dimethylsiloxane) Block Copolymer. *Nano Lett.* **2011,** *11*, 4095-4101.

25. Jung, Y. S.; Ross, C. A., Orientation-Controlled Self-Assembled Nanolithography Using a Polystyrene−Polydimethylsiloxane Block Copolymer. *Nano Lett.* **2007,** *7* (7), 2046-2050.

26. Dai, K. H.; Kramer, E. J., Determining the temperature-dependent Flory interaction parameter for strongly immiscible polymers from block copolymer segregation measurements. *Polymer* **1994,** *35*, 157-161.

27. Hammond, M. R.; Cochran, E.; Fredrickson, G. H.; Kramer, E. J., Temperature Dependence of Order, Disorder, and Defects in Laterally Confined Diblock Copolymer Cylinder Monolayers. *Macromolecules* **2005,** *38*, 6575-6585.

28. Varshney, S. K.; Zhong, X. F.; Eisenberg, A., Anionic homopolymerization and block copolymerization of 4-vinylpyridine and its investigation by high-temperature size-exclusion chromatography in N-methyl-2-pyrrolidinone. *Macromolecules* **1993,** *26*, 701-706.

29. Creutz, S.; Teyssié, P.; Jérôme, R., Living Anionic Homopolymerization and Block Copolymerization of 4-Vinylpyridine at "Elevated" Temperature and Its Characterization by Size Exclusion Chromatography. *Macromolecules* **1997,** *30* (1), 1-5.

30. Yang, R.; Wang, Y.; Wang, X.; He, W.; Pan, C., Synthesis of poly(4-vinylpyridine) and block copoly (4-vinylpyridine–b-styrene) by atom transfer radical polymerization using 5,5,7,12,12,14-hexamethyl-1,4,8,11-tetraazamacrocyclotetradecane as ligand. *Eur. Polym. J.* **2003,** *39* (10), 2029-2033.

31. Meli, M.-V.; Badia, A.; Grütter, P.; Lennox, R. B., Self-Assembled Masks for the Transfer of Nanometer-Scale Patterns into Surfaces: Characterization by AFM and LFM. *Nano Lett.* **2001,** *2*, 131-135.

32. Walish, J. J.; Kang, Y.; Mickiewicz, R. A.; Thomas, E. L., Bioinspired Electrochemically Tunable Block Copolymer Full Color Pixels. *Adv. Mater.* **2009,** *21*, 3078-3081.

33. Kennemur, J. G.; Hillmyer, M. A.; Bates, F. S., Synthesis, Thermodynamics, and Dynamics of Poly(4-*tert*-butylstyrene-*b*-methyl methacrylate). *Macromolecules* **2012,** *45*, 7228-7236.

34. Hahn, J.; Filiz, V.; Rangou, S.; Lademann, B.; Buhr, K.; Clodt, J. I.; Jung, A.; Abetz, C.; Abetz, V., PtBS-b-P4VP and PTMSS-b-P4VP Isoporous Integral-Asymmetric Membranes with High Thermal and Chemical Stability. *Macromol. Mater. Eng.* **2013,** *298*, 1315-1321.

35. Sai, H.; Tan, K. W.; Hur, K.; Asenath-Smith, E.; Hovden, R.; Jiang, Y.; Riccio, M.; Muller, D. A.; Elser, V.; Estroff, L. A.; Gruner, S. M.; Wiesner, U., Hierarchical Porous Polymer Scaffolds from Block Copolymers. *Science* **2013,** *341*, 530-534.

36. Peng, Q.; Tseng, Y.-C.; Darling, S. B.; Elam, J. W., Nanoscopic Patterned Materials with Tunable Dimensions via Atomic Layer Deposition on Block Copolymers. *Adv. Mater.* **2010,** *22*, 5129-5133.

37. Peng, Q.; Tseng, Y.-C.; Darling, S. B.; Elam, J. W., A Route to Nanoscopic Materials via Sequential Infiltration Synthesis on Block Copolymer Templates. *ACS Nano* **2011,** *5*, 4600-4606.

38. Tsitsilianis, C.; Voulgaris, D., Poly(2-vinylpyridine)-based star-shaped polymers. Synthesis of heteroarm star (AnBn) and star-block (AB)n copolymers. *Macromol. Chem. Phys.* **1997,** *198* (4), 997-1007.

39. Klein, J. W.; Lamps, J.-P.; Gnanou, Y.; Rempp, P., Synthesis and characterization of block copolymers containing poly(tert.butyl acrylate) blocks. *Polymer* **1991,** *32* (12), 2278-2282.

40. Lee, S.; Gillard, T. M.; Bates, F. S., Fluctuations, Order, and Disorder in Short Diblock Copolymers. *AIChE J.* **2013,** *59*, 3502-3513.

41. Kim, J. K.; Lee, H. H.; Gu, Q.-J.; Chang, T.; Jeong, Y. H., Determination of Order−Order and Order−Disorder Transition Temperatures of SIS Block Copolymers by Differential Scanning Calorimetry and Rheology. *Macromolecules* **1998,** *31* (12), 4045-4048.

42. Leolukman, M.; Paoprasert, P.; Wang, Y.; Makhija, V.; McGee, D. J.; Gopalan, P., Influence of Architecture, Concentration, and Thermal History on the Poling of Nonlinear Optical Chromophores in Block Copolymer Domains. *Macromolecules* **2008,** *41*, 4651-4660.

Chapter 5. A Single Component Inimer Containing Cross-linkable Ultra-thin Polymer Coating for Dense Polymer Brush Growth

The contents of this chapter have been published in *Langmuir* **2013**, *29*, 3805-3812. Authors are: Sweat, Daniel P.; Kim, Myungwoong; Yu, Xiang; Gopalan, Padma.

Author Contributions: Daniel designed and synthesized the inimer and the copolymers, Myungwoong did the XPS quantification studies, thin film processing and characterization, Xiang performed the ATRP brush growth optimization. Daniel and Myungwoong interpreted the experimental data. All authors contributed towards writing the manuscript.

5.1. Abstract

We have developed a highly versatile universal approach to grow polymer brushes from a variety of substrates with high grafting density by using a single component system. We describe a random copolymer which consists of an inimer, *p*-(2-bromoisobutyloylmethyl)styrene (BiBMS), copolymerized with glycidyl methacrylate (GMA) synthesized by reversible addition-fragmentation chain-transfer (RAFT) polymerization. Thermal cross-linking created a mat that was stable during long exposure in organic solvent even with sonication or during Soxhlet extraction. The absolute bromine density was determined via X-ray photoelectron spectroscopy (XPS) to be 1.86 ± 0.12 Br atoms/nm^3. The ratio of experimental density to calculated absolute initiator density suggests that approximately ~25% of the bromine is lost during cross-linking. Surface-initiated ATRP (SI-ATRP) was used to grow PMMA brushes on the substrate with sacrificial initiator in solution. The brushes were characterized by ellipsometry, XPS and atomic

force microscopy (AFM) to determine thickness, composition and homogeneity. By correlating the molecular weight of polymer grown in solution with the brush layer thickness, a high grafting density of 0.80 ± 0.06 chains/nm^2 was calculated. By synthesizing the copolymer before cross-linking on the substrate, this single-component approach avoids any issues with blend miscibility as might be present for a multi-component curable mixture, while resulting in high chain density on a range of substrates.

5.2. Introduction

Polymer brushes are a broad class of materials consisting of a polymer chain tethered by one chain end to a surface.[1] These brushes have a variety of applications especially in their ability to tune and modify surface properties such as bioadhesion, wettability, and surface activity.[2] Two main methods for their preparation have emerged, namely grafting "to" and grafting "from".[3] The grafting "to" methodology involves the reaction of an end-functionalized polymer chain with an appropriate surface (*e.g.* hydroxyl-terminated polymer with an oxide surface) to anchor the polymer. Although grafting "to" allows for full characterization of the polymer before grafting, it is only applicable to limited substrates and requires terminal functionality on the polymer chain-end, and the grafting efficiency decreases with increasing molecular weight.[4]

Grafting "from" overcomes some of these limitations and has been used extensively with a variety of polymerization techniques such as living anionic, cationic, ring-opening, and conventional free-radical polymerization but perhaps the most widely used are the controlled free radical polymerization techniques, namely atom transfer radical polymerization (ATRP), nitroxide-mediated polymerization (NMP) and reversible addition-fragmentation chain-transfer (RAFT) polymerization.[1] By anchoring a suitable initiator to the substrate, polymer chains can be grown directly by the use of these various polymerization conditions. The vast majority of surface-

anchored initiators involve the formation of a self-assembled monolayer (SAM) on an appropriate substrate.[1] For silicon surfaces, this involves the use of chlorosilanes or alkoxysilanes, whereas for noble metal surfaces such as gold almost exclusively thiol-functionalized initiators are used.[1] While this strategy has obviously worked well , SAMs have limited stability to various reagents and are not substrate-independent, as they require a new initiator for every substrate type.[1]

Surface-initiated ATRP (SI-ATRP) has become the workhorse in the grafting "from" literature due to the ease in polymerizing a wide variety of monomers containing an array of functional groups with a high degree of control.[2] Control in ATRP comes from the reversible redox activation of a dormant polymer chain-end (halide functionalized) by a halogen transfer to a transition metal complex.[5] Many parameters are involved which can be tuned for better control such as type of ligand, Cu^{II} to Cu^{I} ratio, halide, solvent or initiator.[5] This large degree of variability provides an impressive window in which well-controlled polymers of numerous different monomers can be synthesized.

While the most common method for anchoring ATRP initiators to the substrate involves the formation of a SAM (siloxane or thiol based for Si and Au substrates, respectively), some alternative methods have been presented in the literature. von Werne *et al*. describe the inclusion of 10 ~ 20% ATRP inimer in a mixture of curable monomers suitable for photopolymerization.[6] This multi-component solution was designed for microcontact printing or nanoimprint lithography but required a siloxane-based SAM, 3-methacryloxypropyltrichlorosilane, as an adhesion promoter. This work was further extended by the use of an acid-cleavable ATRP inimer, allowing for direct measurement of surface grown brushes and their comparison with polymer grown from sacrificial initiator in solution.[7] An alternate method for creating an inimer layer is to form an adhesive coating which contains moieties for initiator incorporation. For example, layers of

poly(allylamine) (deposited by pulsed plasma polymerization) or catechol-amine (deposited by solution incubation) on various substrates were used for functionalizing the surface with ATRP initiators.[8,9,10] Alternatively, a homopolyer of glycidyl methacrylate was deposited on a Si wafer by dip coating and then ATRP initiator was incorporated by ring-opening with bromoacetic acid.[11] More recently, a catechol-functionalized methacrylamide and a methacrylate ATRP inimer were copolymerized by free radical polymerization and was then deposited on Ti substrates for polymer brush growth.[12]

Here we present a highly versatile universal approach to grow polymer brushes from a variety of substrates with high grafting density by using a single component system. Our previous work has shown that a random copolymer with 4% or less glycidyl methacrylate (GMA) can be thermally cross-linked into a stable cross-linked thin film (mat) on a plethora of surfaces.[13] In this paper, we describe a random copolymer which was designed to have an ATRP inimer as the majority component with a small amount of GMA for cross-linking. Thermal cross-linking created a mat that was stable to long-term exposure to organic solvent even with sonication or Soxhlet extraction. We further present detailed characterization of the mat by X-ray photoelectron spectroscopy (XPS) to determine the *absolute* initiator density (i.e., the number of initiators per unit volume) after thermal cross-linking. We find that this single component system, synthesized from readily available monomers, has a high initiator density which allows for the growth of grafted polymer brushes with high chain density. We study the chain density by correlating the molecular weight of polymer formed in solution and dry brush thickness. Through optimization of the polymerization conditions, excellent control over the grafting density was achieved. By synthesizing the copolymer before cross-linking on the substrate, this single component approach

avoids any issues with blend miscibility as might be present for a multicomponent curable mixture, while resulting in high chain density on a range of substrates.

5.3. Experimental Section

Materials. All chemicals were purchased from Sigma-Aldrich and used without further purification unless otherwise noted. 4-vinylbenzyl alcohol was synthesized according to a literature procedure.[14] Copper(I) bromide (99.999%) was stirred in acetic acid overnight, suction-filtered, washed with ethanol and then dried under vacuum. Styrene, glycidyl methacrylate and methyl methacrylate (MMA) were stirred over calcium hydride and then distilled under vacuum. 4-cyano-4-[(dodecylsulfanylthiocarbonyl)sulfanyl]pentanoic acid was synthesized according to a literature procedure.[15] 2,2'-Azobis(2-methylpropionitrile) (AIBN) was recrystallized from acetone and dried under vacuum.

Synthesis of *p*-(2-bromoisobutyloylmethyl)styrene (BiBMS). 4-vinylbenzyl alcohol (28.18 g, 210 mmol) was dissolved in 750 mL of dichloromethane and chilled *via* an external ice bath under a nitrogen atmosphere. 4-(dimethylamino)pyridine (1.28 g, 10.5 mmol) and triethylamine (38.47 g, 380 mmol) were added to the solution and stirred until dissolved. 2-bromoisobutyryl bromide (59.5 g, 259 mmol) was added slowly by syringe and the reaction stirred at 0 ^{o}C until thin-layer chromatography (TLC) showed complete conversion. The reaction was quenched via the addition of water and the layers separated using a separatory funnel. The organic layer was washed twice with water, 1 M HCl and 1 M NaOH, then dried over sodium sulfate and the solvent was removed by rotary evaporation. The resulting oil was distilled under reduced pressure (~1 Torr) at 130 ^{o}C to give a near colorless oil with a yield of 50 g (84% of theoretical yield). ^{1}H NMR (400 MHz, $CDCl_3$) δ: 7.41 (d, J = 8.3 Hz, 2H), 7.33 (d, J = 8.3 Hz, 2H), 6.71 (dd,

J = 17.6, 10.9 Hz, 1H), 5.76 (dd, *J* = 17.6, 0.9 Hz, 1H), 5.27 (dd, *J* = 17.6, 0.9 Hz, 1H), 5.19 (s, 2H), 1.94 (s, 6H). ^{13}C NMR (101 MHz, $CDCl_3$) δ: 171.49, 137.71, 136.33, 134.89, 128.24, 126.43, 114.44, 67.38, 55.72, 30.81.

Synthesis of *p*-(2-bromoisobutyloylmethyl)ethylbenzene. 4-ethylbenzyl alcohol (5.0 g, 36.7 mmol) was dissolved in 100 mL dichloromethane with 4-(dimethylamino)pyridine (22.4 mg, 0.18 mmol) and triethylamine (6.72 g, 66 mmol) under nitrogen and chilled to 0 ºC. 2-bromoisobutyryl bromide (10.4 g, 45.2 mmol) was added slowly by syringe and the reaction stirred at 0 ºC until TLC showed complete conversion. The reaction was quenched via the addition of water and the layers separated using a separation funnel. The organic layer was washed twice with water, 1 M HCl and 1 M NaOH, then dried over sodium sulfate and the solvent was removed by rotary evaporation. The resulting oil was then passed through a column of basic alumina to yield 9 g (86% yield). ^{1}H NMR (400 MHz, $CDCl_3$) δ: 7.30 (d, *J* = 8.3 Hz, 2H), 7.20 (d, *J* = 8.3 Hz, 2H), 5.17 (s, 2H), 2.65 (q, *J* = 7.6 Hz, 2H), 1.94 (s, 6H), 1.24 (t, *J* = 7.6 Hz, 3H).

Synthesis of P(BiBMS-*r*-GMA). BiBMS (2.55 g, 9 mmol), GMA (0.14 g, 1 mmol), 4-cyano-4-[(dodecylsulfanylthiocarbonyl)sulfanyl]pentanoic acid (40.3 mg, 0.1 mmol), and AIBN (4.1 mg, 0.025 mmol) were added to 1 gram anisole in a 10 mL Schlenk flask equipped with a magnetic stir bar. The mixture was degassed via three freeze-pump-thaw cycles and placed in an oil bath at 85 ºC for 16 hours. The polymerization was quenched by cooling the flask with cold water and exposure to air. The resulting viscous oil was then diluted with THF and precipitated into hexanes. The polymer was collected as a yellow powder and dried under vacuum. The relative composition of the two monomers was determined by ^{1}H NMR spectroscopy.

Synthesis of P(S-*r*-BiBMS-*r*-GMA). BiBMS (0.849 g, 3 mmol), GMA (0.071 g, 0.5 mmol), styrene (0.68 g, 6.5 mmol), 4-cyano-4-[(dodecylsulfanylthiocarbonyl)sulfanyl]pentanoic acid (40.3 mg, 0.1 mmol), and AIBN (4.1 mg, 0.025 mmol) were added to 1 gram anisole in a 10 mL Schlenk flask equipped with a magnetic stir bar. The mixture was degassed via three freeze-pump-thaw cycles and placed in an oil bath at 75 ^{o}C for 16 hours. The polymerization was quenched by cooling the flask with cold water and exposure to air. The resulting viscous oil was then diluted with THF and precipitated into hexanes. The polymer was collected as a yellow powder and dried under vacuum. The relative composition of the three monomers was determined by ^{1}H NMR spectroscopy.

Substrate preparation and thin film formation. A solution of P(BiBMS-*r*-GMA) or P(S-*r*-BiBMS-*r*-GMA) (0.3% w/w) in toluene was spin-coated onto silicon wafers that had been cleaned using piranha acid (7:3 H_2SO_4:H_2O_2, ***caution: reacts violently with organic compounds***). The substrate was then annealed under vacuum at 200 ^{o}C for various times to produce a cross-linked thin film. After annealing, the substrate was soaked in toluene and rinsed copiously with fresh toluene to remove uncross-linked polymer.

Surface-initiated atom transfer radical polymerization (SI-ATRP). MMA (4 grams, 40 mmol), *tris*-(2-pyridylmethyl)amine (60 mg, 0.21 mmol), CuBr (4.0 mg, 0.028 mmol), $CuBr_2$ (6.4 mg, 0.028 mmol), *p*-(2-bromoisobutyloylmethyl)ethylbenzene (7.6 mg, 0.027 mmol) and anisole (40 g) were mixed and sonicated until the copper completely dissolved into the brown solution. Equal amounts of the polymerization mixture was then added to four different flasks containing substrates covered with the cross-linked inimer mat and magnetic stir bars. The flasks were then degassed via three freeze-pump-thaw cycles. After warming to room temperature using a water bath, the flasks were immersed in a 60 ^{o}C oil bath for the requisite amount of time. After the

requisite amount of time elapsed, the flasks were cooled to room temperature using running water and the flask opened to atmosphere. The substrate was then removed from the flask and washed copiously with THF and water. After washing, the substrate was further soaked in THF for 2 hours, then sonicated in THF for 10 minutes, followed by rinsing with THF to remove any ungrafted polymer chains and dried using a stream of nitrogen. Some samples were further subjected to Soxhlet extraction using acetone for 18 hours to ensure that the THF treatment removed any ungrafted polymer.

Characterization. ^{1}H NMR and ^{13}C NMR spectrums were recorded in $CDCl_3$ using a Bruker Avance-400 spectrometer with TMS as internal standard. Gel-permeation chromatography (GPC) was performed using a Viscotek 2210 system equipped with three Waters columns (HR 4, HR 4E, HR 3) and a 1 mL/min flow rate of THF as eluent at 30 °C. Monodisperse PS standards were used for calibration. The film thickness of the samples was measured by ellipsometry (Rudolph Research Auto EL). The surface topography of the cross-linked mat and brush layer was examined using a Nanoscope III Multimode atomic force microscope (Digital Instruments) in tapping mode. Thermal gravimetric analysis was performed on a TA Instruments Q500 using a heating rate of 10 ^{o}C per minute under a nitrogen atmosphere. X-ray photoelectron spectroscopy (XPS) was done on a PerkinElmer 5400 ESCA spectrometer Phi model using a Mg X-ray source (300 W, 15 kV) at a takeoff angle of 45° from the substrate normal. The hemispherical energy analyzer was used in hybrid mode with a 1 mm × 3.5 mm area aperture. Survey spectra were collected at pass energy of 89.45 eV with a scan step size of 1.0 eV. High-resolution multiplex spectra were collected with pass energy of 35.75 eV and a step size of 0.05 eV. Water contact angle was measured with a Dataphysics OCA 15 Plus.

5.4. Results and discussion

Synthesis of random copolymer. Following the pioneering work by Matyjaszewski et. al.,[16] on an ATRP-functionalized methacrylate, namely 2-(2-bromoisobutyryloxy)ethyl methacrylate (BIEM), a whole range of inimers have been developed.[1] The main focus of the work so far with BIEM has been growing bottlebrush type copolymers in solution via the "grafting from" method.[17,18] A styrenic version using the same α-haloester type ATRP initiator, namely *p*-(2-bromoisobutyloylmethyl)styrene (BiBMS), has been recently developed for growing bottlebrush copolymers[19] or hyperbranched polymers.[20] We found that BiBMS is more easily controlled by conventional free radical or RAFT polymerization when copolymerized with GMA. Thus, we synthesized a random copolymer consisting of BiBMS and GMA by RAFT polymerization where the inimer is the majority component of the copolymer and GMA allows for the formation of a cross-linked mat (**Figure 5.1**). The polydispersity of this polymer (2.07, **Figure 5.S1**) was much higher than usual for a RAFT polymerization and the reasons for this are currently under investigation. For the purpose of this work however, the PDI was not of utmost importance as the copolymer was meant to be cross-linked on the surface where the PDI has shown to have little effect on the overall film properties.[13] The composition of the copolymer was determined to be 84% BiBMS and 16% GMA by ^{1}H NMR spectroscopy (**Figure 5.S1**).

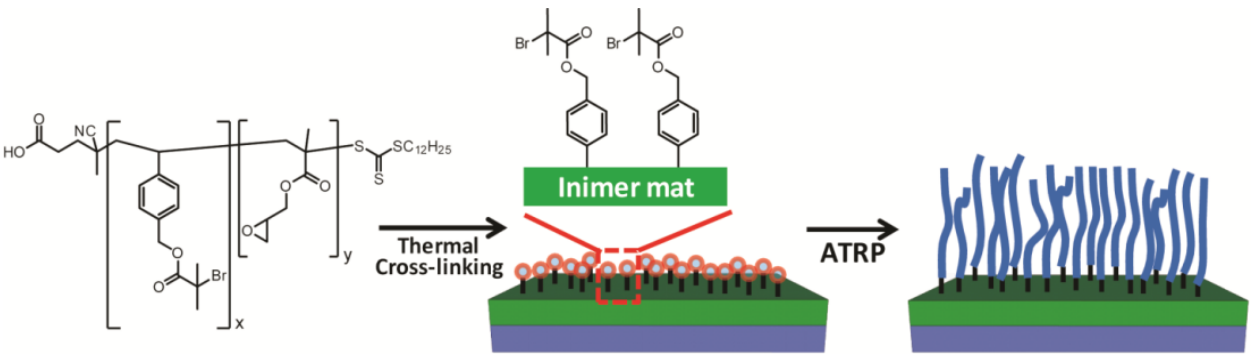

Figure 5.1. Schematic illustration of the process followed for the formation of the inimer mat and the brush growth.

Formation of Cross-linked mat and XPS quantification. TGA shows an initial decomposition step at 230 ^{o}C, likely due to decarboxylation and subsequent loss of propylene through bromide elimination (**Figure 5.S2**). Therefore, a cross-linking temperature of 200 ^{o}C was chosen to avoid unintentional degradation of the polymer during cross-linking while maintaining a rapid cross-linking rate. A 0.3% w/w solution in toluene of random copolymer was spin-coated onto silicon wafers to yield ~ 9 nm thick films. The substrates were then heated under vacuum at 200 ^{o}C for predetermined times and quenched to room temperature. After repeated washing in toluene, the samples were dried under nitrogen and the remaining thickness measured by ellipsometry. The film thickness after cross-linking but prior to washing was used as the initial thickness for determining cross-linking efficiency (**Figure 5.2**).

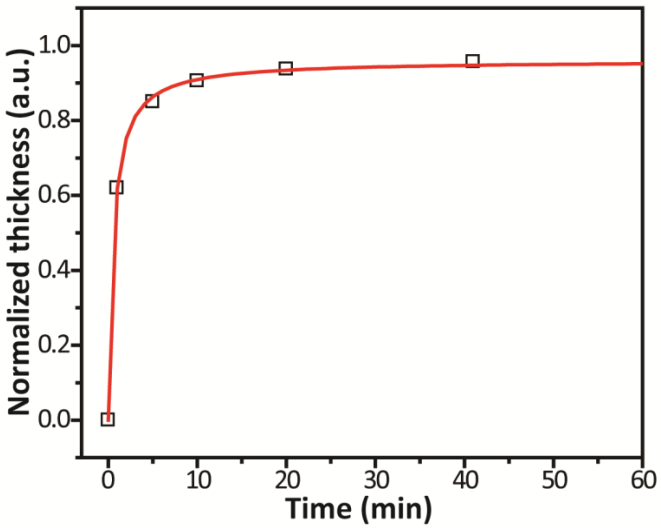

Figure 5.2. The normalized thickness as a function of time for evaluation of cross-linking efficiency at 200 ^{o}C.

After 10 minutes, the normalized thickness starts to plateau at approximately 90% of the original value. Despite the relatively low molecular weight (11.8 kDa), extensive cross-linking is achieved through a comparatively large amount of GMA.[13] To determine the effect of this processing on the initiating units, the amount of bromine in the mat was quantified by XPS. A typical XPS survey spectrum is shown in **Figure 5.3**, clearly showing the presence of bromine and the film thickness was controlled to be less than the typical XPS sampling depth (~ 10 nm) so that Si peaks from the substrate are also visible.

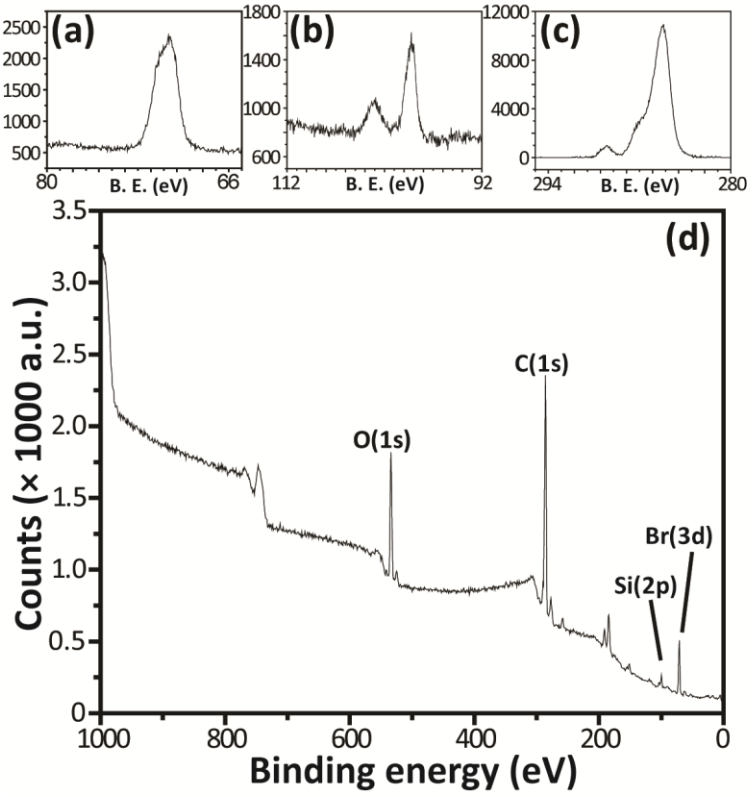

Figure 5.3. XPS spectra of the inimer mat showing: (a) Br(3d), (b) Si(2p), (c) C(1s), (d) survey scan.

The absolute elemental concentration can be determined from the intensity ratio of the element in the organic thin film to an element in the underlying substrate whose atomic density is

known.[21,22] We employed the native oxide layer as a reference as the density of silicon in the oxide is well known and the oxide thickness can be determined experimentally.

In general, the intensity of the XPS signal is given by the equation

$$I_S = I_0 \cdot e^{-\frac{d}{\lambda \cos\theta}} \quad (1)$$

where I_S is the detected intensity, I_0 is the incident electron intensity, d is the depth of the electrons emitted in the material, λ is the inelastic mean free path (IMFP) of electrons in the material and θ is the take-off angle. In these sample, signal from emitted electrons in three different layers contribute to the XPS spectrum: emitted electrons from silicon atoms in the silicon substrate, from silicon atoms in the native oxide and from various elements (C, O and Br) in the cross-linked mat. The intensity of emitted electrons from silicon atoms in the native oxide, I_{Si,SiO_2} can be calculated by integrating the exponential equation

$$I_{Si,\,SiO_2} = N_{Si,\,SiO_2} \cdot \int_0^{T_{ox}} e^{-\frac{z}{\lambda_{Si,SiO_2} \cdot \cos\theta}} dz \quad (2)$$

through the native oxide layer, typically 1.1 nm in our experiments, where N_{Si,SiO_2} is the number density of silicon atoms in native oxide layer (22.06 atoms/nm^3),[23] T_{ox} is the thickness of the native oxide, and λ_{Si,SiO_2} is the IMFP of the electrons from silicon in the native oxide layer. The emitted electrons further travel through the organic thin film layer, and then escape from the material and reach the detector, resulting in the Si(2p) peak at 101.5 ~ 104.5 eV. Therefore, the intensity of the peak is:

$$\frac{A_{Si}}{S_{Si}} = N_{Si,\,SiO_2} \cdot e^{-\frac{L}{\lambda_{Si,organic} \cos\theta}} \cdot \int_0^{T_{ox}} e^{-\frac{z}{\lambda_{Si,SiO_2} \cdot \cos\theta}} dz \quad (3)$$

where A_{Si} is the integrated intensity of the Si(2p) peak of SiO_2, S_{Si} is the relative sensitivity factor of Si(2p), L is the thickness of the organic thin film and $\lambda_{Si,organic}$ is the IMFP of the electrons emitted from silicon traversing the organic thin film layer.

The electrons emitted from the organic layer, specifically from the bromine atoms in the cross-linked mat, travel through the organic layer and reach the detector, resulting in a Br(3d) peak at 69.0 ~ 72.5 eV. Thus, the intensity of the Br(3d) peak can be formulated by the equation of

$$\frac{A_{Br}}{S_{Br}} = N_{Br,\,organic} \cdot \int_0^L e^{-\frac{z}{\lambda_{Br,organic}\cos\theta}} dz \qquad (4)$$

where A_{Br} is the integrated intensity of Br(3d) peak, S_{Br} is the relative sensitivity factor of Br(3d) and $\lambda_{Br,organic}$ is the IMFP of the electrons from bromine in the organic thin film layer. The intensity ratio of Si(2p) to Br(3d) is given by

$$\frac{\frac{A_{Si}}{S_{Si}}}{\frac{A_{Br}}{S_{Br}}} = \frac{N_{Si,\,SiO_2} \cdot e^{-\frac{L}{\lambda_{Si,organic}\cos\theta}} \cdot \int_0^{T_{ox}} e^{-\frac{z}{\lambda_{Si,SiO2}\cdot\cos\theta}} dz}{N_{Br,\,organic} \cdot \int_0^L e^{-\frac{z}{\lambda_{Br,organic}\cos\theta}} dz} \qquad (5)$$

from equation (3) and (4). Equation (5) can be rewritten as

$$N_{Br,\,organic} = \frac{\frac{A_{Br}}{S_{Br}}}{\frac{A_{Si}}{S_{Si}}} \cdot \frac{N_{Si,\,SiO_2} \cdot e^{-\frac{L}{\lambda_{Si,organic}\cos\theta}} \cdot \int_0^{T_{ox}} e^{-\frac{z}{\lambda_{Si,SiO2}\cdot\cos\theta}} dz}{\int_0^L e^{-\frac{z}{\lambda_{Br,organic}\cos\theta}} dz} \qquad (6)$$

Where, $N_{Br,organic}$ is the number density of bromine in the cross-linked mat.

The thickness of the cross-linked mat was 5.8 ± 0.4 nm, and λ_{Si,SiO_2}, $\lambda_{Si,organic}$ and $\lambda_{Br,organic}$ values were obtained from the literature.[24,25] From the high resolution XPS spectra of Br(3d) and Si(2p), the integrated intensity ratio, corrected for the relative sensitivity factors of Br(3d) and Si(2p) (S_{Br} = 1.053 and S_{Si} = 0.339), was found to be 2.23 ± 0.26 [$(A_{Br}/S_{Br})/(A_{Si}/S_{Si})$ in equation

(6)]. From this result, the calculated density of bromine in the cross-linked mat, $N_{Br,organic}$, is 1.86 ± 0.12 Br atoms/nm^3. For comparison, the theoretical amount of initiator per unit volume (ρ_{ini}) calculated using the number average molecular weight (M_n) and the number of inimer units per chain (the same as N_{Br}), as determined from GPC and ^{1}H NMR, respectively can be calculated from the equation

$$\rho_{ini} = \rho_p \cdot N_{av} \cdot N_{Br}/M_n \quad (7)$$

where, N_{av} is Avogadro's number and ρ_p is the density of copolymer which is 1.30 g/cm^3 (assuming the density of copolymer is similar to the weighted average density of the two monomers). Calculated ρ_{ini} is 2.53 initiators/nm^3, which is slightly higher than the experimentally determined value. The ratio of experimental density to calculated absolute initiator density is 0.735, suggesting that approximately 25% of the bromine is lost during processing.

We next compared the calculated results with the *relative* initiator concentration by looking at the ratio of bromine to carbon. To do so, we examined the calculated intensity ratio of Br(3d) to C(1s) peaks from high resolution XPS spectra (N(Br)/N(C)) and the theoretically estimated value from the compositional information obtained from ^{1}H NMR. The experimental data gave a N(Br)/N(C) of 0.0523 ± 0.001, while the theoretical value was 0.0700, resulting in the ratio of experimental value to theoretical value of 0.747. This value obtained from the relative intensity ratio is in excellent agreement with the values of N_{Br}/ρ_{ini} of 0.735 obtained from the quantitative comparison with the Si(2p) peak above.

In order to further verify the quantitative XPS analysis model, we synthesized a different copolymer which reduces the amount of inimer by incorporating an additional monomer that does not have bromine *e.g.* styrene. This copolymer consisted of styrene, BiBMS and GMA (M_n = 11.7 kDa, PDI = 1.61, F_{st} = 0.62, F_{BiBMS} = 0.29, F_{GMA} = 0.09, determined by GPC and ^{1}H NMR). The

cross-linked mat (5.0 ± 0.2 nm) was formed in the same manner as before on native oxide/Si substrate, followed by XPS characterization. Using equation (6) and (7), the experimental (N_{Br}) and the theoretical (ρ_{ini}) number density of initiator were 0.90 ± 0.18 Br atoms/nm^3 and 1.15 initiators/nm^3, respectively. This, again confirms the experimental value to be lower than the theoretical estimate (ratio of experimental to theoretical values is 0.78, comparable to the 0.735 from the previous calculation). Furthermore, it shows that the amount of initiator on the surface can be easily tuned by introducing a comonomer and thereby changing the molar ratio of inimer in the copolymer.

Surface initiated ATRP of PMMA. Following the quantitative analysis of inimer in the cross-linked film, we examined the growth of polymer brushes from this mat. Specifically, we were interested in the resulting chain density of grown polymer brushes considering the sheer density of initiating groups available for polymerization (1.86 Br/nm^3). Therefore, we quantitatively determined the chain density on the surface by correlating the molecular weight of sacrificial polymer grown in solution to the resulting brush layer thickness of the substrate using a well-known monomer, MMA. There is still some debate on the validity of this method[26,27,28] but several papers have cleaved the brushes from the surface for further analysis and shown the molecular weight is quite similar to that grown in solution.[7, 29, 30]

In our first experiments, we used standard ATRP conditions for the solution growth of PMMA (ethyl-2-bromoisobutyrate, CuBr and PMDETA) and indeed, we were able to control the sacrificial polymer grown in solution (PDI <1.2). However, under these conditions, the solution molecular weight did not reasonably correlate to the measured brush thickness. The polymer brush height implied a length longer than the fully-extended contour length of a polymer with the solution molecular weight that was measured. Therefore, several parameters needed to be

optimized.

First, we needed to ensure that the initiating species had as similar a reactivity between solution and substrate as possible. Even though ethyl 2-bromoisobutyrate (**Figure 5.4a**) has the same α-haloester type ATRP initiating moiety as BiBMS (Figure 2.6b), Matyjaszewski *et al*. have shown that going from methyl 2-bromoisobutyrate to ethyl 2-bromoisobutyrate almost halves the ATRP equilibrium constant keeping everything else constant.[31,32] Therefore, it was important to account for this possible reactivity difference. A new ATRP initiator p-(2-bromoisobutyloylmethyl)ethylbenzene (**Figure 5.4c**) was thus synthesized to mimic the propagating reactive sites on the surface by having the same molecular structure with an ethyl moiety instead of vinyl. Secondly, as the monomer is depleted in solution, it is likely that any discrepancy in molecular weight between the surface and the substrate will be magnified due to viscosity and other kinetics issues.[26] A very small amount of initiator (target 1500 DP) was used to initiate the sacrificial polymer in solution which allowed the monomer concentration to stay as constant as possible. A magnetic stir bar was used to promote a homogeneous solution, maintaining consistent concentrations without gradients. Also, copper (II) bromide was found to be the most effective parameter for controlling the brush growth rate. However, by including $CuBr_2$, this slowed the solution growth of the PMMA to an unreasonable extent, hence a stronger ligand (*tris*-(2-pyridylmethyl)amine, TPMA) was used to counteract this effect.[32] The combination of strong ligand and stoichiometrically large amount of $CuBr_2$ allowed for the solution grown PMMA to have a PDI of less than 1.10.

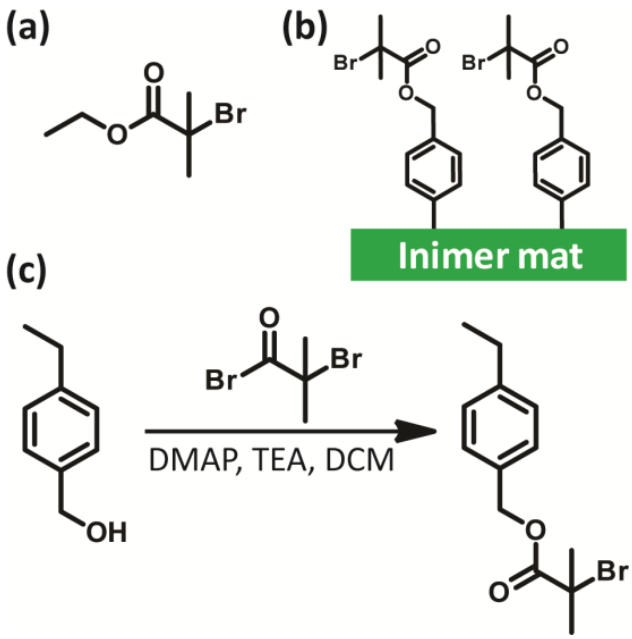

Figure 5.4. Structure of (a) ATRP initiator ethyl 2-bromoisobutyrate, (b) initiating sites on the surface, and (c) the synthetic scheme for the initiator *p*-(2-bromoisobutyloylmethyl)ethylbenzene.

With the conditions for SI-ATRP thus optimized, kinetic studies were done to examine the brush growth over time and its correlation to solution molecular weight. First, the PMMA polymerized in solution exhibits excellent control and linear kinetics as evidenced by the linear increase in M_n with time (due to the low overall conversion of monomer) and the narrow PDI (**Figure 5.5)**. The brush thickness also exhibited a linear relationship with polymerization time, showing a well-controlled polymerization on the surface as well. Ungrafted polymer was removed by soaking the substrates in THF for two hours and followed by sonication for 10 minutes. To ensure this THF treatment was efficient at removing ungrafted polymer, we subjected substrates to Soxhlet extraction with acetone for 18 hours. After extraction, the thickness was identical to the previous results from sonicating in THF, confirming the successful removal of ungrafted polymer, as well as the stability of the mat.

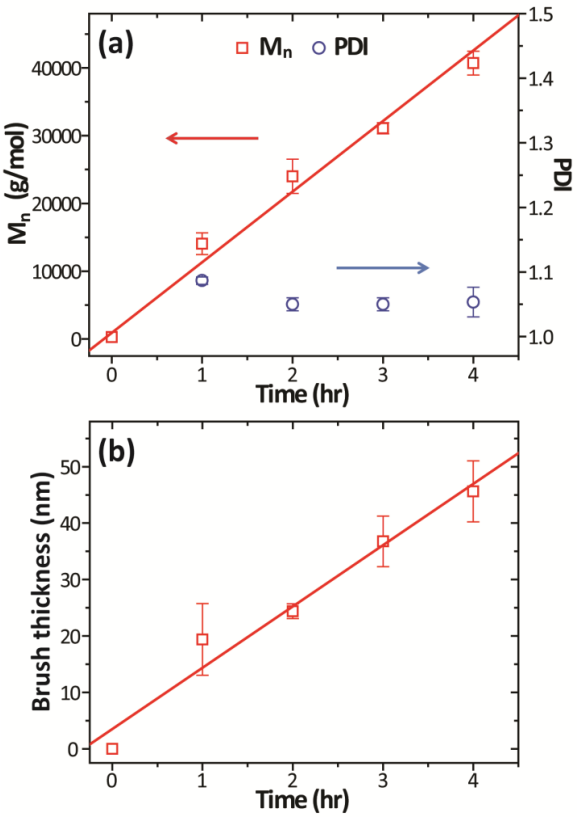

Figure 5.5. Plots showing (a) M_n and PDI of the PMMA grown in solution as a function of polymerization time during SI-ATRP of MMA, and (b) the linear increase in brush thickness as a function of time.

By correlating the dry brush thickness (h) with the M_n of PMMA grown in solution, the chain density (σ) can be calculated using a standard equation (8),

$$\sigma = h \cdot N_{av} \cdot \rho / M_n \quad (8)$$

where ρ = 1.19 g/cm^3 (bulk density of PMMA).[33] As ρ and N_{av} are constant, the relationship between brush thickness and molecular weight is linear, with the chain density as the slope of the line (equal to $\sigma/(N_{av} \cdot \rho)$). In **Figure 5.6a**, the graph showing brush thickness as a function of molecular weight exhibits a clear linear trend over the experimental time examined. Using equation (8), the chain density is calculated to be 0.80 ± 0.06 chains/nm^2, which is considerably

higher than other "very dense" brushes prepared by SI-ATRP.[34] The chain density can also be calculated for each polymerization time by directly applying equation (8) and the resulting data is also plotted in **Figure 5.6b**, demonstrating a high chain density that was constant for the entire polymerization time.

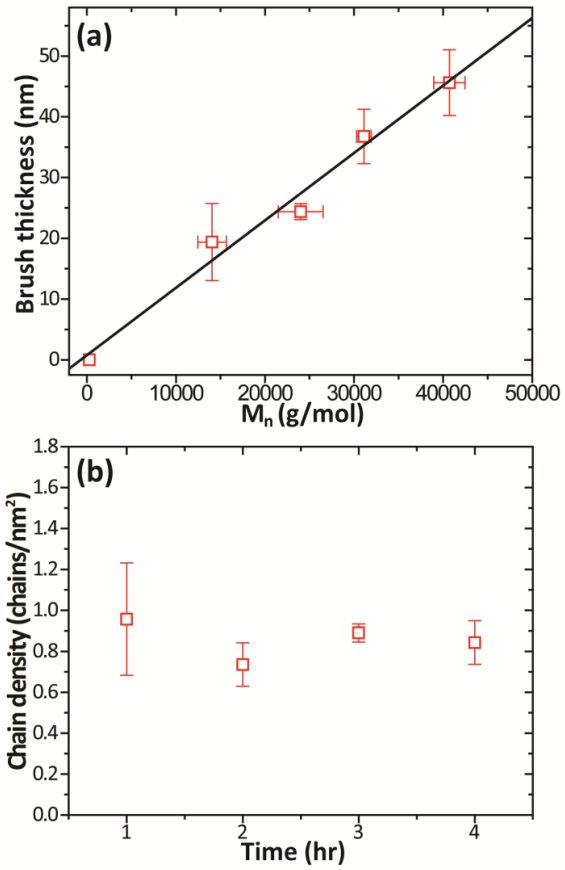

Figure 5.6. Kinetics data from SI-ATRP of MMA showing (a) a linear correlation between the brush thickness and the M_n of the PMMA grown in solution, and (b) the uniform average chain density at various polymerization times.

We also used atomic force microscopy (AFM) to examine the surface morphology of both the inimer mat and grown polymer brush films. **Figure 5.7** shows the AFM height data for the inimer mat and after 3 hours of SI-ATRP. The inimer mat exhibits extremely low roughness with

an average height variation of less than 0.4 nm over a 5 × 5 μm^2 area. All polymer brush films examined showed similar AFM micrographs with a roughness of 1.82 nm, 3.73 nm and 3.56 nm for 1 hour, 2 hours and 3 hours of polymerization, respectively. Typically, there were large flat areas with occasional divots which traversed the full brush thickness down to the inimer mat. The reason for these holes is still under investigation, probably due to inefficient and incomplete initiation in those areas. A slower polymerization rate could allow for an even more uniform film.

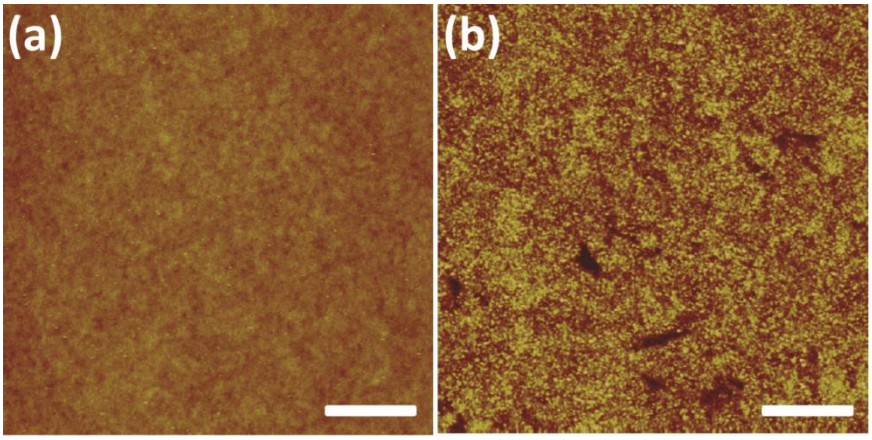

Figure 5.7. Tapping-mode AFM height images of the inimer mat (a) before growth and (b) after 3 hours of polymerization (scale bar is 1 μm).

We also examined the effect of different substrates on the polymer brush growth. In addition to the piranha treated bare Si discussed extensively, we prepared inimer mats on SiO_2/Si, Au/Si and aluminum oxide/Si substrates. SiO_2, Au and aluminum oxide substrates were prepared by evaporation of source materials using e-beam dielectric or metal evaporators onto Si wafers. While the bare silicon was cleaned with piranha acid, the other substrates were not chemically cleaned to preserve their inherent properties. The inimer mat was formed in the same manner as before, through spin-coating and thermal cross-linking. The mats were then subjected to two hours of PMMA polymerization under the optimized conditions discussed earlier. Static water contact angle measurements of the bare substrate, the inimer mat and the brush layer were taken to judge

the efficacy of the film at growing brushes on various substrates (**Figure 5.8**). All of the bare substrates show the expected contact angles while post-deposition of the mat and growth of PMMA brushes, the contact angles for the various substrates became equivalent. The contact angle measured for the grown PMMA brush layer matches well with previous reports.[35]

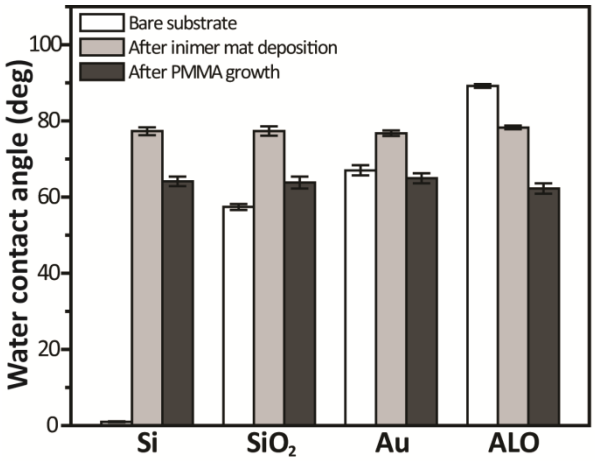

Figure 5.8. Static water contact angles for various substrates before inimer mat formation, after cross-linking and after growth of PMMA brushes.

To further confirm the growth of PMMA on the surface, XPS was used to characterize the brush films (**Figure 5.S3**). The intensity ratio of deconvoluted C-C or C-H, C-O and O=C-O peaks show good agreement with the theoretical ratios for PMMA, providing additional evidence for polymer brush growth.

5.5. Conclusions

In summary, we have developed a new approach to create a cross-linked thin film from a single component system containing an inimer as a comonomer. A random copolymer of BiBMS and GMA was synthesized, fully characterized and cross-linked into an "inimer bearing mat" on a range of substrates. The amount of initiator on the surface can be readily tuned by introducing an additional monomer to reduce the percentage of inimer, providing a facile method to tailor the

surface properties. After thermally cross-linking a thin film of the copolymer which contains 84 mol% BiBMS, the absolute initiator density in the resulting ultra-thin mat characterized using XPS showed a value of 1.86 ± 0.12 Br atoms/nm^3. A uniform polymer chain density over the entire polymerization time frame was achieved by optimization of conditions for SI-ATRP, including the synthesis of a new initiator. Kinetic studies on the growth of PMMA from the surface gave an average chain density for these PMMA brushes of 0.80 ± 0.06 chains/nm^2, which is quite high given the theoretical maximum chain density of PMMA (about 1.4-1.6 chains/nm^2). The inimer containing cross-linkable copolymer can be viewed as a single component ultra-thin polymeric coating which can be applied to a range of substrates to grow high chain density polymer brushes by ATRP. The ease of synthesis, chemical tunability, homogeneity of composition, stability in organic solvents and applicability by simple spin-coating to a wide range of substrates makes this a versatile approach to create functionalized interfaces. We are currently exploring this system for the growth of poly(ethylene glycol)methyl ether methacrylate brushes to resist non-specific cell adhesion.[36]

5.6. Supporting Information

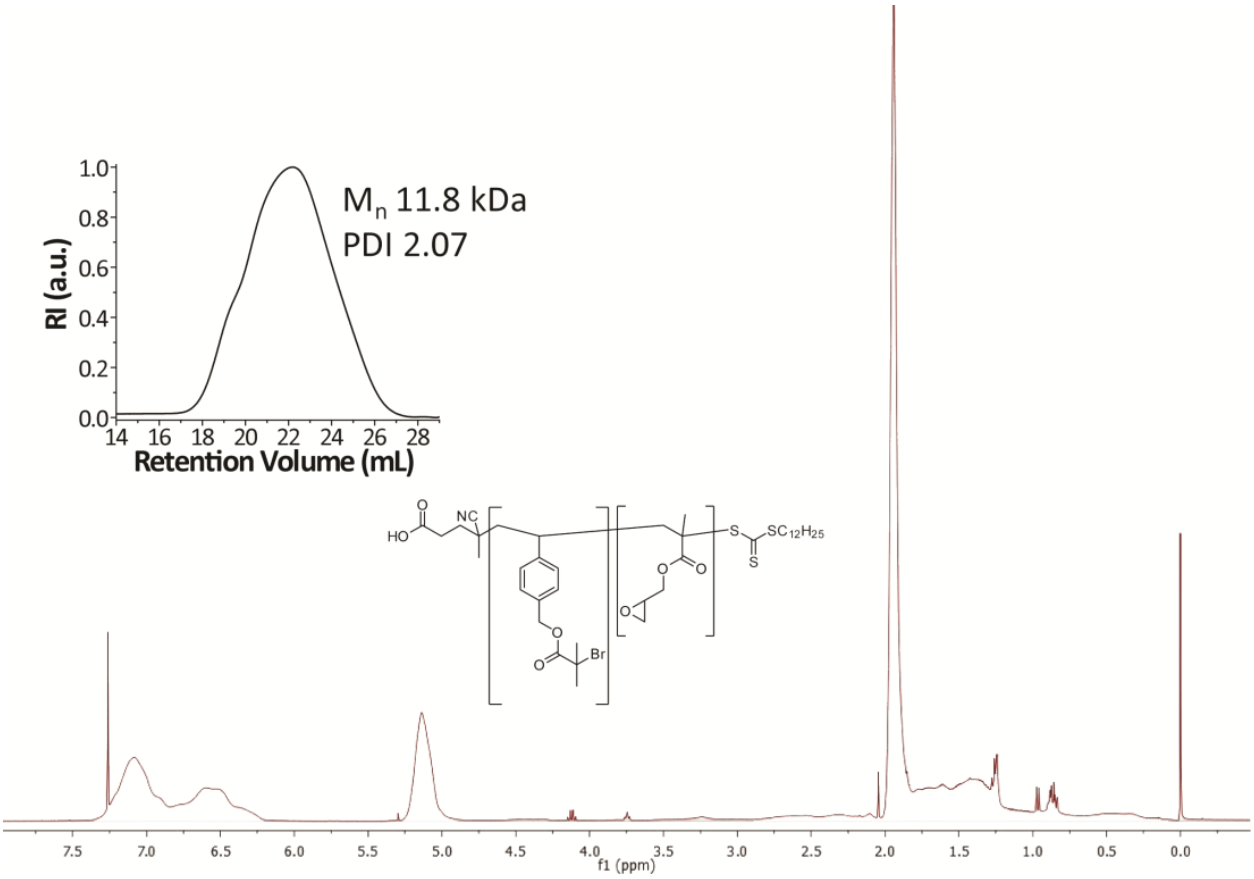

Figure 5.S1. ^{1}H NMR spectrum of P(BiBMS-*r*-GMA) copolymer with GPC (inset).

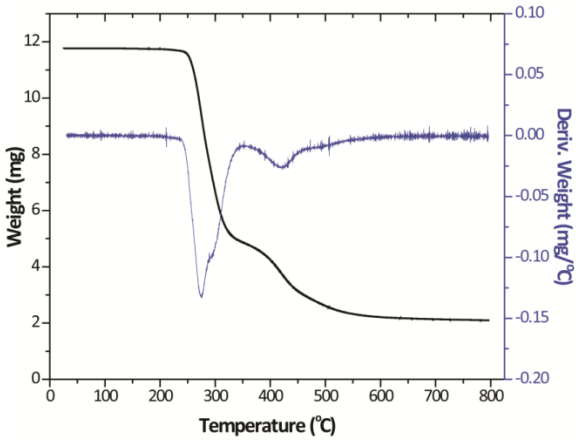

Figure 5.S2. TGA of P(BiBMS-*r*-GMA) copolymer.

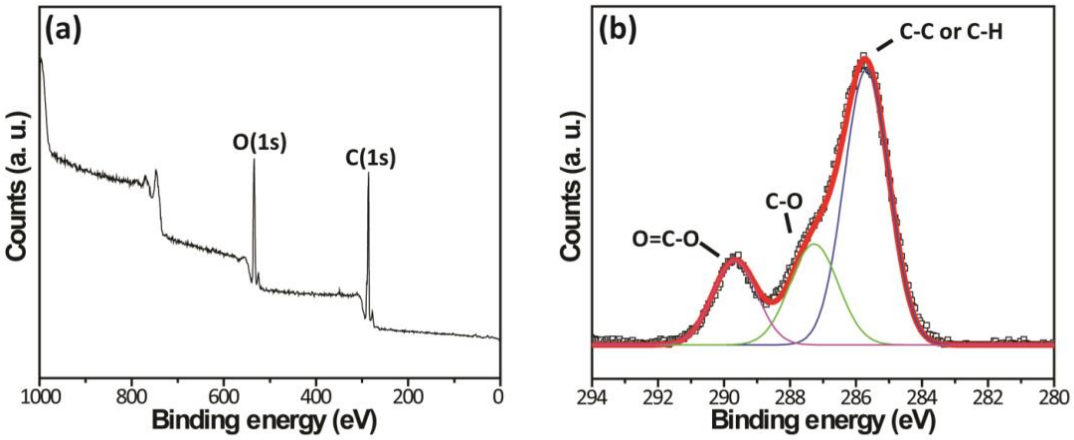

	C-C or C-H	C-O	O=C-O
Position	285.7	287.3	289.7
Theoretical ratio	3	1	1
Intensity ratio	3.30	1.30	1.00

Figure 5.S3. XPS spectra of a PMMA film grown from the inimer mat.

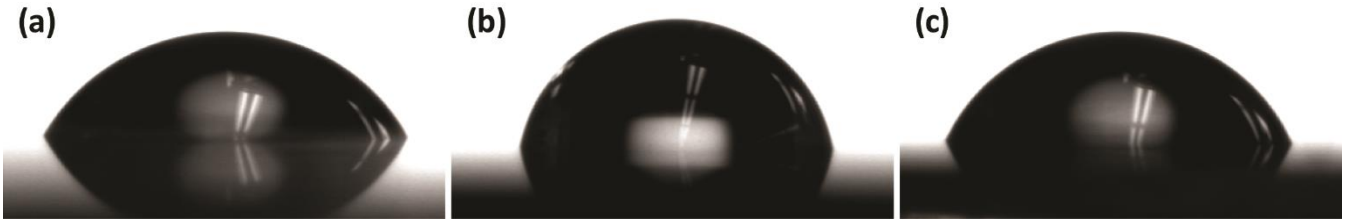

Figure 5.S4. Pictures of sessile water drops on (a) SiO_2, (b) after inimer mat formation and (c) after growth of PMMA brushes.

5.7. References

1. Barbey, R.; Lavanant, L.; Paripovic, D.; Schüwer, N.; Sugnaux, C.; Tugulu, S.; Klok, H.-A., Polymer Brushes via Surface-Initiated Controlled Radical Polymerization: Synthesis, Characterization, Properties, and Applications. *Chem. Rev.* **2009,** *109*, 5437-5527.

2. Edmondson, S.; Osborne, V. L.; Huck, W. T. S., Polymer Brushes *via* Surface-Initiated Polyermizations. *Chem. Soc. Rev.* **2004,** *33*, 14-22.

3. Zhao, B.; Brittain, W., Polymer Brushes: Surface-Immobilized Macromolecules. *J. Prog. Polym. Sci.* **2000,** *25*, 677-710.

4. Balazs, A. C.; Singh, C.; Zhulina, E.; Chern, S.-S.; Lyatskaya, Y.; Pickett, G., Theory of Polymer Chains Tethered at Interfaces. *Prog. Surf. Sci.* **1997,** *55*, 181-269.

5. Matyjaszewski, K.; Xia, J. H., Atom Transfer Radical Polymerization. *Chem. Rev.* **2001,** *101*, 2921-2990.

6. von Werne, T. A.; Germack, D. S.; Hagberg, E. C.; Sheares, V. V.; Hawker, C. J.; Carter, K. R., A Versatile Method for Tuning the Chemistry and Size of Nanoscopic Features by Living Free Radical Polymerization. *J. Am. Chem. Soc.* **2003,** *125*, 3831-3838.

7. Koylu, D.; Carter, K. R., Stimuli-Responsive Surfaces Utilizing Cleavable Polymer Brush Layers. *Macromolecules* **2009,** *42*, 8655-8660.

8. Yameen, B.; Khan, H. U.; Knoll, W.; Förch, R.; Jonas, U., Surface Initiated Polymerization on Pulsed Plasma Deposited Polyallylamine: A Polymer Substrate-Independent Strategy to Soft Surfaces with Polymer Brushes. *Macromol. Rapid Commun.* **2011,** *32*, 1735-1740.

9. Coad, B. R.; Lua, Y.; Meagher, L., A Substrate-Independent Method for Surface Grafting Polymer Layers by Atom Transfer Radical Polymerization: Reduction of Protein Adsorption. *Acta Biomaterialia* **2012,** *8*, 608-618.

10. Fan, X.; Lin, L.; Dalsin, J. L.; Messersmith, P. B., Biomimetic Anchor for Surface-Initiated Polymerization from Metal Substrates. *J. Am. Chem. Soc.* **2005,** *127*, 15843-15847.

11. Liu, Y. K., V; Zdyrko, B; Luzinov, I., Polymer Grafting via ATRP Initiated from Macroinitiator Synthesized on Surface. *Langmuir* **2004,** *20*, 6710-6718.

12. Wang, X.; Ye, Q.; Gao, T.; Liu, J.; Zhou, F., Self-Assembly of Catecholic Macroinitiator on Various Substrates and Surface-Initiated Polymerization. *Langmuir* **2012,** *28*, 2574-2581.

13. Han, E.; Gopalan, P., Cross-Linked Random Copolymer Mats As Ultrathin Nonpreferential Layers for Block Copolymer Self-Assembly. *Langmuir* **2010,** *26*, 1311-1315.

14. Zhao, L. J.; Kwong, C. K. W.; Shi, M.; Toy, P. H., Optimization of Polystyrene-Supported Triphenylphosphine Catalysts for aza-Morita-Baylis-Hillman Reactions. *Tetrahedron* **2005,** *61* (51), 12026-12032.

15. Moad, G.; Chong, Y. K.; Postma, A.; Rizzardo, E.; Thang, S. H., Advances in RAFT Polymerization: the Synthesis of Polymers with Defined End-Groups. *Polymer* **2005,** *46*, 8458-8468.

16. Beers, K. L.; Gaynor, S. G.; Matyjaszewski, K., The Synthesis of Densely Grafted Copolymers by Atom Transfer Radical Polymerization. *Macromolecules* **1998,** *31*, 9413-9415.

17. Bolton, J.; Rzayev, J., Tandem RAFT-ATRP Synthesis of Polystyrene−Poly(Methyl Methacrylate) Bottlebrush Block Copolymers and Their Self-Assembly into Cylindrical Nanostructures. *ACS Macro. Lett.* **2012,** *1*, 15-18.

18. Nese, A.; Li, Y.; Sheiko, S. S.; Matyjaszewski, K., Synthesis of Molecular Bottlebrushes by Atom Transfer Radical Polymerization with ppm Amounts of Cu Catalyst. *ACS Macro. Lett.* **2012,** *1*, 991-994.

19. Chen, Y.; Kushner, A. M.; Williams, G. A.; Guan, Z., Multiphase Design of Autonomic Self-Healing Thermoplastic Elastomers. *Nature Chem.* **2012,** *4*, 467-472.

20. Dong, B.-T.; Dong, Y.-Q.; Du, F.-S.; Li, Z.-C., Controlling Polymer Topology by Atom Transfer Radical Self-Condensing Vinyl Polymerization of p-(2-Bromoisobutyloylmethyl)styrene. *Macromolecules* **2010,** *43*, 8790-8798.

21. Paoprasert, P.; Spalenka, J. W.; Peterson, D. L.; Ruther, R. E.; Hamers, R. J.; Evans, P. G.; Gopalan, P., Grafting of Poly(3-hexylthiophene) Brushes on Oxides Using Click Chemistry. *J. Mat. Chem.* **2010,** *20*, 2651-2658.

22. Franking, R. A.; Landis, E. C.; Hamers, R. J., Highly Stable Molecular Layers on Nanocrystalline Anatase TiO_2 through Photochemical Grafting. *Langmuir* **2009,** *25*, 10676-10684.

23. Gavrilenko, V. P.; Novikov, Y. A.; Rakov, A. V.; Todua, P. A., Measurement of Thickness of Native Silicon Dioxide With a Scanning Electron Microscope. *Proc. of SPIE* **2009,** *7405*, 740507-1.

24. Powell, C. J.; Jablonski, A., Evaluation of Electron Inelastic Mean Free Paths for Selected Elements and Compounds. *Surf. Interface Anal.* **2000,** *29*, 108-114.

25. Laibinis, P. E.; Bain, C. D.; Whitesides, G. M., Attenuation of Photoelectrons in Monolayers of Normal-Alkanethiols Adsorbed on Copper, Silver, and Gold. *J. Phys. Chem.* **1991,** *95*, 7017-7021.

26. Turgman-Cohen, S.; Genzer, J., Simultaneous Bulk- and Surface-Initiated Controlled Radical Polymerization from Planar Substrates. *J. Am. Chem. Soc.* **2011,** *133*, 17567-17569.

27. Gorman, C. B.; Petrie, R. J.; Genzer, J., Effect of Substrate Geometry on Polymer Molecular Weight and Polydispersity during Surface-Initiated Polymerization. *Macromolecules* **2008,** *41*, 4856-4865.

28. Pasetto, P.; Blas, H.; Audouin, F.; Boissière, C.; Sanchez, C.; Save, M.; Charleux, B., Mechanistic Insight into Surface-Initiated Polymerization of Methyl Methacrylate and Styrene via ATRP from Ordered Mesoporous Silica Particles. *Macromolecules* **2009,** *42*, 5983-5995.

29. Devaux, C.; Chapel, J. P.; Beyou, E.; Chaumont, P., Controlled Structure and Density of "Living" Polystyrene Brushes on Flat Silica Surfaces. *Eur. Phys. J. E* **2002,** *7*, 345-352.

30. Husseman, M.; Malmström, E. E.; McNamara, M.; Mate, M.; Mecerreyes, D.; Benoit, D. G.; Hedrick, J. L.; Mansky, P.; Huang, E.; Russell, T. P.; Hawker, C. J., Controlled Synthesis of Polymer Brushes by "Living" Free Radical Polymerization Techniques. *Macromolecules* **1999,** *32*, 1424-1431.

31. Tang, W.; Matyjaszewski, K., Effects of Initiator Structure on Activation Rate Constants in ATRP. *Macromolecules* **2007,** *40*, 1858-1863.

32. Tang, W.; Kwak, Y.; Braunecker, W.; Tsarevsky Nicolay, V.; Coote Michelle, L.; Matyjaszewski, K., Understanding Atom Transfer Radical Polymerization: Effect of Ligand and Initiator Structures on the Equilibrium Constants. *J. Am. Chem. Soc.* **2008,** *130*, 10702-10713.

33. Brandrup, J.; Immergut, E. H.; Grulke, E. A., *Polymer handbook*. 4th ed.; Wiley: 1999.

34. Matyjaszewski, K.; Dong, H.; Jakubowski, W.; Pietrasik, J.; Kusumo, A., Grafting from Surfaces for "Everyone": ARGET ATRP in the Presence of Air. *Langmuir* **2007,** *23*, 4528-4531.

35. Han, E.; Leolukman, M.; Kim, M.; Gopalan, P., Resist Free Patterning of Nonpreferential Buffer Layers for Block Copolymer Lithography. *ACS Nano* **2010,** *4*, 6527-6534.

36. Schmitt, S. K.; Murphy, W. L.; Gopalan, P., Crosslinked PEG mats for peptide immobilization and stem cell adhesion. *J. Mater. Chem. B* **2013,** *1*, 1349-1360.

Chapter 6. A Dual Functional Layer for Block Copolymer Self-Assembly and the Growth of Nanopatterned Polymer Brushes

The contents of this chapter have been published in *Langmuir* **2013**, *29*, 12858-12865. Authors are: Sweat, Daniel P.; Kim, Myungwoong; Yu, Xiang; Schmitt, Samantha K.; Han, Eungnak; Choi, Jonathan W.; Gopalan, Padma.

Author Contributions: Daniel designed and synthesized the copolymers, Myungwoong did the XPS quantification, neutrality studies, thin film processing and characterization, Xiang did the optimization of ATRP conditions, Samantha did the AFM studies, Eungnak designed the concept of dual functional layer and Jonathan contributed towards thin-film studies. Daniel and Myungwoong interpreted the experimental data.

6.1. Abstract

We present a versatile method for fabricating nanopatterned polymer brushes using a cross-linked thin film made from a random copolymer consisting of an inimer (*p*-(2-bromoisobutyloylmethyl)styrene), styrene, and glycidyl methacrylate (GMA). The amount of inimer was held constant at 20 or 30% while the relative amount of styrene to GMA was varied to induce perpendicular domain orientation in an overlying P(S-*b*-MMA) block copolymer (BCP) film for lamellar and cylindrical morphologies. A cylinder forming BCP blend with PMMA homopolymer was assembled to create a perpendicular hexagonal array of cylinders, which allowed access to a nanoporous template without the loss of initiator functionality. Surface-initiated ATRP of 2-hydroxyethyl methacrylate was conducted through the pores to generate a

dense array of nanopatterned brushes. Alternatively, gold was deposited into the nanopores, and brushes were grown around the dots after removal of the template. This is the first example of combining the chemistry of nonpreferential surfaces with surface initiated growth of polymer chains.

6.2. Introduction

Patterned polymer brushes have been synthesized by a variety of techniques for applications in stimuli responsive coatings, photonic crystals, microelectronics and nanofluidics.[1-3] The synthesis of polymer brushes can be accomplished through the use of grafting "to" and grafting "from" strategies, with grafting "from" being the most common.[4] Most polymer brushes are grown from self-assembled monolayers (SAMs) of initiators, which can be combined with top-down patterning, such as electron-beam lithography,[5] to create nanopatterned brushes. Nanopatterned brushes have been defined by many different methods such as e-beam patterning of pregrown brushes,[2] spatially localized photopolymerization of initiators,[6] and by selective placement of initiators on the surface through contact molding.[7] However, the drawbacks of serial processes such as e-beam lithography towards large area applications are well-known.[8] Likewise, the limitations of using SAMs to grow polymer brushes such as lack of long-term stability in various biological mediums[1] as well as lack of substrate independence limits its utility.[9] Ideally, we would like to have a method which can create dense periodic array of nanopatterned polymer brushes in a substrate-independent manner, over large areas using nonlithographic approach, which also addresses the stability issues.

For nanopatterning, block copolymer (BCP) lithography has been used in a variety of applications as it overcomes many of the limitations of serial processes, resulting in high density, large area arrays of nanostructures with feature sizes typically between 5 and 50 nm.[10-15] Among

the various BCP systems, poly(styrene-*block*-methyl methacrylate) [P(S-*b*-MMA)] is most widely used for thin film self-assembly due to the nearly equal surface energies of the two blocks and the ability to selectively degrade the PMMA domains.[16-19] One of the first steps for BCP lithography is to control the domain orientation in thin film. We and others have done an extensive amount of work in developing the chemistry and a fundamental understanding of the factors that control the domain orientation of P(S-*b*-MMA).[18, 20-25] The orientation of the microdomains in thin films is mainly controlled by the interaction of each block with the substrate and the free surface through wetting energetics and polymer confinement effects (resulting from the film thickness).[23, 25-27] Balancing the interfacial interactions of A-*b*-B BCPs using A-*r*-B or A-*r*-B-*r*-C random copolymers, so-called "surface neutralization", provides a simple route for the fabrication of perpendicularly oriented domains in thin BCP films.[23, 28] We will refer to these neutral surfaces as nonpreferential surfaces for the purpose of this article. For P(S-*b*-MMA), random copolymers with varying ratios of styrene and MMA can be used to modify and create a nonpreferential substrate. In fact, different morphologies such as PS cylinders, lamellae and PMMA cylinders have been found to have a distinct "nonpreferential window" based on the fraction of styrene in the copolymer. While this methodology is well-established, the underlying nonpreferential layer offers no additional functionality besides controlling the domain orientation. However, these studies have shown that the composition and the molecular architecture of the nonpreferential layer can be tuned to a large extent, potentially allowing for the incorporation of functionalities.[29]

Recently, we demonstrated the use of a single component, cross-linked thin film (mat) to grow high density polymer brushes from a variety of substrates.[30] This approach of inimer containing mats overcomes both the limitations of SAM based methods simultaneously, namely instability of the SAM over long-term period as well as the lack of substrate independence. The

cross-linked mat consisted of a random copolymer of an ATRP inimer (*p*-(2-bromoisobutyloylmethyl)styrene or BiBMS) and glycidyl methacrylate (GMA), a cross-linkable monomer. We further showed that the initiator density can be tuned by the incorporation of a third comonomer, such as styrene (S). If the surface energy can be tuned by adjusting the ratio of S to BiBMS and GMA, then nonpreferential conditions can be identified to direct the assembly of an overlying BCP film. In this paper, we present a versatile chemistry for fabricating nanopatterned polymer brushes over large areas from these nonpreferential inimer containing mats. Our approach is the very first to combine nonpreferential brush chemistry for controlling BCP domain orientation with inimer chemistry to *grow dense periodic arrays of patterned brushes*. The spot size of these nanopatterned brushes is very small, ~ 15 nm, which is difficult to achieve by any of the existing methods. This is a large area approach, which overcomes many of the limitations of other approaches based on patterning a SAM of initiators by serial top-down lithographic techniques.

6.3. Materials and Methods

Materials. All chemicals were purchased from Sigma-Aldrich and used without further purification unless otherwise noted. P(S-*b*-MMA) BCPs (46 kDa (PS) – 21 kDa (PMMA), 50 kDa (PS) – 20 kDa (PMMA) and 18 kDa (PS) – 18 kDa (PMMA)) and PMMA homopolymer (20 kDa) were purchased from Polymer Source and used as received. Styrene, glycidyl methacrylate (GMA) and 2-hydroxyethyl methacrylate (HEMA) were stirred over calcium hydride and then distilled under vacuum. Poly(ethylene glycol) methyl ether methacrylate (M_n 300) was passed through an alumina column to remove inhibitor. 2,2'-Azobis(2-methylpropionitrile) (AIBN) was recrystallized from acetone and dried under vacuum. *p*-(2-bromoisobutyloylmethyl)styrene (BiBMS) was synthesized according to the literature procedure.[30] 4-vinylbenzyl alcohol was synthesized according to the literature procedure.[31]

Synthesis of P(S-*r*-BiBMS-*r*-GMA). A series of P(S-*r*-BiBMS-*r*-GMA) was synthesized via free radical polymerization with varied feed ratio of styrene (0.79-0.55), BiBMS (0.20-0.30) and GMA (0.01-0.15). As a typical example, BiBMS (0.849 g, 3 mmol), GMA (0.071 g, 0.5 mmol), styrene (0.68 g, 6.5 mmol), and AIBN (4.1 mg, 0.025 mmol) were added to 3 g anisole in a 10 mL Schlenk flask equipped with a magnetic stir bar. The mixture was degassed via three freeze-pump-thaw cycles and placed in an oil bath at 60 ^{o}C for 16 hours with vigorous stirring. The polymerization was quenched by cooling the flask with cold water and exposure to air. The resulting viscous oil was then diluted with tetrahydrofuran (THF) and precipitated into hexane. The polymer was collected as a white powder and dried under vacuum.

Substrate preparation and thin film formation. A solution of P(S-*r*-BiBMS-*r*-GMA) (0.3% w/w) in toluene was spin-coated onto silicon wafers that had been cleaned using piranha acid (7:3 H_2SO_4:H_2O_2, *caution: reacts violently with organic compounds*). The substrate was then annealed under vacuum at 220 ^{o}C for 5 min. After annealing, the substrate was soaked in toluene and rinsed copiously with fresh toluene to remove un-cross-linked polymer, resulting in 5-11 nm thick cross-linked thin films. On these cross-linked mats, a solution of cylinder forming P(S-*b*-MMA) (M_n(PS) ~ 46k, M_n(PMMA) ~ 21k) in toluene (1.0 wt%) or a binary blend of cylinder forming P(S-*b*-MMA) (M_n(PS) ~ 50k, M_n(PMMA) ~ 20k) and PMMA (M_n ~ 20k) in toluene (1.0 wt% or 1.5 wt%, weight ratio of PMMA to P(S-*b*-MMA) = 0.114) was spin-coated at 4000 rpm to produce films with BCP thicknesses of 25 nm or 37 nm. All BCP films were annealed at 220 ^{o}C for 10 min under vacuum to drive self-assembly of BCP domains. Annealed samples were further treated with acetic acid for 20 min, followed by DI water rinsing, to create porous structure by extracting PMMA homopolymer. For Au dot arrays, 2.5 nm of Cr (0.4 Å/sec) and 4.5 nm of Au (0.4 Å/sec) were subsequently deposited onto the nanoporous template made from 1.5 wt% P(S-

b-MMA) and PMMA blend solution using an e-beam evaporator under vacuum (~2×10^{-6} Torr). Lift-off of P(S-*b*-MMA) template and overlying metal layer was carried out by soaking the samples in boiling acetone for 10 min and subsequent sonication for 30 ~ 60 min. Resulting samples were further rinsed with acetone, isopropyl alcohol and toluene prior to use.

Surface-initiated atom transfer radical polymerization (SI-ATRP). HEMA (2.5 grams, 19.21 mmol), *tris*-(2-pyridylmethyl)amine (100 mg, 0.34 mmol), CuCl (35 mg, 0.35 mmol), $CuCl_2$ (6 mg, 0.45 mmol), and methanol (100 ml) were mixed and sonicated until the copper completely dissolved into the yellow-green solution. The mixture was then added to the flask containing substrates covered with porous BCP template. The flasks were then degassed via three freeze-pump-thaw cycles. After warming to room temperature using a water bath, the flasks were immersed in a 35 ^{o}C oil bath for various amounts of time. After the requisite amount of time elapsed, the flasks were cooled to room temperature using running water and the flask opened to atmosphere. The substrate was then removed from the flask and washed copiously with water. After washing, the substrate was further soaked in THF for 2 hours, then sonicated in THF for 10 minutes, followed by rinsing with THF to remove porous BCP template and ungrafted polymer chains and dried using a stream of nitrogen.

SI-ATRP from Au-dot arrays. Poly(ethylene glycol) methyl ether methacrylate (PEGMEMA) (4.0 g, 13.3 mmol), *tris*-(2-pyridylmethyl)amine (100 mg, 0.34 mmol), CuBr (30 mg, 0.21 mmol), and isopropanol (100 ml) were mixed and sonicated until the copper completely dissolved into the yellow-green solution. The mixture was then added to the flask containing substrates covered with Au dot arrays sample and magnetic stirring bar. The flasks were then degassed via three freeze-pump-thaw cycles. After warming to room temperature using a water bath, the flasks were immersed in a 35 ^{o}C oil bath for the requisite amount of time. After the

requisite amount of time elapsed, the flasks were cooled to room temperature using running water and the flask opened to atmosphere. The substrate was then removed from the flask and washed copiously with water. After washing, the substrate was further soaked in THF for 2 hours. The resulting sample was soaked in 0.02 M HCl aqueous solution for 10 min, then rinsed with DI water and blow-off. Finally, the sample was immersed in ethanol for 24 h and then rinsed with ethanol.

Characterization. ^{1}H NMR spectra were recorded in $CDCl_3$ using a Bruker Avance-400 spectrometer with TMS as internal reference. Gel-permeation chromatography (GPC) was performed using a Viscotek 2210 system equipped with three Waters columns (HR 4, HR 4E, HR 3) and a 1 mL/min flow rate of THF as eluent at 30 °C. Monodisperse PS standards ranging from 1 kDa to 400 kDa were used for calibration. The film thickness of the samples was measured by ellipsometry (Rudolph Research Auto EL). The surface topography of the cross-linked mat and patterned brushes was examined using a Nanoscope III Multimode atomic force microscope (Digital Instruments) in tapping mode. Top-down scanning electron microscope (SEM) images of the BCP microdomains were acquired using a LEO-1530 field-emission instrument using an accelerating voltage of 1 kV. X-ray photoelectron spectroscopy (XPS) was done on a PerkinElmer 5400 ESCA spectrometer Phi model using a Mg X-ray source (300 W, 15kV) at a takeoff angle of 45° from the substrate normal. The hemispherical energy analyzer was used in hybrid mode with a 1 mm × 3.5 mm area aperture. Survey spectra were collected at pass energy of 89.45 eV with a scan step size of 1.0 eV. High-resolution multiplex spectra were collected with pass energy of 35.75 eV and a step size of 0.05 eV. The resulting spectra were deconvoluted and analyzed using AugerScan software. Integrated intensity and peak positions were analyzed by fitting multiplex spectra with Voigt function after a baseline correction of the raw data.

6.4. Results and Discussion

In a previous paper, we demonstrated the applicability of cross-linkable random copolymers containing ATRP inimers towards the substrate-independent growth of dense polymer brushes.[30] A styrenic version of a α-haloester type ATRP initiator, namely BiBMS, was copolymerized with GMA by reversible addition-fragmentation chain-transfer (RAFT) polymerization to yield a copolymer where the inimer is the majority component with a small amount of GMA to facilitate thermal covalent cross-linking of the film. The resulting mat was highly polar in nature due to the high percentage of GMA (84% BiBMS and 16% GMA by ^{1}H NMR spectroscopy). In order to design an inimer mat which is also nonpreferential to an overlying P(S-*b*-MMA) BCP film, the first step is to decrease the polarity by incorporating a nonpolar monomer such as styrene as a third comonomer. Hence, we synthesized a range of copolymers using free radical polymerization (**Figure 6.1**) with varying ratios of styrene (S), BiBMS (SI) and GMA (G) (denoted as SSIG f_{St}), with number average molecular weights (M_n) between 16 kDa and 23 kDa and polydispersities (PDI) between 1.7 and 2.1 (**Table 6.1**). BiBMS was held constant at either 20% or 30% of the monomer feed while the ratio of styrene to GMA was varied. Using the method in our previous paper,[30] we calculated the bromine density on a SSIG 78 mat of 0.83 Br atoms/nm^3, which is sufficient to ensure a high chain density in grown brushes.

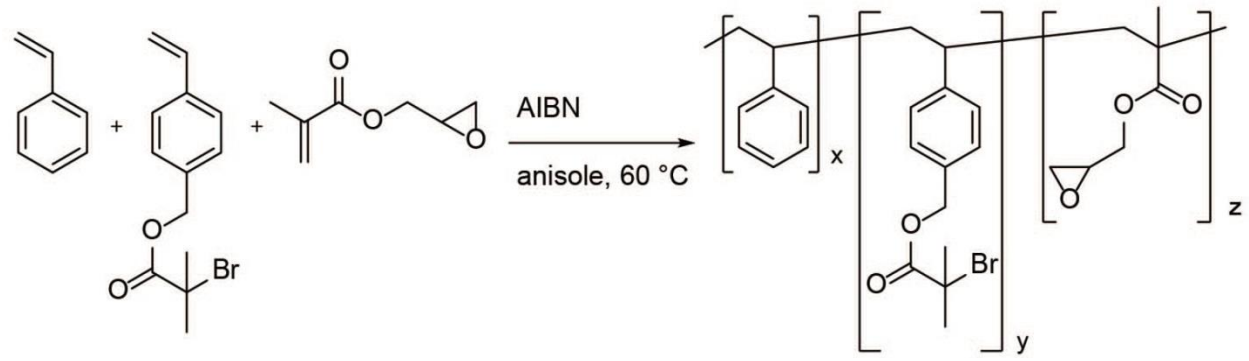

Figure 6.1. Scheme for synthesis of the sytrenic inimer containing random copolymers.

Table 6.1 Characteristic data for the various polymers synthesized.

Polymer	f_{St} [a]	F_{St} [b]	f_{BiBMS} [a]	F_{BiBMS} [b]	M_n (kDa) [c]	PDI
SSIG 55	0.55	0.45	0.30	0.32	22.8	2.0
SSIG 60	0.60	0.48	0.30	0.34	23.3	2.1
SSIG 65	0.65	0.55	0.30	0.32	16.0	2.1
SSIG 76	0.76	0.69	0.20	0.22	23.9	1.9
SSIG 77	0.77	0.71	0.20	0.21	15.9	2.1
SSIG 78	0.78	0.71	0.20	0.23	20.5	1.8
SSIG 79	0.79	0.72	0.20	0.23	19.5	1.7

[a] f_{St} and f_{BiBMS} are the mole fractions of styrene and BiBMS in the feed, [b] F_{St} and F_{BiBMS} are the mole fractions in the resulting copolymer as determined by ^{1}H-NMR. [c] Molecular weights and PDIs were determined by GPC.

Following the synthesis and characterization of the random copolymers, we tested their nonpreferentiality towards the self-assembly of an overlying P(S-*b*-MMA) film. 10 nm thick cross-linked random copolymer thin films were prepared by spin-coating the copolymer solution onto silicon wafers and heating the substrates at 220 ^{o}C for 5 minutes under vacuum. Toluene was used to remove un-cross-linked chains and then either a lamellar (18 kDa-18 kDa) or PMMA cylinder (46 kDa-21 kDa) forming BCP thin film was deposited onto the cross-linked surface and then annealed at 220 ^{o}C under vacuum for 10 minutes to drive the self-assembly of the BCP. SEM was used to determine the nonpreferentiality of the surfaces for P(S-*b*-MMA) assembly (**Figure 6.S1**).

From the SEM micrographs, compositional windows for the nonpreferential surface were identified for both lamellar and PMMA cylinder forming BCPs. SSIG 65 showed perpendicular lamellar orientation while the less polar copolymers SSIG 76 through 79 all showed perpendicular orientation of PMMA cylinders. These results are consistent with our previous studies on nonpreferential layers where the compositional window for perpendicular PMMA cylinders is shifted to higher PS compositions compared to that for a lamellar BCP.[23] We thus used SSIG 78 for all further experiments involving PMMA cylinder forming P(S-*b*-MMA).

The minority PMMA cylinder block of the assembled BCP was removed by UV exposure and subsequent acetic acid immersion.[17] The selective removal of PMMA by this process was verified by SEM where an observed increase in contrast confirms the formation of a nanoporous template. However, no growth of polymer brushes was observed after SI-ATRP through the nanopores, indicating that the inimer had been degraded in the process of removal of the PMMA cylinders. This was confirmed by XPS examination of the inimer film, where the concentration of bromine was undetectable after exposure to UV (**Figure 6.2**).

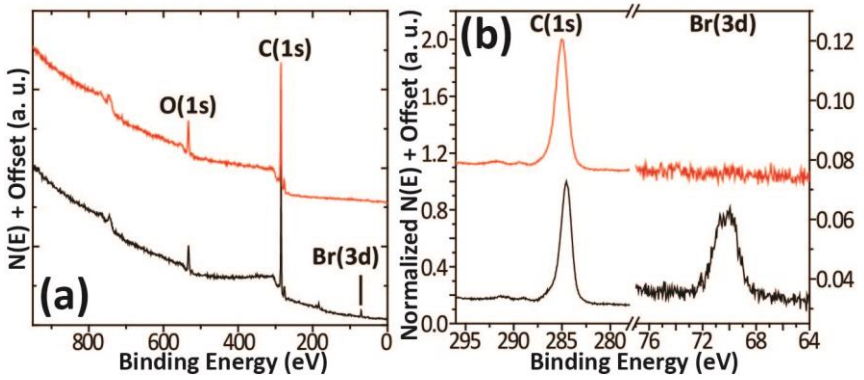

Figure 6.2. (a) XPS survey spectra of a SSIG 78 film after processing steps and removal of overlying BCP template by toluene with UV ($\lambda = 254$ nm, 1 J/cm^2) etching (red trace) and without UV etching (black trace). (b) Multiplex spectra for C(1s) and Br(3d).

To avoid this incidental bromine cleavage by UV etching, we elected to use a blend of BCP and PMMA homopolymer (40 wt % homopolymer relative to the PMMA block), as the homopolymer is incorporated into the PMMA cylinders and can then be extracted using acetic acid as a selective solvent (**Figure 6.3**).[32] After treatment with acetic acid, there is a large increase in contrast between PS and the cylindrical areas in the SEM, indicating the formation of nanopores. After PMMA removal, XPS confirmed that bromine was still present on the surface (**Figure 6.2**). This process was attempted with lamella forming BCP as well but we were unable to generate a well-ordered nanoporous structure due to pattern collapse during the homopolymer removal.

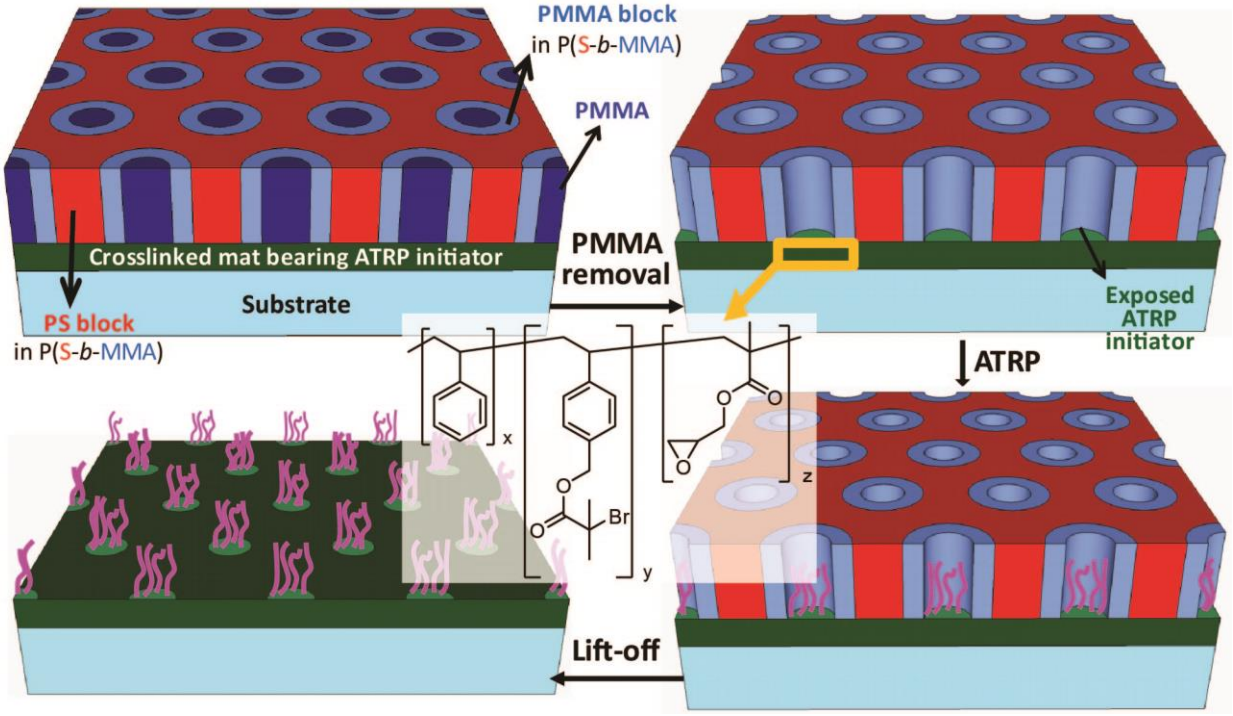

Figure 6.3. Scheme for the formation of BCP nanoporous template and subsequent brush growth.

The choice of solvent and monomer for brush growth through the nanopores is important to prevent dissolution of the PS template itself. We therefore chose 2-hydroxyethyl methacrylate (HEMA) as a model monomer for brush growth due to its ease of polymerization by ATRP as well as solubility in alcohols.[33, 34] Polymerization times from 1 to 4 h were examined and the resulting

brushes characterized by SEM, atomic force microscopy (AFM) and XPS. Before BCP deposition, the cross-linked thin film exhibited a RMS roughness of ~0.35 nm as measured by AFM (**Figure 6.4**a). After PMMA homopolymer removal and SI-ATRP, a small difference in contrast can be seen in SEM before the removal of PS template (**Figure 6.4d**). This contrast is due to copper being trapped by the P(HEMA) brushes as metals tend to be bright when imaged by SEM. After the PS template is removed by THF, AFM clearly showed height and phase variations which mirror the pattern from the nanoporous template itself (**Figure 6.4g,h**). After 1 h of polymerization, the height of the polymer dots is approximately 1.5 nm. The periodicity of the dots matches well with the BCP template (~45 nm). The size of brush dots is impressively small, a diameter of ~15 nm, which is not trivial to accomplish with conventional photolithography or nanoimprint lithography over large areas.

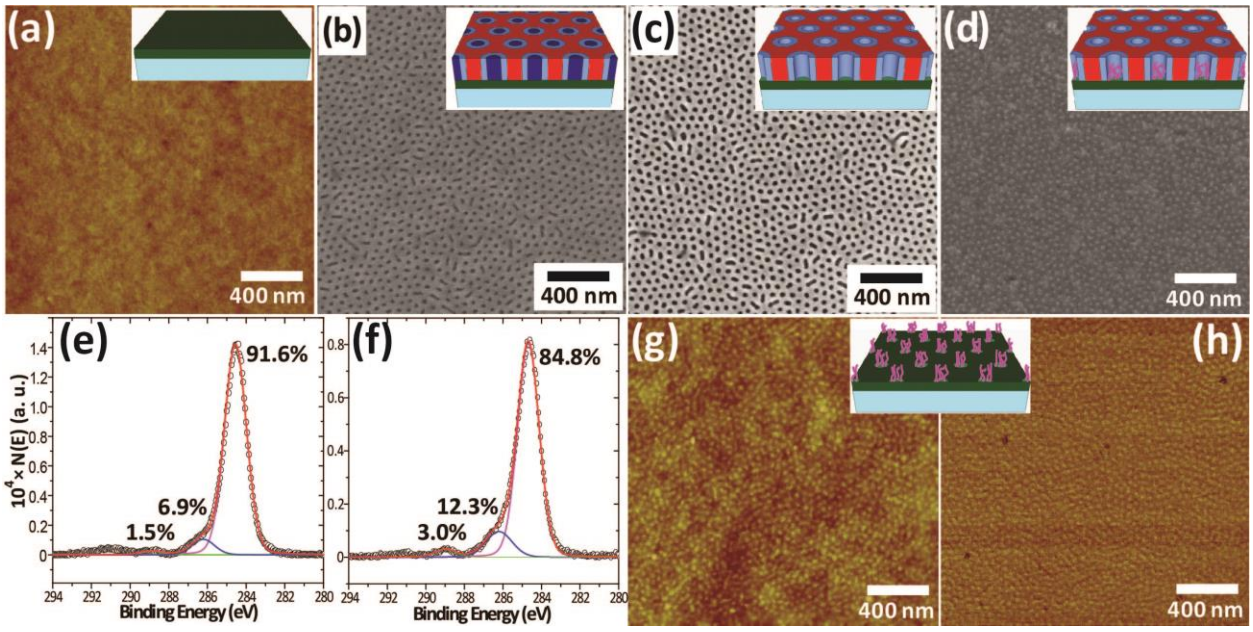

Figure 6.4. AFM height (a, g), AFM phase (h) and SEM (c, d) images of the films of (a) inimer mat after cross-linking and washing, (b) assembled blend of P(S-*b*-MMA) and PMMA homopolymer on inimer mat, (c) nanoporous template before brush growth, (d) template after

brush growth, (e) XPS C(1s) multiplex spectrum of bare inimer mat, (f) XPS C(1s) multiplex spectrum after SI-ATRP for 1 h, and (g, h) polymer brushes after removal of the PS template.

When polymerized for longer than two h, the substrates no longer exhibit regular features by AFM (**Figure 6.5b**). As the PS template is still intact (as seen from the SEM before lift-off using THF, **Figure 6.5a**), it is likely that the brushes grew long enough to generate an essentially featureless surface after removal of the PS template with THF. The solubility parameter of P(HEMA) is around 26.93 $MPa^{1/2}$ and that of *n*-hexane is 14.93 $MPa^{1/2}$ (compared to THF with a solubility parameter of 18.61 $MPa^{1/2}$).[35] Hence, *n*-hexane can act as a better non-solvent than THF towards PHEMA to collapse the brushes. Thus, the patterned brushes were incubated in *n*-hexane overnight, thereby collapsing the brushes to their minimum feature size. After overnight immersion in hexanes, a regular dot array was observed by AFM with an increase in height from 5.75 nm (**Figure 6.5d**) to 6.45 nm (**Figure 6.S2**) as the polymerization time increased from 3 to 4 h. XPS was used to further characterize the growth of P(HEMA) brushes, showing clear increases in C-O and O-C=O energy regions which corresponds to the higher concentrations of P(HEMA) on the surface (**Figure 6.4e,f and Figure 6.S3**).

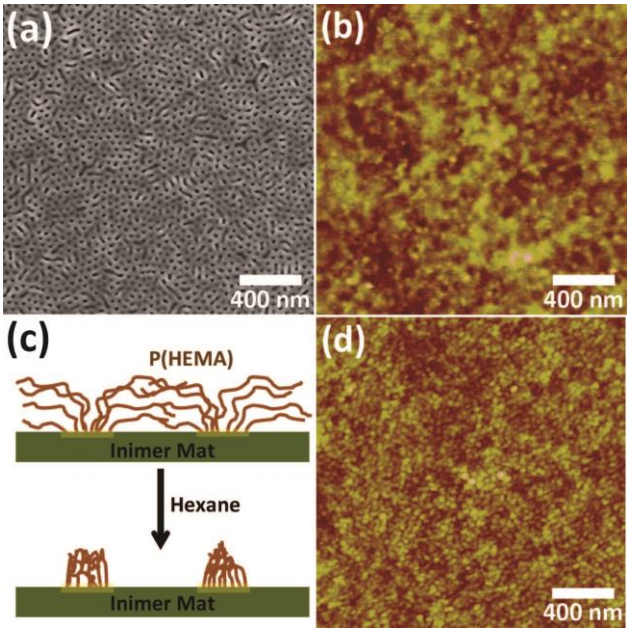

Figure 6.5. SEM (a) and AFM height (b, d) images: (a) after 3 h polymerization, (b) after template removal with THF, (d) same substrate after soaking in *n*-hexane overnight, and (c) an illustration of brush collapse via hexane treatment.

It would be ideal to know the grafting density of these patterned brushes; however, the most common way to do so is to compare the molecular weight of polymer grown from free initiators in solution with the height of the polymer brushes.[30] The validity of this method is already a subject of debate: polymerization kinetics on surfaces would differ from that in bulk or solution,[36] and also in nanoconfined areas, the molecular weight of brushes grown can often be overestimated.[37] The only alternative would be to cleave the grown brushes from the substrate and analyze them separately but the practical issues of extremely low amounts of polymer and difficulty in separating the brush from the inimer mat make this approach challenging as well. As an example, assuming a 1 cm^2 substrate, a grafting density of 0.5 chains/nm^2 and a P(HEMA) degree of polymerization (DP) of 100 on an unpatterned substrate, we expect ~1.1 μg of P(HEMA) brush on the surface. Patterning the substrate would further decrease the amount of polymer. In

addition, the grafting density and even the molecular weight of the P(HEMA) brushes are likely to vary across the diameter of the dot itself as the edge of the nanopore would have larger steric constraints in comparison to the center. This is a fundamental question which we are interested in pursuing for future studies as to the best of our knowledge the growth of patterned brush dot arrays of this small size (15 nm) and high density (~5×10^{10} cm^{-2}) has not been investigated before. One possibility to address this will be the use of cleavable inimers such as those pioneered by Koylu et al. for the direct determination of molecular weight and grafting density.[38]

The processing conditions used here preserve the initiators in the mat underneath the template while allowing for the directed assembly of a BCP/homopolymer blend and the subsequent growth of nanopatterned polymer brushes. The activity of the initiators in the mat can be further verified by growing brushes from the area under the majority PS domains of the BCP (**Figure 6.6**). To do so we deposited Au in the nanoporous template after PMMA homopolymer removal and lifted off the polymer layer to leave Au nanodots on the inimer mat (**Figure 6.7a**). Poly(ethylene glycol) methyl ether methacrylate (PEGMEMA) brushes were then grown by SI-ATRP around the Au dots, yielding an "antidot" array of PEGMEMA brushes.

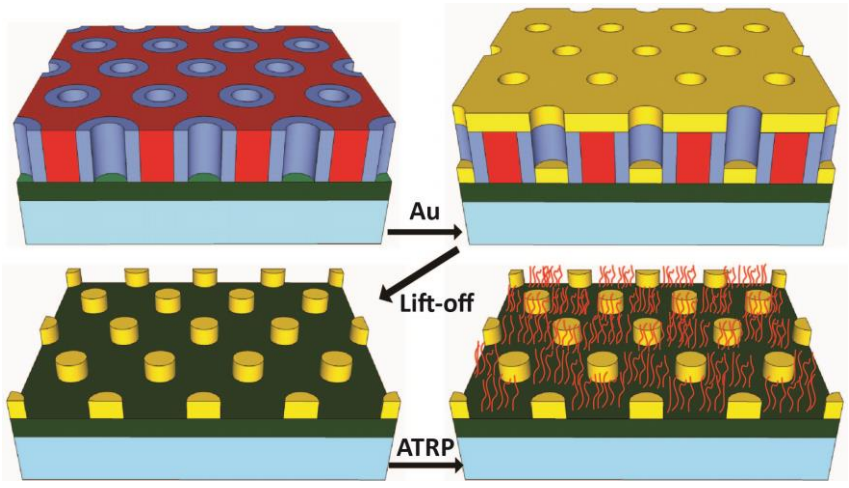

Figure 6.6. Process for forming Au dot arrays followed by surrounding brush growth.

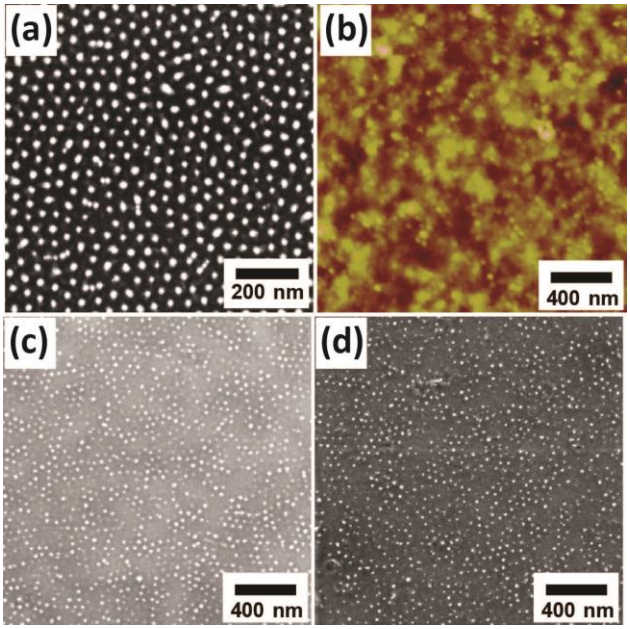

Figure 6.7. (a) Top down SEM image of Au dot arrays after template lift off. (b) AFM height image after growth of PEGMEMA brushes for 30 min. Top-down SEM images of PEGMEMA brushes grown around Au dot arrays after (c) 30 min and (d) 1.5 h.

After the growth of PEGMEMA, AFM showed no regular features in the height image while SEM clearly showed the presence of the Au dots (**Figure 6.7b-d**). After Au deposition and lift-off of the BCP template, ellipsometry gave a thickness of 20 nm. This thickness increases to 31 nm and 38 nm after SI-ATRP of PEGMEMA for 30 min and 1.5 h, respectively. As previously discussed, the bromine density for this inimer mat is estimated at 0.83 Br/nm^3 which should be sufficient for dense brush growth.[30] Although determining the chain density is still challenging as mentioned earlier, by examining the ratio of initiator density to the theoretical maximum chain density of PEGMEMA, we can estimate if a high PEGMEMA chain density is feasible for this surface. We assume that a fully extended single PEGMEMA chain forms a cylinder perpendicular to the surface. The radius of this cylinder is assumed to be the size of a ~ 300 g/mol pendant PEG coil ($2R_g$ ~ 1.06 nm, estimated from the literature[39]) plus the ester linkage between the PEG side

chain and the polymer backbone (~0.3 nm). As a consequence, a single PEGMEMA chain occupies an area of ~ 5.8 nm^2 [$\pi(1.06 + 0.3)^2$], resulting in a theoretical maximum chain density of 0.17 chains/nm^2 for PEGMEMA. These calculations show that the inimer surface used here contains about 5 times higher density of initiators (0.83 initiators/nm^3) than what is needed to achieve the maximum chain density for PEGMEMA. Thus, the dual functional layer is expected to provide sufficient initiating sites for high grafting density. XPS was also used to characterize the Au dot arrays before and after PEGMEMA growth. Peaks from the Au (4f) and (4d) orbitals were clearly observed in the survey spectrum before PEGMEMA growth and disappeared after SI-ATRP with a concomitant rise in C-O and O-C=O intensities (**Figure 6.8a,b**). The sampling depth of XPS is approximately 10 nm, and the lack of Au peaks is consistent with the measured thickness from ellipsometry. SEM can penetrate more deeply into the film and the Au dots are clearly visible due to their high electronic contrast compared to the surrounding materials.[40]

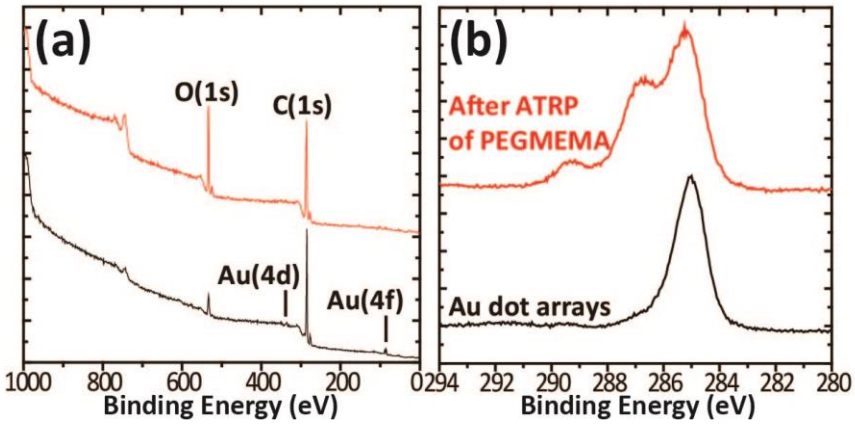

Figure 6.8. (a) XPS survey and (b) multiplex C(1s) spectra confirming the growth of PEGMEMA brushes (red trace) around Au dot arrays (black trace).

6.5. Conclusions

In this paper, we have successfully demonstrated an organic thin film with dual functionality, namely nonpreferentiality for controlling BCP domain orientation and an embedded inimer to *grow dense periodic arrays of patterned brushes*. This is a large area approach, which overcomes many of the limitations of other methods based on patterning a SAM of initiators by serial top-down lithographic techniques. By varying the ratio of styrene, BiBMS and GMA, nonpreferential surface compositions were found for both lamellar and PMMA cylinder forming P(S-*b*-MMA) BCPs that promoted perpendicular domain orientation. A binary blend of BCP and homopolymer was used to circumvent problems associated with UV etching, generating a nanoporous template over large areas while maintaining initiator functionality as XPS confirmed the presence of bromine after all the processing steps were completed. Furthermore, the resulting template was stable to polymerization in methanol for over 4 h without degradation. P(HEMA) brushes were grown through the nanopores in the template, and the height of the brushes was controlled by varying the polymerization time. XPS also showed an increase in C-O and O-C=O bonding regions in the C(1s) region, further confirming the growth of P(HEMA) brushes. We also demonstrated the growth of PEGMEMA brushes around Au nanodots generated from the nanoporous template, showing the versatility of this technique. The chemistry developed through this work on dual functionality lays the groundwork for potentially incorporating a whole range of electronic, biological or optical functionalities in nonpreferential layers.

6.6. Supporting Information

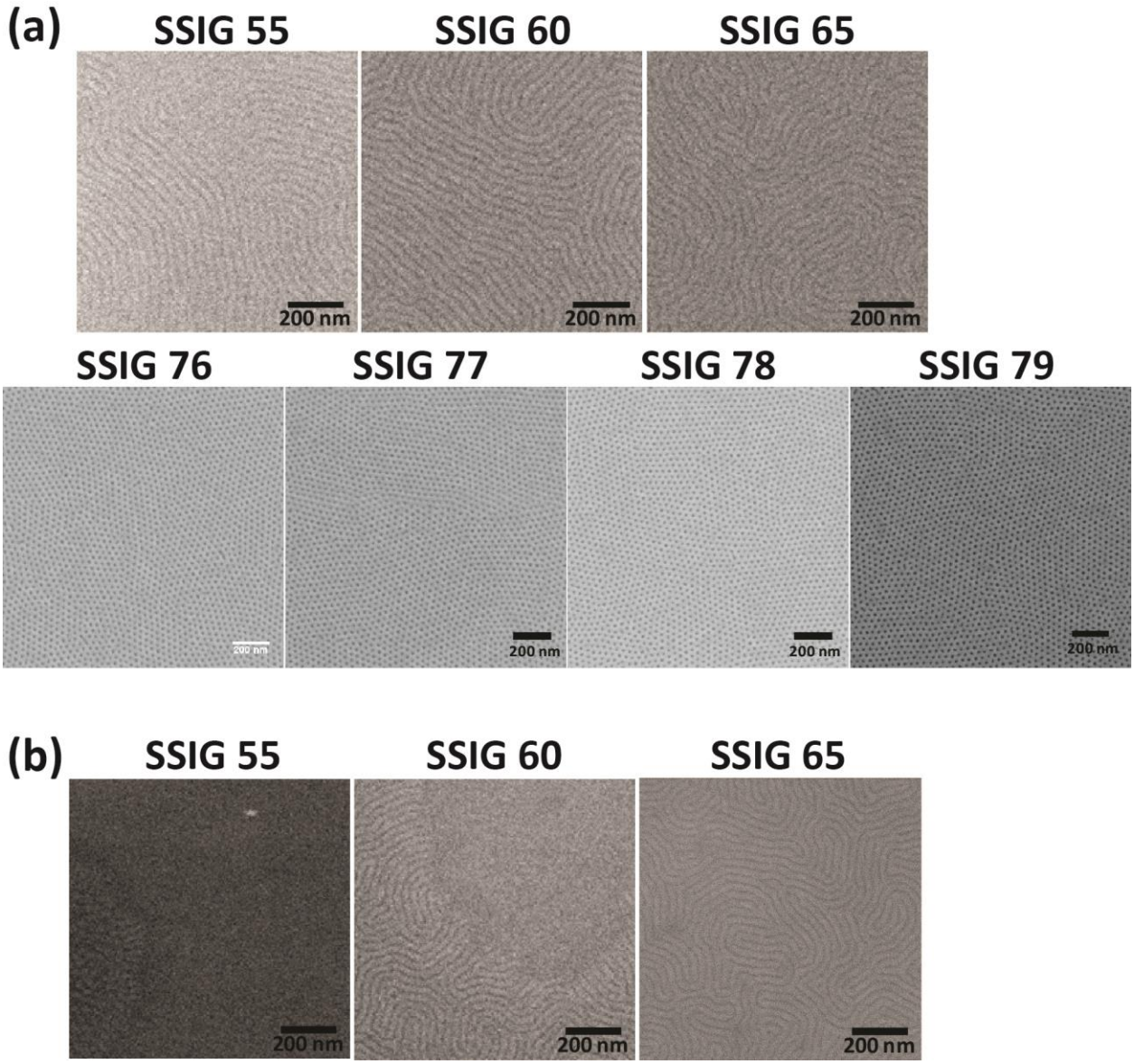

Figure 6.S1. Top view SEM images of self-assembled BCP. (a) C4621 on crosslinked mats from SSIG 55 ~ SSIG 79, (b) L1818 on crosslinked mats from SSIG 55 ~ SSIG 65.

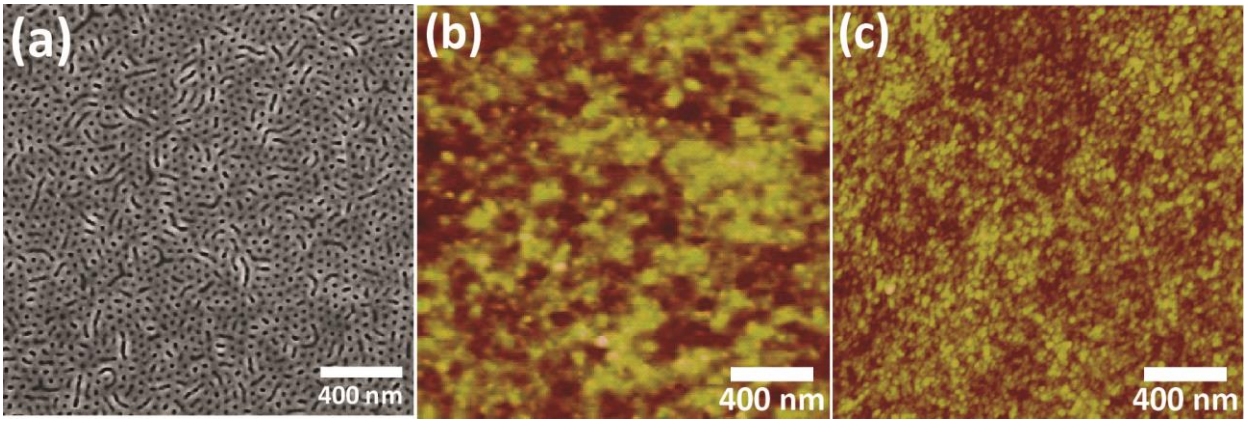

Figure 6.S2. SEM (a) and AFM height (b, c) images of the template and brushes after SI-ATRP. AFM z-axis scale is 0 - 15 nm. (a) SEM images show the substrate before PS lift-off after polymerization for 4 h. AFM images show the substrate (b) after PS lift-off using THF after polymerization for 4 h and (c) after immersion in hexane.

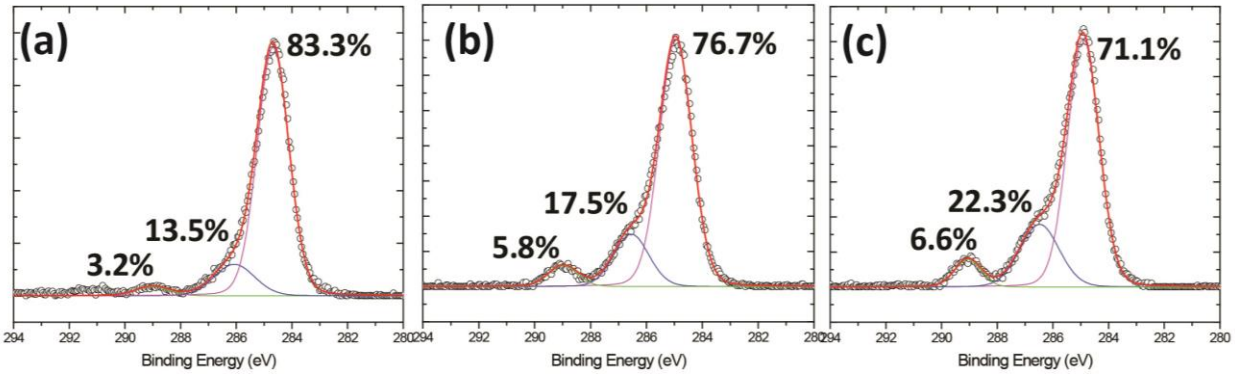

Figure 6.S3. XPS C(1s) multiplex spectra of P(HEMA) brushes grown for various times: (a) 2 h, (b) 3 h and (c) 4 h.

6.7. References

1. Chen, T.; Amin, I.; Jordan, R., Patterned Polymer Brushes. *Chem. Soc. Rev.* **2012,** *41*, 3280-3296.

2. Rastogi, A.; Paik, M. Y.; Tanaka, M.; Ober, C. K., Direct Patterning of Intrinsically Electron Beam Sensitive Polymer Brushes. *ACS Nano* **2010,** *4*, 771-780.

3. Nie, Z.; Kumacheva, E., Patterning Surfaces with Functional Polymers. *Nat. Mater.* **2008,** *7*, 277-290.

4. Barbey, R.; Lavanant, L.; Paripovic, D.; Schüwer, N.; Sugnaux, C.; Tugulu, S.; Klok, H.-A., Polymer Brushes via Surface-Initiated Controlled Radical Polymerization: Synthesis, Characterization, Properties, and Applications. *Chem. Rev.* **2009,** *109*, 5437-5527.

5. Jonas, A. M.; Hu, Z. J.; Glinel, K.; Huck, W. T. S., Chain Entropy and Wetting Energy Control the Shape of Nanopatterned Polymer Brushes. *Macromolecules* **2008,** *41*, 6859-6863.

6. Schuh, C.; Santer, S.; Prucker, O.; Ruhe, J., Polymer Brushes with Nanometer-Scale Gradients. *Advanced Materials* **2009,** *21* (46), 4706-4710.

7. von Werne, T. A.; Germack, D. S.; Hagberg, E. C.; Sheares, V. V.; Hawker, C. J.; Carter, K. R., A Versatile Method for Tuning the Chemistry and Size of Nanoscopic Features by Living Free Radical Polymerization. *J. Am. Chem. Soc.* **2003,** *125*, 3831-3838.

8. Xia, Y.; Rogers, J. A.; Paul, K. E.; Whitesides, G. M., Unconventional Methods for Fabricating and Patterning Nanostructures. *Chem. Rev.* **1999,** *99*, 1823-1848.

9. Ayres, N., Polymer Brushes: Applications in biomaterials and nanotechnology. *Polym. Chem.* **2010,** *1*, 769-777.

10. Stoykovich, M. P.; Nealey, P. F., Block Copolymers and Conventional Lithography. *Mater. Today* **2006,** *9*, 20-29.

11. Black, C. T.; Ruiz, R.; Breyta, G.; Cheng, J. Y.; Colburn, M. E.; Guarini, K. W.; Kim, H.-C.; Zhang, Y., Polymer self assembly in semiconductor microelectronics. *IBM J. Res. Dev.* **2007,** *51*, 605-633.

12. Segalman, R. A., Patterning with block copolymer thin films. *Materials Science and Engineering: R: Reports* **2005,** *48* (6), 191-226.

13. Hawker, C. J.; Russell, T. P., Block Copolymer Lithography: Merging "Bottom-Up" with "Top-Down" Processes. *MRS Bull.* **2005,** *30*, 952-966.

14. Bratton, D.; Yang, D.; Dai, J.; Ober, C. K., Recent progress in high resolution lithography. *Polym. Adv. Technol.* **2006,** *17* (2), 94-103.

15. Tseng, Y.-C.; Darling, S. B., Block Copolymers Nanostructures for Technology. *Polymers* **2010,** *2*, 470-489.

16. Cheng, J. Y.; Sanders, D. P.; Truong, H. D.; Harrer, S.; Friz, A.; Holmes, S.; Colburn, M.; Hinsberg, W. D., Simple and Versatile Methods to Integrate Directed Self-Assembly with Optical Lithography Using a Polarity-Switched Photoresist. *ACS Nano* **2010,** *4*, 4815-4823.

17. Kim, M.; Safron, N. S.; Han, E.; Arnold, M. S.; Gopalan, P., Electronic Transport and Raman Scattering in Size-Controlled Nanoperforated Graphene. *ACS Nano* **2012,** *6*, 9846-9854.

18. Ryu, D. Y.; Shin, K.; Drockenmuller, E.; Hawker, C. J.; Russell, T. P., A Generalized Approach to the Modification of Solid Surfaces. *Science* **2005,** *308*, 236-239.

19. Thurn-Albrecht, T.; Steiner, R.; DeRouchey, J.; M. Stafford, C.; Huang, E.; Bal, M.; Tuominen, M.; Hawker, C. J.; Russell, T. P., Nanoscopic Templates from Oriented Block Copolymer Films. *Adv. Mater.* **2000,** *12*, 787-791.

20. Mansky, P.; Liu, Y.; Huang, E.; Russell, T. P.; Hawker, C., Controlling Polymer-Surface Interactions with Random Copolymer Brushes. *Science* **1997,** *275*, 1458-1460.

21. Han, E.; Gopalan, P., Cross-Linked Random Copolymer Mats As Ultrathin Nonpreferential Layers for Block Copolymer Self-Assembly. *Langmuir* **2010,** *26*, 1311-1315.

22. Han, E.; In, I.; Park, S.-M.; La, Y.-H.; Wang, Y.; Nealey, P. F.; Gopalan, P., Photopatternable Imaging Layers for Controlling Block Copolymer Microdomain Orientation. *Adv. Mater.* **2007,** *19*, 4448-4452.

23. Han, E.; Stuen, K. O.; La, Y.-H.; Nealey, P. F.; Gopalan, P., Effect of Composition of Substrate-Modifying Random Copolymers on the Orientation of Symmetric and Asymmetric Diblock Copolymer Domains. *Macromolecules* **2008,** *41*, 9090-9097.

24. In, I.; La, Y.-H.; Park, S.-M.; Nealey, P. F.; Gopalan, P., Side-Chain-Grafted Random Copolymer Brushes as Neutral Surfaces for Controlling the Orientation of Block Copolymer Microdomains in Thin Films. *Langmuir* **2006,** *22*, 7855-7860.

25. Kim, M.; Han, E.; Sweat, D. P.; Gopalan, P., Interplay of surface chemical composition and film thickness on graphoepitaxial assembly of asymmetric block copolymers. *Soft Matter* **2013,** *9* (26), 6135-6141.

26. Ham, S.; Shin, C.; Kim, E.; Ryu, D. Y.; Jeong, U.; Russell, T. P.; Hawker, C. J., Microdomain Orientation of PS-b-PMMA by Controlled Interfacial Interactions. *Macromolecules* **2008,** *41* (17), 6431-6437.

27. Suh, H. S.; Kang, H.; Nealey, P. F.; Char, K., Thickness Dependence of Neutral Parameter Windows for Perpendicularly Oriented Block Copolymer Thin Films. *Macromolecules* **2010,** *43* (10), 4744-4751.

28. Huang, E.; Pruzinsky, S.; Russell, T. P.; Mays, J.; Hawker, C. J., Neutrality Conditions for Block Copolymer Systems on Random Copolymer Brush Surfaces. *Macromolecules* **1999,** *32* (16), 5299-5303.

29. Bates, C. M.; Strahan, J. R.; Santos, L. J.; Mueller, B. K.; Bamgbade, B. O.; Lee, J. A.; Katzenstein, J. M.; Ellison, C. J.; Willson, C. G., Polymeric Cross-Linked Surface Treatments for Controlling Block Copolymer Orientation in Thin Films. *Langmuir* **2011,** *27*, 2000-2006.

30. Sweat, D. P.; Kim, M.; Yu, X.; Gopalan, P., A Single-Component Inimer Containing Cross-Linkable Ultrathin Polymer Coating for Dense Polymer Brush Growth. *Langmuir* **2013,** *29*, 3805-3812.

31. Zhao, L. J.; Kwong, C. K. W.; Shi, M.; Toy, P. H., Optimization of Polystyrene-Supported Triphenylphosphine Catalysts for aza-Morita-Baylis-Hillman Reactions. *Tetrahedron* **2005,** *61* (51), 12026-12032.

32. Jeong, U.; Kim, H.-C.; Rodriguez, R. L.; Tsai, I. Y.; Stafford, C. M.; Kim, J. K.; Hawker, C. J.; Russell, T. P., Asymmetric Block Copolymers with Homopolymers: Routes to Multiple Length Scale Nanostructures. *Adv. Mater.* **2002,** *14*, 274-276.

33. Robinson, K. L.; Khan, M. A.; de Paz Báñez, M. V.; Wang, X. S.; Armes, S. P., Controlled Polymerization of 2-Hydroxyethyl Methacrylate by ATRP at Ambient Temperature. *Macromolecules* **2001,** *34* (10), 3155-3158.

34. Beers, K. L.; Boo, S.; Gaynor, S. G.; Matyjaszewski, K., Atom Transfer Radical Polymerization of 2-Hydroxyethyl Methacrylate. *Macromolecules* **1999,** *32* (18), 5772-5776.

35. Lee, J.; Kim, E. H.; Jhon, M. S., The Swelling and Mechanical Properties of Hydrogels of Tactic Poly (2-Hydroxyethyl Methacrylate). *Bull. Korean Chem. Soc.* **1983,** *4*, 162-169.

36. Turgman-Cohen, S.; Genzer, J., Simultaneous Bulk- and Surface-Initiated Controlled Radical Polymerization from Planar Substrates. *J. Am. Chem. Soc.* **2011,** *133,* 17567-17569.

37. Gorman, C. B.; Petrie, R. J.; Genzer, J., Effect of Substrate Geometry on Polymer Molecular Weight and Polydispersity during Surface-Initiated Polymerization. *Macromolecules* **2008,** *41,* 4856-4865.

38. Koylu, D.; Carter, K. R., Stimuli-Responsive Surfaces Utilizing Cleavable Polymer Brush Layers. *Macromolecules* **2009,** *42,* 8655-8660.

39. Lee, H.; Venable, R. M.; MacKerell, A. D.; Pastor, R. W., Molecular Dynamics Studies of Polyethylene Oxide and Polyethylene Glycol: Hydrodynamic Radius and Shape Anisotropy. *Biophys. J.* **2008,** *95,* 1590-1599.

40. Bunk, J. K. G.; Drechsler, A.; Rauch, S.; Uhlmann, P.; Stamm, M.; Rennekamp, R., The Distribution of Hydrophobized Inorganic Nanoparticles in Thermoresponsive Polymer Nanocomposite Films Investigated by Scanning Probe and Electron Microscopy. *Eur. Polym. J.* **2013,** *49,* 1994-2004.

Appendix 1: List of Publications Resulting from Work During the Thesis

7. **Sweat, D. P.**; Kim, M.; Larson, Steven R.; Choi, J. W.; Choo, Y.; Osuji, C. O.; Gopalan, P. Rational Design of a Block Copolymer with a High Interaction Parameter. *Submitted (August 2014).*

6. **Sweat, D. P.***; Kim, M.*; Schmitt, A. K.; Perroni, D. V.; Mahanthappa, M. K.; Fry, C. G.; Gopalan, P. Phase Behavior of Poly(4-hydroxystyrene-*block*-styrene) Synthesized by Living Anionic Polymerization of an Acetal Protected Monomer. *Accepted to Macromolecules*. **Denotes equal contribution*

5. **Sweat, D. P.**; Yu, X.; Kim, M.; Gopalan, P. Synthesis of Poly(4-hydroxystyrene)-based Block Copolymers Containing Acid-Sensitive Blocks by Living Anionic Polymerization. *J. Polym. Sci. Part A: Polym. Chem.* **2014**, *52*, 1458-1468.

4. **Sweat, D. P.***; Kim, M.*; Yu, X.; Schmitt, S. K.; Han, E.; Choi, J. W.; Gopalan, P. A Dual-Functional Layer for Block Copolymer Self-Assembly and the Growth of Nanopatterned Polymer Brushes. *Langmuir* **2013**, *29*, 12858-12865. **Denotes equal contribution*

3. **Sweat, D. P.***; Kim, M.*; Yu, X.; Gopalan, P. A Single-Component Inimer Containing Cross-Linkable Ultrathin Polymer Coating for Dense Polymer Brush Growth. *Langmuir* **2013**, *29* (11), 3805-3812. **Denotes equal contribution*

2. Kim, M.; Han, E.; **Sweat, D. P.**; Gopalan, P. Interplay of Surface Chemical Composition and Film Thickness on Graphoepitaxial Assembly of Asymmetric Block Copolymers. *Soft Matter* **2013**, *9*, 6135-6141.

1. Paoprasert, P.; Kandala, S.; **Sweat, D. P.**; Ruther, R.; Gopalan, P., Versatile grafting chemistry for creation of stable molecular layers on oxides. *J. Mater. Chem*. **2012**, *22* (3), 1046-1053.